Gas-Phase Conversion of Glycerol to Methanol Over Magnesium Oxide Catalysts

Thesis submitted in accordance with the requirement of Cardiff University for the degree of Doctor of Philosophy

Karl S. Mugford

School of Chemistry

Cardiff University

2022

Summary of Thesis

The gas phase conversion of aqueous glycerol feedstocks to methanol has been investigated over a series of MgO catalysts, conducted at atmospheric pressure and in the absence of external reductants. MgO catalysts with characteristics altered by varying the preparation heat treatment temperature were studied. Glycerol reactions were carried out over the samples. The samples exhibited a complex product distribution. Major products observed included hydroxyacetone, ethylene glycol, acetaldehyde, acrolein and methanol. Gaps in the carbon mass balance occurred the catalysts. These were proposed to be due to high weight molecular products, which can form *via* bi-molecular condensation reactions. Promotion of condensation reactions was linked to strong O^{2-} basic sites on MgO. These are proposed to readily dissociate water, which can lead to hydroxylation of the sites *in-situ*. It was theorised that the hydroxylation of the catalysts surface promoted glycerol conversion and condensation reactions, due to substrate stabilisation. The catalyst treated at 650 °C was found to not require the dissociation of water to activate glycerol and exhibited more coke than the other samples. This was proposed to be linked to its morphology which differed from the others, resulting in a less prominent ratio of the O^{2-} sites. This sample exhibited a high carbon mass balance over all conditions tested. This was concluded to be due to it suppressing the formation of high weight molecular products. The high carbon balance resulted in a higher yield to the identified products. The catalyst exhibited a higher methanol STY of 93 g h^{-1} kg cat^{-1} than the other catalysts tested. Finally, reactions investigating the mechanism were conducted using intermediates products. It was concluded that hydroxyacetone and glycolaldehyde C-C bond cleavage was unlikely to be the primary route to methanol. Instead, it is proposed to be the initial homolytic C-C cleavage of glycerol.

Acknowledgements

I have thoroughly enjoyed my time at Cardiff University conducting my research in the Cardiff Catalysis Institute, developing my knowledge, and broadening my perspective. I feel privileged to have been given the opportunity to study at such a prestigious institution and have found my research here incredibly rewarding.

I would like to thank my supervisors Prof. Stuart Taylor and Prof. Graham Hutchings for giving me the opportunity to undertake this project. Their oversight and guidance have proven invaluable, and I am hugely grateful to them for sharing their time and expertise which were vital to my studies.

A massive thank you goes to Dr Mark Douthwaite, Dr Nicholas Dummer and Dr Louise Smith. Their input and support throughout the four years, along with their understanding of the project, have been of huge importance to the success of this thesis.

Thank you to Dr Dave Willock for your computational work into the complex chemistry investigated. I would like to thank the advisory board, Prof. Donald Bethell, Prof. David Knight and Prof. Mark Howard for their input and expertise in our meetings on directing this project and furthering its aims.

Special thanks to Dr Greg Shaw for his assistance and expertise in the laboratory. Thanks to Dr Tom Davies for his expertise and help with SEM and TEM analysis. And Tom Williams for help with LCMS analysis. I am also very grateful to all of the staff members of the School of Chemistry who have helped with this project.

Finally, I would like to thank my partner Gary for all of his support and reassurance through often stressful and all-consuming times during my PhD; and my family without whose support I would not have reached this stage.

Abbreviations and units

% – Percent

°C – Degrees Celsius

Å – Angstrom (10^{-10} meters)

Atm – standard atmosphere pressure

a.u – arbitrary units

BET – Brunauer–Emmett–Teller

BDE – bond dissociation energy

C – carbon

CC/g – cubic centimetres per gram

CAT – catalyst

CHN – Carbon, hydrogen, and nitrogen

CMB – carbon mass balance

CO – Carbon monoxide

CO_2 – Carbon dioxide

CO_x – Carbon oxides

DFT – Density functional theory

DNPH – 2,4-dinitrophenylhydrazine

DRIFTS – Diffuse reflectance infrared Fourier transform spectroscopy

DTA – differential thermal analysis

EXAFS – Extended X-ray absorption fine structure

FAME – Fatty acid methyl esters fame

FFA – free fatty acids

FID – flame ionisation detector

FWHM – full width half maximum

g – gram

GC – gas chromatography

GHSV – gas hourly space velocity

HRTEM – high resolution transmission electron microscopy

HWMP – high weight molecular products

hrs – hours

K – kelvin

Kg - Kilogram (10^3 g)

LCMS – liquid chromatography mass spectrometry

MBOH – 2-methyl-but-3-yn-2-ol

MS - mass spectrometry

M/Z- mass to charge ratio

MgO – Magnesium oxide

M – Molar (mol dm^{-3}) MeOH

mg – Milligram (10^{-3} g)

MPV – Meerwein-Ponndorf-Verley

nm – Nanometre (10^{-9} m)

PBEsol – Perdew Burke Ernzerhof adapted for solids

QM/MM – quantum mechanics/molecular mechanics

SEM – Scanning electron microscopy

SiC – Silicon carbide

STY – Space time yield

SSNMR – solid state nuclear magnetic resonance

TCD – Thermal conductivity detector

TGA – Thermogravimetric analysis

TOC – total organic carbon

TEM – Transmission electron microscopy

TMP – trimethylphosphine

TPD – Temperature programmed

XRD – Powder X-ray diffraction

XPS – X-ray photoelectron spectroscopy

XAS – X-ray absorption spectroscopy

wt.% – Weight percent

Table of Contents

Chapter 1

Introduction

1.1 Introduction to green chemistry

Over the last 120 years, the global population has rapidly grown from approximately 1.6 billion to almost 7.9 billion in 2021.[1] This exponential growth and the accompanied demand for resources has put significant pressures on the environment. The demand on industry and scientific research to produce solutions to feed, dress, shelter and energise this burgeoning global population has subsequently increased. Catalysis has often been at the forefront of important industrial developments. An understanding of the discipline being instrumental in areas such as medicine, fuels, fertilization and production of consumer and industrial goods.

As demand for resources increases, science and engineering have often been able to answer the call and allow for optimisation of earth's natural resources, which in turn, has resulted in further increases in population. The Haber-Bosch process is an great example of this and is often credited for facilitating exponential population growth.[2,3] This has allowed for the yield of arable land to increase significantly, making it possible to reliably feed significantly more people than would have been previously possible. The Haber-Bosch process, in which ammonia is produced from atmospheric nitrogen reacted with hydrogen under high temperature and pressure, is also known as nitrogen fixation. The catalyst used is usually an iron based heterogenous catalyst with various promoters, which promote the hydrogenation of N_2.[4] This process is mainly used to produce fertilizer, which allows for significant increases in food production. Catalysis is a crucial tool in current and future chemical processes. Without this technology, keeping society running at the current population would not be possible. The production of adequate amounts of important materials such as petroleum, certain pharmaceuticals and food would not be possible.

1.1.2 Principles of green chemistry

Driven by economic, legislative, and environmental reasons, there has been a push towards efficient and greener chemical processes. Economic reasons, however, remain at the forefront of driving change. If a process can be made more efficient, using less energy, and producing less waste to deal with, this could also be advantageous to producers as it would reduce operation costs. Nowadays there is emphasis in modern scientific research to provide cheaper, efficient, sustainable, and greener alternatives to past and alternative processes.

To limit impact on the environment and protect the health of the population, the production of chemical commodities needs to be conducted in a safe and responsible manner. Chemical products that find their way into the environment can have deleterious effects. Examples of this occurring include acid rain caused by the mixing of emitted sulphur dioxide and nitrogen oxide damaging forest cover.[5] In the event of liquid chemical waste reaching natural waterways, this would be extremely detrimental as it would limit access to safe water sources for local populations and could cause an increase in health problems.[6] There is evidence that large amounts of agricultural fertilizer reaching seas and oceans can result in uncontrolled algae blooms, which consume excessive quantities of oxygen in the waters, leading to coastal and riverine dead spots.[7] The earth's ozone layer is also depleted, due to the production and release of chlorofluorocarbons, halon and similar compounds.[8]

With the aim of reducing the occurrence of the aforementioned and similar problems; there has been development of governmental legislative bodies such as the environmental protection agency in the USA, which was formed in 1970. The UK has also put forward a series of different environmental acts and developed several governing bodies. One of the first was the alkali act in 1863 which was used to enact some control upon sewage, town planning and housing. However, this did little to combat the emissions causing smog, a serious problem in the UK industrial and urban areas during the late Victorian period. Since joining the EU in 1973, and especially over the last 30 years, there has been an increase in the amount and specifications of UK environmental laws and restrictions.

With the legislative, environmental, health and economical demand for a greener future, a framework for the basis of what constitutes as 'green' practice within chemistry has been proposed. This takes the legislation laid out by USA and European directives further with a series of core principles for the chemists and chemical engineers to try and operate within.[9] The main goal being to ensure that the chemicals, processes, and commercial products do not lead to toxic products and waste, but also that more sustainable methods are used which are less energy intensive.

In 1998, the 12 core principles to green chemistry were laid proposed by Paul Anastas and John Warner.[9,10] One of the key principles is that 'it is better to prevent waste than to treat and clean up created waste'. Waste for a process can be measured by the E-Factor, a relation between the mass of waste to desired product.[11,12] It is also important that when waste is produced it is benign and degradable. In reducing waste, the atom economy is also important which can be calculated by:

$$\% \text{ Atom Economy} = (\text{FW of atoms utilized}/\text{FW of all reactants}) \times 100 \text{ }^{[13]}$$

Traditionally, efficiency was measured by percentage yield. But with some reactions even if a 100% of the possible yield is achieved the atomic efficiency can be significantly lower as some of the atoms are tied up in unused co-products and waste. In catalysis this may be seen by achieving a high mass balance in the desired product, where atoms within the feedstock are mostly accounted for and not lost in unwanted side reactions, coking and fouling. Safety is also key to the principles, both in laboratory safety and disposal of waste that is produced. When there are several possible reactants or products to serve a purpose, the choice should be predominantly based on which are the least hazardous.

1.2 Catalysis

Use of catalysis whenever possible is a key feature of the green principles. This principle is a core focus of this thesis, with a catalytic transformation being the main subject of investigation. Catalysis is highly important in chemical synthesis. It allows for reactions which under normal conditions are not energetically favourable to be directed over other less desired routes. This can result in reagents that would not normally interact react. Catalysts instigate these reactions by providing an alternative reaction pathway. Catalytic processes have also been directly used for clean-up of pollutants before expulsion into the environment. A famous and common example of this is the catalytic convertors found in the exhaust systems of vehicles.[14]

The importance of catalysis in the chemistry industry is difficult to overstate. Up to 90% of industrial chemical processes involve catalysis and they are necessary for several expansive industries.[15–19] The production of the important industrial chemical sulphuric acid for example is created *via* the catalytic oxidation of SO_2 to SO_3. In industrialised countries, catalysis is estimated to be responsible for about $1/6^{th}$ of the value of all manufactured goods.[20] As detailed by the aforementioned principles of green chemistry, catalysis has a significant role to play. The creation of future chemical products and processes should focus on these principles to reduce waste and eliminate unnecessarily hazardous chemicals. Catalysis has played an important role in the transformation of chemistry to a more responsible and sustainable industry.[21]

One of the first uses of the term 'catalyst' in its current meaning was by the scientist Berzelius in 1835.[22] However, the industrial application of inorganic catalysts go somewhat further back, to the late 1700's. It was discovered that certain reactions could be made to proceed non-stoichiometrically in the presence of certain substances. Many initial investigations involved oxidation over platinum, which would remain a mainstay in catalysis to the present day. The first investigation which provided a detailed explanation as to how heterogeneous catalytic oxidation proceeds over platinum was reported by Ambrogio Fusinieri in a paper published in 1824.[22]

The simplest definition of a catalyst is a substance that increases the rate of reaction but which itself is not consumed.[20] On physical terms a catalyst is a component which is added to a chemical reaction. Usually in heterogeneous catalysis, the catalyst is a solid or in homogenous catalysis a liquid (often a metal complex) which reacts with the substrates to increase and direct the rate of a chemical reaction. In this process the catalyst must not in principle be used up itself i.e., it is not a stoichiometric reagent. This is important as allows for a continuous cycle to theoretically persist where the catalyst facilitates the transformation many times to produce numerous substrate molecules. This allows for only a small amount of catalyst to be used, relative to the substrate(s). The role of the catalyst varies, but usually it speeds up the reaction by providing an alternative reaction pathway. In this case a pathway with a lower overall activation energy, with no deep troughs or peaks in the associated energy level diagram of the reaction. However, in the case of the biological enzymes, the catalyst stabilises molecular transition states to allow for further reaction in bio-catalytic systems. When enacting an alternative pathway, it will require a lower activation energy and thus, often require a shorter amount of time and lower temperature to achieve than the associated non-catalysed reaction. However, the overall thermodynamic energy of reaction will be the same. In practice, many reactions that proceed over a catalyst could also proceed without one, but the rate would be much slower or counteracted by the reversibility of the reaction.

One of the most important parameters when assessing a catalysts performance in a reaction, is the product selectivity. A highly selective catalyst will yield a high proportion of the desired product with minimal amounts of unintended side products (by-products). This can often be one of the most challenging aspects of catalyst design, with great efforts being enacted to make even small increases in pre-existing catalysts selectivity. As well as an intrinsic ability of the said catalyst, the selectivity observed is often highly dependent on the conditions of reaction, such as temperature, pressure, and reactant concentration. Balancing all these factors to achieve a high selectivity is therefore important. From an economic perspective, there is a high incentive to increase selectivity as higher amounts of the desired product will be made from the same amount of substrate and less waste will be generated. There are only a few instances where selectivity is not a huge concern. These would normally be simple reactions with only one thermodynamically viable product, such as the formation of NH_3 from H_2 and N_2.

1.2.1 Types of catalyst

There are two distinct areas of research in non-biological catalysis. These are heterogeneous and homogeneous catalysis.

1.2.1.1 Homogeneous catalysts

Homogeneous catalysts are usually based on organometallic compounds and coordination complexes. They are classified as homogeneous catalysts if they exist in the same phase as their reagents. This is in practice often a metal complex which is dissolved with its ligands and the reagents within a solvent.

Homogeneous catalysis is known for having several advantages and disadvantages compared to heterogeneous catalysis. These lead to the application of the different types depending on the operation aims and scale. Homogeneous catalysis often relies on a smaller scale and more complex, but directable reactions. The principal advantages of homogeneous catalysis are the excellent atom efficiency and reaction selectivity which can be obtained with them. The nature of the ligand framework means it is often very specific to a certain substrate, and steric effects of the designed ligands help direct the reaction to a specific product. Also, as homogeneous catalysts are usually dissolved in a solution, every single molecule of catalyst is accessible to the reagents and thus very high activity is attainable. Their reaction mechanisms are often also easier to deduce and evaluate as it is often easier to identify the specific active site of the catalyst.[20]

One of the disadvantages is that these catalysts can often be complex to synthesise themselves. The choice of metal and ligands influences the oxidation state of the active centre and thus, the associated coordination number. This can have big implication on the stereoselective properties of the catalyst. The catalyst may take many complex synthesis steps to prepare, which would need to be optimised to obtain acceptable yields and purity. These extra steps required for the production of the catalyst can be responsible for significant amounts of waste themselves. Another limitation of homogeneous catalysis is that while the existence of same phase reactions can be advantageous to rate and selectivity, it makes separation of the catalyst from product and solvent difficult. This can lead to loss of catalyst in the product, or just not being reliably extracted from the product mixture. In this way, while less would be needed than a stoichiometric reagent there would still need to be a continuous process of production to reclaim the catalyst after reaction.

While the metal complex catalysts may require a multistep synthesis, it is practicable to obtain their crystal structure quite reliably *via* X-ray crystallography. This knowledge of the metal and ligands allows for them to be rationally designed to emphasise certain parameters. The organic ligands themselves can, in many cases, be optimised. This provides a further element of control and thus, the specificity of the active site and the selectivity can be excellent.

There are many types of reactions where homogenous catalysts have been used, such as alkene metathesis[23], hydrogenation of alkenes[24] and hydroformylation.[25] One recent and highly applicable

example was the 2010 Nobel Prize for chemistry winning work by Heck, Negishi and Suzuki on Pd complexes for C-C cross coupling reactions.[26] The 2021 nobel prize in chemistry was again awarded in the field of homogeneous catalysis to Benjamin List and Davi W. C Macmilian for their work on Enamine and iminium ion-mediated organocatalysis.[27] Most industrial chemistry processes which use catalysts however do not use homogeneous catalysts, regardless of their generally excellent selectivity. This is due to the additional time and money required for the synthesis of these catalysts and extraction of products. Interesting work is on-going, where homogeneous catalysts are tethered to solids resulting in the "hetero-genising" and pairing with heterogeneous catalyst supports, allowing for much simpler extraction and reuse.[28,29] Further advancements in this field could see more commercial applications for homogeneous catalysts moving forward.

1.2.1.2 Heterogeneous catalysis

Heterogeneous solid catalysts are used more in industry and in large scale bulk processes. The world catalyst market size was estimated at USD 33.9 billion in 2019 with a predicted compound annual growth rate of 4.4% to 2027 which would lead to forecasted value of 48 billion USD. Heterogenous catalysts hold 72.1 % of the catalyst market share in 2019.[30] This shows that they are the dominant type of catalyst over homogeneous catalyst at this point in time. MgO is an example of a simple heterogeneous catalyst. Heterogeneous catalysts exhibit several benefits that, from an economical industrial standpoint, make them more practical. Heterogeneous catalysts can be far more robust to high temperatures, flows and pressures. Thus, high reaction temperatures can be used to enhance activity in systems which are not thermodynamically limited. They can be more environmentally friendly as they are easy to separate from the products. Separation is especially easy in fixed bed flow reactors which also allow for large scale reactions to take place and are relatively easily scalable. In such processes, a simple tubular reaction vessel will be used where the reagents, in liquid or gas, are passed over a bed of the catalyst and collected the other end. A disadvantage of this, however, is that the catalyst (as a solid) is not dissolved with the reagents and therefore only the catalyst surface is available for reaction. This can result in mass transfer limitations, where the diffusion from the bulk substrate *via* adsorption and desorption to the solid surface can limit the rate of reaction.[31] This means that heterogeneous solid catalysts are often designed to have the highest surface area possible to give the optimum reactivity. An example of this includes zeolites such as ZSM-5, which are highly porous solids, this allows for reagents to penetrate deep within their solid structure resulting in impressively high surface areas. A more common approach however is multiphasic catalysts where a high surface support provides a surface where smaller catalyst particles are deposited. Such supported metal catalysts are abundant within heterogeneous catalysis. A vast variety of different metals have proven to be affective when

supported in such a way. The choice of metal used is often related to the intrinsic property of the metal and the specific reaction under investigation.[32] Pt group and noble metals are often used. Examples of supported metal catalysts include Pd catalysts supported on alumina and carbon.[33] Pd supported catalysts are commonly used in hydrogenation reactions for fine chemical production.[34] Pd/C catalysts are also used in bulk chemical production such as for terephthalic acid.[35] Development in the use of Au in heterogenous catalysis has led to several breakthroughs in the area.[36] Examples includes Au/C supported catalysts, which can be used as effective acetylene hydrochlorination to vinyl chloride catalyst[37] and Au/FeOx for CO oxidation.[38]

1.3 Base catalysed reactions on metal oxides

Compared to the abundance of research on acid catalysts, the study of basic heterogeneous catalysts is somewhat limited.[39,40] It was noted by Tanabe and Holderich in their 1999 survey of industrial processes that only 10 out of 127 major processes they identified were solely base catalysed, there were also 14 acid-base catalysed reactions, but the rest were acid catalysed.[41] However, these materials are increasingly being seen as an alternative to acid catalysts.

Acid and base sites on a catalyst surface can serve as active sites for catalytic reactions. The strong robust nature of solid catalysts means that both Lewis acids and basic sites can co-exist on a catalyst surface without reacting with each other to form adducts. This can allow for unique catalyst reactivity, that would not be possible in solution. These types of sites tend to be highly active for the dehydration of alcohols and the isomerisation of alkenes. Bifunctional sites can be seen on γ-Al_2O_3 which, with its high surface area and acidity/basicity, allow for its wide employment as a support for metal nanoparticles.[42] These surface metal sites are then used as the active sites for the catalytic conversion, with the reactants that have absorbed on the support surface. In catalytic convertors, γ-Al_2O_3 is used as a support for the Pt/Rh alloys metal sites.[20]

An example of a base catalysed industrial process is alkyl aromatic alkylation. Here, the basic catalysts can be used for their different specificity compared to an acid catalyst. Basic catalysts alkylate the side chain rather than the ring of the molecule, which is typically what is observed over acid catalysts.[39] MgO promoted with various alkaline and alkali earth oxides can catalyse the synthesis of α,β-unsaturated ketones from the aldol condensation of acetone.[43] In the selective hydrogenation of nitriles over base/metal bifunctional catalysts, base promoters are used to help poison acid sites on the surface responsible for the undesirable coupling reactions.[44]

Alkali metal oxides can also serve as basic catalysts; their basic strength increases as you descend group I, with Li_2O being the weakest. They are usually studied as supports and modifiers, the literature on using them as a solitary catalytic material is far less explored. Caesium oxide is highly

basic and as such, it too had been utilised frequently. As a catalyst however, it typically requires a high activation temperature and is susceptible to poisoning by water and CO_2.[39] Regardless, there has been significant research into the use of Caesium based catalysts. Several important processes involve the use of supported alkali metal oxide catalysts and are being developed in industry. 4-Methylthiazole, which is used as a fungicide and in the pharmaceutical industry, can be produced by zeolite supported caesium catalysts. However, the selectivity is only low (*ca.* 60 %) and the activity halves within two weeks.[39] A similar catalyst has been used for aldol reactions, such as the reaction between methyl propionate and formaldehyde.[45] Other research has also investigated the aldol condensation of butanal for 2-ethylhexenal.[46]

The alkaline earth oxides have a large body of work focussing on them, especially based on magnesium and calcium-based oxides.[47,48] CaO has been found to be a useful catalyst in biodiesel production.[49,50] Both MgO and CaO have been found to have applications in the sequestration of CO_2 from the atmosphere. This process would also yield calcium carbonates which have commercial value.[51,52] The rest of this thesis will specially focus on MgO as a basic catalyst, where the uses and preparation of will be discussed in detail in the next section.

1.4 MgO

MgO is a basic rock salt solid, which can be prepared in a variety of ways. As will be shown, the conditions and reagents used in its preparation can result in significant changes to its physical properties. These include its specific surface area (SA), its basicity (strength and site distribution), its porosity, crystallite size and morphology.

As with the alkali metals, MgO catalysts need to be activated under high temperatures to remove hydroxides and carbonates. Therefore, attention must be given to these as such species can re-emerge readily through exposure to air.[53] MgO as a basic solid has already been used in a variety of base catalysed reactions. There has been both experimentation with the metal oxide as the catalyst itself, as a support and with alkali metals to promote its basic strength. It exhibits a low solubility compared to alkaline earth metals, which can assist with its stability and reusability. The Hammett constant for it is *H- = + 26.0,* making it relatively average for a basic oxide.[54]

1.4.1 Calcination from Mg(OH)$_2$

A common and simple way of preparing MgO is *via* the thermal degradation of a Mg(OH)$_2$. This needs to be done at temperatures in excess of 350 °C. One of the first investigations pioneered in this area was by Anderson and Horlock (1962).[55]

The formula for the dehydration of Magnesium hydroxide is as follows:

$$Mg(OH)_2 \rightarrow MgO + H_2O$$
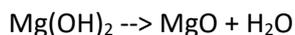
This is relatively straight forward example of thermal degradation, both MgO and $Mg(OH)_2$ possess only one crystal structure. $Mg(OH)_2$ consists of a hexagonal hydroxide lattice, which undergoes a crystallographic transformation to a cubic oxide lattice. Anderson and Horlock reported that the hydroxide powder upon investigation by electron microscopy consisted of fairly well-defined hexagonal discs, with a diameter of approximately 1000 Å.[55] Upon decomposition to MgO the sample consisted of an aggregate mass of oxide, which consisted as a 'sponge-like' structure, reminiscent of the original hydroxide structure.

Anderson and Horlock discussed the reaction as proceeding in three stages.[55] The first stage was the hydroxide lattice being slightly altered *via* the interaction of neighbouring hydroxyl ions. The thermal energy causes dimensional changes which stress the large brucite crystals, resulting in poly-crystallisation. This is the process of the larger crystallites transforming into more numerous small species. Next, water is removed from the lattice and recrystallization of the dehydrated products occurs, resulting in the formation of an MgO periclase structure. It is generally found that higher heat treatments lead to larger crystallite sizes, lower surface area and thus, a lower total amount of basic sites.[56,57] MgO prepared from the precipitation of $Mg(OH)_2$ are known to be highly defective, which has been confirmed using high resolution transmission electron microscopy (HRTEM) and can be advantageous from a catalytic perspective.[58]

1.4.2 Calcination from various precursors

There are many more examples of producing MgO from the calcination of other substrates (in addition to $Mg(OH)_2$. High surface area MgO was prepared by calcination of $(MgCO_3)_4$-$Mg(OH)_2$, or rehydrated $Mg(OH)_2$ at 450 °C for 2 h.[59] Here, temperatures above 400 °C were employed to remove hydroxide species, which were deemed to be far less reactive. Between calcination temperatures of 400 and 500 °C, the highest surface area material obtained a surface area of over 300 $m^2\,g^{-1}$. This, logically, decreased upon exposure to higher temperatures, as the catalyst became more crystalline. [58]

Ruckenstein and Hu,[60] also investigated the preparation of preparing MgO supports *via* decomposing a variety of different Mg precursors. The MgO samples were made *via* calcination of either $Mg(NO_3)_2$, $Mg(OH)_2$ and $[MgCO_3]_4Mg(OH)_2$. $Mg(NO_3)_2$, $Mg(OH)_2$, which were treated at 400 °C for 3 hrs. The authors also conducted additional treatments at 1000 °C for an additional 3 hrs, for comparison. $[MgCO_3]_4Mg(OH)_2$ was prepared by a 400 °C treatment at 3 hrs or a 800 °C for 1.5

hrs or 1100 °C for 10 minutes. These conditions led to varied characteristics in the catalyst. Most exhibited very low surface areas, except for the sample prepared through decomposition of $[MgCO_3]_4Mg(OH)_2$ at 400 °C for 3 hrs.

The effects of increasing calcination temperature were tested on trapezoid like MgO.[61] These were made from $Mg(NO)_3$-$6H_2O$ dissolved in water and treated with $Na_2C_2O_4$. This gave MgC_2O_4-$2H_2O$ which was then calcined from 400 – 1000 °C. The crystal plane underwent significant changes as the temperature increased. At 400 – 600 °C, meso-crystals were observed, changing to a polycrystalline sample at 700 °C. This then proceeded to a pseudo-morphic structure between 800 – 900 °C and finally into a cubic single crystal structure when approaching 1000 °C. This was accompanied by the smooth surface fracturing as sintering occurred.

MgO samples were prepared by the calcination of $(MgCO_3)_4$-$Mg(OH)_2$ by Chunli Xu *et al.*[62] Temperature had a significant effect on the MgO properties. An ideal range between 450 °C to about 700 °C allowed for high surface area and adequate pore structure. For example, the sample made at 450 °C exhibited 292 m^2 g^{-1} and 0.33 cm^3 g^{-1} pore volume. Below these temperatures however, residual $MgCO_3$ attributed to the observed lower surface area and pore volume. At higher temperatures the surface became homogenised, and the pore structure collapsed. For example, the sample calcined at 800 °C only exhibited a surface area of 17 m^2 g^{-1} and a pore volume of 0.08 cm^3 g^{-1}.

MgO can also be synthesised with specific morphologies. These can sometimes be complex procedures but a simple method was developed by Cui *et al*; the heating of $MgCl_2$ powder at 750 °C for 1.5 hours in a flow of 9:1 argon to hydrogen yielded well defined nanorods.[63]

1.4.3 Precipitation and calcination preparations

Procedures involving precipitation steps can also yield MgO with different and targeted characteristics. Aramendía *et al.*[64] prepared MgO in a variety of ways, including: precipitation of the nitrate and sulphate precursors, a sol-gel preparation and a urea precipitation. Precipitations from $Mg(NO_3)_2$-$6H_2O$ and $MgSO_4$-$7H_2O$ were performed with 1 M KOH followed by a 600 °C calcination for 2 hours. The sol-gel sample was made using 0.1 mol of magnesium ethoxide refluxed with 100 mL of ethanol, 20 mL of water and 3 mL of concentrated HCl. Following the dissolution of the ethoxide, concentrated NH_4OH was added until a pH of 9 was reached, after which it was left for 36 hours, centrifuged, and calcined at 600 °C for 2 hours. The precipitation in urea involved a ratio of urea to Mg^{2+} of 3.8. For this, 42 g of urea and 0.2028 moles of $MgSO_47H_2O$ were dissolved in half a litre of water. This was then refluxed for 3 days, yielding a gel that was washed and filtered, followed by 600 °C calcination for 2 hours. The sol-gel procedure resulted in the formation of large

MgO crystallite sizes of 270 Å, which was comparable to that of the hydroxide sample of 277 Å. The Urea precipitation on the other hand, produced MgO with the smallest crystallite size of 97 Å and the rest of the samples were similar, exhibiting sizes of around 110 – 164 Å. When investigated by CO_2 TPD, it was found that each of the samples possessed a variety of different basic site densities. These were seen to exist in three distinct forms, strong unidentate carbonate, medium bidentate carbonate, and weak bicarbonate. The commercial MgO sample, used for comparison, was determined to the least basic, but when this was rehydrated and calcined, it led to the most basic catalyst observed. The materials prepared *via* the sol-gel and urea precipitation methods yielded relatively low, but similar basicity.

Another precipitation technique, put forward by Sutradhar *et al.*[65], can be used for the synthesis of well-defined MgO nanorods. The nanorods, which were up to 100 nm in length, were formed *via* the precipitation of a 0.2 M solution of $MgNO_3$ with 0.2 M $(NH_4)_2CO_3$. This gave a carbonate which was then heat treated at 450 °C to 800 °C in air or N_2. Lattice defects and low coordinate ions were enhanced in the rods when treated at lower temperatures.

1.4.4 Other techniques for MgO preparation

Research carried out by Dummer *et al.*[66] involved the use of MgO prepared *via* a surfactant controlled route. This route used hydrothermal conditions and the surfactants used were sodium dodecyl sulphate, sodium hydroxide, which were reacted with a quaternary ammonium ion. This preparation method allowed for the controlled formation of $Mg(OH)_2$ hexagonal plates. These were subsequently thermally transformed to MgO under 420 °C for 2 hours, retaining the morphology. This method of MgO synthesis, using surfactants, was also investigated by Khairallah.[67]

A variety of different MgO morphologies were made by Sutradhar *et al.*[68] They investigated the synthesis of nanoflakes of a random, flower and grid like shape. Spheres, cubes, and hexagonal plates were also formed. These were made by the calcination of magnesium carbonate hydrates, which were made *via* hydrothermal and supercritical methods using $MgNO_3$ and nesquehonite rods with $(NH_4)_2CO_3$. The different forms were obtained through varying the pH and carbonate concentration. Hydrolysis of $MgSO_4$ in an aqueous ammonium hydroxide solution in hydrothermal conditions leads to $Mg(OH)_2$ rods which can then be calcined to MgO nanorods.

Attempts to tune the basic properties of nanocrystalline MgO was investigated by Menezes *et al.*[58] The distribution of basic sites was dependent on the preparation method. Surface heterogeneity was found to promote basic site concentration. Medium strength sites were more prominent on samples made *via* hydrothermal or precipitation aging treatments, while precipitation techniques gave a more even amount of medium and strong sites.

1.5 Reactions using MgO as a basic catalyst

MgO is commonly used in heterogeneous catalysis, both by itself and as a support in bimetallic systems. Aldol condensation reactions,[39,43,69–71] Henry reactions,[72] alcohol coupling,[73] transesterification of vegetable oils to biodiesel,[39,62,74,75] double bond isomerisation,[76] Cannizzaro reactions,[77] Michael additions,[59] CO_2 reforming of CH_4[60], Tischenko reactions[78] and Claisen condensation reactions[65,68] are all examples of reactions where MgO has been employed as a catalyst. MgO nano rods have also been used to increase performance in Bi/Pb 2223 super-conductors.[63] This all shows that it is a flexible and important material.

Overall, basic site strength and density is deemed to be important for catalysis over MgO and is found to have significant effects in a variety of reactions. For example: Aramendía *et al.*[64] found, when testing for the Meerwein-Ponndorf-Verley (MPV) reduction, that there was a strong correlation with the basicity of the sample and its activity. Higher concentrations of stronger basic sites led to a quicker hydrogen transfer from cyclohexanone with isopropyl alcohol (IPA).

Wei *et al.,* [79] investigated the basic properties of MgO and CaO for the synthesis of dimethyl carbonate from propylene carbonate and methanol. The authors were specifically interested in how basic strength and density affected this transformation. Predictably, higher strength basicity led to an increase in activity, but at the expense of selectivity. The main role of the base was to activate methanol by abstracting a proton. This gave MeO^- which would react with the propylene carbonate yielding dimethyl carbonate. Stronger base sites result in a more negative and reactive MeO^-, and thus, increased activity for dimethyl carbonate production. However, this also increased the rate of propylene carbonate polymerization, resulting in a decreased selectivity to the desired product.

Chunli Xu *et al.*[59] explored a variety of reactions over MgO. It was found that MgO could efficiently convert α, β unsaturated carbonyl compounds with a 1,4 addition to chalcone, obtaining yields of above 80 %. MgO was interestingly found to be more active than previously explored catalysts for this transformation and simpler to prepare. The reaction was tested using varied donor species. The use of ethyl cyanoacetate and diethyl malonate led to fast rates. But changing these to more acidic donors led to a full loss in activity. This was reported to be due to a *cis*-enol species forming, which was very strongly bound to the MgO surface resulting in the active sites being blocked. There is limited examples of work utilizing MgO as a catalyst in liquid reactions due to low activity exhibited at lower temperatures,[41] especially with use of H_2O as a solvent, which would result in the formation and dissolution of $Mg(OH)_2$.[80]

Chunli Xu et al,[59] also investigated base catalysed Knoevenagel condensation over MgO. Here, a variety of aromatic carbonyl compounds were reacted with malononitrile and ethyl cyanoacetate. When using aldehydes, the reaction proceeded relatively fast. In the contrary, with ethyl cyanoacetate, the reaction rate was much lower. This was proposed to be due to the low acidity of the molecule, thus, requiring more thermal energy for the proton abstraction. In this example, the MgO catalyst exhibited high reaction rates and selectivity across the board, again surpassing literature examples in several instances. Dummer et al.[66] also investigated the Knoevenagel condensation of benzaldehyde and ethyl cyanoacetate. It was found that the amount of surface hydroxyl species was found to drive the catalysts activity, but the distribution of -O^{2-} sites was also identified as being important for product yields.

In another publication Chunli Xu et al. also investigated the use of MgO as a transesterification catalyst.[62] In these experiments, it was found to be an effective catalyst when used with methanol and at a temperature of 200 °C. The reaction temperatures were also needed to be relatively high; at lower temperatures (such as 60 °C), MgO showed little activity and large quantities of methanol was required to obtain acceptable yields. This is undesirable due to the fossil fuel derived nature of methanol and resultant requirement for solvent disposal. The catalyst did however stand out, as relatively high yields could be obtained compared to previous catalysts which often required doping with Li^+ and led to leaching. Unfortunately, the catalyst exhibited a decrease in pore size when undergoing reactivation procedures, which resulted in a decrease in activity upon each reuse.

Bartley and Chunli Xu focused on testing MgO in several other reactions including MPV reduction.[56] In this report, they examined how transfer hydrogenation occurred between benzaldehyde and a variety of different alcohols such as 1-butanol, 2-butanol, 2-methyl-1-propanol, and 2-methyl-2-propanol. It was determined that, especially with the higher surface MgO samples, they were highly effective catalysts for this reaction. For the catalyst to be highly effective for the MPV reaction it needed to include no left over $MgCO_3$ but also retain a high surface area. The optimum catalyst was acquired from calcination at 450 °C. It was thought that the rate determining step of the reaction was the adsorption of the alcohol onto the basic site. This proceeds to dissociate into an alkoxide which then undergoes a hydride transfer to the carbonyl group. In this reaction, when using 2-methyl-2-propanol a very low conversion is observed. The authors proposed that this was due to hydrogen being required for an intermediate 6-member ring state. These factors combined with its high catalytic effectiveness, allows MgO to represent a very real alternative to the more difficult to handle and less environmentally friendly aqueous bases such as aluminium isopropoxide, which is traditionally used as a catalyst for MPV reduction.[81]

Zhang et al.[61] investigated MPV reduction of benzaldehyde with ethanol. Catalyst characteristics were very important. The conversion decreased from 90 % to 57 % over the calcination temperature range (400 °C – 1000 °C) as the catalyst underwent crystal plane changes. Selectivity to benzyl alcohol was determined to decrease until 700 °C then increasing to almost a 100 % at 1000 °C. The opposite trend was seen with cinnamaldehyde which increased to 700 °C and then dropped to less than 10 %, as the calcination temperature approached 1000 ˚C.

Overall, there is a huge variety of both preparation procedures for the synthesis of MgO and applications for its use in heterogenous catalysis. Basicity and other characteristics such as its surface area, porosity, crystallite structure and nanoscale morphology have been identified to be important factors for catalyst performance. Certain reactions may prevail with better selectivity if the catalyst exhibits specific distribution and density of different strength basic sites on its surface. Other factors such as pore density and size could lead to more directed reactions. Understanding these characteristics and accurately identifying are vital for improving catalyst development.

1.6 Characterization of MgO basicity

Determining the basicity of MgO is critical for understanding its performance as a catalyst. To further understand how such materials could be more efficiently utilised, effective methods for the characterisation of the surface basic sites are required. Lewis-basicity would commonly be analysed using acidic probe molecules such as CO_2.

1.6.1 Types of sites

MgO sites have previously been described by Chizallet et al.[82] MgO (100) is the most common, stable and characterised exposed MgO plane. It is unlikely to present a perfect flat surface, resulting in the exposure of a high degree of different types of Mg^{2+} - O^{2-} depending where they are present on the morphology of the surface. On an ideal MgO (100) surface, the terrace situated Mg and O atoms are five coordinated, corner sites are 4 coordinated and edge sites are 3 atom coordinated.[53] Mg^{2+}-O^{2-} pairs on a (100) surface can exhibit a variety of coordination types, lower coordinated sites (typically donated $_{LC}$) exist on a corner, edge, or terrace, this leads them being (respectively) three-, four- and five-fold coordinated. Higher coordinated sites will however exist in the bulk of the material.

Hydroxyl groups can form on low coordinate O^{2-} basic sites and are known to promote basic reactions.[69,83] The hydroxylated site (Mg-OH) of MgO can even achieve higher activity than oxide ions in certain situations.[84] Several theoretical and experimental studies have shown that H_2O can undergo dissociative adsorption to the MgO surface.[85–91] Hydroxyl groups form on the surface of MgO in the presence of H_2O.

1.6.2 Instrumentation and techniques for the analysis of basic sites

There is a variety of instrumentation and methods which can be used to probe the basic site strength and distribution in MgO materials.

1) Diffuse reflectance infrared Fourier transform spectroscopy (DRIFTS). This technique is based on IR spectroscopy and allows for the semi-quantitative analysis of adsorbed molecules on the surface of a powdered sample. DRIFTS can be used to detect how a probe molecule adsorbs, making it an ideal technique to study acid and base sites on metal oxides using suitable probe molecules. Through analysing the energy(ies) of vibrations observed when passing a probe molecule over a metal oxide surface, the mode of its adsorption can be deduced. This can in turn be used to determine the type of basic (or acidic) sites which are present. For the purpose of probing basic sites in a sample, analysis using CO_2 as a probe molecule is most suitable. There are three main types of basic site which can exist on MgO. These are all indicative of different carbonate species which can form, from exposing the surface to CO_2. Absorption bands for carbonates on MgO surfaces are located between 1800 cm^{-1} to 1200 cm^{-1}. These values can vary, however, due to preparation procedures and morphological features and a review of literature values for different types of sites is presented in Table 1.

2) Temperature programmed desorption (TPD). TPD can also be used to measure basicity and acidity of solid materials, again using probe molecules.[98] When investigating basicity, CO_2 is typically employed as the probe molecule. For this, CO_2 is passed over a clean surface sample, and then desorbed by increasing temperature. The amount of CO_2 detected as it desorbs allows for basic site quantification, thus, basicity per gram or m^2 of catalyst can be acquired. The temperature the CO_2 desorbs at also allows for determination of the relative strength of a given site. This can be combined with other techniques, such as DRIFTS, which can identify the actual nature of these sites.

3) Microscopy can also be used to investigate the basicity of a sample. This would likely need to be used in conjunction with other techniques to identify morphological patterns that may correspond to changes in quantified basicity. It is predicted that lower coordination and step sites of MgO would exhibit a higher basic strength.[99] Crystallite sizes and exposed facets can be identified by TEM. Montero et al.[100] found that there was a correlation between features such as kinetic energy and crystallite size that predicted the surface base strength of MgO to increase with increasing crystallite size, corresponding to a change of (100) to a stepped (110) face. The faces (110) and (111) were found to be more basic than the (100) face and were obtained via high temperature annealing.

Table 1. Literature values for DRIFTS adsorption bands basic sites and CO_2 species.

Reference	OH Bicarbonate / hydrogen carbonates (cm^{-1})	O^{2-} Monodentate carbonates (cm^{-1})	Mg^{2+}-O^2 Bidentate & tridentate carbonates (cm^{-1})
[53]	1220 asymmetric 1480 asymmetric 1650 asymmetric	1360–1400 symmetric 1510 – 1560 asymmetric	1610 – 1630 symmetric 1320–1340 symmetric
[92]		1370–1590 general area attributed 1440 v_{3high} DFT (110) 1378 v_{3low} DFT (110)	1270 – 1390 general area attributed 1620 – 1710 general area attributed 1680 v_{3high} Drifts 1650-1730 v_{3high} DFT 1125-1200 v_{3low} DFT 1651 v_{3high} Drifts (tridentate 100) 1304 v_{3low} Drifts (tridentate 100) 1600-1650 v_{3high} DFT (tridentate 100) 1280-1300 v_{3low} DFT (tridentate 100) 1516 v_{3high} Drifts (tridentate 100) 1347 v_{3low} Drifts (tridentate 100) 1560 v_{3high} DFT (tridentate 100) 1330 v_{3low} DFT (tridentate 100)
[93]	1655–1658 v_2 1405–1419 v3 1220–1223 v4	1510–1550 v_{3high} 1390–1410 v_{3low} 1035–1050 v_1	
[94]	1480 v_3 1250 v_4	1590,1510 v_{3high} 1415 v_{3low}	1385,1335 v_{3low}
[58]	1650 v_2 1510,1408 v3 1220 v4		
[95]		1550 v_{3high} 1410 v_{3low} 1050 v_1	
[96]		1520 v_{3high} 1370 v_{3low} 1060 v_1	1670, 1630 v_{3high} 1270 v_1
[97]		1550 v_{3high} 1410 v_{3low} 1050 v_1	1670,1630 v_{3high} 1315,1280 v_{3low} 1000,850 v_1 950,830 v_1

4) Solid state nuclear magnetic resonance (SSNMR). SSNMR is another spectroscopic technique which can be used for the characterisation of atomic structure of undissolved solid materials, such as powders and single crystals.[101] *In-situ* SSNMR is a well-established tool and can be a useful technique in the characterisation of heterogeneous catalysts.[102] It can be combined with other

techniques such as gas chromatography (GC).[103] *In-situ* SSNMR and can be used for the determination of the structure of adsorbed reactants, in this way it can provide significant insight into the mechanism of reaction that proceeds over a catalysts surface, allowing for identification of intermediates products that might not otherwise be isolated on collection. Using probe molecules there adducts on the sample surface can be detected and quantified by analysing the intensity and chemical shift. Depending on equipment availability, cost restrictions and the type of catalytic system being investigated *in-situ* solid state NMR can be conducted in a bath reactor, which is cheaper and simpler or a continuous flow reactor.

5) X-ray photoelectron spectroscopy (XPS) is a technique which can determine the elements in or on the surface of a sample, the chemical state and electronic structure. XPS can be used to detect the different electron states of MgO, such as the 1s, 2p and O 1s in detail.[104] The changes of observed binding energies can be used to detect different components on the surface and in the case of hydrated carbonates on MgO the different forms.[105] XPS's ability to detect regions related to carbonate and hydrated species could be used to help identify basic sites with the *in-situ* addition of probe molecules.

6) X-ray absorption spectroscopy (XAS) is a technique for analysing the atomic energy structure of a sample. Extended X-ray absorption fine structure (EXAFS) reveals details about interatomic distances, the coordination number of neighbouring species and information about the samples lattice dynamics. X-ray absorption near edge structure allows for investigation of the valence state, energy bandwidth and bond angles.[106] XAS has various uses in the study of heterogeneous catalysis.[107] The combination of data such as coordination numbers and use of probe molecules could be useful for evaluating different active sites on a metal oxide surface.

1.6.3 Limitations of single probe molecule studies

Techniques using probe molecules are well developed.[102,108] Techniques such as CO_2 TPD and CO_2 DRIFTS rely on the use of probe molecules to investigate Lewis basic sites in isolation. However, this may not account for the interaction of acid base site pairs on substrates or Brønsted basicity on MgO. Fu *et al.*[109] developed a way to simultaneously analyse the acid and basic sites of sample. This uses probe molecules to attach to the solid surface, which are subsequently detected *via* NMR. ^{13}C and ^{31}P MAS NMR using $^{13}CO_2$ and trimethylphosphine (TMP) were used as the investigative probe molecules, respectively. They found that these influenced each other and gave varied and perhaps more insightful results to the nature of the sites on the samples surface. It was found that three main basic sites existed on metal oxides, which were termed strong, medium, and weak. These could be identified by their chemical shift. The strong sites were represented by the CO_2 forming

unidentate species on low coordinated O^-. TMP on the adjacent metal cation can donate electrons, this results in a stronger base strength on the oxygen site and a stronger acidity on the metal. With the medium strength sites CO_2 formed a bidentate carbonate species on $M^+ - O^-$ pairs. With this, again, the TMP donates electrons resulting in a stronger base site, but due to the bidentate carbonate species interacting with a M^+, the overall acidic site density detected decreases. It was reported that CO_2 adsorbing on weak basic sites would produce bidentate carbonates with slightly lower chemical shifts. These were produced *via* hydroxyls forming from the adsorbed CO_2, the OH proton then interacts with the TMP phosphorous atom, resulting in a decrease in electron density and thus basic strength for the O site.

This experiment raises the important point that acidic sites may co-exist with their conjugate basic site on basic catalysts and the when the reactants are adsorbed on basic or acidic sites, this could change the nature of the conjugate site. This means that co-adoptive techniques, may provide a more accurate picture of basic sites on an oxide surface, compared to sole adsorption techniques alone.

Focusing predominantly on Lewis type interactions may understate Brønsted interactions, under actual reaction conditions on a basic oxide such as MgO. As discussed previously, a common first step in a catalysed reaction over MgO is the deprotonation of an organic molecule (RH). This is attributed to Brønsted basicity, ergo, the ability of the catalyst to protonate its surface sites.[110] As protic molecules dissociate favourably, this makes them useful for measuring the thermodynamic Brønsted basicity on a basic surface.[82,111]

$$R\text{-}H + M^{n+}\text{-}O^{2-} \rightleftharpoons \overset{\displaystyle [R^-] \;\; [H^+]}{\underset{\displaystyle M^{n+}\text{-}O^{2-}}{\big| \qquad \big|}} \longrightarrow Products$$
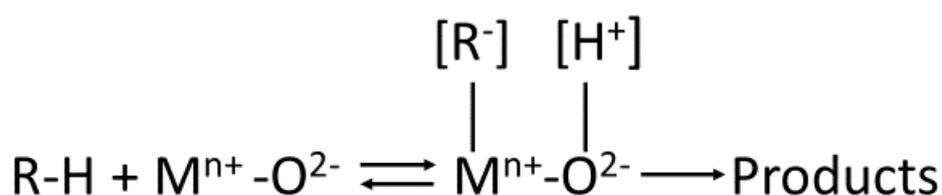
Figure 1. Acid base pair on a metal oxide

Figure 1 would require a Lewis acid and base site: O^{2-} to deprotonate the organic molecule (RH) and the M^{n+} to stabilise an anionic intermediate (R-). The degree of this stabilisation will influence the absorption time and thus, influence which products are formed.[84] This shows that the basic sites do not act alone and the acid-base pair should be considered.

Brønsted basicity of the MgO surface was investigated using the deprotonation of methanol and propyne and the conversion of 2-methyl -but-3-yn-2-ol (MBOH). Hydroxyl surface groups are known to be basic and can catalyse basic reactions.[69,83] There has also been cases where they have been

observed to exhibit a higher activity than clean MgO O^{2-} ions.[84] This was attributed to a v_{OH} infrared stretching band in the narrow high frequency region. The experimenters tried to identify these sites using DFT calculations to model low coordination ion irregularities on MgO surfaces. *(mono- and di-atomic steps for 4C ions, corners, kinks and divacancies for 3C ions).* All but the kinks and divacancies with isolated OH groups were found to be able to dissociate water. When tested for the conversion of MBOH the higher degree of non-hydroxylated oxide ions, the higher the conversion became. The thermodynamic Brønsted basicity was the key factor here. It was reported that the conversion of the MBOH on a clean MgO surface correlated with the deprotonation ability the same surface had with methanol and propyne.[112] Deprotonation of propyne was evidenced by the appearance of C≡C stretch on oxide ions. When the heterolytic dissociation of water occurred over MgO, there were two main species of OH surface groups expected. OH groups can be generated by the protonation of the surface oxide ions. This results in the hydroxyl group being multi or single coordinated to Mg^{2+} cations.

This type of underlying co-ordination to the surface ions should result in different spectroscopic and acid-basic properties. The hydrogen bonding that can form between different hydroxyl surface groups can also impose a significant effect. The clean surface was found to be more active for the deprotonation of methanol than hydroxylated surfaces activated at 673 K. This led to the conclusion that the thermodynamic Bronsted basicity of OH groups at 673 K were lower than the O^{2-} low coordinated ions. However, at higher activated temperatures of up to 973 K, this was reversed with the hydroxylated sample exhibiting a higher activity. Where OH groups measured at 3740 cm^{-1} correlated with MBOH conversion. However, it seemed only the ones measured at that wavenumber were involved as overall, OH concentration did not correlate.

DFT modelling provided several interesting conclusions. The first saw that OH groups were not always formed by low coordinate Mg^{2+}, because whenever possible, bridging between several Mg^{2+} cations would give a more stable configuration. Also, isolated OH group formation is limited to only specific locations such as on kinks and divacancies only. The degree of hydrogen bonding seems to be one of the most important factors. H donor OH groups exhibit low stretching as they are located on corners and steps. H Bond acceptors on the other hand exhibit high frequencies which correspond to single coordinated OH groups near a corner or di-coordinated bridging, through the edge and underlying plane. O_{3c}-H coordinated species form on kinks and divacancies through multiple bridging. IR band data showed that O_{3c}-H and O_{4c}-H groups on kinks and divacancies, respectively, are not responsible for basic activity. On the other hand, the mono and di-coordinated OH groups were extremely active.

These conclusions ultimately highlight how an integrated approach involving multiple techniques is important to understanding the different types of basic sites present on a sample surface and how they would actually interact with reaction substrates *in-situ.* As presented in previous sections, there is a developed understanding of MgO preparation, characteristics and use in a variety of reaction systems. MgO has many applications and can be tailored for specific purposes. With this in mind, MgO may also have potential as a catalyst in the areas associated with the upgrading of platform chemicals and sustainable chemistry.

1.7 Trans-esterification of triglycerides to biodiesel and sustainable chemistry

In recent decades, there has been a considerable shift towards research into sustainable chemistry. This has resulted in a drive for research into sustainable methods for the production of liquid fuels and products, which are currently derived from petrochemical feedstocks.[17,113] The use of renewable or carbon neutral feedstocks has therefore become an attractive prospect for researchers and much emphasis has been placed on reducing dependency on fossil fuel derived feedstocks.

Consequentially, the biodiesel industry has seen growth in recent years. While the rising sale and demand of electric road vehicles is expected to somewhat hinder biodiesel demand, there is an expected compound annual growth rate of 8.4 % in the marine industry and a 4.6 % for power generation between 2017-2025.[114]

The majority of biodiesel produced commercially occurs through the production of fatty acid methyl esters (FAME). Shown in Figure 2 this process involves the transesterification of triglycerides, where methanol and a base, such as potassium hydroxide, are employed as a reagent and catalyst, respectively.[115,116] Biodiesel is non-toxic and in-theory, an environmentally benign energy source. Biodiesel is sourced mainly from vegetable oil; however, animal fat waste is also used.[117] Hydrolysis of the triglycerides results in the formation of a glycerol molecule; *ca.* 1 ton of glycerol is produced for every ten tons of biodiesel.[117,118] Glycerol is therefore a major by-product of the biodiesel industry, which has ultimately resulted in an oversupply of glycerol. Due to the current limited uses for this extra glycerol, the majority of by-product crude glycerol is sent to water treatment for digestion or burnt for energy.[119,120] Therefore, effective methods for the conversion of crude glycerol to high-value chemicals is an important and fluid area of research.
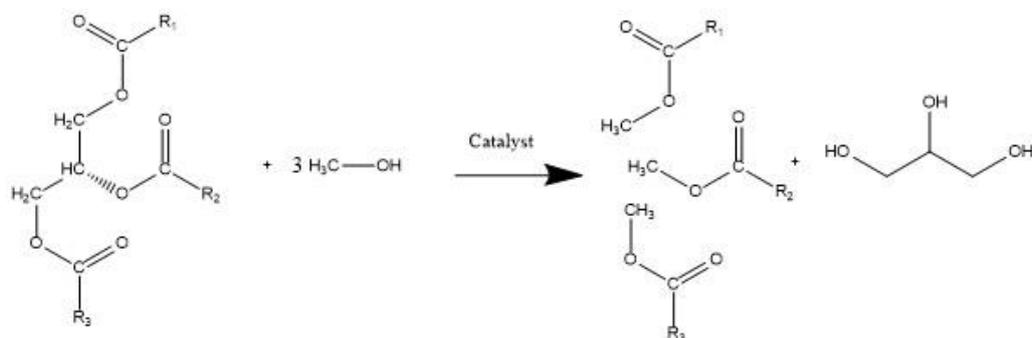
Figure 2. Transesterification of triglycerides to fatty acid methyl esters and glycerol

1.7.1 Crude glycerol (composition and considerations)

A barrier to the utilisation of glycerol as a platform chemical is that, in its crude form, it can have a purity as low as 10 %.[117] As feedstock and refining processes vary, the grade and impurities present within the glycerol can differ significantly. Crude glycerol is reported to possess many impurities and can exhibit a brown/green murky appearance. These impurities can include: the transesterification catalyst, such as KOH, NaCl, water, oligomers, biodiesel, methanol, other alcohols, salts, polymers of glycerol, di-glycerides, soap, ash, free fatty acids (FFA), nitrogen containing compounds and various metals. [121–124] The purity can vary immensely, with glycerol sourced from the soap industry often surpassing a purity of 80 %. In the contrary, glycerol from the biodiesel industry can vary between 14 % - 87 %, and from the triglyceride industry averaging at 42 %. The source oil can also effect the composition, shown in Table 2.[124] Due to the abundance and its impurities, it is therefore unsurprising that refined crude glycerol only possessed a value of between *ca* 200 – 250 € per tonne over the past year.[125] This has however increased substantially to almost 400 euros a tonne around (March 2020), due to a significant decrease in biodiesel production in europe.[125]

Individual studies of biodiesel sourced crude glycerol also reveal a large variation. In a study of 11 samples from 7 different biodiesel manufacturers, it was found that the glycerol content varied from 38 % to 96 %. Significant contaminants were observed with up to 29 % ash and 14 % methanol content.[126] Hu *et al.* analysed 5 samples procured from the same producer.[127] It was found that 85 % of the mass of crude glycerol was methanol FAMEs, soap and water and less than 15 % was glycerol free fatty acids and ash. The glycerol concentration varied from 23 % to 63 %. The impure nature of crude glycerol and the inconsistency between batches, raises a significant problem for its effective utilisation and thus commercial usage. Purification of said crude glycerol is desired, but this can present additional costs.

Table 2. Composition of crude glycerol reproduced from data collated by Kumar, L. R.; Yellapu, S. K.; Tyagi, R. D.; Zhang, X. A Review on Variation in Crude Glycerol Composition, Bio-Valorization of Crude and Purified Glycerol as Carbon Source for Lipid Production. Bioresource Technology. 2019. https://doi.org/10.1016/j.biortech.2019.122155.

Feedstock	IdaGold	PacGold	Rapeseed	Canola	Soybean	Crambe	Waste cooking oil
Ca (ppm)	11.7	23	24	19.7	11	163.3	–
K (ppm)	–	–	–	–	–	216.7	–
Mg (ppm)	3.9	6.6	4	5.4	6.8	126.7	0.4
P (ppm)	25.3	48	65	58.7	53	136.7	12
S (ppm)	21	16	21	14	–	128	19
Carbon (% wt)	24	24.3	25.3	26.3	26	24	37.7
Fat (% wt)	2.03	1.11	9.74	13.1	7.98	8.08	60.1
Na (% wt)	1.17	1.23	1.06	1.07	1.2	1.1	1.4
Ash (% wt)	2.8	1.9	0.7	0.65	2.73	0.25	5.5

In a review by Ardi et al.[128] methods for the purification of crude glycerol were discussed and three main steps to the process were revealed. The degree of purification required depends on usage, generally for industrial processes requires purities $\geq 96\%$ and pharmaceuticals would require $\geq 99.5\%$. The first step in the glycerol purification process requires neutralisation of the substrate. This is done using an acid catalyst such as H_2SO_4, which can convert the soap to free fatty acids which rise to the top for removal. The acid can react with a residual base catalyst to produce salts which will form on the bottom. Using H_2SO_4 to obtain pH of 1 allows for a glycerol yield of 93%.[129] Methanol which was added during the biodiesel process now needs to be recovered for reuse due to its toxicity. Methanol is removed with water by vacuum evaporation to give an average purity of glycerol of around 85%. Finally, a last purification and refining stage is required. Vacuum distillation is commonly used to purify the remaining glycerol. This is conducted under vacuum to avoid glycerol polymerisation and degradation, which can occur at elevated temperatures.

Purified glycerol does however have a variety of applications in the food, tobacco and pharmaceuticals industries.[118,130,131] While there is applications for high value purified glycerol, the purification process can be costly and the infrastructure is not always available; especially for smaller biodiesel producers. The supply of crude glycerol significantly outstrips demand for its pure form for conventional uses. The development of processes for the large scale consumption of glycerol has been severely limited due to the price of its purification.[119,121,132] Hence, there is a drive

to develop processes and infrastructure that can utilise crude glycerol directly as a feedstock with possible significant cost and energy savings.

A significant review, published in 2016, investigated the difference of crude and pure glycerol utilisation in a variety of processes.[133] Overall, the results with crude glycerol samples were inferior to that achieved with pure glycerol. This is due to the contaminants which can lead to reactor fouling and the poisoning of catalyst active sites, which in turn leads to a reduction in yields.[122] However due to the variation between crude glycerol sources, it's hard to make comparisons between processes. A selection for comparison is presented in Table 3. As can be seen in some cases, where the crude glycerol is relatively pure it compares well to the pure glycerol experiment.

However, most research into glycerol valorisation utilises pure glycerol. This allows for the true nature of the reactions and effect of catalysts to be analysed and restricts variation based on glycerol batch. While the goal of most valorisation methods is to convert crude glycerol to useful products, the heterogeneity of the sources would make comparable research difficult. For catalyst caused effects to be identified accurately, purified glycerol is used to avoid the complications of crude variation. This allows for differences observed to be pinned purely to conditions and the catalyst and not the specific batch of glycerol. This also allows for more accurate comparisons with fellow researchers. It is hoped that the insight gained from pure glycerol experiments and any effective catalysts for transformations would still be relatively effective when exposed to less pure product streams. Therefore, in this thesis the catalytic transformations of glycerol discussed use purified glycerol unless otherwise stated.

Table 3. A series of reactions using crude and pure glycerol as feedstock are compared. C = conversion, S = selectivity, Y = yield. Reproduced from data collated in P. S. Kong, M. K. Aroua and W. M. A. W. Daud, Renew. Sustain. Energy Rev., 2016, 63, 533–555.[133]

Product	Route	Crude glycerol contents	Crude glycerol	Pure glycerol
H_2	Steam reforming	Glycerol 70–90 % Methanol & H_2O ≤ 15 % Glycerol 70–90 % Methanol & H2O ≤ 15 % Salt ≤ 5% Polyglycerol 5 %	C = 100 %	C = 97 %
H_2	Supercritical water reform	Glycerol 42.3 % Methanol 20.8 % FAMEs 33.1 % Glycerol 71.12 % Methanol 2.6 % MONG 25.9 % Ash 2.6% H_2O 0.01%	18.9 % mol-H_2/mol-C Tar 21 %	24.1 % mol-H_2/mol-C Tar = 0 %
H_2	Aqueous phase reforming	Glycerol 68.5 % Methanol 15.5 % FAEs 0.7 % H_2O 1.5 % Soap 16.2 %	C = 46 % S = 1 %	C= 100 % S = 64 %
1,2 propanediol	Hydrogenolysis (dehydroxylation of glycerol) CG;PG;	Glycerol 80 wt % Methanol ≤ 1 % MONG ≤ 20 % Ash ≤ 0.1 %	C= 71 % S = 56 %	C = 99 % S= 87%
Acrolein	Dehydration	Glycerol 92 % Methanol 4 % Soap 3.3 %	Y = 80 mol %	Y= 82.3 mol %
glyceric acid (GA),	oxidation	Glycerol 95.5 % Methanol 0.131 % H_2O 0.001 % Soap 3.23 % FAMEs 0.029 % FFAs 0.1 % CH_3ONa 0.056 %	C = 35 % S = 22.2 %	C= 35 % S = 62.9 %
Glycerol tertiary butyl ether (GTBE)	etherication	Methanol 3.46 % FAEs 2.8 % H_2O 0.053 % K 2.33 % Na 0.012 %	C = 6 %	C = 52 %
Dioxolane and dioxane	Condensation	Glycerol 87 wt %	Y = </ 1 %	Y = 42 %
Polyesters	Poly condensation	Glycerol 15.4 % Soap 22.4 % FFA 2.1 % FAME 30.9 % Methanol 15.5 % Water 5.1 % Ash 4.2 %	Y = 53 %	Y = 84.4 %

1.8 Valorisation of glycerol to other platform chemicals

Due to the abundance of crude glycerol, valorisation to important value added platform chemicals has become a common goal.[134] There are many possible processes for the conversion of glycerol to value added products including: oxidation, dehydration, acetylation, esterification, reforming, reduction, etherication, ammoxidation and acetalization.[130] Some of the primary areas of focus in

recent years has been the dehydration of glycerol over acid catalysts,[135] glycerol hydrogenolysis to 1,2 and 1,3 propanediol,[136] glycerol halogenation to epichlorhydrin and the liquid phase aqueous oxidation of glycerol oxidation to a variety of products such as dihydroxyacetone, glyceric acid and tartronic acid.[137] Further brief discussion on some of these processes is presented below, along with more extensive discussion relating to research published on routes from glycerol to methanol.

1.8.1 Reforming

Reforming of glycerol (Figure 3) is an important example and allows for the small-scale production of H_2 from a renewable source with a low CO content.[117,119,120,123] While mostly done in the gas phase, reactions in the aqueous phase have also been explored and would be highly applicable for use in fuel cells. In this process, glycerol has been reacted with water to form CO_2 and H_2 over a Pt-Re catalyst in a one step process at relatively low temperatures of 200 °C to 250 °C.[138]

$$HO \diagup \diagdown ^{OH} \diagdown OH \ + \ 3\,H_2O \ \longrightarrow \ 7H_2 \ + \ 3CO_2$$
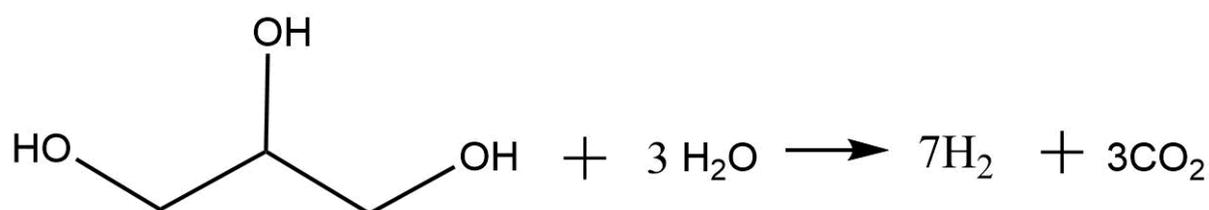
Figure 3. Glycerol reforming overall reaction.[139]

Detailed investigation on the steam reforming of glycerol is covered by a recent review.[120] Steam reforming of glycerol is a source for, theoretically, carbon neutral bio-hydrogen, which could help meet the global increasing hydrogen demand.[140] The process of hydrogen production currently is 95 % fossil fuel derived.[141] Nickel based catalysts are thought to be the most promising for the steam reforming process, especially under optimal conditions (between 650 – 900 °C and atmospheric pressure). Catalysts used are typically noble or transition metals co-precipitated or impregnated on metal oxide supports. In this process, glycerol is converted to synthesis gas which has a high hydrogen content. High temperatures are required to reduce the chances of methanisation. Under high temperatures glycerol can degrade to CO and hydrogen but can also react with water to give CO_2 and hydrogen. A water gas shift reaction can also occur, converting the CO formed to CO_2 and further H_2 molecules.[119,120]

1.8.2 Reduction

1,2- and 1,3-propanediols are important value-added chemicals which can be made from glycerol through catalytic hydrogenolysis. 1,2 propanediol is used in a variety of products such as paint, polyester resins, cosmetics, feed, and detergents. It is normally sourced from the fossil fuel originating propylene oxide. Glycerol can be dehydrated to hydroxyacetone and undergo a

sequential hydrogenation to 1,2 propanediol over variety of catalysts.[142,143] A Cr_2O_3 material at 200 °C, is currently used in industry.[143]

1,3 propanediol is used as the monomer in polymethylene terephthalate (PTT) or polypropylene terephthalate (PTT).[144] Its production value is growing at a rate of 10.4 % a year, making it a key area for research.[145] It can be produced *via* a selective reduction of glycerol with H_2 over a metal catalyst. These are often bifunctional, usually involving a noble metal like Ir, Rh or Pt combined with a Brønsted acid component, such as tungsten, heteropolyacid or rhenium.[145,146] However these routes from glycerol to 1,3-propanediol need more research to be economically viable. High selectivity to 1,3 propanediol is a significant challenge and more complex to achieve than 1,2-propanediol. The catalyst needs to remove specifically only the sterically hindered secondary alcohol group of glycerol.[147,148] This means that any changes in catalyst structure can result in loss of selectivity.

1.8.3 Formation of acrolein.

Another common target molecule for the conversion of glycerol is acrolein, which can be achieved *via* the catalytic dehydration of the molecule.[149] Several reviews have been produced on the subject and a wide variety of usually acidic catalysts are used.[150–152] A variety of conditions can be used both in the gas and liquid phase at varying temperature and pressure. Examples of previous work on acrolein production includes the work carried out by Haider *et al.*[153,154] The catalysts used here included zirconium doped mesoporous silica catalysts, zirconia and ceria on alumina supports, and silico-tungstic acid. WO_3 on Al_2O_3 catalysts were investigated by Aihara *et al.*[155] under gas phase conditions of 315 °C, at ambient pressure. Selectivity was about 80 % regardless of loading but the 20 wt.% WO_3 loaded achieved the highest yields of between 75-80 %. Heteropoly acid based catalysts, zeolites, mixed metal oxides, phosphates and pyrophosphates have been used. [150–152] Basic catalysts have seen limited used in this reaction. CeO_2, La_2O_3 and MgO have been investigated, but they only exhibited a low selectivity to acrolein. The range of products was wide with over 60 mol % remaining unidentified. [156]

As described, there is a variety of uses for glycerol being developed, however none, as yet, have succeeded in depleting the crude glycerol reserves. The complex chemistry and wide range of products glycerol can undergo leaves it opens to further study as a platform chemical. There have been several recent developments in the production of useful alcohols from glycerol. Methanol being a primary one which is the focus of this thesis.

1.9 Green methanol from glycerol

1.9.1 Previous work on MgO and CeO$_2$ valorisation of gas phase glycerol to methanol

In 2015 Haider *et al.*[157] discovered that glycerol, when passed over bulk oxide catalysts such as MgO,[158] and CeO$_2$[159], can be transformed into methanol with considerable selectivity. Theoretically, this could have multiple economic and environmental benefits if achieved with high efficiency. For instance, given that methanol is used as a reagent in the FAME process, it could be envisaged that commercial biodiesel plants develop infrastructure to recycle the waste glycerol they produce, to use in further processing. Currently, methanol is derived from fossil fuels and the process cannot therefore be considered fully sustainable. Another application of methanol is that it can be converted into formaldehyde, which can subsequently be used in the production of plastics.[160]

The methanol used in the bio-diesel process often represents a large quantity of the industries overheads. The molar ratio of methanol to the oil used in the transesterification reaction is a significant parameter, affecting the efficiency of conversion, yield and cost of the resultant biodiesel.[74,161] The stoichiometric ratio is typically 3:1 for the reaction.[162] However due to the reversibility of the reaction and low miscibility of the reactants, significantly higher molar ratios are required.[161,163] Using a CaO catalyst at 65 °C, an optimum ratio of 9:1 methanol to oil was used. [164,165] Using an approximate methanol price of € 260 metric ton,[166] this would result in the methanol costs equating to *ca.* € 85 of investment per 1 ton of biodiesel produced. The 'green' methanol produced from such a process would therefore be useful for increasing the process sustainability and reduce the current economic barriers which exist between the biodiesel industry and conventional energy production.

The valorisation of glycerol to methanol in the vapour phase over MgO and CeO$_2$ has been the feature of several previous works. The aforementioned research article by Haider *et al.*[157] provided the foundational platform in this area, which demonstrated that methanol could be produced as a major product at low glycerol feeds using this methodology. Operating this process at higher glycerol feeds however (up to 50 wt.%), led to reduced methanol space time yields (STYs) and reduced carbon mass balances (CMB). Since this seminal work, significant improvements in the understanding of the reaction mechanism and individual pathways has been developed.[158,159,167] A more complete reaction scheme was devised and a variety of catalyst-free and reactions over MgO were performed under various conditions by Smith *et al.*[159] It was identified that the CMB of the reactions, operating at 50 wt.% glycerol feeds, was typically around 75 %. Of this missing 25 % of carbon, up to 10 % was attributed to coke and *ca.* 15 % attributed to the formation of high molecular weight products. The formation of the latter was proposed to be attributed to various

bimolecular condensation reactions.[159] The methanol space time yields were found to be highest with MgO with increases in temperature. A reaction temperature of 400 °C gave 205 (g h^{-1} kg$_{cat}$$^{-1}$) with 50 wt.% glycerol and 0.5 g MgO. A higher space time yield was observed 255 (g h^{-1} kg$_{cat}$$^{-1}$) with lower catalyst mass and glycerol concentration of 0.1 g and 10 wt.% respectively.

Investigation using crude glycerol was performed in the initial paper found that the catalysts were relatively tolerant to the impurities within the batch of crude glycerol used. This crude glycerol was provided by Biodiesel Amsterdam BV and was treated before testing with decantation of the aqueous phase and a simple charcoal filtration. The conversion, methanol selectivity and methanol yield were slightly lower compared to pure glycerol and this difference increased with reaction time and feed concentration. However, the difference was minimal which was promising for the direct use of crude glycerol.

Significant further work was carried out focusing on the use of CeO_2 as a catalyst for the valorisation of glycerol by Smith *et al.*[159] Investigations were carried out with 50 wt.% over a range of temperatures. It was found that higher temperatures produced a higher space time yield 15 – 145 methanol g h^{-1} kg$_{cat}$$^{-1}$ from 320 °C - 440 °C. Temperature also altered the product distribution, leading to more acetaldehyde, CO_2, coke, and undetectable products. Using different surface area catalysts but with the same normalised total bed surface area, it was found that there was no relationship between defect site quantity and catalyst performance. This led to the hypothesis that the sample morphology drove the reaction.

Synthesis and testing of well-defined CeO_2 cubic, rodlike and polyhedral morphologies for glycerol conversion was subsequently carried out.[168] There was a significant difference between the different morphological samples. The cubic structure sample was found to be relatively poorly active due to high acidity, low surface area and possible tendency to be hydroxylated. At 400 °C, the polyhedral sample was far more active resulting in a space time yield more than four times that of the cubic 47 to 201 methanol g h^{-1} kg$_{cat}$$^{-1}$. When comparable conversions were achieved over the samples at 320 °C, it was found that they exhibited different product distributions. The cubic sample only exhibited a low selectivity to hydroxyacetone of 15 % with selectivity of *ca.* 45 % for the rods and polyhedra. This is a major intermediate and this difference of selectivity here indicates the cubes primarily promote a different reaction mechanism than the other catalysts. The cube sample also produced acrolein, a double dehydration product as its primary product. This indicates that the cubic sample catalysed the C2 dehydration of glycerol preferentially to the C1 dehydration.

CeO_2 based catalysts were further explored. Studies conducted doped CeO_2 with Pr and Zr which were made *via* co-precipitation and tested for conversion of glycerol.[169] While Zr had little effect,

the inclusion of Pr resulted in a higher degree of defects, which was found to promote the methanol space time yield per unit of surface area. While the $CePrO_2$ had a reduced surface area, it still exhibited a high selectivity to methanol indicating that the degree of defects directed the reaction through a different pathway.

1.9.2 Other research on glycerol to methanol

There are also several other instances of investigation into the production of bio-derived methanol from glycerol. A two-step process which was proposed, involves the reforming of glycerol within supercritical water to syngas.[170] This was done over a Ni based catalyst with high temperatures and low pressures of glycerol. This syngas can then be converted into methanol over a commercial Cu based methanol synthesis catalyst. This means the gas composition from the reforming process was important for high yields. The authors managed to obtain 60 % carbon yield of methanol from the glycerol.

Glycerol has also been converted to methanol over zeolite-based catalysts. Mohamed *et al.*[171] investigated Ni and Cu loaded HZSM-5 and found that a 5 wt.%. Cu loaded gave the best methanol yield. Ni and Cu/Ni bimetallic catalysts were unsuitable due to carbon coking causing deactivation. However only 6.7 % methanol yield was obtained from fully converted glycerol.

Decomposing glycerol in supercritical water can also yield a significant amount of methanol in solution.[172] Highest yields were obtained at 450 °C and 300 bar. Ethyl-sulfide promotes the reaction rate but had no effect on directing the products. Under the described conditions, approximately 1 mol of methanol per mol of glycerol was obtained, corresponding to 1/3 carbon yield from the converted glycerol.

Maneewuthiworasakul,[173] investigated modified MgO catalysts for the conversion of glycerol to methanol. These experiments saw the use of 10 wt.% glycerol feed, with 0.1 mL min^{-1} flow rates at 330 °C. The catalysts investigated included 3% Ca/MgO, 3 % Co/MgO and 3 % Cu/MgO made by wet impregnation. The impregnated catalysts resulted in enhanced activity compared to MgO. At high conversions of glycerol, 20 % methanol yield was obtained with the 3 % Ca/ MgO sample. The impact of using crude and pure glycerol with Ca/MgO catalysts in vapor phase glycerol transformation were also investigated.[173] It was observed here that the methanol yield was not affected but the conversion was, with higher but less stable conversion of glycerol seen with the crude sample.

Similar investigations have been conducted which focussed on other alcohols such as ethanol as a target molecule. Kostyniuk *et al.*[174] achieved the one step gas phase conversion of glycerol to

ethanol using a caesium promoted ZSM-5. They achieved high conversion and selectivity of 92 carbon mol % after 52 h time-time-online. Zhao *et al.* also investigated the production of ethanol from glycerol. A novel catalyst was prepared in which nano sized Co particles were embedded in ZnO plates. They obtained 58 % ethanol selectivity and a high productivity of 1.45 (g ethanol g cat h^{-1}). Ethanol direct synthesis is promising, with impressive yields obtained.

In all, glycerol to methanol and other alcohols has been gaining traction, with several papers reporting promising results. Direct one-step transformations, however, still have a lot of room for improvement. Product selectivity and yield will need to increase and there is a large scope for investigation with different catalysts and preparations. Significant problems that need to be overcome is the use of low partial pressures and maintaining a high carbon balance.

1.10 Reaction mechanism for the MgO basic catalysed conversion of gas phase glycerol

Understanding the reaction mechanism is critical for improving catalyst preparation and reaction parameters. Extensive work has been conducted to understand the reaction scheme for the glycerol to methanol reaction.[157–159,167] The scheme in Figure 4 shows the initial one proposed by Haider *et al*.[157] This was subsequently updated by Smith *et al.*[158], to account for the greater complexity in the product distribution which arose from the use of higher concentrations of feedstock. However, it is important to note that this is still somewhat of a simplification, with many unknown products produced experimentally which are not accounted for here. It is however useful for trying to understand the primary reaction routes and how catalyst and conditions can influence product distribution.

The scheme shows that there are three main routes for the conversion of glycerol, two can lead to methanol and a third route to acrolein. These branch away for a variety of side products. Previous reactions starting from methanol, ethanol, 1 and 2 propanol, acetone and acrolein led to these being concluded to be unreactive and terminal products.[157]
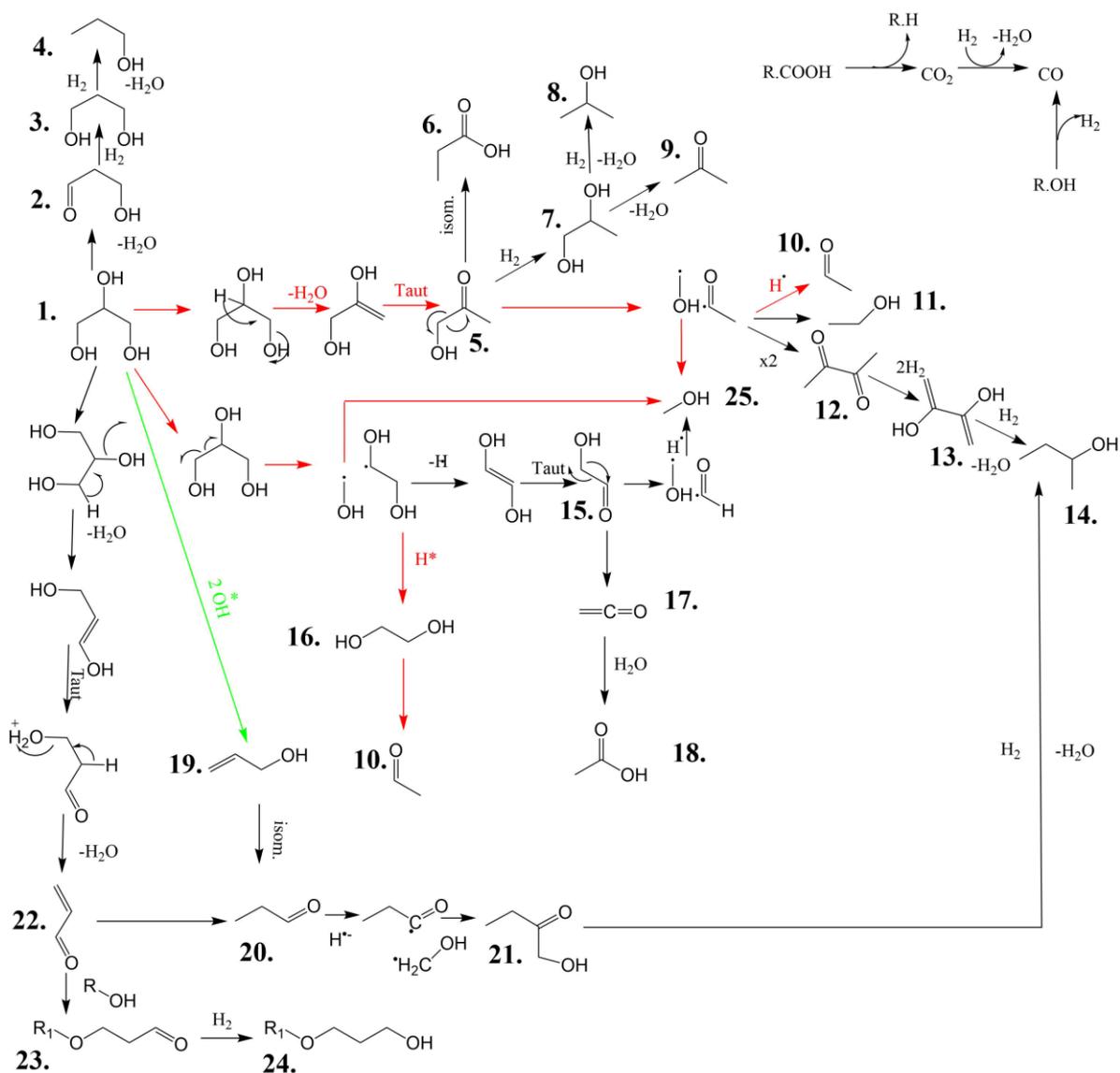
Figure 4. Proposed reaction network for the catalytic transformation of glycerol into a range of different products over MgO. Red arrows correspond to dominant reaction pathways over MgO. The green arrow corresponds to a dominant pathway occurring in the absence of MgO. 1. Glycerol; 2. 3-hydroxypropenal; 3. 1,3-propanediol; 4. 1-propanol; 5. hydroxyacetone; 6. propanoic acid; 7. 1,2-propanediol; 8. 2-propanol; 9. acetone; 10. acetaldehyde; 11. ethanol; 12. 2,3-butanedione; 13. 2,3-butandiol; 14. 2-butanol; 15. glycolaldehyde; 16. ethylene glycol; 17. ethenone; 18. acetic acid; 19. allyl alcohol; 20. 1-propanal; 21. 1-hydroxyl-2-butanone; 22. acrolein; 23. 3-alkoxypropanal; 24. 3-alkoxy propanol; 25. Methanol. Reproduced from work presented in L. R. Smith, P. J. Smith, K. S. Mugford, M. Douthwaite, N. F. Dummer, D. J. Willock, M. Howard, D. W. Knight, S. H. Taylor and G. J. Hutchings, Catal. Sci. Technol., 2019, 19–22.[158]

1.10.1 Acrolein double dehydration C2 pathway

It was proposed that the most likely mechanism by which glycerol would first react is *via* a thermal dehydration and radical fragmentation in a reductive steam atmosphere. Double dehydration leads directly to acrolein through the intermediate (1E)-1-propene-1,3-diol, which can then undergo a tautomeric shift to reuterin, followed by a secondary dehydration to result in acrolein. Acrolein itself can form 1-propanal. In the presence of H• radicals and hydroxy-methyl radicals this could react to form 1-hydroxyl-2-butanaone, dehydration and the addition of hydrogen can then lead to 2-butanol. Upon the addition of R-OH containing molecules, acrolein can proceed through to a 3-alkoxypropanal containing compound, which under reducing conditions, results in the formation of a 3-alkoxy propanol derivative.

1.10.2 Hydroxyacetone C1 dehydration pathway

The single dehydration route of glycerol exhibits many possible alternative products. A single dehydration leads to 3 – hydroxy-propenal, which can subsequently be reduced in the presence of H_2 to 1,3 propanediol. This is seen in small amounts. Further dehydration and reduction of 1,3 propanediol forms 1 – propanol as a terminal product. One of the major routes for glycerol involves it undergoing a tautomeric shift as it is initially dehydrated. This results in an enol proceeding to hydroxyacetone. This is a significant route, with this intermediate often exhibiting ≥ 20 % selectivity in most reactions over MgO. Hydroxyacetone is relatively stable over MgO, with high basicity and temperature needed to convert it. When hydroxyacetone reacts, there are several further possible reactions which can occur. The most desirable (to produce methanol), is a radical fragmentation *via* C-C bond cleavage. This yields an acetyl and hydroxymethyl radical precursors to acetaldehyde and methanol, respectively. This radical fragmentation shows similarities to a Norrish type-1 process (Appendix section 6.1).[157,175] On introduction of an hydrogen source to the hydroxymethyl radical, methanol can be obtained. The acetyl radical will also result in acetaldehyde with capture of a proton. Further reduction can yield ethanol. Radical self-reactions can result in two acetyl fragments producing 2,3-butanedione. This itself, can be reduced to 2,3-butanediol in the presence of molecular H_2. A further dehydration reduction would result in 2-butanol.

Propanoic acid is seen from a simple isomerisation of hydroxyacetone and exists in the reactions in relative proportion of it (< 2 % carbon mole selectivity %). Reducing hydroxyacetone with H_2 results in 1,2 propanediol (< 5 %) dehydration of 1,2 propanediol results in either acetone or 2-propanol when reduced. The little acetone that is produced is highly reactive and likely to self-condense.[69]

CO and CO_2 are detected in relatively consistent amounts of under < 3 %. These are sourced from the disintegration of R. COOH moieties for CO_2, which itself can undergo a reverse water gas shift reaction to yield CO.

1.10.3 Ethylene glycol C-C cleavage

The third main pathway for the conversion of glycerol is initiated by C-C bond cleavage. This results in the hydroxy methyl radical precursor (also seen in the hydroxyacetone fragmentation route) and an ethylene glycol radical. Loss of a hydrogen atom from this radical gives enediol and its tautomeric pair; hydroxy-ethanal (glycolaldehyde). This can then undergo a fragmentation, like with hydroxyacetone, to form formaldehyde and methanol radical precursor. This route can give a higher yield of methanol, as two hydroxymethyl precursor molecules are produced, rather the one from the hydroxyacetone pathway. The formaldehyde precursor itself can theoretically be reduced to methanol, but can also convert through ethenone to acetic acid, which is consistently seen in small amounts. Ethylene glycol is observed to be relatively stable intermediate product, likely reduced by H radicals present, further fragmentation of this product gives acetaldehyde, which along with the source from the acetyl radical produced *via* the hydroxyacetone route, results in acetaldehyde as one of the dominant products, existing in selectivity of at least 10 %.

1.10.4 Allyl alcohol formation

The route to allyl alcohol was proposed by Smith *et al.*[158] Allyl alcohol is present in most reactions over MgO in small amounts. In catalyst free empty tube reactions at 400 and 480 °C, it was found to be a major product. A product selectivity of *ca.* 17 % observed gave a yield of 2.5 % alcohol at 11 % conversion at 480 °C. SiC filled tubes resulted in a slightly higher selectivity of allyl alcohol of 35 % at 360 °C and 22 % at 480 °C. This was paired with a decrease with unknowns and both effects were thought to be due to the increased contact with SiC compared to the empty tube, allowing for more substrate and intermediate activation on hot surfaces. It was concluded that the formation of allyl alcohol, as a major product under the MgO free conditions, was indicative that the glycerol reacts *via* a dehydration pathway at either its C1 or C3 position to produce hydroxyacetone. C2 dehydration in the presence of H_2 would result in acrolein.[150] However H_2 is not present in the reaction product stream in substantial quantities. Thus, a new radical mechanism was derived for the formation allyl alcohol. Glycerol dehydroxylates at the C2, followed by the C3 position resulting in allyl alcohol. Due to the lower observed occurrence of allyl alcohol and acrolein over MgO, it is likely that MgO lowers the energy required for the activation of a primary alcohol group. This leads to the formation of hydroxyacetone or ethylene glycol being more favourable than a radical reaction to allyl alcohol.

1.10.5 Condensation reactions over MgO.

It was previously postulated that the loss of carbon mass balance observed in vapor phase glycerol to methanol reactions was likely due to formation of high weight molecular products (HWMP) that go undetected from analysis by GC-FID.[158] Biomolecular condensation reactions are commonly observed over MgO.[39,43,53,59,70,176] Aldol condensation reactions are a common example, a simplified scheme of which is shown in Figure 5. This means that it is not unlikely, that catalysts such as MgO can catalyse these reactions between various intermediates in the product stream.

MgO is known to serve as an efficient heterogenous catalyst for the Knoevenagel reaction under liquid phase conditions.[59] MgO has also been investigated for the vapour phase aldol condensation of acetone to form α, β - unsaturated ketones.[43] The self-condensation of acetone was evidenced to be catalysed by MgO's basic sites. The α, β – unsaturated carbonyl compounds are formed by consecutive aldol and / or Michael addition condensation reactions. These reactions were carried out with a temperature of 300 °C and under 1 atm of pressure. It is anticipated that acetone is formed during the glycerol to methanol reaction, but only trace quantities have been observed. However it may react quickly into other products.[158]
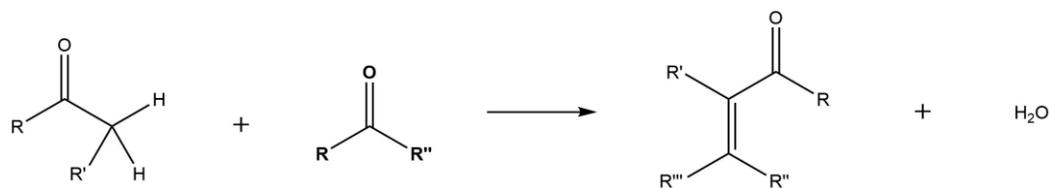
Figure 5. Simple aldol condensation scheme

A major concern is acetaldehyde self-condensation and its reaction with other formyl reaction products. Acetaldehyde is produced in significant amounts over MgO and can form from both the hydroxyacetone and ethylene glycol pathway. Acetaldehyde is known to undergo condensation reactions in the presence of basic catalysts such as MgO. 3-hydroxybutanal is a product, which in turn can undergo a dehydration to crotonaldehyde [176] Crotonaldehyde can undergo further condensation reactions with itself and acetaldehyde to result in a variety of products such as ortho and para tolualdehyde, 2,4,6 octatrienal and 2,4 hexadienal.[177]

Propanal is another aldehyde present in the glycerol over MgO scheme that could contribute to these products, however it is not a dominant product so its influence may be minor. The gas phase aldol condensation of propanal has also been investigated over zeolitic and calcium-based catalysts.[178] Subsequent addition of this monomer could lead to dimers and trimers after formation

of the initial aldol product. It was found that in this type of reaction, a higher degree of basic sites to a slower deactivation of the catalysts.

Another possible source of the loss of carbon in reactions of glycerol over MgO is oligomerisation. Glycerol oligomerisation has been investigated in the presence of alkali metal oxide by Weckhuysen and co-workers.[179,180] However, in this study, the more basic alkali metal oxides exhibited much higher activity and selectivity for glycerol oligomerisation than MgO.

If it can be determined over which catalyst characteristics these condensation products form over, and which intermediates lead preferentially to them it may be possible to direct catalyst design. If these routes can be suppressed through improved catalyst design, higher selectivity to desirable reaction products could be achievable.

1.11 Computational DFT mechanistic studies of the hydrogen transfer to methanol on MgO surface.

It is important for catalyst design purposes, that a solid understanding of the individual reaction steps is achieved. Computational modelling can be used to develop an understanding of specific stages of a reaction that could otherwise, be difficult to isolate experimentally. *Sainna et al.*[167] investigated key mechanistic steps in the formation of methanol from glycerol over MgO. Specifically, a series of computational experiments investigated the source and role of hydrogen atoms in the final step of converting the hydroxymethyl radicals to methanol. In our reaction the homolytic cleavage of the C3 feedstock glycerol leads to an ethylene glycol and hydroxymethyl radical or with glycerol's dehydration product hydroxyacetone, a hydroxymethyl and acetyl radical. Glycolaldehyde cleavage also results in a hydroxy methyl radical. The produced hydroxymethyl radical requires a hydrogen atom to form methanol. This is thought to be abstracted from another species in the product stream, as H_2 is not present in significant quantities under the inert gas conditions of the reaction.

One major conclusion from this work was that a disproportionation mechanism was considered to be a favourable route. The hydroxymethyl radicals would disproportionate between methanol and formaldehyde. Formaldehyde has been identified as present in the reaction mixture but not quantified.

Using DFT calculations, the researchers investigated which of the present sources would give the lowest energy for the required hydrogen transfer. The bond dissociation energies for the X-H cleavage of them was calculated for each species in isolation without influence of a catalyst surface. The disproportionation route was calculated and concluded to be the most favourable and thus,

the dominant route to methanol over a MgO (100) surface. This was investigated due to a very low calculated bond dissociation energy for the hydroxy methyl alcohol group, calculated *via PBE0* as -254 kJ mol^{-1}. This mechanism would proceed *via* the adsorption of two hydroxy methyl radical species, the second which would donate a proton to the surface anion. This results in formaldehyde and a surface methoxy anion, respectively.

This could result in an optimal amount of methanol but would also produce formaldehyde as an undesirable side product and would ultimately limit the possible methanol yield which is attainable from this process. The mechanism for this process was also considered using PBEsol +D3 theory. A dissociated radical on a clean surface followed by a second hydroxymethyl radical both adsorb readily with similar energy. -105 and -107 kJ mol^{-1}, respectively. The H atom is transferred to form a methyl group which immediately takes up another proton from the surface OH group to result in methanol. The formaldehyde left from the transfer is strongly bound to the surface with an interaction distance of 1.553 Å. Sainna *et al.* Showed that this reaction is likely to be highly energetically favourable as it indicated a termination of a radical reaction sequence, rather than further radical products with the alternative routes.

1.12 Thesis aims

A considerable amount of research has been conducted on the conversion of glycerol to value added products, such as: 1,3 propanediol, lactic acid and acrolein. More recently however, a route to produce methanol from glycerol, in a one-step process, has been developed, and could represent a sustainable route to green methanol.[157–159,168,169,173] This methanol could subsequently be used in the production of fatty acid methyl esters, eliminating the need for commercial biodiesel plants to purchase fossil derived methanol. This could reduce the environmental impact and cost associated with biodiesel synthesis, making it a more economically competitive liquid fuel. While moderate yields of methanol can already be achieved, it is accompanied by a variety of other products. Furthermore, a large proportion of these products remain unquantified and are unlikely to be of economic benefit. Ultimately, these issues limit the overall potential of this process, and more research is required to understand whether this process can be realised on a commercial platform.

The following chapter (Chapter 2) will focus on describing the techniques and methods used through the result chapters (Chapters 3 and 4). Chapter 3 focusses on the preparation and characterisation of MgO and its performance for gas phase conversions of glycerol. Chapter 4 investigates the mechanism *via* the conversion of the more stable detected intermediates.

The main aim and purpose of the research presented in this thesis was to further investigate glycerol to methanol process. Several main areas were investigated. A better understanding of how

the catalyst properties could influence reaction pathways was needed. It was considered that changing the catalysts preparation method could help suppress the promotion of undesirable reaction pathways which could result in HWMP. It was also important to consider the importance of water and reaction conditions on product selectivity. In attempt to understand which of the proposed reaction pathways are preferential for the production of methanol the reaction of hydroxyacetone and ethylene glycol were used as substrates. It was also investigated if cofeeding species could help promote methanol formation. It is hoped that through these investigations it will be possible to develop better catalysts for the glycerol valorisation over MgO reaction, allowing for higher yields of desired products. The overall conclusions of the thesis will be presented in the final chapter 5. Further research will be suggested based on the conclusions discovered which could strengthen the presented hypothesis and potentially improve the understanding of the reaction.

1.13 References

(1)   Kaneda, T.; Greenbaum, C.; Haub, C. *World Population Data Sheet 2021*. https://www.prb.org/collections/data-sheets/.

(2)   Smil, V. Population Growth and Nitrogen: An Exploration of a Critical Existential Link. *Popul. Dev. Rev.* **1991**. https://doi.org/10.2307/1973598.

(3)   Smil, V. Detonator of the Population Explosion. *Nature*. 1999. https://doi.org/10.1038/22672.

(4)   Appl, M. The Haber-Bosch Process and the Development of Chemical Engineering. In *A Century of Chemical Engineering*; Plenum Press: New York, 1982; pp 29–54.

(5)   Grennfelt, P.; Engleryd, A.; Forsius, M.; Hov, Ø.; Rodhe, H.; Cowling, E. Acid Rain and Air Pollution: 50 Years of Progress in Environmental Science and Policy. *Ambio* **2020**, *49* (4), 849–864. https://doi.org/10.1007/s13280-019-01244-4.

(6)   Rahman, M. M.; Alam, K.; Velayutham, E. Is Industrial Pollution Detrimental to Public Health? Evidence from the World's Most Industrialised Countries. *BMC Public Health* **2021**, *21* (1), 1175. https://doi.org/10.1186/s12889-021-11217-6.

(7)   Schindler, D. W.; Vallebtyne, J. R. *The Algal Bowl : Overfertilization of the World's Freshwaters and Estuaries.*, 1st ed.; Routledge: London, 2008.

(8)   Chipperfield, M. P.; Hossaini, R.; Montzka, S. A.; Reimann, S.; Sherry, D.; Tegtmeier, S. Renewed and Emerging Concerns over the Production and Emission of Ozone-Depleting Substances. *Nat. Rev. Earth Environ.* **2020**, *1* (5), 251–263. https://doi.org/10.1038/s43017-020-0048-8.

(9)   Anastas, P. T. .; Warner, J. C. *Green Chemistry: Theory and Practice, 12 Principles of Green Chemistry*; 1998.

(10)   Anastas, P.; Eghbali, N. Green Chemistry: Principles and Practice. *Chem. Soc. Rev.* **2010**, No. 39, 301–312. https://doi.org/10.1039/b918763b.

(11)   Sheldon, R. A. The E Factor: Fifteen Years On. *Green Chem.* **2007**. https://doi.org/10.1039/b713736m.

(12)   Jimenez-Gonzalez, C.; Ponder, C. S.; Broxterman, Q. B.; Manley, J. B. Using the Right Green Yardstick: Why Process Mass Intensity Is Used in the Pharmaceutical Industry to Drive More Sustainable Processes. *Org. Process Res. Dev.* **2011**. https://doi.org/10.1021/op200097d.

(13)   Trost, B. M. The Atom Economy - A Search for Synthetic Efficiency. **1991**.

https://doi.org/10.1126/science.1962206.

(14)   Milton, B. E. Chapter 8 - Control Technologies in Spark-Ignition Engines. In *Handbook of Air Pollution From Internal Combustion Engines*; Sher, E., Ed.; Academic Press: San Diego, 1998; pp 189–258. https://doi.org/https://doi.org/10.1016/B978-012639855-7/50047-8.

(15)   Scurrell, M. S. Heterogeneous Catalysis on Metal Oxides. *Annu. Reports Prog. Chem. Sect. A Phys. Inorg. Chem.* **1973**, *70*, 87–122. https://doi.org/10.1039/PR9737000087.

(16)   Armor, J. N. A History of Industrial Catalysis. *Catal. Today* **2011**. https://doi.org/10.1016/j.cattod.2009.11.019.

(17)   Alonso, D. M.; Bond, J. Q.; Dumesic, J. A. Catalytic Conversion of Biomass to Biofuels. *Green Chem.* **2010**. https://doi.org/10.1039/c004654j.

(18)   Ma, F.; Hanna, M. A. Biodiesel Production: A Review. *Bioresour. Technol.* **1999**. https://doi.org/10.1016/S0960-8524(99)00025-5.

(19)   Busacca, C. A.; Fandrick, D. R.; Song, J. J.; Senanayake, C. H. The Growing Impact of Catalysis in the Pharmaceutical Industry. *Advanced Synthesis and Catalysis*. 2011. https://doi.org/10.1002/adsc.201100488.

(20)   Atkins, P.; Overton, T. Catalysis. In *Inorganic Chemistry*; Oxford University Press, 2010; pp 690–720.

(21)   Sheldon, R. A.; Arends, I. W. C. E.; Hanefeld, U. *Green Chemistry and Catalysis*; 2007. https://doi.org/10.1002/9783527611003.

(22)   Wisniak, J. The History of Catalysis. From the Beginning to Nobel Prizes. *Educ. Quim.* **2010**. https://doi.org/10.1016/S0187-893X(18)30074-0.

(23)   Astruc, D. The Metathesis Reactions: From a Historical Perspective to Recent Developments. *New Journal of Chemistry*. 2005. https://doi.org/10.1039/b412198h.

(24)   Young, J. F.; Osborn, J. A.; Jardine, F. H.; Wilkinson, G. Hydride Intermediates in Homogeneous Hydrogenation Reactions of Olefins and Acetylenes Using Rhodium Catalysts. *Chem. Commun.* **1965**. https://doi.org/10.1039/C19650000131.

(25)   Trzeciak, A. M. Hydroformylation. In *Comprehensive Inorganic Chemistry II (Second Edition): From Elements to Applications*; 2013. https://doi.org/10.1016/B978-0-08-097774-4.00602-1.

(26)   Johansson Seechurn, C. C. C.; Kitching, M. O.; Colacot, T. J.; Snieckus, V. Palladium-Catalyzed Cross-Coupling: A Historical Contextual Perspective to the 2010 Nobel Prize. *Angewandte Chemie - International Edition*. 2012. https://doi.org/10.1002/anie.201107017.

(27)   The Nobel Committee for Chemistry. Scientific Background on the Nobel Prize in Chemistry 2021 Enamine and Iminium Ion–Mediated Organocatalysis. *R. Swedish Acad. Sci.* **2021**, *50005*, 1–19.

(28)   Gao, H.; Angelici, R. J. Combination Catalysts Consisting of a Homogeneous Catalyst Tethered to a Silica-Supported Palladium Heterogeneous Catalyst: Arene Hydrogenation [10]. *Journal of the American Chemical Society*. 1997. https://doi.org/10.1021/ja9710058.

(29)   Cole-Hamilton, D. J. Homogeneous Catalysis - New Approaches to Catalyst Separation, Recovery, and Recycling. *Science*. 2003. https://doi.org/10.1126/science.1081881.

(30)   *Catalyst Market Size, Share & Trends Analysis Report By Raw Material (Chemical Compounds, Zeolites, Metals), By Product (Heterogeneous, Homogeneous), By Application, By Region, And Segment Forecasts, 2020 - 2027*. https://www.grandviewresearch.com/industry-analysis/catalyst-market.

(31)   Klaewkla, R.; Arend, M.; F., W. A Review of Mass Transfer Controlling the Reaction Rate in Heterogeneous Catalytic Systems. In *Mass Transfer - Advanced Aspects*; 2011. https://doi.org/10.5772/22962.

(32) Liu, L.; Corma, A. Metal Catalysts for Heterogeneous Catalysis: From Single Atoms to Nanoclusters and Nanoparticles. *Chem. Rev.* **2018**, *118* (10), 4981–5079. https://doi.org/10.1021/acs.chemrev.7b00776.

(33) Pellegrini, R.; Leofanti, G.; Agostini, G.; Groppo, E.; Lamberti, C. Investigation of Carbon and Alumina Supported Pd Catalysts during Catalyst Preparation. In *Scientific Bases for the Preparation of Heterogeneous Catalysts*; Gaigneaux, E. M., Devillers, M., Hermans, S., Jacobs, P. A., Martens, J. A., Ruiz, P., Eds.; Studies in Surface Science and Catalysis; Elsevier, 2010; Vol. 175, pp 437–440. https://doi.org/https://doi.org/10.1016/S0167-2991(10)75079-5.

(34) Blaser, H.-U.; Indolese, A.; Schnyder, A.; Steiner, H.; Studer, M. Supported Palladium Catalysts for Fine Chemicals Synthesis. *J. Mol. Catal. A Chem.* **2001**, *173* (1), 3–18. https://doi.org/https://doi.org/10.1016/S1381-1169(01)00143-1.

(35) Pernicone, N.; Cerboni, M.; Prelazzi, G.; Pinna, F.; Fagherazzi, G. An Investigation on Pd/C Industrial Catalysts for the Purification of Terephthalic Acid. *Catal. Today* **1998**, *44* (1), 129–135. https://doi.org/https://doi.org/10.1016/S0920-5861(98)00183-7.

(36) Hutchings, G. J. Heterogeneous Gold Catalysis. *ACS Cent. Sci.* **2018**, *4* (9), 1095–1101. https://doi.org/10.1021/acscentsci.8b00306.

(37) Johnston, P.; Carthey, N.; Hutchings, G. J. Discovery, Development, and Commercialization of Gold Catalysts for Acetylene Hydrochlorination. *J. Am. Chem. Soc.* **2015**, *137* (46), 14548–14557. https://doi.org/10.1021/jacs.5b07752.

(38) He, Q.; Freakley, S. J.; Edwards, J. K.; Carley, A. F.; Borisevich, A. Y.; Mineo, Y.; Haruta, M.; Hutchings, G. J.; Kiely, C. J. Population and Hierarchy of Active Species in Gold Iron Oxide Catalysts for Carbon Monoxide Oxidation. *Nat. Commun.* **2016**, *7* (1), 12905. https://doi.org/10.1038/ncomms12905.

(39) Khalaf, A. J.; Hargreaves, J.; David, J. S. Base Catalysis with Metal Oxides. In Metal Oxide Catalysis. *Met. Oxide Catal.* **2009**. https://doi.org/doi:10.1002/9783527626113.ch21.

(40) Hattori, H. Solid Base Catalysts : Generation , Characterization , and Catalytic Behavior of Basic Sites Solid Base Catalysts : Generation , Characterization , and Catalytic Behavior of Basic Sites. *J. Japan Pet. Inst.* **2004**, *47* (2), 67–81. https://doi.org/10.1627/jpi.47.67.

(41) Tanabe, K.; Hölderich, W. F. Industrial Application of Solid Acid-Base Catalysts. *Appl. Catal. A Gen.* **1999**. https://doi.org/10.1016/S0926-860X(98)00397-4.

(42) Trueba, M.; Trasatti, S. P. γ-Alumina as a Support for Catalysts: A Review of Fundamental Aspects. *Eur. J. Inorg. Chem.* **2005**, *2005* (17), 3393–3403. https://doi.org/https://doi.org/10.1002/ejic.200500348.

(43) Di Cosimo, J. I.; Dïez, V. K.; Apesteguía, C. R. Base Catalysis for the Synthesis of α,β-Unsaturated Ketones from the Vapor-Phase Aldol Condensation of Acetone. *Appl. Catal. A Gen.* **1996**. https://doi.org/10.1016/0926-860X(95)00289-8.

(44) Busca, G. Bases and Basic Materials in Chemical and Environmental Processes. Liquid versus Solid Basicity. *Chem. Rev.* **2010**, *110* (4), 2217–2249. https://doi.org/10.1021/cr9000989.

(45) Ai, M. Formation of Methyl Methacrylate by Condensation of Methyl Propionate with Formaldehyde over Silica-Supported Cesium Hydroxide Catalysts. *Appl. Catal. A Gen.* **2005**, *288* (1), 211–215. https://doi.org/https://doi.org/10.1016/j.apcata.2005.04.027.

(46) Hamilton, C. A.; Jackson, S. D.; Kelly, G. J. Solid Base Catalysts and Combined Solid Base Hydrogenation Catalysts for the Aldol Condensation of Branched and Linear Aldehydes. *Appl. Catal. A Gen.* **2004**. https://doi.org/10.1016/j.apcata.2003.12.009.

(47) Hattori, H. Solid Base Catalysts: Generation, Characterization, and Catalytic Behavior of Basic Sites. *J. Japan Pet. Inst.* **2004**, *47* (2), 67–81. https://doi.org/10.1627/jpi.47.67.

(48) Hattori, H.; Ono, Y. 4 - Catalysts and Catalysis for Acid–Base Reactions. In *Metal Oxides*; Védrine, J.

C. B. T.-M. O. in H. C., Ed.; Elsevier, 2018; pp 133–209. https://doi.org/https://doi.org/10.1016/B978-0-12-811631-9.00004-1.

(49) Marinković, D. M.; Stanković, M. V.; Veličković, A. V.; Avramović, J. M.; Miladinović, M. R.; Stamenković, O. O.; Veljković, V. B.; Jovanović, D. M. Calcium Oxide as a Promising Heterogeneous Catalyst for Biodiesel Production: Current State and Perspectives. *Renew. Sustain. Energy Rev.* **2016**, *56* (January), 1387–1408. https://doi.org/10.1016/j.rser.2015.12.007.

(50) Mazaheri, H.; Ong, H. C.; Amini, Z.; Masjuki, H. H.; Mofijur, M.; Su, C. H.; Anjum Badruddin, I.; Khan, T. M. Y. An Overview of Biodiesel Production via Calcium Oxide Based Catalysts: Current State and Perspective. *Energies* . 2021. https://doi.org/10.3390/en14133950.

(51) Zevenhoven, R.; Fagerlund, J. 16 - Mineralisation of Carbon Dioxide (CO2). In *Woodhead Publishing Series in Energy*; Maroto-Valer, M. M. B. T.-D. and I. in C. D. (CO2) C. and S. T., Ed.; Woodhead Publishing, 2010; Vol. 2, pp 433–462. https://doi.org/https://doi.org/10.1533/9781845699581.4.433.

(52) Miller, B. G. 13 - Carbon Dioxide Emissions Reduction and Storage; Miller, B. G. B. T.-C. C. E. T. (Second E., Ed.; Butterworth-Heinemann, 2017; pp 609–668. https://doi.org/https://doi.org/10.1016/B978-0-12-811365-3.00013-2.

(53) Di Cosimo, J. I.; Díez, V. K.; Ferretti, C.; Apesteguía, C. R. Basic Catalysis on MgO: Generation, Characterization and Catalytic Properties of Active Sites. *Catalysis* **2014**, *26* (3000), 1–28. https://doi.org/10.1039/9781782620037-00001.

(54) Gervasini, A.; Auroux, A. Acidity and Basicity of Metal Oxide Surfaces II. Determination by Catalytic Decomposition of Isopropanol. *J. Catal.* **1991**. https://doi.org/10.1016/0021-9517(91)90335-2.

(55) Anderson, P. J.; Horlock, R. F. Thermal Decomposition of Magnesium Hydroxide. *Trans. Faraday Soc.* **1962**. https://doi.org/10.1039/tf9625801993.

(56) Bartley, J. K.; Xu, C.; Lloyd, R.; Enache, D. I.; Knight, D. W.; Hutchings, G. J. Simple Method to Synthesize High Surface Area Magnesium Oxide and Its Use as a Heterogeneous Base Catalyst. *Appl. Catal. B Environ.* **2012**, *128*, 31–38. https://doi.org/10.1016/j.apcatb.2012.03.036.

(57) Xu, C.; Bartley, J. K.; Enache, D. I.; Knight, D. W.; Hutchings, G. J. High Surface Area MgO as a Highly Effective Heterogeneous Base Catalyst for Michael Addition and Knoevenagel Condensation Reactions. *Synthesis (Stuttg).* **2005**. https://doi.org/10.1055/s-2005-918467.

(58) Menezes, A. O.; Silva, P. S.; Hernández, E. P.; Borges, L. E. P.; Fraga, M. A. Tuning Surface Basic Properties of Nanocrystalline MgO by Controlling the Preparation Conditions. *Langmuir* **2010**, *26* (5), 3382–3387. https://doi.org/10.1021/la903149y.

(59) Xu, C.; Bartley, J. K.; Enache, D. I.; Knight, D. W.; Hutchings, G. J. High Surface Area MgO as a Highly Effective Heterogeneous Base Catalyst for Michael Addition and Knoevenagel Condensation Reactions. *Synthesis (Stuttg).* **2005**, No. 19, 3468–3476. https://doi.org/10.1055/s-2005-918467.

(60) Ruckenstein, E.; Hu, Y. H. The Effect of Precursor and Preparation Conditions of MgO on the CO2 Reforming of CH4 over NiO/MgO Catalysts. *Appl. Catal. A Gen.* **1997**, *154* (1–2), 185–205. https://doi.org/10.1016/S0926-860X(96)00372-9.

(61) Zhang, X.; Zheng, Y.; Feng, X.; Han, X.; Bai, Z.; Zhang, Z. Calcination Temperature-Dependent Surface Structure and Physicochemical Properties of Magnesium Oxide. *RSC Adv.* **2015**, *5* (105), 86102–86112. https://doi.org/10.1039/c5ra17031a.

(62) Xu, C.; Enache, D. I.; Lloyd, R.; Knight, D. W.; Bartley, J. K.; Hutchings, G. J. Mgo Catalysed Triglyceride Transesterification for Biodiesel Synthesis. *Catal. Letters* **2010**, *138* (1–2), 1–7. https://doi.org/10.1007/s10562-010-0365-5.

(63) Cui, Z.; Meng, G. W.; Huang, W. D.; Wang, G. Z.; Zhang, L. D. Preparation and Characterization of MgO Nanorods. *Mater. Res. Bull.* **2000**, *35* (10), 1653–1659. https://doi.org/10.1016/S0025-5408(00)00369-X.

(64)   Aramendía, M. A.; Borau, V.; Jiménez, C.; Marinas, J. M.; Ruiz, J. R.; Urbano, F. J. Influence of the Preparation Method on the Structural and Surface Properties of Various Magnesium Oxides and Their Catalytic Activity in the Meerwein-Ponndorf-Verley Reaction. *Appl. Catal. A Gen.* **2003**, *244* (2), 207–215. https://doi.org/10.1016/S0926-860X(02)00213-2.

(65)   Sutradhar, N.; Sinhamahapatra, A.; Roy, B.; Bajaj, H. C.; Mukhopadhyay, I.; Panda, A. B. Preparation of MgO Nano-Rods with Strong Catalytic Activity via Hydrated Basic Magnesium Carbonates. *Mater. Res. Bull.* **2011**, *46* (11), 2163–2167. https://doi.org/10.1016/j.materresbull.2011.02.024.

(66)   Dummer, N. F.; Joyce, L.; Ellicott, H.; Jiang, Y. Surfactant Controlled Magnesium Oxide Synthesis for Base Catalysis. *Catal. Sci. Technol.* **2016**, *6* (6), 1903–1912. https://doi.org/10.1039/c5cy01107h.

(67)   Khairallah, F.; Glisenti, A. Synthesis, Characterization and Reactivity Study of Nanoscale Magnesium Oxide. *J. Mol. Catal. A Chem.* **2007**, *274* (1–2), 137–147. https://doi.org/10.1016/j.molcata.2007.04.039.

(68)   Sutradhar, N.; Sinhamahapatra, A.; Pahari, S. K.; Pal, P.; Bajaj, H. C.; Mukhopadhyay, I.; Panda, A. B. Controlled Synthesis of Different Morphologies of MgO and Their Use as Solid Base Catalysts. *J. Phys. Chem. C* **2011**, *115* (25), 12308–12316. https://doi.org/10.1021/jp2022314.

(69)   Zhang, G.; Hattori, H.; Tanabe, K. Aldol Addition of Acetone, Catalyzed by Solid Base Catalysts: Magnesium Oxide, Calcium Oxide, Strontium Oxide, Barium Oxide, Lanthanum (III) Oxide and Zirconium Oxide. *Appl. Catal.* **1988**. https://doi.org/10.1016/S0166-9834(00)80114-1.

(70)   Díez, V. K.; Apesteguía, C. R.; Di Cosimo, J. I. Aldol Condensation of Citral with Acetone on MgO and Alkali-Promoted MgO Catalysts. *J. Catal.* **2006**, *240* (2), 235–244. https://doi.org/10.1016/j.jcat.2006.04.003.

(71)   Ji, W.; Chen, Y.; Kung, H. H. Vapor Phase Aldol Condensation of Acetaldehyde on Metal Oxide Catalysts. *Appl. Catal. A Gen.* **1997**. https://doi.org/10.1016/S0926-860X(96)00390-0.

(72)   Xi, Y.; Davis, R. J. Nanocrystalline MgO Catalysts for the Henry Reaction of Benzaldehyde and Nitromethane. *J. Mol. Catal. A Chem.* **2011**. https://doi.org/10.1016/j.molcata.2011.03.018.

(73)   Gines, M. J. L.; Iglesia, E. Bifunctional Condensation Reactions of Alcohols on Basic Oxides Modified by Copper and Potassium. *J. Catal.* **1998**. https://doi.org/10.1006/jcat.1998.2009.

(74)   Ma, F.; Hanna, M. A. Biodiesel Production: A Review. *Bioresour. Technol.* **1999**, *70* (1), 1–15. https://doi.org/10.1016/s0960-8524(99)00025-5.

(75)   Lee, A. F.; Wilson, K. Recent Developments in Heterogeneous Catalysis for the Sustainable Production of Biodiesel. *Catal. Today* **2015**, *242* (Part A), 3–18. https://doi.org/10.1016/j.cattod.2014.03.072.

(76)   Gorzawski, H.; Hoelderich, W. F. Preparation of Superbases and Their Use as Catalysts for Double-Bond Isomerization. *J. Mol. Catal. A Chem.* **1999**. https://doi.org/10.1016/S1381-1169(98)00363-X.

(77)   Wang, Z. Cannizzaro Reaction. In *Comprehensive Organic Name Reactions and Reagents*; 2010. https://doi.org/10.1002/9780470638859.

(78)   Tsuji, H.; Hattori, H. Dynamic Behavior of Basic Sites of MgO in Tishchenko Reaction. **2006**, *116*, 239–243. https://doi.org/10.1016/j.cattod.2006.01.034.

(79)   Wei, T.; Wang, M.; Wei, W.; Sun, Y.; Zhong, B. Effect of Base Strength and Basicity on Catalytic Behavior of Solid Bases for Synthesis of Dimethyl Carbonate from Propylene Carbonate and Methanol. *Fuel Process. Technol.* **2003**. https://doi.org/10.1016/S0378-3820(03)00065-1.

(80)   Douthwaite, M.; Huang, X.; Iqbal, S.; Miedziak, P. J.; Brett, G. L.; Kondrat, S. A.; Edwards, J. K.; Sankar, M.; Knight, D. W.; Bethell, D.; Hutchings, G. J. The Controlled Catalytic Oxidation of Furfural to Furoic Acid Using AuPd/Mg(OH)2. *Catal. Sci. Technol.* **2017**, *7* (22), 5284–5293. https://doi.org/10.1039/C7CY01025G.

(81)   Wilds, A. L. Reduction with Aluminum Alkoxides. In *Organic Reactions*; American Cancer Society,

2011; pp 178–223. https://doi.org/https://doi.org/10.1002/0471264180.or002.05.

(82)   Chizallet, C.; Costentin, G.; Lauron-Pernot, H.; Krafft, J. M.; Bazin, P.; Saussey, J.; Delbecq, F.; Saufet, P.; Che, M. Role of Hydroxyl Groups in the Basic Reactivity of MgO: A Theoretical and Experimental Study. *Oil Gas Sci. Technol.* **2006**, *61* (4), 479–488. https://doi.org/10.2516/ogst:2006023a.

(83)   Hoq, M. F.; Nieves, I.; Klabunde, K. J. Mechanistic Studies of Hydrocarbon CH/D2 Exchange over Thermally Activated Magnesium Oxide. *J. Catal.* **1990**. https://doi.org/10.1016/0021-9517(90)90134-6.

(84)   Laurence, M.; Chizallet, C.; Costentin, G.; Krafft, J. M.; Lauron-Pernot, H.; Che, M. A Spectroscopy and Catalysis Study of the Nature of Active Sites of MgO Catalysts: Thermodynamic Brønsted Basicity versus Reactivity of Basic Sites. *J. Catal.* **2005**. https://doi.org/10.1016/j.jcat.2005.09.004.

(85)   Giordano, L.; Goniakowski, J.; Suzanne, J. Partial Dissociation of Water Molecules in the (3×2) Water Monolayer Deposited on the MgO (100) Surface. *Phys. Rev. Lett.* **1998**. https://doi.org/10.1103/PhysRevLett.81.1271.

(86)   Odelius, M. Mixed Molecular and Dissociative Water Adsorption on MgO[100]. *Phys. Rev. Lett.* **1999**. https://doi.org/10.1103/PhysRevLett.82.3919.

(87)   Henderson, M. A.; Epling, W. S.; Perkins, C. L.; Peden, C. H. F.; Diebold, U. Interaction of Molecular Oxygen with the Vacuum-Annealed TiO2(110) Surface: Molecular and Dissociative Channels. *J. Phys. Chem. B* **1999**. https://doi.org/10.1021/jp990655q.

(88)   Delle Site, L.; Alavi, A.; Lynden-Bell, R. M. The Structure and Spectroscopy of Monolayers of Water on MgO: An Ab Initio Study . *J. Chem. Phys.* **2000**. https://doi.org/10.1063/1.1287276.

(89)   Lynden-Bell, R. M.; Delle Site, L.; Alavi, A. Structures of Adsorbed Water Layers on MgO: An Ab Initio Study. *Surf. Sci.* **2002**. https://doi.org/10.1016/S0039-6028(01)01669-7.

(90)   Kim, Y. D.; Lynden-Bell, R. M.; Alavi, A.; Stulz, J.; Goodman, D. W. Evidence for Partial Dissociation of Water on Flat MgO(100) Surfaces. *Chem. Phys. Lett.* **2002**. https://doi.org/10.1016/S0009-2614(02)00009-X.

(91)   Kim, Y. D.; Stultz, J.; Goodman, D. W. Dissociation of Water on MgO(100). *J. Phys. Chem. B* **2002**. https://doi.org/10.1021/jp012306d.

(92)   Cornu, D.; Guesmi, H.; Krafft, J. M.; Lauron-Pernot, H. Lewis Acido-Basic Interactions between CO 2 and MgO Surface: DFT and DRIFT Approaches. *J. Phys. Chem. C* **2012**, *116* (11), 6645–6654. https://doi.org/10.1021/jp211171t.

(93)   Kwon, H. H.-K.; Park, D.-G. G. Infra-Red Study of Surface Carbonation on Polycrystalline Magnesium Hydroxide. *Bull. Korean Chem. Soc.* **2009**, *30* (11), 2567–2573. https://doi.org/10.5012/BKCS.2009.30.11.2567.

(94)   V. Stark, J.; G. Park, D.; Lagadic, I.; J. Klabunde, K. Nanoscale Metal Oxide Particles/Clusters as Chemical Reagents. Unique Surface Chemistry on Magnesium Oxide As Shown by Enhanced Adsorption of Acid Gases (Sulfur Dioxide and Carbon Dioxide) and Pressure Dependence. *Chem. Mater.* **1996**, *8* (8), 1904–1912. https://doi.org/10.1021/cm950583p.

(95)   Yang, J.; Li, Y.; Zhao, X.; Fan, W. Critical Role of Water and Oxygen Defects in C–O Scission during CO2 Reduction on Zn2GeO4(010). *Langmuir* **2018**, *34* (12), 3742–3754. https://doi.org/10.1021/acs.langmuir.7b03360.

(96)   Lind, A.; Thorshaug, K.; Anne Andreassen, K.; Blom, R.; Arstad, B. The Role of Water during CO2 Adsorption by Ca-Based Sorbents at High Temperature. *Ind. & Eng. Chem. Res.* **2018**, *57* (8), 2829–2837. https://doi.org/10.1021/acs.iecr.7b04052.

(97)   Yanagisawa, Y.; Takaoka, K.; Yamabe, S.; Ito, T. Interaction of CO2 with Magnesium Oxide Surfaces: A TPD, FTIR, and Cluster-Model Calculation Study. *J. Phys. Chem.* **2002**, *99* (11), 3704–3710. https://doi.org/10.1021/j100011a043.

(98)   Jentoft, F. C. 7.09 - Solid Acids and Bases. In *Comprehensive Inorganic Chemistry II (Second Edition)*; Reedijk, J., Poeppelmeier, K., Eds.; Elsevier: Amsterdam, 2013; pp 205–230. https://doi.org/https://doi.org/10.1016/B978-0-08-097774-4.00720-8.

(99)   Pacchioni, G.; Ricart, J. M.; Illas, F. Ab Initio Cluster Model Calculations on the Chemisorption of CO2 and SO2 Probe Molecules on MgO and CaO (100) Surfaces. A Theoretical Measure of Oxide Basicity. *J. Am. Chem. Soc.* **1994**, *116* (22), 10152–10158. https://doi.org/10.1021/ja00101a038.

(100)   Montero, J. M.; Gai, P.; Wilson, K.; Lee, A. F. Structure-Sensitive Biodiesel Synthesis over MgO Nanocrystals. *Green Chem.* **2009**, *11* (2), 265–268. https://doi.org/10.1039/B814357A.

(101)   Duer, M. J. The Basics of Solid-State NMR. In *Solid-State NMR Spectroscopy Principles and Applications*; John Wiley & Sons, Ltd, 2001; pp 1–72. https://doi.org/https://doi.org/10.1002/9780470999394.ch1.

(102)   Zhang, W.; Xu, S.; Han, X.; Bao, X. In Situ Solid-State NMR for Heterogeneous Catalysis: A Joint Experimental and Theoretical Approach. *Chem. Soc. Rev.* **2012**, *41* (1), 192–210. https://doi.org/10.1039/C1CS15009J.

(103)   Hunger, M.; Seiler, M.; Horvath, T. A Technique for Simultaneous in Situ MAS NMR and On-Line Gas Chromatographic Studies of Hydrocarbon Conversions on Solid Catalysts under Flow Conditions. *Catal. Letters* **1999**, *57* (4), 199–204. https://doi.org/10.1023/A:1019064003201.

(104)   Khairallah, F.; Glisenti, A. XPS Study of MgO Nanopowders Obtained by Different Preparation Procedures. *Surf. Sci. Spectra* **2006**, *13* (1), 58–71. https://doi.org/10.1116/11.20060601.

(105)   Rheinheimer, V.; Unluer, C.; Liu, J.; Ruan, S.; Pan, J.; Monteiro, P. J. M. XPS Study on the Stability and Transformation of Hydrate and Carbonate Phases within MgO Systems. *Mater. (Basel, Switzerland)* **2017**, *10* (1), 75. https://doi.org/10.3390/ma10010075.

(106)   Alp, E. E.; Mini, S. M.; Ramanathan, M. *X-Ray Absorption Spectroscopy: EXAFS and XANES - A Versatile Tool to Study the Atomic and Electronic Structure of Materials*; United States, 1990.

(107)   Meitzner, G. In Situ XAS Characterization of Heterogeneous Catalysts. In *In-Situ Spectroscopy in Heterogeneous Catalysis*; John Wiley & Sons, Ltd, 2002; pp 179–194. https://doi.org/https://doi.org/10.1002/3527601589.ch7.

(108)   Deng, F.; Yang, J.; Ye, C. Solid State NMR Characterization of Solid Surface of Heterogeneous Catalysts. In *Modern Magnetic Resonance*; Webb, G. ., Ed.; Springer, 2008; pp 205–211. https://doi.org/https://doi.org/10.1007/1-4020-3910-7_25.

(109)   Fu, Y.; Zhang, L.; Yue, B.; Chen, X.; He, H. Simultaneous Characterization of Solid Acidity and Basicity of Metal Oxide Catalysts via the Solid-State NMR Technique. *J. Phys. Chem. C* **2018**, *122* (42), 24094–24102. https://doi.org/10.1021/acs.jpcc.8b06827.

(110)   Brönsted, J. N. Einige Bemerkungen Über Den Begriff Der Säuren Und Basen. *Recl. des Trav. Chim. des Pays-Bas* **1923**. https://doi.org/10.1002/recl.19230420815.

(111)   Chizallet, C.; Bailly, M. L.; Costentin, G.; Lauron-Pernot, H.; Krafft, J. M.; Bazin, P.; Saussey, J.; Che, M. Thermodynamic Brønsted Basicity of Clean MgO Surfaces Determined by Their Deprotonation Ability: Role of Mg2+-O2- Pairs. *Catal. Today* **2006**. https://doi.org/10.1016/j.cattod.2006.01.030.

(112)   Petitjean, H.; Guesmi, H.; Lauron-Pernot, H.; Costentin, G.; Loffreda, D.; Sautet, P.; Delbecq, F. How Surface Hydroxyls Enhance MgO Reactivity in Basic Catalysis: The Case of Methylbutynol Conversion. *ACS Catal.* **2014**. https://doi.org/10.1021/cs5010807.

(113)   Sudarsanam, P.; Zhong, R.; Van Den Bosch, S.; Coman, S. M.; Parvulescu, V. I.; Sels, B. F. Functionalised Heterogeneous Catalysts for Sustainable Biomass Valorisation. *Chemical Society Reviews*. 2018. https://doi.org/10.1039/c8cs00410b.

(114)   *Biodiesel Market Analysis By Feedstock [Vegetable Oils (Canola Oil, Soybean Oil, Palm Oil, Corn Oil), Animal Fats (Poultry, Tallow, White Grease)], By Application (Fuel, Power Generation), And Segment*

Forecasts, 2018 - 2025; 2017. https://doi.org/GVR-1-68038-513-7.

(115) Lotero, E.; Liu, Y.; Lopez, D. E.; Suwannakarn, K.; Bruce, D. A.; Goodwin, J. G. Synthesis of Biodiesel via Acid Catalysis. *Ind. Eng. Chem. Res.* **2005**, *44* (14), 5353–5363. https://doi.org/10.1021/ie049157g.

(116) López, D. E.; Jr, J. G. G.; Bruce, D. A. Transesterification of Triacetin with Methanol on Nafion ® Acid Resins. **2007**, *245*, 381–391. https://doi.org/10.1016/j.jcat.2006.10.027.

(117) Dou, B.; Song, Y.; Wang, C.; Chen, H.; Xu, Y. Hydrogen Production from Catalytic Steam Reforming of Biodiesel Byproduct Glycerol: Issues and Challenges. *Renewable and Sustainable Energy Reviews*. 2014. https://doi.org/10.1016/j.rser.2013.11.029.

(118) Rossi, M.; Pagliaro, M. Glycerol: Properties and Production. In *Future of Glycerol: New Usages for a Versatile Raw Material*; 2008. https://doi.org/10.1016/S1351-4180(08)70291-5.

(119) Slinn, M.; Kendall, K.; Mallon, C.; Andrews, J. Steam Reforming of Biodiesel By-Product to Make Renewable Hydrogen. *Bioresour. Technol.* **2008**. https://doi.org/10.1016/j.biortech.2007.10.003.

(120) Adeniyi, A. G.; Ighalo, J. O. A Review of Steam Reforming of Glycerol. *Chem. Pap.* **2019**, *73* (11), 2619–2635. https://doi.org/10.1007/s11696-019-00840-8.

(121) Thompson, J. C.; He, B. B. Characterization of Crude Glycerol from Biodiesel Production from Multiple Feedstocks. *Appl. Eng. Agric.* **2006**, *2* (22), 261–265. https://doi.org/10.13031/2013.20272.

(122) Yang, F.; Hanna, M. A.; Sun, R. Value-Added Uses for Crude Glycerol--a Byproduct of Biodiesel Production. *Biotechnol. Biofuels* **2012**. https://doi.org/10.1186/1754-6834-5-13.

(123) Schwengber, C. A.; Alves, H. J.; Schaffner, R. A.; Da Silva, F. A.; Sequinel, R.; Bach, V. R.; Ferracin, R. J. Overview of Glycerol Reforming for Hydrogen Production. *Renewable and Sustainable Energy Reviews*. 2016. https://doi.org/10.1016/j.rser.2015.12.279.

(124) Kumar, L. R.; Yellapu, S. K.; Tyagi, R. D.; Zhang, X. A Review on Variation in Crude Glycerol Composition, Bio-Valorization of Crude and Purified Glycerol as Carbon Source for Lipid Production. *Bioresource Technology*. 2019. https://doi.org/10.1016/j.biortech.2019.122155.

(125) Independent Commodity Intelligence Service (ICIS). *Europe glycerine spot prices post triple-digit rises on fears of further biodiesel output cuts | ICIS*. 2020/04/03. https://www.icis.com/explore/resources/news/2020/04/03/10490229/europe-glycerine-spot-prices-post-triple-digit-rises-on-fears-of-further-biodiesel-output-cuts (accessed 2020-06-01).

(126) Hansen, C. F.; Hernandez, A.; Mullan, B. P.; Moore, K.; Trezona-Murray, M.; King, R. H.; Pluske, J. R. A Chemical Analysis of Samples of Crude Glycerol from the Production of Biodiesel in Australia, and the Effects of Feeding Crude Glycerol to Growing-Finishing Pigs on Performance, Plasma Metabolites and Meat Quality at Slaughter. *Anim. Prod. Sci.* **2009**, *49* (2), 154–161. https://doi.org/10.1071/EA08210.

(127) Hu, S.; Luo, X.; Wan, C.; Li, Y. Characterization of Crude Glycerol from Biodiesel Plants. *J. Agric. Food Chem.* **2012**, *60* (23), 5915–5921. https://doi.org/10.1021/jf3008629.

(128) Ardi, M. S.; Aroua, M. K.; Hashim, N. A. Progress, Prospect and Challenges in Glycerol Purification Process: A Review. *Renew. Sustain. Energy Rev.* **2015**, *42*, 1164–1173. https://doi.org/https://doi.org/10.1016/j.rser.2014.10.091.

(129) Kongjao, S.; Damronglerd, S.; Hunsom, M. Purification of Crude Glycerol Derived from Waste Used-Oil Methyl Ester Plant. *Korean J. Chem. Eng.* **2010**, *27* (3), 944–949. https://doi.org/10.1007/s11814-010-0148-0.

(130) Pagliaro, M.; Ciriminna, R.; Kimura, H.; Rossi, M.; Pina, C. Della. Recent Advances in the Conversion of Bioglycerol into Value-Added Products. *European Journal of Lipid Science and Technology*. 2009. https://doi.org/10.1002/ejlt.200800210.

(131) Bagheri, S.; Julkapli, N. M.; Yehye, W. A. Catalytic Conversion of Biodiesel Derived Raw Glycerol to

Value Added Products. *Renew. Sustain. Energy Rev.* **2015**.
https://doi.org/10.1016/j.rser.2014.08.031.

(132) Johnson, D. T.; Taconi, K. A. The Glycerin Glut: Options for the Value-Added Conversion of Crude Glycerol Resulting from Biodiesel Production. *Environ. Prog.* **2007**.
https://doi.org/10.1002/ep.10225.

(133) Kong, P. S.; Aroua, M. K.; Daud, W. M. A. W. Conversion of Crude and Pure Glycerol into Derivatives: A Feasibility Evaluation. *Renew. Sustain. Energy Rev.* **2016**, *63*, 533–555.
https://doi.org/10.1016/j.rser.2016.05.054.

(134) Pagliaro, M.; Ciriminna, R.; Kimura, H.; Rossi, M.; Della Pina, C. From Glycerol to Value-Added Products. *Angew. Chemie - Int. Ed.* **2007**, *46* (24), 4434–4440.
https://doi.org/10.1002/anie.200604694.

(135) Pathak, K.; Reddy, K. M.; Bakhshi, N. N.; Dalai, A. K. Catalytic Conversion of Glycerol to Value Added Liquid Products. *Appl. Catal. A Gen.* **2010**, *372* (2), 224–238.
https://doi.org/10.1016/j.apcata.2009.10.036.

(136) Chaminand, J.; Djakovitch, L. auren.; Gallezot, P.; Marion, P.; Pinel, C.; Rosier, C. Glycerol Hydrogenolysis on Heterogeneous Catalysts. *Green Chem.* **2004**, *6* (8), 359.
https://doi.org/10.1039/b407378a.

(137) Dodekatos, G.; Schünemann, S.; Tüysüz, H. Recent Advances in Thermo-, Photo-, and Electrocatalytic Glycerol Oxidation. *ACS Catal.* **2018**, *8* (7), 6301–6333.
https://doi.org/10.1021/acscatal.8b01317.

(138) Liu, S.; Okuyama, Y.; Tamura, M.; Nakagawa, Y.; Imai, A.; Tomishige, K. Catalytic Conversion of Sorbitol to Gasoline-Ranged Products without External Hydrogen over Pt-Modified Ir-ReOx/SiO2. *Catal. Today* **2016**, *269* (C), 122–131. https://doi.org/10.1016/j.cattod.2015.10.023.

(139) Adhikari, S.; Fernando, S. D.; Haryanto, A. Hydrogen Production from Glycerin by Steam Reforming over Nickel Catalysts. *Renew. Energy* **2008**, *33* (5), 1097–1100.
https://doi.org/https://doi.org/10.1016/j.renene.2007.09.005.

(140) Behr, A.; Eilting, J.; Irawadi, K.; Leschinski, J.; Lindner, F. Improved Utilisation of Renewable Resources: New Important Derivatives of Glycerol. *Green Chem.* **2008**, *10* (1), 13–30.
https://doi.org/10.1039/b710561d.

(141) Adhikari, S.; Fernando, S.; Gwaltney, S. R.; Filip To, S. D.; Mark Bricka, R.; Steele, P. H.; Haryanto, A. A Thermodynamic Analysis of Hydrogen Production by Steam Reforming of Glycerol. *Int. J. Hydrogen Energy* **2007**. https://doi.org/10.1016/j.ijhydene.2007.03.023.

(142) Nakagawa, Y.; Tomishige, K. Heterogeneous Catalysis of the Glycerol Hydrogenolysis. *Catal. Sci. Technol.* **2011**, *1* (2), 179–190. https://doi.org/10.1039/c0cy00054j.

(143) Dasari, M. A.; Kiatsimkul, P. P.; Sutterlin, W. R.; Suppes, G. J. Low-Pressure Hydrogenolysis of Glycerol to Propylene Glycol. *Appl. Catal. A Gen.* **2005**, *281* (1–2), 225–231.
https://doi.org/10.1016/j.apcata.2004.11.033.

(144) Liu, H.; Xu, Y.; Zheng, Z.; Liu, D. 1,3-Propanediol and Its Copolymers: Research, Development and Industrialization. *Biotechnol. J.* **2010**, *5* (11), 1137–1148.
https://doi.org/https://doi.org/10.1002/biot.201000140.

(145) Samudrala, S. P. Glycerol Transformation to Value-Added 1,3-Propanediol Production: A Paradigm for a Sustainable Biorefinery Process. In *Glycerine Production and Transformation*; Frediani, M., Bartoli, M., Rosi, L., Eds.; IntechOpen: Rijeka, 2019. https://doi.org/10.5772/intechopen.83694.

(146) Kurosaka, T.; Maruyama, H.; Naribayashi, I.; Sasaki, Y. Production of 1,3-Propanediol by Hydrogenolysis of Glycerol Catalyzed by Pt/WO3/ZrO2. *Catal. Commun.* **2008**, *9* (6), 1360–1363.
https://doi.org/10.1016/j.catcom.2007.11.034.

(147) Zhao, X.; Wang, J.; Yang, M.; Lei, N.; Li, L.; Hou, B.; Miao, S.; Pan, X.; Wang, A.; Zhang, T. Selective Hydrogenolysis of Glycerol to 1,3-Propanediol: Manipulating the Frustrated Lewis Pairs by Introducing Gold to Pt/WOx. *ChemSusChem* **2017**, *10* (5), 819–824. https://doi.org/https://doi.org/10.1002/cssc.201601503.

(148) Samudrala, S. P.; Kandasamy, S.; Bhattacharya, S. Turning Biodiesel Waste Glycerol into 1,3-Propanediol: Catalytic Performance of Sulphuric Acid-Activated Montmorillonite Supported Platinum Catalysts in Glycerol Hydrogenolysis. *Sci. Rep.* **2018**, *8* (1), 7484. https://doi.org/10.1038/s41598-018-25787-w.

(149) Rosas, I. P.; Larios, J. L. C.; Zeifert, B.; Blásquez, J. S. Catalytic Dehydration of Glycerine to Acrolein. In *Glycerine Production and Transformation*; Frediani, M., Bartoli, M., Rosi, L., Eds.; IntechOpen: Rijeka, 2019. https://doi.org/10.5772/intechopen.85751.

(150) Talebian-Kiakalaieh, A.; Amin, N. A. S.; Hezaveh, H. Glycerol for Renewable Acrolein Production by Catalytic Dehydration. *Renew. Sustain. Energy Rev.* **2014**, *40*, 28–59. https://doi.org/10.1016/j.rser.2014.07.168.

(151) Katryniok, B.; Paul, S.; Bellière-Baca, V.; Rey, P.; Dumeignil, F. Glycerol Dehydration to Acrolein in the Context of New Uses of Glycerol. *Green Chem.* **2010**, *12* (12), 2079–2098. https://doi.org/10.1039/c0gc00307g.

(152) Katryniok, B.; Paul, S.; Capron, M.; Dumeignil, F. Towards the Sustainable Production of Acrolein by Glycerol Dehydration. *ChemSusChem* **2009**, *2* (8), 719–730. https://doi.org/10.1002/cssc.200900134.

(153) Haider, M. H.; D'Agostino, C.; Dummer, N. F.; Mantle, M. D.; Gladden, L. F.; Knight, D. W.; Willock, D. J.; Morgan, D. J.; Taylor, S. H.; Hutchings, G. J. The Effect of Grafting Zirconia and Ceria onto Alumina as a Support for Silicotungstic Acid for the Catalytic Dehydration of Glycerol to Acrolein. *Chem. - A Eur. J.* **2014**, *20* (6), 1743–1752. https://doi.org/10.1002/chem.201302348.

(154) Haider, M. H.; Dummer, N. F.; Zhang, D.; Miedziak, P.; Davies, T. E.; Taylor, S. H.; Willock, D. J.; Knight, D. W.; Chadwick, D.; Hutchings, G. J. Rubidium- and Caesium-Doped Silicotungstic Acid Catalysts Supported on Alumina for the Catalytic Dehydration of Glycerol to Acrolein. *J. Catal.* **2012**, *286*, 206–213. https://doi.org/10.1016/j.jcat.2011.11.004.

(155) Aihara, T.; Asazuma, K.; Miura, H.; Shishido, T. Highly Active and Durable WO3/Al2O3 Catalysts for Gas-Phase Dehydration of Polyols. *RSC Adv.* **2020**, *10* (61), 37538–37544. https://doi.org/10.1039/D0RA08340B.

(156) Chai, S. H.; Wang, H. P.; Liang, Y.; Xu, B. Q. Sustainable Production of Acrolein: Investigation of Solid Acid-Base Catalysts for Gas-Phase Dehydration of Glycerol. *Green Chem.* **2007**, *9* (10), 1130–1136. https://doi.org/10.1039/b702200j.

(157) Haider, M. H.; Dummer, N. F.; Knight, D. W.; Jenkins, R. L.; Howard, M.; Moulijn, J.; Taylor, S. H.; Hutchings, G. J. Efficient Green Methanol Synthesis from Glycerol. *Nat. Chem.* **2015**, *7* (12), 1028–1032. https://doi.org/10.1038/nchem.2345.

(158) Smith, L. R.; Smith, P. J.; Mugford, K. S.; Douthwaite, M.; Dummer, N. F.; Willock, D. J.; Howard, M.; Knight, D. W.; Taylor, S. H.; Hutchings, G. J. New Insights for the Valorisation of Glycerol over MgO Catalysts in the Gas-Phase. *Catal. Sci. Technol.* **2019**, 19–22. https://doi.org/10.1039/C8CY02214C.

(159) Smith, P. J.; Smith, L.; Dummer, N. F.; Douthwaite, M.; Willock, D. J.; Howard, M.; Knight, D. W.; Taylor, S. H.; Hutchings, G. J. Investigating the Influence of Reaction Conditions and the Properties of Ceria for the Valorisation of Glycerol. *Energies* **2019**, *12* (7), 1359. https://doi.org/10.3390/en12071359.

(160) Waters, T.; O'Hair, R. A. J.; Wedd, A. G. Catalytic Gas Phase Oxidation of Methanol to Formaldehyde. *J. Am. Chem. Soc.* **2003**. https://doi.org/10.1021/ja028839x.

(161) Musa, I. A. The Effects of Alcohol to Oil Molar Ratios and the Type of Alcohol on Biodiesel

Production Using Transesterification Process. *Egypt. J. Pet.* **2016**, *25* (1), 21–31. https://doi.org/10.1016/j.ejpe.2015.06.007.

(162) KoohiKamali, S.; Tan, C. P.; Ling, T. C. Optimization of Sunflower Oil Transesterification Process Using Sodium Methoxide. *Sci. World J.* **2012**, *2012*, 475027. https://doi.org/10.1100/2012/475027.

(163) Lee, J. S.; Saka, S. Biodiesel Production by Heterogeneous Catalysts and Supercritical Technologies. *Bioresource Technology*. 2010. https://doi.org/10.1016/j.biortech.2010.04.071.

(164) Sánchez, M.; Marchetti, J. M.; El Boulifi, N.; Aracil, J.; Martínez, M. Kinetics of Jojoba Oil Methanolysis Using a Waste from Fish Industry as Catalyst. *Chem. Eng. J.* **2015**. https://doi.org/10.1016/j.cej.2014.09.088.

(165) Gebremariam, S. N.; Marchetti, J. M. The Effect of Economic Variables on a Bio-Refinery for Biodiesel Production Using Calcium Oxide Catalyst. *Biofuels, Bioprod. Biorefining* **2019**, *13* (5), 1333–1346. https://doi.org/10.1002/bbb.2039.

(166) Methanex. *Methanex Methanol Price Sheet*. May 28. https://www.methanex.com/our-business/pricing.

(167) Sainna, M. A.; Nanavati, S.; Black, C.; Smith, L.; Mugford, K.; Jenkins, H.; Douthwaite, M.; Dummer, N. F.; Catlow, C. R. A.; Hutchings, G. J.; Taylor, S. H.; Logsdail, A. J.; Willock, D. J. A Combined Periodic DFT and QM/MM Approach to Understand the Radical Mechanism of the Catalytic Production of Methanol from Glycerol. *Faraday Discuss.* **2020**, *34* (4), 240–241. https://doi.org/10.19009/jjacg.34.4_240.

(168) Smith, L. R.; Sainna, M. A.; Douthwaite, M.; Davies, T. E.; Dummer, N. F.; Willock, D. J.; Knight, D. W.; Catlow, C. R. A.; Taylor, S. H.; Hutchings, G. J. Gas Phase Glycerol Valorization over Ceria Nanostructures with Well-Defined Morphologies. *ACS Catal.* **2021**, *11* (8), 4893–4907. https://doi.org/10.1021/acscatal.0c05606.

(169) Devlia, J.; Smith, L.; Douthwaite, M.; Taylor, S. H.; Willock, D. J.; Hutchings, G. J.; Dummer, N. F. The Formation of Methanol from Glycerol Bio-Waste over Doped Ceria-Based Catalysts: Doped Ceria Based Catalysts. *Philos. Trans. R. Soc. A Math. Phys. Eng. Sci.* **2020**, *378* (2176). https://doi.org/10.1098/rsta.2020.0059.

(170) van Bennekom, J. G.; Venderbosch, R. H.; Heeres, H. J. Biomethanol from Glycerol. In *Biodiesel*; Fang, Z., Ed.; IntechOpen: Rijeka, 2012. https://doi.org/10.5772/53691.

(171) Mohamed, M.; Ting, T. S.; Amin, N. A. S.; Abdullah, T. A. T.; Mat, R. Conversion of Glycerol to Methanol in the Presence of Zeolite Based Catalysts. In *2011 IEEE Conference on Clean Energy and Technology (CET)*; 2011; pp 389–393. https://doi.org/10.1109/CET.2011.6041503.

(172) Carr, A. G.; Shi, X.; Domene, C.; Leung, A. K.; Green, W. H. Methanol Formation from the Treatment of Glycerol in Supercritical Water and with Ethylsulfide. *J. Supercrit. Fluids* **2016**, *117*, 80–88. https://doi.org/https://doi.org/10.1016/j.supflu.2016.05.017.

(173) Maneewuthiworasakul, M. Direct Methanol Synthesis from Glycerol over Modified Basic Metal Oxide Catalysts; Silpakorn University, 2019.

(174) Kostyniuk, A.; Bajec, D.; Likozar, B. One-Step Synthesis of Ethanol from Glycerol in a Gas Phase Packed Bed Reactor over Hierarchical Alkali-Treated Zeolite Catalyst Materials. *Green Chem.* **2020**, *22* (3), 753–765. https://doi.org/10.1039/C9GC03262B.

(175) Braslavsky, S. E.; Braun, A. M.; Cassano, A. E.; Emeline, A. V.; Litter, M. I.; Palmisano, L.; Parmon, V. N.; Serpone, N. Glossary of Terms Used in Photocatalysis and Radiation Catalysis (IUPAC Recommendations 2011). *Pure Appl. Chem.* **2011**. https://doi.org/10.1351/PAC-REC-09-09-36.

(176) Fan, D.; Dong, X.; Yu, Y.; Zhang, M. A DFT Study on the Aldol Condensation Reaction on MgO in the Process of Ethanol to 1,3-Butadiene: Understanding the Structure-Activity Relationship. *Phys. Chem. Chem. Phys.* **2017**, *19* (37), 25671–25682. https://doi.org/10.1039/c7cp04502f.

(177) Lusardi, M.; Struble, T.; Teixeira, A. R.; Jensen, K. F. Identifying the Roles of Acid–Base Sites in Formation Pathways of Tolualdehydes from Acetaldehyde over MgO-Based Catalysts. *Catal. Sci. Technol.* **2020**, *10* (2), 536–548. https://doi.org/10.1039/C9CY01927H.

(178) Hernández-Giménez, A. M.; Ruiz-Martínez, J.; Puértolas, B.; Pérez-Ramírez, J.; Bruijnincx, P. C. A.; Weckhuysen, B. M. Operando Spectroscopy of the Gas-Phase Aldol Condensation of Propanal over Solid Base Catalysts. *Top. Catal.* **2017**, *60* (19–20), 1522–1536. https://doi.org/10.1007/s11244-017-0836-7.

(179) Martin, A.; Richter, M. Oligomerization of Glycerol - a Critical Review. *European Journal of Lipid Science and Technology*. 2011. https://doi.org/10.1002/ejlt.201000386.

(180) Calatayud, M.; Ruppert, A. M.; Weckhuysen, B. M. Theoretical Study on the Role of Surface Basicity and Lewis Acidity on the Etherification of Glycerol over Alkaline Earth Metal Oxides. *Chem. - A Eur. J.* **2009**. https://doi.org/10.1002/chem.200900487.

Chapter 2

Experimental

2.1 Chemicals (Source, Purity)

Routinely used chemicals for the reaction testing included: cyclohexanol (Sigma-Aldrich, 99 %), D_2O (Sigma-Aldrich, 99 %), glycerol (Sigma-Aldrich, ≥ 99.5 %) silicon carbide (SiC) (≥ 97.5 %, Sigma Aldrich, 40–50 mesh size) and Magnesium (II) hydroxide ($Mg(OH)_2$ (Sigma-Aldrich, ≥ 99.0 %). Argon gas (99.998%) and CO_2 (> 99.99%) was supplied by BOC. All purchased materials were used as received. Deionised water was provided in house.

Other less used chemicals used for identification of products and calibrations included:

Acetaldehyde (Sigma-Aldrich, > 99.5 %)

Acetaldehyde in helium (BOC, 1000 ppm)

Acetic acid (Sigma-Aldrich, ≥ 99 %)

Acetone (Sigma-Aldrich, ≥ 99.9 %)

Acrolein (Sigma-Aldrich ≥ 99 %)

Allyl alcohol (Sigma-Aldrich, ≥ 99 %)

2,3-Butanedione (Sigma-Aldrich, 97 %)

2-Butanol (Sigma-Aldrich, 99.8 %)

Butyraldehyde (Sigma-Aldrich, 99 %)

Cyclopentanone (Sigma-Aldrich, ≥ 99 %)

Ethanol (Sigma-Aldrich, ≥99.5 %)

3-Ethoxy-1-propanol (Sigma-Aldrich, 97 %)

Ethylene glycol (Sigma-Aldrich, ≥ 99 %)

Glycidol (Sigma-Aldrich, 96 %)

3-Hexanone (Sigma-Aldrich, 98 %)

2-Hexanone (Sigma-Aldrich, 98 %)

Hydroxyacetone (Sigma-Aldrich, ≥ 90.0 %)

Methanol (Sigma-Aldrich, ≥ 99.9 %)

2-Methyl-1-propanol (Sigma-Aldrich, 99.5 %)

Phenol (Sigma-Aldrich, ≥ 99.5 %)

1-Propanol (Sigma-Aldrich, ≥ 99.9 %)

2-Propanol (Sigma-Aldrich, > 99.5 %)

1,2 Propanediol (Sigma-Aldrich, ≥ 99.5 %)

1,3-Propanediol (Sigma-Aldrich, ≥ 99.6 %)

Propionaldehyde (Sigma-Aldrich, ≥ 98 %)

Propionic acid (Sigma-Aldrich, ≥ 99.5 %).

2.2 Calculations and Definitions

Equation (1) and (2) are used for the calculations quantifying the amount of CO_2 desorbed in temperature programmed desorption (TPD) experiments in terms of moles per g^{-1} (1) and moles per m^2 (2) of catalyst.

$$CO_2 \; desorbed \; (mol \; g^{-1}) = \frac{\left(I\,(mV) \middle/ F\,(mV\,mol^{-1}) \right)}{M_{cat}\,(g)} \tag{1}$$

Where I = detector response (mV), F = calibrated response factor, M_{cat} = catalyst mass (g) SA_{cat} = surface area (SA) of catalyst $m^2\,g^{-1}$.

$$CO_2 \; desorbed \; (mol \; m^{-2}) = \frac{mol \; CO_2 \; g_{cat}^{-1}}{SA_{cat} \; m^2 g^{-1}} \tag{2}$$

The following equations 3-8 were used in the reaction results calculations. (Eqn (3)) was used to calculate the glycerol conversion (C_{gly}) based on the molar difference between the carbon moles of glycerol fed into the reactor g_{mi} compared to those detected in the reaction mixture g_{mo}:

$$C_{GLY} \; (\%) = \left(\frac{g_{mi} - g_{mo}}{g_{mi}} \right) \times 100 \tag{3}$$

g_{mi} was calculated in relation to the concentration of glycerol solution used in mol/L multiplied by the volume injected (flow rate x time) to give the amount of glycerol moles injected. The carbon moles were calculated by multiplying the amount of glycerol moles by number of carbon atoms in a glycerol molecule (x 3). g_{mo} was determined *via* gas chromatography (GC) with use of an external standard as detailed in section 2.4.4, calibration curve shown in appendix Figure 1.

The product selectivity (S_x) for any product, x, was calculated from the moles of carbon recovered in product x, (x_{cm}) divided by the sum of moles of carbon in all detected products, y_{Cm} (4):

$$S_x \; (\%) = \left(\frac{X_{cm}}{\sum_y y_{cm}} \right) \times 100 \tag{4}$$

The carbon balance X_{cb} (5) was calculated by dividing the sum of the carbon moles of the reaction products X_{cp}, coke X_{coke} and unreacted glycerol g_{mol} by the amount of carbon moles injected into the reactor g_{mi}. The sum of reaction product carbon moles was calculated *via* combining the products

identified in the liquid fractions, (GC1: method 1) with that of the gas fraction of the reaction stream (GC1: method 2).

$$X_{cb}(\%) = \left(\frac{X_{cp} + X_{coke} + g_{mo}}{g_{mi}}\right) \text{x } 100 \tag{5}$$

Carbon deposition in the form of catalyst coke (6) was estimated from the mass loss *via* thermogravimetric analysis (TGA) of the post reaction catalyst. The mass of carbon lost was converted to the number of moles of carbon retained on the catalyst (X_{coke}) and divided by the number of carbon moles in the glycerol feed (g_{mi}).

$$Coke\ (\%) = \left(\frac{m_{lost}}{g_{mi}}\right) \times 100 \tag{6}$$

Space time yield of product *x* was calculated (7) from the mass of product m_x produced per hour (reaction time Rt), per mass of catalyst ($m_{cat,}$ Kg).

$$STY_X\ \left(g_X\ h^{-1}\ kg_{cat}^{-1}\right) = \left(\frac{m_X\ (g)}{Rt(h)\ x\ m_{cat}(kg)}\right) \tag{7}$$

Catalyst activity (8) expressed as grams of glycerol converted per hour per gram of catalyst (g_{gly} h^{-1} g$^{-1}_{cat}$) was calculated by subtracting the number of grams of glycerol fed out (g_{Mo}) from the injected (g_{Mi}) to obtain the amount in grams converted, this is followed by dividing by reaction time (Rt(h)) and mass of catalyst (M_{cat}).

$$Activity_{cat}\ \left(g_{gly}\ h^{-1}\ g_{cat}^{-1}\right) = \left(\frac{g_{Mi} - \dfrac{g_{Mo}}{Rt(h)}}{M_{cat}}\right) \tag{8}$$

2.3 Catalyst preparation

The preparation method used to synthesise a particular catalyst can greatly affect its chemical and physical properties. Even the properties of a simple material, such as MgO, can be altered significantly, with the use of different starting materials and heat treatment temperatures.[1–3] Optimising properties such as basicity and SA is thought to be crucial for controlling the activity and selectivity of MgO catalysts.[3–5] For this purpose, a preparative procedure for the synthesis of MgO, where the heat treatment conditions were varied, was used to assess how different properties influenced reactivity.

MgO catalysts, used in this study, were prepared by following a previously established procedure,[6,7] using commercial Mg(OH)$_2$ as a starting material. For all the samples, Mg(OH)$_2$ (5 g) was first calcined in a tubular Carbolite furnace at 450 °C in air for 2 hours (heating ramp 10 °C min^{-1}). The

solid obtained was subsequently refluxed in water (15 mL g^{-1}) for 3 hours at 100 °C, before the resulting slurry was dried in an oven at 110 °C for 24 hours. 4 g of the resulting product was then heat treated at 450 °C, 550 °C, 650 °C or 750 °C (10 °C min^{-1}) for three hours, under a steady flow of N$_2$ (150 mL min^{-1}). These materials are denoted as MgO_450, MgO_550, MgO_650 and MgO_750, respectively. Before use in catalytic reactions, the sample was pelleted, crushed and sieved. Pelleting was done *via* a pelleting press; 2 g of samples was pressurised under 1 ton for 1 minute. The resulting pellet was then crushed with a pestle and pressed through a series of sieves to obtain particles with diameters of between 250 - 425 μm were collected for catalytic testing

2.4 Catalyst Reaction Testing
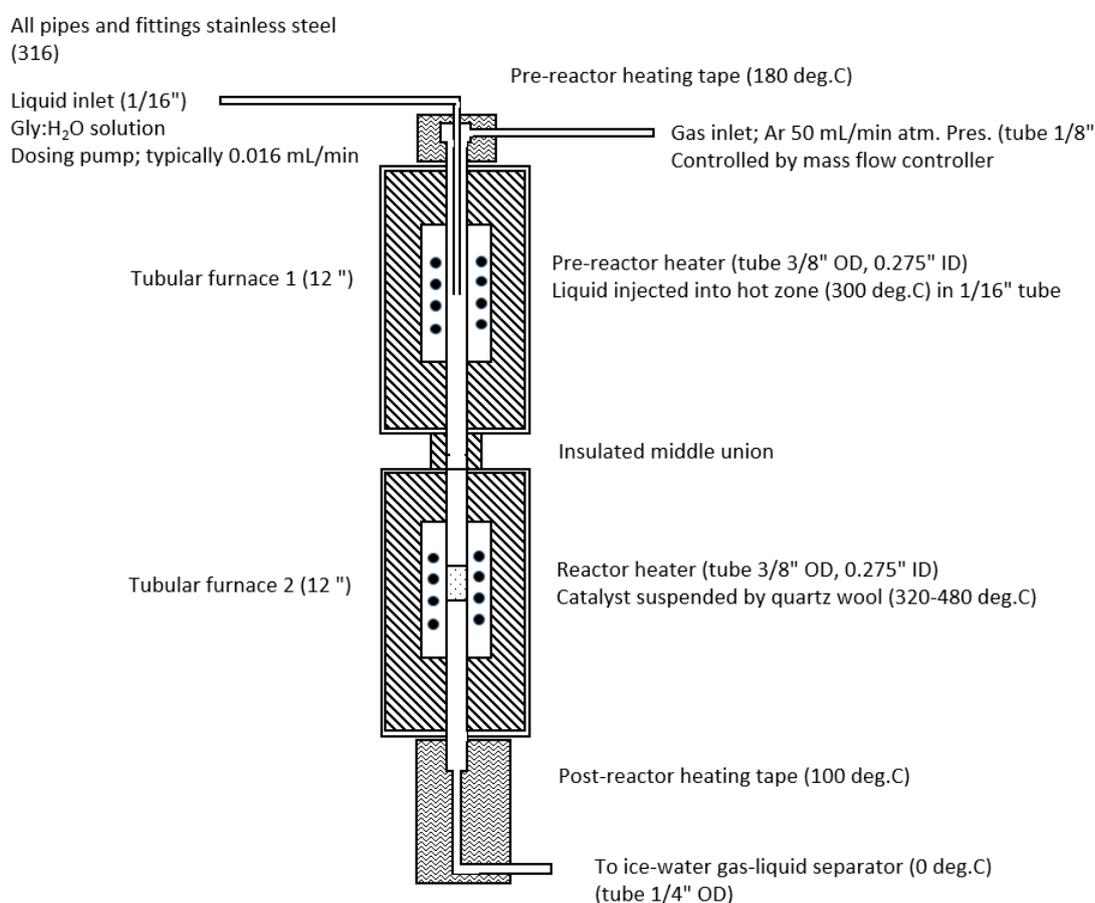
Figure 1. Catalyst reactor design schematic

The catalytic conversion of glycerol over the different MgO materials was investigated using a gas-phase flow fixed bed reactor (Figure 1). The aqueous glycerol feedstock (50 wt.% in H$_2$O) was introduced to the reactor by a HPLC pump, set to a flow of 0.016 mL min^{-1}. The vaporised feed was subsequently carried through the system in a flow of argon typically 50 mL min^{-1} for 3 hours, unless stated otherwise. The pelleted catalyst (typically 0.5 g) was made up to 1 mL with SiC as a diluent. This was then mixed and packed into an 8 mm stainless-steel tube between plugs of quartz wool.

The catalyst bed was then. The feed first passed a pre-reactor heating tape which was set to 180 °C. The inlet introduced the feed into the pre-heater chamber at 300 °C. This proceeded to the catalyst bed which was heated at 320 - 440 °C).

The catalyst bed was heated using an electric furnace (LPC elements), which was fixed in place around the reactor tube. The bed temperature was monitored using a thermocouple. The temperature, post catalyst bed, was controlled using heating tape to avoid condensation of reaction products before collection. The liquid reaction products were passed through a 2–way tap, which for the first 2 hours and 15 minutes was fed through to a waste reservoir. After this time, when the reaction had reached steady state, they were collected.[6] The liquid reaction products were condensed in a cold trap for collection, this consisted of coiled loop leading from the reactor into a sealed vessel, both of which were cooled *via* submersion in ice water within a dewar. Uncondensed products and carrier gas were collected in the attached 10 L gas bag.

Subsequent analysis (and quantification) of the liquid and gaseous components was achieved by gas chromatography (GC). Qualitative analysis of the liquid phase was also conducted by Liquid chromatography – mass spectrometry (LC-MS), following a previously established method outlined by Smith *et al.*[7] Carbon-Hydrogen-Nitrogen (CHN) analysis was performed externally by Exeter Analytical UK Ltd. for total organic carbon analysis.

2.4.1 Product analysis

After reactions were completed, the condensed reaction solution was collected from the cold trap and a fixed quantity of cyclohexanol external standard (67 μ mol, 0.2 mL, 0.34 M) and 3 mL of H_2O was added. GC was used for the quantification of the reaction products. This was done by injecting both the collected liquid sample and the gaseous components into a GC. The different GC methods used are outlined in section 2.4.4.

2.4.2 Chromatography

The earliest uses of chromatography was in the arts and textile industries in the late 19th century, to separate pigments in paint mixtures.[8] This would occur *via* capillary action; cloth or paper would act as the stationary phase and water or alcohol (containing the pigments); the mobile phase. The largest pigment molecules would travel at a slower rate than smaller ones, this results in separation. In chromatography the sample mixture is passed into a mobile phase, which serves as a carrier, transporting the components through to a stationary phase. When passed into the stationary phase, the different chemical constituents will begin to separate as they interact based on their physical and chemical characteristics. Things that commonly affect this are their polarity and mass,

but this is often dependent on the nature of the stationary phase. Eventually, the compounds will elute from the stationary phase and be passed (by the mobile phase) to the detector. The time taken for a compound to pass through the stationary phase (from injection to detection) is known as the retention time.

The main forms of chromatography used in laboratories are gas chromatography (GC), liquid chromatography (LC), thin layer chromatography (TLC) and ion exchange chromatography. LC is similar to GC, but the substance is dissolved in a liquid and then passed through a solid stationary silica column. Different varieties of LC are either normal or reverse phase, this is in conjunction to the mobile and stationary phase polarities. TLC is a simple technique which uses a thin layer of solid, usually a silica material. The substance is dissolved and applied to the plate. Next the plate is placed upright in the mobile phase which will rise through it, this results in separation as the molecules travel at varying speed. Ion exchange chromatography uses the charge of substances to separate them. In this way using different pH mobile phases, the cation and anions can be separated as they interact differently.

2.4.3 Gas Chromatography (GC)

GC is a widely used, versatile analytical technique. It is generally accredited to be invented in 1952 by A.T. James and A.J.P. Martin.[9,10] As a form of chromatography, it is used for the separation and subsequent quantification of chemical compounds in solutions. It is an accurate and reliable technique for a wide range of organic compounds. A simplified schematic of a GC is shown in Figure 2.

In organic synthesis, GC is useful for purity analysis of a synthesised compound - allowing for an accurate % purity to be determined. Due to its ability to separate organic components, it can also be used to determine and quantify constituents in a solution. This makes it useful in the catalytic sciences, where it can be used to monitor the reactants produced and determine important factors, such as substrate conversion and reaction selectivity. It is also commonly employed in other industries. Its routinely used for quality control in manufacturing, especially with pharmaceuticals and fine chemicals, but also for water and environmental monitoring, food industries and other research purposes.[11–13]

In GC the mixture is vaporised and then carried through a column (stationary phase) to a detector, by a mobile phase (often N_2 or He).[14,15] The column can consist of variety of pore sizes, diameters, and linings, such as wax and other substances. Samples are introduced to the instrument by injection. A specific volume of sample will be taken into a syringe, which will then be injected into the inlet chamber. This can be done by hand, or, for higher reproducibility, an autosampler. An

autosampler also allows the running of many samples or reinjections without supervision. The mobile phase must be inert, so as not to change the nature and concentration of the compounds which have been introduced. A variety of different mobile phases can be used, such as He, N_2, Ar or H_2. Due to the increase in price and availability of He, there has been a collective move away from using it as a carrier gas as cheaper, more abundant, alternatives can now be used instead.[16] Once the sample is injected into the inlet, it is heated to a set point which is ideally above the substrates boiling point. The pressure can also be manipulated to vaporise the sample. A rubber septum sits on top of the inlet to stop the mobile phase and sample from being lost. Once vapourised, the sample will progress into the column which resides in an oven. Here, a temperature ramp is normally adopted to assist with the separation of the different substances. Often more than one type of column, which can vary by length, will be employed. The column will typically be up to 10 m but can be as long as 150 m, and will possess and internal diameter of between 0.1 and 0.53 mm. This will have the silica or wax, or other stationary phase coated on its insides, which the constituents in the sample will interact with.
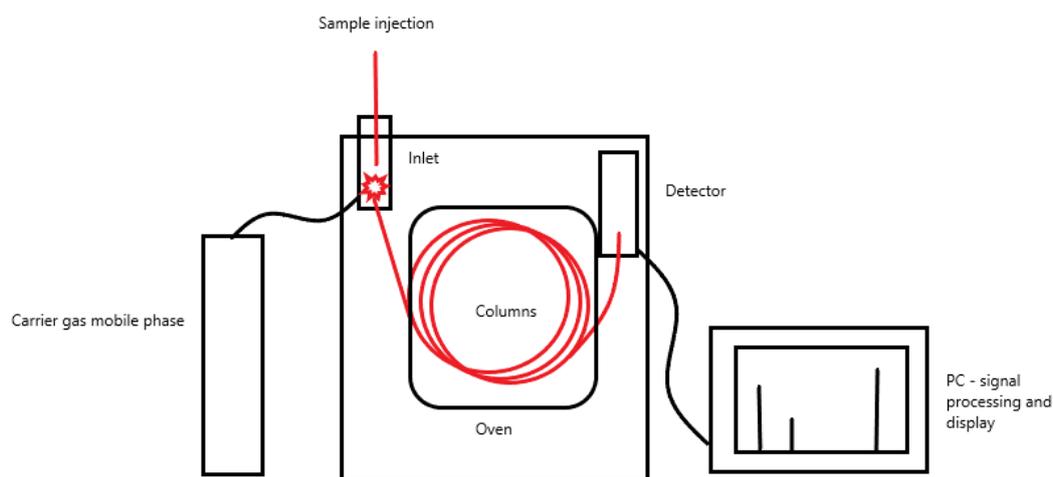
Figure 2. GC instrumentation schematic.

Several types of detectors can be employed in GC. These include detectors such as flame ionisation detectors (FID), temperature conductive detectors (TCD) and others, depending on the analytes and conditions of the analysis.

FIDs (shown in Figure 3) are commonly used the analysis of organic chemicals. These detectors are well suited for the detection of a wide range of hydrocarbons. FID can detect any molecules which undergo ionisation in a hydrogen-air flame. A 200-V polarization is applied across the flame jet and collector area. The hydrocarbons are combusted and ionised. These ions are then attracted by a potential difference towards the electrode, producing a small amount of current in the picometre scale. As solutes elute from the GC columns and are passed into the FID, they produce a current which is proportionate to the concentration of solute present.[17,18] The current is then converted

into a voltage and processed, to produce a signal on the associated chromatogram. This allows for quantification of a known solute once a response factor is determined *via* calibration.

Some of the advantages of FIDs are that they often generate a linear response. They also have a wide detection range, are relatively cheap and are typically low maintenance. They are however often poor for the detection of both highly oxygenated compounds and compounds which possess many different functional groups. For the detection of CO_2 and CO by FID, a methanizer is required. Methanizers are therefore extremely useful and rely on the hydrogenation of such compounds to allow for detection. A limitation of methanizers is that they possess a Ni catalyst, which can be easily poisoned.[19]
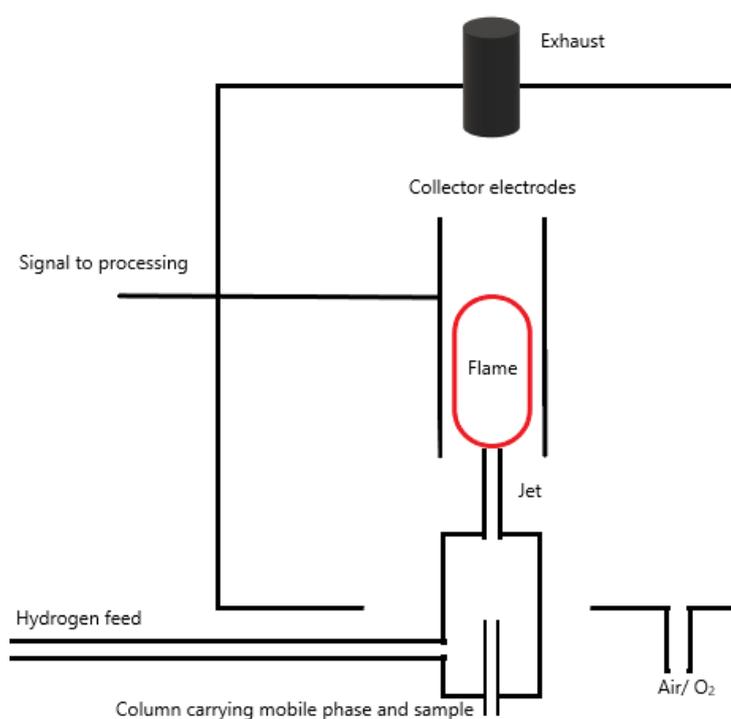
Figure 3. **FID schematic**

TCDs are another common detector used in conjunction with GC. TCDs are cheaper, rugged and dependable when a low concentration analysis is not required.[18] They do not require any extra gas, apart from the carrier. A TCD analyses the bulk conductivity of the effluent. It generates a response by comparing the difference in conductivity of the carrier gas and the column exhaust gas. He is commonly used as the carrier gas for TCDs. When no sample is present, there is a stable heat flow between the filament and detector. When a sample is present, the thermal conductivity of the effluent is altered leading to a difference in filament temperature and resistance. This change produces a signal that can be analysed to quantify the amount of sample present.

GC (and LC) is also commonly combined with mass spectrometers (MS), which can allow for more accurate identification of unknown compounds.[20] MS measures the mass to charge ratio of ions. An electron beam bombards the analyte resulting in positively charged ions or fragments of the analyte. These can be separated by their mass to charge ratio by exposure to a magnetic field. This can be used to help determine the identity of analytes by their known molecular mass and characteristic fragmentation pattern.[21]

Column choice is important in GC. Generally two types of columns are used: closed packed columns and capillary columns.[22]. Selection of an appropriate column composition and length is exceptionally important to achieve adequate separation. In a packed column, the stationary phase is coated directly onto the column. The first commercial instruments only used packed columns. They are often made of stainless steel and possess a diameter of between 0.32 to 0.64 cm. An inert, relatively high SA solid support within the column is impregnated with 5 – 20 % stationary phase. Packed columns are used due to relative low price, ruggedness, and better separation of non-polar samples.

Capillary columns are more commonly used today, accounting for around 80 % of use in 2015.[22] They are often longer, but more fragile and expensive, and exhibit excellent separation resolution and efficiency. They are also better for the separation of polar samples than packed columns. The tube is not packed, it is only coated on the walls. This produces less resistance and pressure build up. There are three general categories of capillary columns; wall coated open tubular columns, support-coated open tubular columns and porous layer open tubular columns.

There are several limitations for GC. For example, the GC inlet must operate within an appropriate temperature range high enough to vaporise the analytes of interest but not lead to thermal decomposition. If this range is small, it can lead to difficulties in accurate analysis at high substrate concentrations. Liquid and gas substrates with boiling points in the applicable range can be routinely analysed by GC. Solid samples would first need to be dissolved in an appropriate solvent. Upon injection, the samples are converted to the gas phase as they are passed into a heated inlet. Therefore, for accurate analysis, a molecule needs to be volatile and thermally stable, as not to degenerate into other products upon vaporisation. Thus, careful consideration of the molecular weights and boiling points of expected products is required, when designing an analysis method for a specific mixture.

2.4.4 Gas chromatography Experimental

Liquid and gas products were analysed offline by gas chromatography using an Agilent gas chromatograph (GC1) equipped with the following columns: a ZB-Wax plus - 30 m x 0.53 mm x 1

μm column, an 8 Ft molecular sieve 5A with 60/80 mesh column and 2 & 4 Ft Unibeads IS with 60/80 mesh column. Two GC methods were used, detailed below. This was necessary as the liquid and gaseous products were collected separately (in a cold trap and gas bag respectively). These had to be injected in separate runs on the GC. A separate run was needed for the gas bag sample to achieve good separation of the gas phase products. To separate and pass only CO and CO_2 over the TCD for analysis and the organics over the FID a separate method utilising the molecular sieve columns was required. A series of timed valve changes separated the CO and CO_2 from the organics directing them into the molecular sieves and over the TCD.

GC1: Method 1

The injector port was maintained at 250 °C and samples were introduced through a split-less injection. After injection of the liquid sample, the sample was passed through the ZB-Wax plus - 30 m x 0.53 mm x 1 μm column, a column temperature of 40 °C was held for 2 mins, before being ramped (20 °C min^{-1}) to 60 °C where it was held for a further 2 minutes. After this, the column temperature was increased to 220 °C (20 °C min^{-1}), where it was held for a further 15 minutes. Products were analysed using an FID, the temperature of which was maintained at 300 °C for the duration of the method. A glycerol calibration curve is shown in (appendix Figure 1); all liquid products were calibrated this way. (Appendix section see Figures 2 - 6)

GC1: Method 2

The initial column temperature was set to 60 °C and held for 2 minutes, before it was ramped to 220 °C (20 °C min^{-1}). Products were analysed using an FID and TCD, the temperature of these detectors were maintained at 300 °C and 250 °C, respectively.

Retention times for the liquid reaction components were identified by injection of standard samples into the GC, using the methods outlined above. For a typical liquid sample injection, a 1 μL syringe was used to inject 0.1 μL of sample by manual injection. For this, 3 mL of water and 0.2 mL (67 μ mol) of external standard (cyclohexanol, 0.34 M) solution. Quantification of reaction components was conducted using an external calibration method; response factors for analysis of liquid components were calculated by the injection of various concentrations of substrate in the expected concentration range. Glycerol was calibrated by preparing a range of samples, which represented different levels of conversion. The concentrations of the glycerol solutions prepared (and used for calibration) were analogous to 99 %, 95 %, 75 %, 50 %, 25 % and 0 % glycerol conversion, in a typical reaction. 0 % representing the substrate feed. The area of the substrate peak is divided by the external standard peak to give an area ratio and then plotted against the mole ratio to give a

calibration line where the slope was the response factor. (Appendix Figure 1) The gas phase organic analysis involved injecting known amounts of the organic dissolved in Ar into the GC and plotting ppm against area.

Table 1. Product list from GC analysis.

Product	Retention time		
	GC1 (liq FID) method 1	GC1 (gas FID) method 2	GC1 (gas TCD) method 2
Acetaldehyde	2.1	2.05	
propionaldehyde	2.6		
acetone	2.8	2.35	
acrolein	3.0	2.64	
butyraldehyde	3.3		
methanol	3.5	2.95	
2-propanol	3.9		
ethanol	4.0		
2,3-butanedione	4.6		
2-butanol	5.4		
1-propanol	5.7		
3-hexanone	6.0		
2-hexanone	6.3		
2-methyl-1-propanol	6.9		
allyl alcohol	7.0		
cyclopentanone	8.6		
hydroxyacetone	8.8		
3-ethoxy-1-propanol	8.9		
acetic acid	9.4		
Glycidol	9.9		
propionic acid	10.1		
1,2-propanediol	10.8		
ethylene glycol	11.0		
1,3-propanediol	12.3		
phenol	15.2		
unreacted glycerol	17.2		
CO			4.5

CO₂			5.4

Total selectivity to unknown products was estimated using the cumulative peak area of the unidentified GC chromatogram peaks and assuming an average of 3 carbon atoms per molecule. The approximate response factor was based on the average of the detected products response factors. The retention times of each product and the method which was used to quantify them are listed in Table 1. Product analysis results from the gas and liquid analysis were combined to give the full product analysis.

2.4.5 Liquid Chromatography – Mass spectroscopy.

Some additional qualitative analysis of the post reaction effluent was conducted by liquid chromatography-mass spectrometry (LCMS). Samples were diluted 100 x and then submitted for LCMS analysis. This was conducted on a Bruker Amazon SL ion trap mass spectrometer which was operated in positive electrospray ion mode and coupled to a Thermo Ultimate HPLC system. The HPLC was equipped with a C-18 column (maintained at 40 °C) and utilized a stepped elution. The stepped elution is shown in Table 2 consisting of 0.1% formic acid in H_2O (A) and 0.1% formic acid in acetonitrile (B). 10 µL of sample was injected. Detection parameters are fixed at 100 - 1000 m/z.

Table 2. The makeup of the mobile phase for the gradient elution Time

Time (min)	A (%)	B (%)
0.0	98	2
1.0	98	2
15.0	2	98
17.0	2	98
18.0	98	2
20.0	98	2

2.4.6 Carbon-Hydrogen-Nitrogen (CHN)

CHN analysis can be used to accurately measure the elemental concentration of carbon, hydrogen or nitrogen in a given sample. This is done *via* combustion analysis. Flash combustion results in oxidisation of the sample into simple molecules such as CO_2 which are then detected *via* TCD or infrared spectroscopy. CHN analysis was performed externally by Exeter Analytical UK Ltd. for total organic carbon (TOC) analysis.

2.5 Catalyst Characterisation

A variety of analytical and spectroscopic techniques were used to characterise the solid MgO catalysts prepared in this thesis. Many techniques are considered key for the characterisation of MgO and both qualitative and quantitative data can be obtained.

2.5.1 Powder X-ray diffraction (XRD)

X-ray diffraction (XRD), also known as X-ray crystallography, is an analytical technique which can be used to help determine key characteristics of a crystalline sample. It produces a characteristic spectrum, which can be matched to the international centre for diffraction data (ICDD) catalogue. Other parameters such as the crystallites size can also be determined using the Scherrer equation (Eqn. 10). This utilizes the full width half maximum (FWHM) of key crystal plain reflections. It is an important technique in the evaluation of heterogeneous catalysts.[23,24]

In XRD, an X-ray source is focussed onto the sample. The samples' crystalline structure causes the incident X-rays to diffract into a variety of angles. The intensity and angle of these can be measured and shown visually. This allows the user to see a 3D picture of the density of electrons within the crystal lattice. The data gained can be used to calculate the positions of atoms, chemical bonds, and a variety of other parameters.

XRD is widely used, but the sample needs to exhibit some crystallinity to be analysed. However, it is still widely applicable as a large variety of materials can form crystal structures. A variety of other naturally occurring crystals of inorganic materials such as salts, metals, and semiconducting and biological material can also form crystals, thus, making them applicable for study by XRD.

Common applications for the use of XRD in catalytic research is structure related; determination of crystallites formed, determination of crystallite purity, identification of component phases and crystallite size. These parameters will relate to the surface structure of the catalyst and can be used to identify key and important characteristics that can affect a catalysts effectiveness. There are often relationships with specific catalytic preparation procedures and observed physiochemical properties. For example, higher heat treatments will often result in the sintering of a material, this will affect characteristics such as the SA decreasing and thus, result in an increase in crystallite size.[25] There are several important laws and equations needed in XRD. Bragg's law (Eqn.9) can be used to calculate parameters such as the lattice spacing in a particular sample.[26] The lattice parameter is used to describe the dimension of a unit cell (repeating contained unit) within the crystal lattice of the sample. Depending on the type of structure, the lattice of a crystal possesses three different constants referred to as a, b, and c. These would normally coincide with the x, y and

z planes respectively. Generally, the average lattice parameter would be given for a particular temperature. This is important as it is unlikely that this will be homogeneous in an imperfect sample, specifically near the samples surface where it may deviate from this determined average significantly.

The calculation of the lattice parameter spacing requires knowledge of the X-ray wavelength order of reflection, in addition to the incident angle (θ), as shown below:

$$n\lambda = 2d \sin \theta \qquad (9)$$

Eqn 9. Bragg's law for obtaining the lattice parameter from XRD data. Where n = an integer representing the reflection order, λ = the electromagnetic radiation wavelength, d = lattice spacing and θ = the diffraction angle.

When reflections are detected, a plot of reflection intensity *vs* incident angle can be constructed. Using this, the crystallite size of a given reflection can be determined using the Scherrer equation (Eqn 10). For this, the FWHM of the most intense diffraction peaks are used, those which are identified as being characteristic of a specific phase. The more crystalline the sample, the more intense and narrow the peaks will appear. On the contrary, less intense peaks which are broad is typically indicative of poor crystallinity.

$$\tau = K\lambda \, / \, \beta \, COS \, \theta \qquad (10)$$

Eqn 10. Scherrer Equation for the calculation of crystallite sizes from reflection data obtained from powder XRD. Where τ = crystallite size in the direction perpendicular to the reflecting plane, K = a constant normally between 0.9-1 based on the crystallite shape. λ = X-ray wavelength, β = peak width, θ beam angle.

The schematic in Figure 4 shows how incident X-rays are elastically scattered. Using the Bragg equation (Eqn 9.), the scattering angle (Θ) can be used to identify the lattice spacing (d) of the sample and the wavelength (λ) of the incident X-ray radiation. In operation, X-rays need to be first generated in an X-ray tube. This occurs by the bombardment of a copper surface with high energy free electrons. This causes excitation in the Cu electron shell to higher levels. When the excited electrons relax back to their ground state, they release energy as Kα and Kβ X-rays. Kα emission is produced from an electron transitioning from a n=2 L shell to n=1 K shell, Kβ X-rays are produced from a transition from n=3 M shell to the n=1 K shell. Kα is usually required for XRD when using a Cu source, so a filter is used to remove the Kβ X-rays from the stream. Kα is more intense and monochromatic and Cu Kα also has a wavelength of 1.5406 Å which should be smaller than the

interatomic size allowing for the scattering diffraction to take place. Kβ wavelength is more variable and can lead to higher degree of noise to signal.
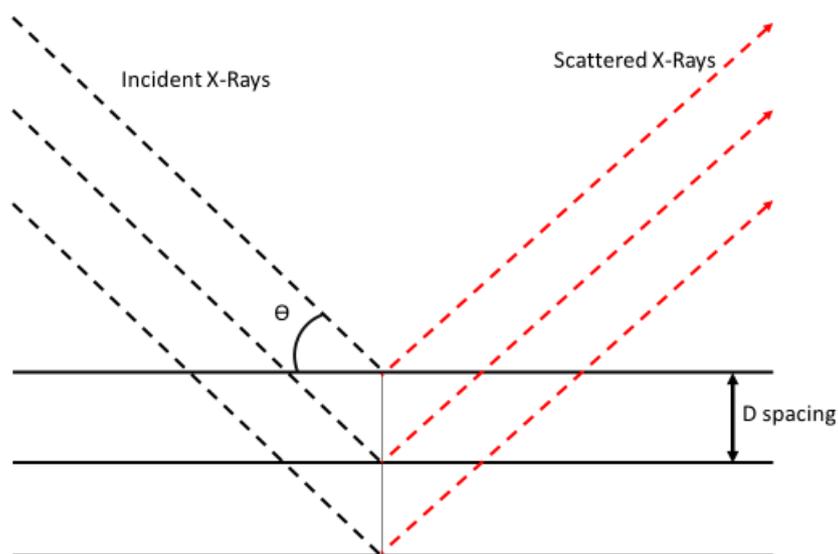
Figure 4. X- ray scattering in accordance to the braggs law.[26,27]

This beam of Kα X-rays can then be focussed onto the sample under investigation. During the experiment, the X-ray source angle moves across a range, usually 10 ° to 80 ° allowing for the X-rays to be focussed on the sample from a variety of angles. When the X-rays meet the substrate's crystal lattice, they are scattered by the sample's atom and either constructively or destructively interfere. The scattered radiation is observed using a detector. If the sample is highly crystalline it is more likely to result in higher intensity constructive interference, which results in large intensity reflection peaks recorded. However, if the sample exhibits a lower degree of crystallinity, then there will be more destructive interference observed, reducing reflection intensity.

The detector scans the wide range of angles over the progress of the sample run. This is important as it allows for all the different possible angles of diffraction from the crystals to be observed. In the powder, the sample powder particles will be randomly orientated, so scanning from every direction is necessary to build up a full spectrum.

2.5.2 XRD Experimental

Powder XRD was conducted using a PANalytical X'Pert Pro system fitted with a CuKα X-ray source run at 40 kV and 40 mA. An X'Celerator detector was used to assess the scattered media. Each sample was scanned over a 2θ range of 10° to 80° with a step size of 0.016° for 30 minutes. Catalysts

were ground into a fine powder and loaded onto a silicon wafer. The resultant data was subsequently compared directly with data held in the ICDD library.

2.5.3 Surface Area (SA) Analysis

SA of solid substances is measured using specialised instruments. These instruments usually rely on monitoring gas adsorption and desorption to calculate a materials SA, and other characteristics. They typically use BET theory (Brunauer – Emmett – Teller)[14,28], BJH theory (Barrett, Joyner, and Halenda) and t-plot analysis (discussed later). BET typically involves the measurement of SA using a 5-point isotherm. In such experiments, N_2 is normally used as a probing adsorption gas, as it is unlikely to react with the substance in question. When N_2 is used, it is required that the temperature of the experiment is cooled to the boiling temperature of N_2 (77K or -196 °C). However other absorbates can also be used such as argon, carbon dioxide and water, depending on the experiment being conducted. N_2 is traditionally used as the adsorptive due to its abundance. However, the quadrupole moment of a N_2 molecule can lead to uncertainty in the value of the molecular cross-sectional area; up to 20 % depending on sample surface chemistry.[29] Argon can be used for more reliable analysis due to its lack of quadrupole moment and it is more inert than N_2. This makes it less likely to interact with surface functional groups. However, a temperature of 87K is required, so liquid argon or a cryostat is needed for accurate analysis. Argon is especially good for micropore analysis, as can result in a faster equilibrium and a higher adsorption isotherm resolution than N_2.[30] This is due to argon at 87K filling narrow micropores at a higher relative pressure than N_2 at 77K.[31]

The BET theory of multilayer gas adsorption is based on a modified version of the Langmuir theory, which is usually only applicable to monolayer molecular adsorption (Figure 5). The BET method accounts for several of the assumptions made in Langmuir theory. The Langmuir adsorption model theory [32] makes many assumptions; (i) the adsorbate behaves as an ideal gas while the temperature remains stable and that the surface of adsorption is a perfectly flat plane and that the gas becomes immobile once it adsorbs, (ii) that all site energies are identical, (iii) that only one molecule and be adsorbed to a site *via* mono layer adsorption and (iV) there are no interactions between neighbouring sites.

The BET theory amends this to be more flexible and accurate to real experimental conditions and different types of adsorptions such as multi-layer adsorption (Figure 5), allowing for infinite layers to form. Other amendments to the hypothesis include: the gas molecules can interact with adjacent layers; the Langmuir adsorption model is applicable to an individual layer. The enthalpy of adsorption has the highest energy for the first layer, this energy is the same for liquefaction for the subsequent layers.

The BJH method is used to calculate pore size distributions from experimental isotherms.[33] It can be used to determine pore sizes in the mesopore and macropore range. It uses the Kelvin model for pore filling [34] and is based on the Wheeler theory of combined physical adsorption. It analyses the N_2 desorption isotherm to compute the pore size and distribution throughout a wide range of pore sizes.

T-plot analysis developed by de Boer *et al.*[35] allows for the calculation of micropore area and volume. Using this method, these estimations can be derived without measuring the low pressure micropore portion of the isotherm. It is applicable for use in a range of multi-layer adsorption, with instrumentation which do not possess the necessary low pressure analysis capabilities.
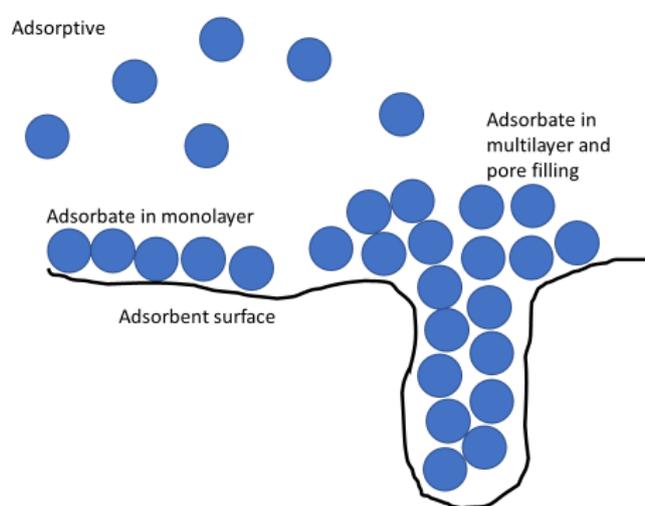
Figure 5. **Adsorption of probe gas on a samples surface.**

In practice, SA analysis works due to the assumption that the maximum amount of gas adsorbed onto a sample surface depends on the area of the exposed surface. Factors such the pressure of absorbent, temperature, the adsorbate gas, and the surfaces affinity for each other also affect the volume of gas adsorbed. While N_2 has a relatively high level of interaction with solids, generally, this would be negligible at room temperature, so the sample is cooled with the liquid N_2. This allows for far higher degrees of adsorption to be achieved which, in turn, allows for detection and measurement. A partial vacuum is created, and small but measured amounts of N_2 are released into the sample cell. The pressure of N_2 is then gradually increased, leading to more adsorption. Once no more adsorption is observed the saturation pressure has been reached. After saturation, the sample is removed from the cold trap and warmed to allow for desorption to be measured. These changes of pressure and volume adsorbed can be plotted as an isotherm, from which data can be utilized to determine various parameters.

2.5.4 BET Surface Area (SA) and BJH pore size Analysis Experimental

SA and porosity measurements were estimated through conducting 5-point or 20-point N_2 adsorption 20-point desorption isotherms at 77 K on a Quadrasorb evo™ Gas Sorption Surface Area and Pore Size Analyser. The BET method was used to calculate SA, using a 5-point isotherm. Pore size distributions were estimated using the BJH method, this was done through analysing the desorption curves from 20-point adsorption/desorption isotherms. These isotherms are presented in the appendix Figures 8-11. Prior to the analysis, *ca.* 0.1 g of samples were degassed at 220 °C for 3 h, under vacuum. These were then weighed to obtain the final catalyst mass and transferred to the Quadrasorb evo instrument. Liquid nitrogen was used for sample cooling and an automated program was used to run the 5- and 20-point experiments. The instrument software calculated the SA using the BET method and the pore sizes using the BJH method.

2.5.5 CO_2 Temperature Programmed Desorption (CO_2 TPD)

TPD is a technique that monitors interactions between an adsorbed molecule and a samples surface. TPD is commonly used for measuring catalyst characteristic parameters such as a basicity and acidity.[36] TPD can also investigate other gas solid adsorption characteristics such as binding energies, energies of activation of desorption, rate constants and reaction orders.[37] When investigating acidic sites, a basic molecule such as ammonia is used as the probe molecule. On the contrary for investigating basicity, CO_2 is employed. Through using these probe molecules, the strength of basic and acid sites in a sample, and their relative proportions, can be established.

Common methodology for this process is to insert a known quantity of the solid sample into a glass U-shaped tube, which is connected to the instrument (Figure 6). This sample tube would reside in the furnace of the instrument. The sample can then undergo a pre-treatment, where it is exposed to an inert gas flow, such as He, and heated to a pre-set temperature. This temperature will depend on the type of catalyst and preparation it underwent. The temperature of the pre-treatment should be high enough to remove surface adsorbed species, but not sufficiently high to induce any structural changes to the sample. The pre-treatment process is important, as it removes any surface impurities or atmospheric adsorbents from the sample surface, prior to analysis, as these could interfere with the experimental data acquired. For example, the adsorption of atmospheric water could result in the formation of surface hydroxides, and adsorption of atmospheric CO_2 could lead to the formation of carbonates. This is to make sure that the response seen is accurate to the sample's actual characteristics and atmospheric adsorbents are not blocking the active sites that

would otherwise lead to adsorption of the probe molecule. Such pre-treatments are therefore critical for deriving accurate quantitative data.

After the pre-treatment, the sample is cooled to room temperature under an inert gas and then the absorbate molecule can be flowed over it at a defined flow rate, for a defined time. After this period, the carrier gas is then switched back to an inert gas flow, and the samples is heated at a fixed rate. This results in the desorption of CO_2, or similar species, from the surface which then passes through the instrument and over a TCD, which records a response. The amount of CO_2 passing over the detector at a given temperature can be quantified, through reference to response factors from external calibrations. In this way different strength sites can be identified, as well as their density on the surface. Desorption at lower temperatures would be indicative of low strength sites, as the probe molecule is weakly bound and could include physisorbed species. Desorption at higher temperatures would be indicative of strong sites, where the probe molecule it is strongly (chemically) bound.
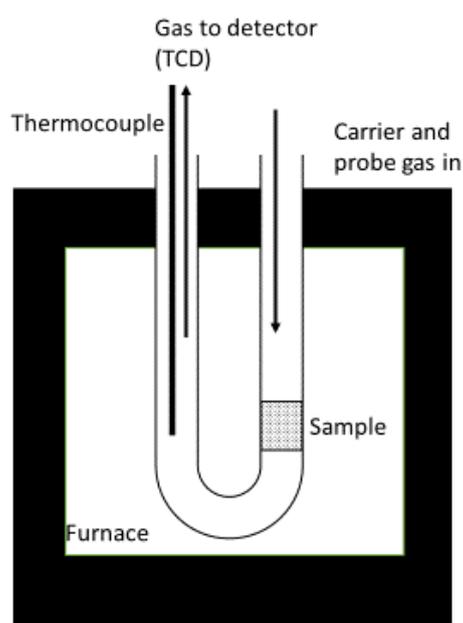
Figure 6. **TPD Sample compartment**

2.5.6 CO_2 Temperature Programmed Desorption (CO_2 TPD) Experimental

CO_2 temperature programmed desorption was conducted on a Quantachrome ChemBET TPR. 0.1 g of sample (300 - 425 mesh) was pre-treated at 400 °C (15 °C min^{-1}) for 1 hour, under flowing He (80 mL min^{-1}). CO_2 was subsequently passed over the material at room temperature, for 20 minutes. Physiosorbed CO_2 was then removed by heating the sample to 110 °C (15 °C min^{-1}) under flowing

He (80 mL min^{-1}) and holding for 1 hour. Chemisorbed CO_2 was subsequently desorbed by heating the sample to 900 - 1100 ^{0}C (15 °C min^{-1}) under flowing He (80 mL min^{-1}). Desorbed CO_2 was monitored by using a TCD detector (180 mV) and quantified using an external calibration method.

Quantification of basicity was calculated by using the integration value from the CO_2 desorption and dividing it by the calibration factor to obtain the number of moles of CO_2 desorbed. (Appendix Figure 7). This was then divided by the catalyst mass to obtain the number of moles of CO_2 desorbed per gram of catalyst (eqn. (1)). This value could then be divided by the catalysts SA_{cat} to determine the number of moles of CO_2 desorbed per m^2 of catalyst (eqn. (2)).

2.5.7 Thermogravimetric analysis (TGA)

Thermogravimetric analysis (TGA) is a useful technique for studying mass changes in a sample. The technique is usually simple to carry out and does not require significant sample preparation. It can be used to determine factors and transformations caused by thermal input, which result in a measurable change in mass. Physical changes that can occur to a sample can include changes of state of the sample such as fusion, sublimation, vaporisation, phase and crystalline transitions, desorption, adsorption, and absorption.[38] It can also measure chemical changes, including: chemisorption, decomposition and oxidation and reduction reactions.[39] This can be combined with MS to provide detailed information on the substances desorbing from the sample at different temperatures. For these reasons, TGA is important tool for catalyst characterisation and due to its ease of use, is commonly employed in catalytic sciences. A schematic diagram of a typical TGA instrument is shown in Figure 7. .

In the study of heterogeneous catalysis, TGA is often employed to observe and quantify residual coke on a catalyst post reaction. Such information is therefore critical for assessing catalyst stability. It can also be used to calculate the cokes contribution to the carbon balance, by estimating the carbon lost to coke formation in a particular reaction.[40–42]

Changes in state of the sample, that result in a change of the samples mass, is recorded, and plotted against temperature. Often, a sample may exhibit several changes of mass, over a range of temperatures, indicting different changes in state.

TGA is often combined with differential thermal analysis (DTA) and differential scanning calorimetry (DSC). DTA is used determine whether the transitions observed are endothermic or exothermic. Endothermic reactions such as the sample melting will cause a dip in temperature of the sample compared to a reference. Exothermic reactions which produce heat will see a peak. DSC provides similar information but measures the amount of energy used to keep both samples the same

temperature. TGA-DSC can be used to measure heat of reactions in catalytic systems, allowing for a quick analysis of activity.[43]
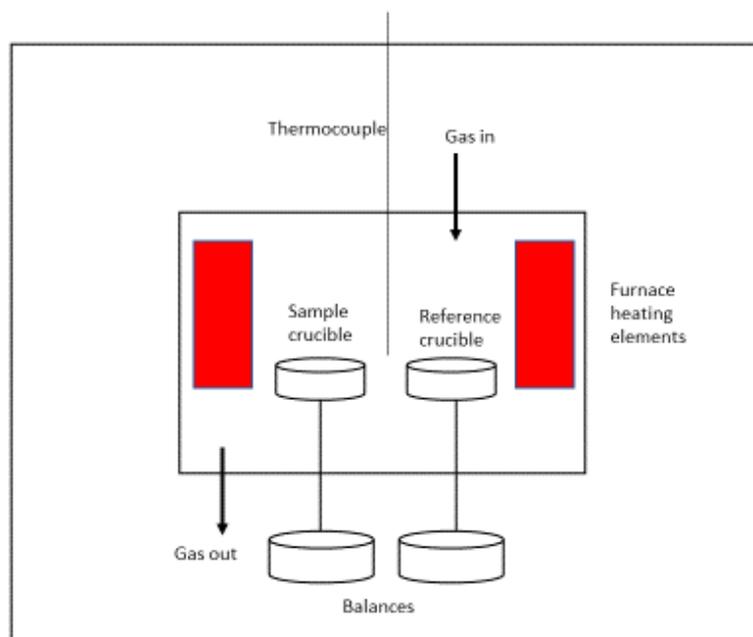
Figure 7. TGA instrument schematic

2.5.8 Thermogravimetric Analysis (TGA) Experimental

Carbon deposition following a catalytic reaction was monitored by thermal gravimetric analysis (TGA) and differential thermal analysis (DTA) and performed on a Setaram Labsys 1600 instrument. Samples (50 mg) were loaded into alumina crucibles and heated to 800 °C (5 °C min^{-1}) in a flow of synthetic air (50 mL min^{-1}). Carbon deposition in the form of catalyst coke (eqn. 6) was estimated from the mass loss *via* TGA of the post reaction catalyst. The mass of carbon lost was converted to the number of moles of carbon retained on the catalyst (X_{coke}) and divided by the number of carbon moles in the glycerol feed (g_{mi}). Phase transitions were monitored by analysing the temperature of mass changes over fresh material samples.

2.5.9 CO$_2$ Adsorption Diffuse Reflectance Infrared Fourier Transform Spectroscopy (DRIFTS)

Diffuse reflectance infrared Fourier transform spectroscopy (DRIFTS) is an IR spectroscopy technique than can be used on powder samples.[44] In infrared spectroscopy, the interaction of the infrared light produced from a source and the sample is measured (Figure 8). This can give the user information on a variety of parameters, such as the chemical structure of the surface. Absorption, emission, and reflection are all important. A chemical compound will have a unique fingerprint spectrum which can be used to identify it. Information such as specific types of bonds and functional groups will be observable on the surface of a sample.

The mid-infrared region, which is between 4000-400 cm^{-1}, is the region which is of most interest in IR spectroscopy. Absorbance, observed in IR spectroscopy, is due to how molecules absorb different frequencies of IR light. This is unique to an individual molecules structure and is otherwise known as resonant frequency – between the light and the molecules vibrational frequency. The types of vibrational modes which can be observed with simple organic molecules include two types of radial stretching: symmetric and asymmetric, and the various types of bending: longitudinal twisting/wagging and latitudinal Rocking/scissoring. Some of the more important bands you can see for an IR species are excitations, where a molecules energy is promoted from its ground state.

DRIFTS is especially useful in study of heterogenous catalysts,[45–48] as it can help identify surface species present, without exposing them to conditions which may remove or change such species. DRIFTS can also be used for *in-situ* experiments under reaction conditions, it can be used to see the consumption of substrate, production of intermediates and products.[45,46,49] The samples rough surface diffusely reflects the instruments incident light in all directions, which are then collected and directed to the detector by a paraboloid or ellipsoid mirror. The properties of the materials surface, such as the colour and roughness effect the amount of the IR light which is reflected. The sample is typically contained in a glass chamber, in which different in-situ conditions can be enacted, such as heating and the flowing and adsorption of specific gases. This allows for it to be a good supplemental experiment for CO_2 TPD, where the nature of the bonds of the sites with CO_2 observed at different temperatures can be investigated. In DRIFTS experiments, probe molecules such as CO_2 can cause chemical bonds with the sample surface, this results in absorbances characteristic of different bonding geometries. This can help the identification of different types of sites on a basic surface, as they would adsorb probe molecules in different ways.

2.5.10 CO_2 Adsorption Diffuse Reflectance Infrared Fourier Transform Spectroscopy Experimental

DRIFTS measurements were carried out using a Brüker DRIFT tensor 27 FTIR spectrometer using CO_2 as the probe molecule. The instrument was fitted with a mercury cadmium telluride (MCT) detector, which was cooled with liquid N_2. DRIFTS spectra were recorded in the 4000-1000 cm^{-1} range, using a spectral resolution of 6 cm^{-1} (64 scans/spectrum) using a Praying Mantis high-temperature (HVC-DRP-4) in situ cell with KBr windows. Samples were first pre-treated in-situ at 400 °C for 2 hours in flowing N_2 (18 mL/min^{-1}). Background spectra were recorded at 400 °C, 300 °C, 200 °C, 100 °C and room temperature. After cooling, CO_2 was subsequently passed over the sample (3 mL/min^{-1}) in N_2 (18 mL/min^{-1}) for 20 minutes. Spectra were then taken at room temperature, 100 °C, 200 °C, 300 °C and 400 °C.
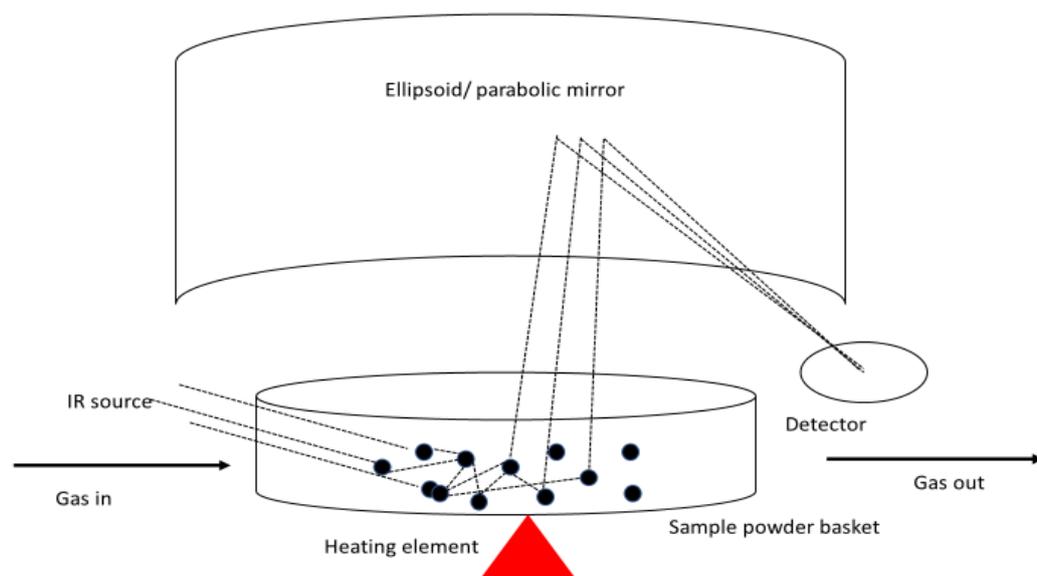
Figure 8. DRIFTS instrumentation sample chamber schematic

2.5.11 Electron microscopy

Electron microscopy is an extremely useful technique in materials science. Often, extremely high magnifications are possible, which allows the user to visualise a samples surface at the nanoscale. Morphological features, which may only be observable at this scale, can be exceptionally important to catalyst performance. Electron microscopes utilize magnetic field 'lens' to control and focus electron beams. There are two primary types of electron microscopes used in the catalytic sciences: scanning electron microscopes (SEM) and the transmission electron microscopes (TEM). These microscopes can be used to acquire information on a range of different properties, including: morphology, unit cell measurements, particle size measurements, elemental mapping, tomography and the *in-situ* analysis of a materials surface upon exposure to different temperatures or chemicals.[50,51]

2.5.11.1 Scanning electron microscopy (SEM)

SEM does not typically achieve as high magnification level as TEM. In SEM, images are constructed as a focussed electron beam scans across a samples surface. Scan speed and energy of the beam are all important parameters which need to be controlled to optimise resolution and detail.

In SEM, the electron beam is usually emitted from a tungsten filament cathode. Tungsten is commonly used due to its high melting temperature. This beam is focussed through a condenser lens to a point, typically between 0.4 to 5 nm. The image is created *via* raster scanning of the electrons across the sample, as the beam is swept across the x and y axis of the samples surface.

The electron beams used in SEM interact with the sample in a teardrop shaped penetration, termed the interaction volume. Random scattering and adsorption cause energy exchange between the beam and sample.

Secondary electrons are species that are inelastically scattered when ejected from the specimens' shells by beam interactions. The secondary electrons are the often most analysed and detected electrons and exhibit a low energy of less the 50 electron volts. Due to being ejected from the samples valence or conduction bands they will be sourced from near the surface, usually only a couple of nanometres down at most. The energy of these electrons in increased with attraction to a 400 V + grid followed by a 2000 V scintillator which causes cathodoluminescence, which can be detected and shown in a video display of intensity. This results in the formation of the image of the samples surface. Secondary electron detection in SEM can produce well-defined images with a strong 3-D quality, due to high depth perception. Edges and steep sides appear bright, this is because; as the angle of beam incidence increases, the interaction volume increases. This allows for more secondary electrons to be emitted. The more electrons emitted the brighter the visualisation will be.

Beam-sample interactions also cause high energy elastically scattered electrons, known as back scattered electrons (BSE) and electromagnetic radiation. BSE result from the incident beam electrons being reflected or scattered elastically. BSE can be used to help detect distribution of different types of atoms depending on the energy they are scattered with. BSE detection uses a detector placed in a ring arrangement above the sample. An advantage of SEM over TEM is that it requires significantly less sample preparation and can be done with larger bulk samples.

2.5.11.2 Transmission Electron Microscopy (TEM)

TEM (Figure 9) is a very powerful tool for catalyst surface analysis, allowing for exceptionally high magnification.[52] The higher level of magnification allows for resolutions of up to the low nanometres or picometre range. There are several extra parameters that can be explored using TEM, the magnification level can allow for the measuring of crystal planes and crystallite sizes, which can be used to confer with XRD results. For analysis by TEM, a sample must be prepared as a thin layer; *ca.* 100 nm or less in thickness, which is more time consuming than SEM preparation. This is required as in TEM the electron beam needs to penetrate entirely through the sample as the transmitted beam must interact with the atoms of the sample.

For the electron beam to be focussed enough to achieve atomic resolution, it must pass through a series of lenses. Lens in TEM usually consist of a solenoid coil surrounded by a ferromagnetic

material. This directs electrons in the beam, concentrating them to a focussed point. Controlling the lens current allows for the magnification level to be changed. Magnification range is wide with atomic resolutions possible up to mm scales. Another important component is the apertures. Apertures serve several purposes. They help reduce x-ray generation, improve vacuum performance, and stop electrons passing outside the lens. This reduces the effect of aberrations. Aperture placement below the sample can produce a crystal diffraction pattern. Projector lenses are employed to produce the image on a fluorescent screen which can be subsequently recorded.
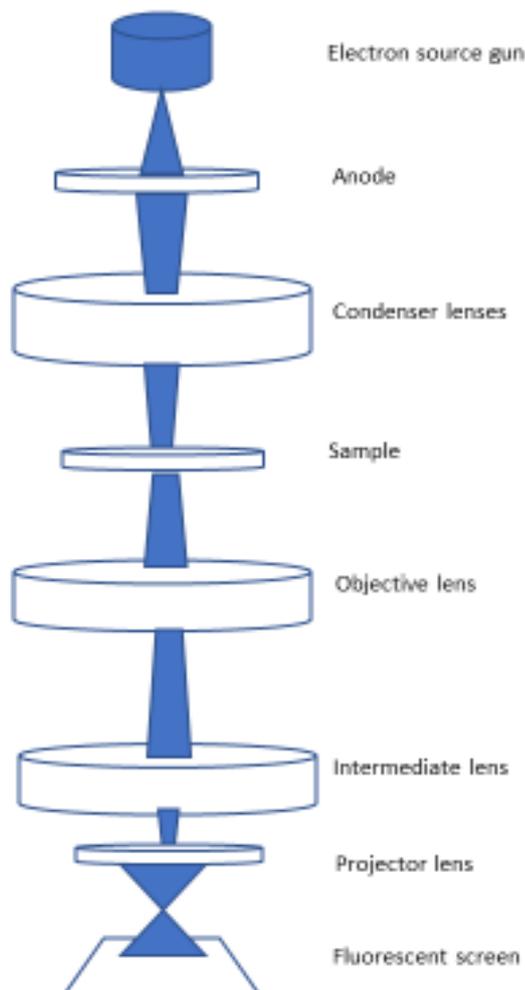
Figure 9. **Simplified typical TEM**

2.5.12 Electron Microscopy Experimental

Microscopy was performed on a Tescan Maia3 field emission gun scanning electron microscope (FEGSEM) fitted with an Oxford Instruments XMAXN 80 energy dispersive X-ray detector (EDX). Images were acquired using the secondary electron and backscattered electron detectors. Samples were dispersed as a powder onto 300 mesh copper grids coated with holey carbon film.

Transmission electron microscopy (TEM) and scanning transmission electron microscopy (STEM) were performed on a JEOL JEM-2100 operating at 200 kV. Samples were prepared by dispersion in ethanol by sonication and deposited on 300 mesh copper grids coated with holey carbon film

2.6 References

(1)   Xu, C.; Bartley, J. K.; Enache, D. I.; Knight, D. W.; Hutchings, G. J. High Surface Area MgO as a Highly Effective Heterogeneous Base Catalyst for Michael Addition and Knoevenagel Condensation Reactions. *Synthesis (Stuttg).* **2005**. https://doi.org/10.1055/s-2005-918467.

(2)   Bartley, J. K.; Xu, C.; Lloyd, R.; Enache, D. I.; Knight, D. W.; Hutchings, G. J. Simple Method to Synthesize High Surface Area Magnesium Oxide and Its Use as a Heterogeneous Base Catalyst. *Appl. Catal. B Environ.* **2012**, *128*, 31–38. https://doi.org/10.1016/j.apcatb.2012.03.036.

(3)   Di Cosimo, J. I.; Díez, V. K.; Ferretti, C.; Apesteguía, C. R. Basic Catalysis on MgO: Generation, Characterization and Catalytic Properties of Active Sites. *Catalysis* **2014**, *26* (3000), 1–28. https://doi.org/10.1039/9781782620037-00001.

(4)   Calatayud, M.; Ruppert, A. M.; Weckhuysen, B. M. Theoretical Study on the Role of Surface Basicity and Lewis Acidity on the Etherification of Glycerol over Alkaline Earth Metal Oxides. *Chem. - A Eur. J.* **2009**. https://doi.org/10.1002/chem.200900487.

(5)   Khalaf, A. J.; Hargreaves, J.; David, J. S. Base Catalysis with Metal Oxides. In Metal Oxide Catalysis. *Met. Oxide Catal.* **2009**. https://doi.org/doi:10.1002/9783527626113.ch21.

(6)   Haider, M. H.; Dummer, N. F.; Knight, D. W.; Jenkins, R. L.; Howard, M.; Moulijn, J.; Taylor, S. H.; Hutchings, G. J. Efficient Green Methanol Synthesis from Glycerol. *Nat. Chem.* **2015**, *7* (12), 1028–1032. https://doi.org/10.1038/nchem.2345.

(7)   Smith, L. R.; Smith, P. J.; Mugford, K. S.; Douthwaite, M.; Dummer, N. F.; Willock, D. J.; Howard, M.; Knight, D. W.; Taylor, S. H.; Hutchings, G. J. New Insights for the Valorisation of Glycerol over MgO Catalysts in the Gas-Phase. *Catal. Sci. Technol.* **2019**, 19–22. https://doi.org/10.1039/C8CY02214C.

(8)   Williams, K. R. Colored Bands: History of Chromatography. *J. Chem. Educ.* **2002**, *79* (8), 922. https://doi.org/10.1021/ed079p922.

(9)   Bartle, K. D.; Myers, P. History of Gas Chromatography. *TrAC Trends Anal. Chem.* **2002**, *21* (9), 547–557. https://doi.org/https://doi.org/10.1016/S0165-9936(02)00806-3.

(10)   James, A. T.; Martin, A. J. P. Gas-Liquid Partition Chromatography: The Separation and Micro-Estimation of Volatile Fatty Acids from Formic Acid to Dodecanoic Acid. *Biochem. J.* **1952**, *50* (5), 679–690. https://doi.org/10.1042/bj0500679.

(11)   Vetter, W. Current Use of Gas Chromatography and Applications. In *Analytical Separation Science*; American Cancer Society, 2015; pp 849–882. https://doi.org/https://doi.org/10.1002/9783527678129.assep026.

(12)   Rohn, S. Gas Chromatography in Food Analysis. In *Practical Gas Chromatography: A Comprehensive Reference*; Dettmer-Wilde, K., Engewald, W., Eds.; Springer Berlin Heidelberg: Berlin, Heidelberg, 2014; pp 745–766. https://doi.org/10.1007/978-3-642-54640-2_21.

(13)   Grob, R. L.; Kaiser, M. A. Chapter 5 The Use Of Gas Chromatography In Environmental Analyses. In *Environmental Problem Solving Using Gas and Liquid Chromatography*; Grob, R. L., Kaiser, M. A., Eds.; Journal of Chromatography Library; Elsevier, 1982; Vol. 21, pp 137–186. https://doi.org/https://doi.org/10.1016/S0301-4770(08)70100-3.

(14)   Harris, D. C. Gas Chromatography. In *Quantitative chemical analysis*; W.H Freeman & company, 2016; p 667.

(15)   Turner, D. *Gas Chromatography – How a Gas Chromatography Machine Works*. Technology networks - analysis and separations. https://www.technologynetworks.com/analysis/articles/gas-chromatography-how-a-gas-chromatography-machine-works-how-to-read-a-chromatograph-and-gcxgc-335168.

(16)   Heseltine, J. Hydrogen as a Carrier Gas for GC and GC–MS. *LCGC North Am.* **2010**, *28* (1), 16–27.

(17)   Hinshaw, J. V. *The Flame Ionization Detector*. LCGC North America. https://www.chromatographyonline.com/view/flame-ionization-detector.

(18)   McMinn, D. CHROMATOGRAPHY: GAS | Detectors: General (Flame Ionization Detectors and Thermal Conductivity Detectors); Wilson, I. D. B. T.-E. of S. S., Ed.; Academic Press: Oxford, 2000; pp 443–447. https://doi.org/https://doi.org/10.1016/B0-12-226770-2/00171-X.

(19)   Porter, K.; Volman, D. H. Flame Ionization Detection of Carbon Monoxide for Gas Chromatographic Analysis. *Anal. Chem.* **1962**, *34* (7), 748–749. https://doi.org/10.1021/ac60187a009.

(20)   Sparkman, O. D.; Penton, Z. E.; Kitson, F. G. Chapter 1 - Introduction and History. In *Gas Chromatography and Mass Spectrometry (Second Edition)*; Sparkman, O. D., Penton, Z. E., Kitson, F. G., Eds.; Academic Press: Amsterdam, 2011; pp 2–13. https://doi.org/https://doi.org/10.1016/B978-0-12-373628-4.00001-0.

(21)   Downard, K. The Mass Spectrometer. In *Mass Spectrometry: A Foundation Course*; RSC, 2004; pp 22–66. https://doi.org/10.1039/9781847551306.

(22)   Rahman, M. M.; Abd El-Aty, A. M.; Choi, J.-H.; Shin, H.-C.; Shin, S. C.; Shim, J.-H. Basic Overview on Gas Chromatography Columns. In *Analytical Separation Science*; American Cancer Society, 2015; pp 823–834. https://doi.org/https://doi.org/10.1002/9783527678129.assep024.

(23)   Hargreaves, J. S. J. Powder X-Ray Diffraction and Heterogeneous Catalysis. *Crystallogr. Rev.* **2005**, *11* (1), 21–34. https://doi.org/10.1080/08893110500078324.

(24)   Perego, G. Characterization of Heterogeneous Catalysts by X-Ray Diffraction Techniques. *Catal. Today* **1998**, *41* (1), 251–259. https://doi.org/https://doi.org/10.1016/S0920-5861(98)00054-6.

(25)   Moya, J. S.; Baudín, C.; Miranzo, P. Sintering; Meyers, R. A. B. T.-E. of P. S. and T. (Third E., Ed.; Academic Press: New York, 2003; pp 865–878. https://doi.org/https://doi.org/10.1016/B0-12-227410-5/00694-3.

(26)   Bragg, W. H.; Bragg, W. L. The Reflection of X-Rays by Crystals. *Proc. R. Soc. London. Ser. A, Contain. Pap. a Math. Phys. Character* **1913**, *88* (605), 428–438. https://doi.org/10.1098/rspa.1913.0040.

(27)   Jeffery, G. A. Elements of X-Ray Diffraction (Cullity, B. D.). *J. Chem. Educ.* **1957**, *34* (4), A178. https://doi.org/10.1021/ed034pA178.

(28)   Brunauer, S.; Emmett, P. H.; Teller, E. Adsorption of Gases in Multimolecular Layers. *J. Am. Chem. Soc.* **1938**, *60* (2), 309–319. https://doi.org/10.1021/ja01269a023.

(29)   Thommes, M.; Kaneko, K.; Neimark, A. V.; Olivier, J. P.; Rodriguez-Reinoso, F.; Rouquerol, J.; Sing, K. S. W. Physisorption of Gases, with Special Reference to the Evaluation of Surface Area and Pore Size Distribution (IUPAC Technical Report). *Pure Appl. Chem.* **2015**, *87* (9–10), 1051–1069. https://doi.org/10.1515/pac-2014-1117.

(30)   Thommes, M.; Kaneko, K.; Neimark, A. V; Olivier, J. P.; Rodriguez-Reinoso, F.; Rouquerol, J.; Sing, K. S. W. Physisorption of Gases, with Special Reference to the Evaluation of Surface Area and Pore Size Distribution (IUPAC Technical Report). *Pure Appl. Chem.* **2015**, *87* (9–10), 1051–1069. https://doi.org/doi:10.1515/pac-2014-1117.

(31)   Rouquerol, F. *Adsorption by powders and porous solids : principles, methodology and applications*; 1999. https://doi.org/https://doi.org/10.1016/B978-0-12-598920-6.X5000-3.

(32)   Langmuir, I. THE ADSORPTION OF GASES ON PLANE SURFACES OF GLASS, MICA AND PLATINUM. *J. Am. Chem. Soc.* **1918**, *40* (9), 1361–1403. https://doi.org/10.1021/ja02242a004.

(33) Barrett, E. P.; Joyner, L. G.; Halenda, P. P. The Determination of Pore Volume and Area Distributions in Porous Substances. I. Computations from Nitrogen Isotherms. *J. Am. Chem. Soc.* **1951**, *73* (1), 373–380. https://doi.org/10.1021/ja01145a126.

(34) Haynes, J. M. Pore Size Analysis According to the Kelvin Equation. *Matériaux Constr.* **1973**, *6* (3), 209–213. https://doi.org/10.1007/BF02479035.

(35) de Boer, J. H.; Lippens, B. C.; Linsen, B. G.; Broekhoff, J. C. P.; van den Heuvel, A.; Osinga, T. J. Thet-Curve of Multimolecular N2-Adsorption. *J. Colloid Interface Sci.* **1966**, *21* (4), 405–414. https://doi.org/https://doi.org/10.1016/0095-8522(66)90006-7.

(36) Jentoft, F. C. 7.09 - Solid Acids and Bases. In *Comprehensive Inorganic Chemistry II (Second Edition)*; Reedijk, J., Poeppelmeier, K., Eds.; Elsevier: Amsterdam, 2013; pp 205–230. https://doi.org/https://doi.org/10.1016/B978-0-08-097774-4.00720-8.

(37) Barrie, P. J. Analysis of Temperature Programmed Desorption (TPD) Data for the Characterisation of Catalysts Containing a Distribution of Adsorption Sites. *Phys. Chem. Chem. Phys.* **2008**, *10* (12), 1688–1696. https://doi.org/10.1039/B717430F.

(38) Coats, A. W.; Redfern, J. P. Thermogravimetric Analysis. A Review. *Analyst* **1963**, *88* (1053), 906–924. https://doi.org/10.1039/AN9638800906.

(39) Parameshwaran, R.; Sarı, A.; Jalaiah, N.; Karunakaran, R. Chapter 13 - Applications of Thermal Analysis to the Study of Phase-Change Materials. In *Recent Advances, Techniques and Applications*; Vyazovkin, S., Koga, N., Schick, C., Eds.; Handbook of Thermal Analysis and Calorimetry; Elsevier Science B.V., 2018; Vol. 6, pp 519–572. https://doi.org/https://doi.org/10.1016/B978-0-444-64062-8.00005-X.

(40) Hernandez, D.; Velasquez, M.; Ayrault, P.; Lopez, D.; Fernandez, J. J.; Santamaria, A.; Batiot-Dupeyrat, C. Gas Phase Glycerol Conversion over Lanthanum Based Catalysts: LaNiO3and La2O3. *Appl. Catal. A Gen.* **2013**, *467*, 315–324. https://doi.org/10.1016/j.apcata.2013.07.016.

(41) Li, B.; Gonzalez, R. D. The Measurement of Small Amounts of Coke by a Sensitive TGA/FTIR Technique. *Catal. Letters* **1998**, *54* (1), 5–8. https://doi.org/10.1023/a:1019055200591.

(42) Zhang, H.; Shao, S.; Xiao, R.; Shen, D.; Zeng, J. Characterization of Coke Deposition in the Catalytic Fast Pyrolysis of Biomass Derivates. *Energy and Fuels* **2014**, *28* (1), 52–57. https://doi.org/10.1021/ef401458y.

(43) Loskyll, J.; Maier, W. F.; Stoewe, K. Application of a Simultaneous TGA-DSC Thermal Analysis System for High-Throughput Screening of Catalytic Activity. *ACS Comb. Sci.* **2012**, *14* (11), 600–604. https://doi.org/10.1021/co3000659.

(44) Fuller, M. P.; Griffiths, P. R. Diffuse Reflectance Measurements by Infrared Fourier Transform Spectrometry. *Anal. Chem.* **1978**, *50* (13), 1906–1910. https://doi.org/10.1021/ac50035a045.

(45) Hu, J.; Zhu, K.; Chen, L.; Kübel, C.; Richards, R. MgO(111) Nanosheets with Unusual Surface Activity. *J. Phys. Chem. C* **2007**, *111* (32), 12038–12044. https://doi.org/10.1021/jp073383x.

(46) Meunier, F. C.; Reid, D.; Goguet, A.; Shekhtman, S.; Hardacre, C.; Burch, R.; Deng, W.; Flytzani-Stephanopoulos, M. Quantitative Analysis of the Reactivity of Formate Species Seen by DRIFTS over a Au/Ce(La)O2 Water-Gas Shift Catalyst: First Unambiguous Evidence of the Minority Role of Formates as Reaction Intermediates. *J. Catal.* **2007**, *247* (2), 277–287. https://doi.org/10.1016/j.jcat.2007.02.013.

(47) Stavitski, E.; Weckhuysen, B. M. Infrared and Raman Imaging of Heterogeneous Catalysts. *Chem. Soc. Rev.* **2010**, *39* (12), 4615–4625. https://doi.org/10.1039/C0CS00064G.

(48) Concepción, P. Application of Infrared Spectroscopy in Catalysis: Impacts on Catalysts Selectivity. *Infrared Spectrosc. - Princ. Adv. Appl.* **2019**.

(49) Meunier, F. C. Pitfalls and Benefits of: In Situ and Operando Diffuse Reflectance FT-IR Spectroscopy

(DRIFTS) Applied to Catalytic Reactions. *React. Chem. Eng.* **2016**, *1* (2), 134–141. https://doi.org/10.1039/c5re00018a.

(50)   Yang, J. C.; Small, M. W.; Grieshaber, R. V; Nuzzo, R. G. Recent Developments and Applications of Electron Microscopy to Heterogeneous Catalysis. *Chem. Soc. Rev.* **2012**, *41* (24), 8179–8194. https://doi.org/10.1039/C2CS35371G.

(51)   Thomas, J. M. Reflections on the Value of Electron Microscopy in the Study of Heterogeneous Catalysts. *Proc. R. Soc. A Math. Phys. Eng. Sci.* **2017**, *473* (2197), 20160714. https://doi.org/10.1098/rspa.2016.0714.

(52)   Pennycook, S. J. Transmission Electron Microscopy: A Textbook for Materials Science, Second Edition. David B. Williams and C. Barry Carter. Springer, New York, 2009, 932 Pages. ISBN 978-0-387-76500-6 (Hardcover), ISBN 978-0-387-76502-0 (Softcover). *Microsc. Microanal.* **2010**, *16* (1), 111–111. https://doi.org/10.1017/S1431927609991140.

Chapter 3

MgO catalyst characterisation and vapour phase glycerol reaction testing

3.1 Introduction

Understanding how the physical and chemical properties of magnesium oxide (MgO) influences the vapour phase conversion of glycerol is key to improving desirable product yields. In previous investigations using MgO for the vapor phase conversion of glycerol, a 'standard' preparation of MgO was used.[1,2] This sample was prepared by calcining $Mg(OH)_2$ for 24 hours at 450 °C, followed by refluxing in H_2O for 3 hours. The precipitate was then dried and subsequently heat treated at 450 °C for 3 hours in flowing N_2. This sample is referred to as (MgO_STD) in this thesis. There were several motivations for the use of this preparation. Firstly commercial MgO and $Mg(OH)_2$ have a low surface area (SA) of around 20-30 m^2 g^{-1}, in the procedure the reflux rehydration stage allows for a significant increase in the catalyst SA.[3] Another advantage with this preparation procedure is that it is relatively simple and reliable way to produce significant amounts of catalyst. While energy is required for the thermal transitions, the preparation is otherwise environmentally benign as there is no requirement for expensive or hazardous reagents and solvents, only $Mg(OH)_2$ H_2O and N_2 are used. The results are presented in Smith *et al.*[1] MgO_STD was tested for the vapour phase conversion of glycerol, the results for the experiments using a 50 wt.% glycerol feedstock are shown in Table 1. Methanol space time yields (STY) of 131 g^1 h^{-1} kg_{cat}^{-1} was observed at 360 °C, increasing to 205 g^1 h^{-1} kg_{cat}^{-1} at 400 °C, further temperature increases did not yield a higher amount of methanol, with the STY staying stable at 204 g^1 h^{-1} kg_{cat}^{-1}. However, the carbon mass balance (CMB) for this reaction was 77 %, this indicated that some of the products were not quantified. It was deemed unlikely that the missing carbon was due entirely to reactor fouling, especially at 360 °C, and was postulated to be possibly due to condensation products not detected reliably *via* GC-FID.

Investigations into glycerol concentration, temperature and catalyst free tests have been conducted using the same prepared sample of MgO_STD.[1,2] However unlike with CeO_2,[4,5] there has not been any work investigating how the properties of the MgO itself would affect its reaction performance. This means that trends between MgO catalyst characteristics such as its basicity, surface area (SA) and crystallinity are yet to be developed for this reaction. This chapter focuses on simple variations to the catalyst preparation technique and how this has a significant impact on catalyst characteristics and reaction performance. Specifically, attempts were made to make

catalyst samples with altered basicity characteristics. The aim here was to investigate a possible expected link between the sample basicity and the CMB.

Table 1. Glycerol conversion and product distribution over MgO at different temperatures. Reaction conditions: 50 wt % glycerol (0.016 mL min⁻¹), 0.5 g MgO, 50 mL min⁻¹ Ar, 3 hours. Data reproduced from L. R. Smith, P. J. Smith, K. S. Mugford, M. Douthwaite, N. F. Dummer, D. J. Willock, M. Howard, D. W. Knight, S. H. Taylor and G. J. Hutchings, Catal. Sci. Technol., 2019, 19– 22.

Condition (°C)	Conversion %	CMB % () includes C in coke	Methanol STY $(g^1 h^{-1} kg_{cat}^{-1})$	Carbon deposition (mg g^{-1})
360	74	74 (77)	131	81
400	90	73 (77)	205	122
440	100	68 (73)	204	125
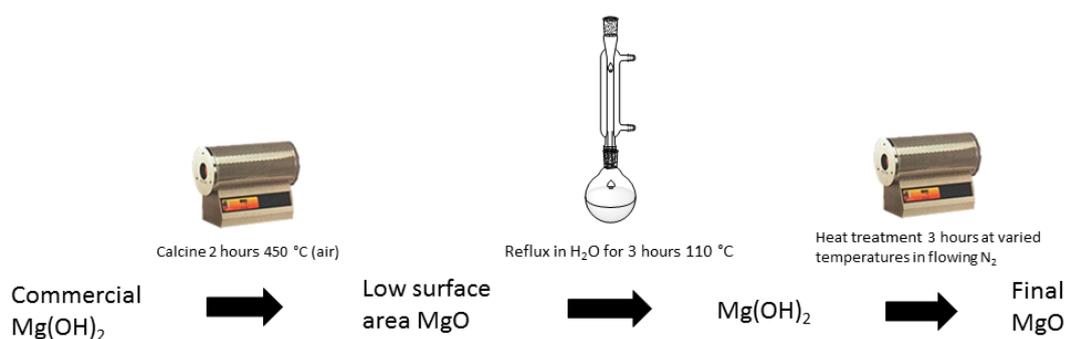
Figure 1. MgO varied heat treatment temperature preparation scheme.

For this reason, a series of MgO catalysts were synthesised, extensively characterised, and employed as catalysts for this reaction. As to only alter minimal characteristic parameters, a simple alteration was made to each catalyst's preparation; the final heat treatment under N_2. The primary goal was to change properties such as the SA and basicity. The series of MgO catalysts, apart from using different heat treatment conditions, were synthesised based on an established preparation method of MgO_STD.[1,2] This modified method of MgO synthesis involves two heat treatment steps: the first a calcination of commercially sourced $Mg(OH)_2$ in a static air furnace at 450 °C for 2 hours and the second, in an inert N_2 atmosphere for 3 hours (Figure 1). In between these two treatments the calcined sample was refluxed in water to promote rehydroxylation. The MgO obtained from the commercially available $Mg(OH)_2$ at 450 °C has a low SA of 24 m^2 g^{-1} and crystallite size of 8 nm. Therefore, methods that involve techniques such as calcining/rehydrating or hydrothermal treatments are a necessary step to increase the SA of samples for catalysis.[6–8] XRD patterns for each stage of preparation are available in appendix Figure 12. The MgO_STD has a SA of 129 m^2 g^{-1} and

crystallite size of 8 nm.[8] (XRD pattern - Figure 2). MgO samples were produced with varied final heat treatment in N_2, with 450 °C, 550 °C, 650 °C and 750 °C. These were termed MgO_450, MgO_550, MgO_650 and MgO_750 respectively.

3.2 Results and discussion

After synthesis, the catalyst samples were characterised using a variety of methods, this was to build a full picture of their surface and chemical attributes. Following this, the influence of the physicochemical properties on the catalyst performance was evaluated.

3.2 Characterisation

3.2.1 X-ray diffraction

First, the samples were probed by X-ray diffraction (XRD). This was to identify that MgO had been successfully prepared, the phase type and that $Mg(OH)_2$ was not present to a significant degree. Diffraction patterns were obtained from experiments over the powder materials processed through comparison with a Si standard to estimate the associated crystallite sizes of the samples. The Scherrer equation was used to calculate the approximate crystallite size from the MgO (200) diffraction peaks. Crystallite sizes are expected to be inversely proportional to SA; lower SA materials are predicted to have larger crystallite sizes than their higher SA counterparts. The corresponding diffraction patterns for the series of MgO samples are displayed in Figure 2(a). All the samples exhibited well defined sharp reflections, indicating a high level of crystallinity. The samples exhibited a high concurrence with established reference patterns obtained from the International Centre for Diffraction Data (ICDD),[9] which indicated that the each of the materials possessed a periclase type crystal structure.

As the temperature of the second heat treatment was increased, the calculated crystallite sizes of the materials increased relatively linearly until exceeding 650 °C. First the crystallite size increases between MgO_450 to MgO_550 from 6.2 nm to 7.5 nm (Table 2). When the calcination temperature was increased from MgO_550 to MgO_650 the crystallite size increased from 7.5 nm to 8.4 nm. When the temperature is increased further for production of MgO_750, a sharp increase of crystallite size takes place of approximately 70 %. The calculated lattice parameters show a mirrored trend to this (Figure 2 (b)). Sharp increases in parameters such as crystallite size are not unknown. A similarly large increase in crystallite size, albeit at a lower temperature, was observed by Di Cosimo *et al.*[10] In this study, the authors observed that the crystallite size increased marginally from 7.4 nm to 7.7 nm when raising the temperature from 400 °C to 500 °C. However, when the temperature was increases to 600 °C the crystallite size increased dramatically to 14.3 nm. Once a specific temperature is surpassed, it seems that the crystallites size increases dramatically. It is

therefore plausible to suggest that the higher temperatures may drive some kind of morpholgical change.
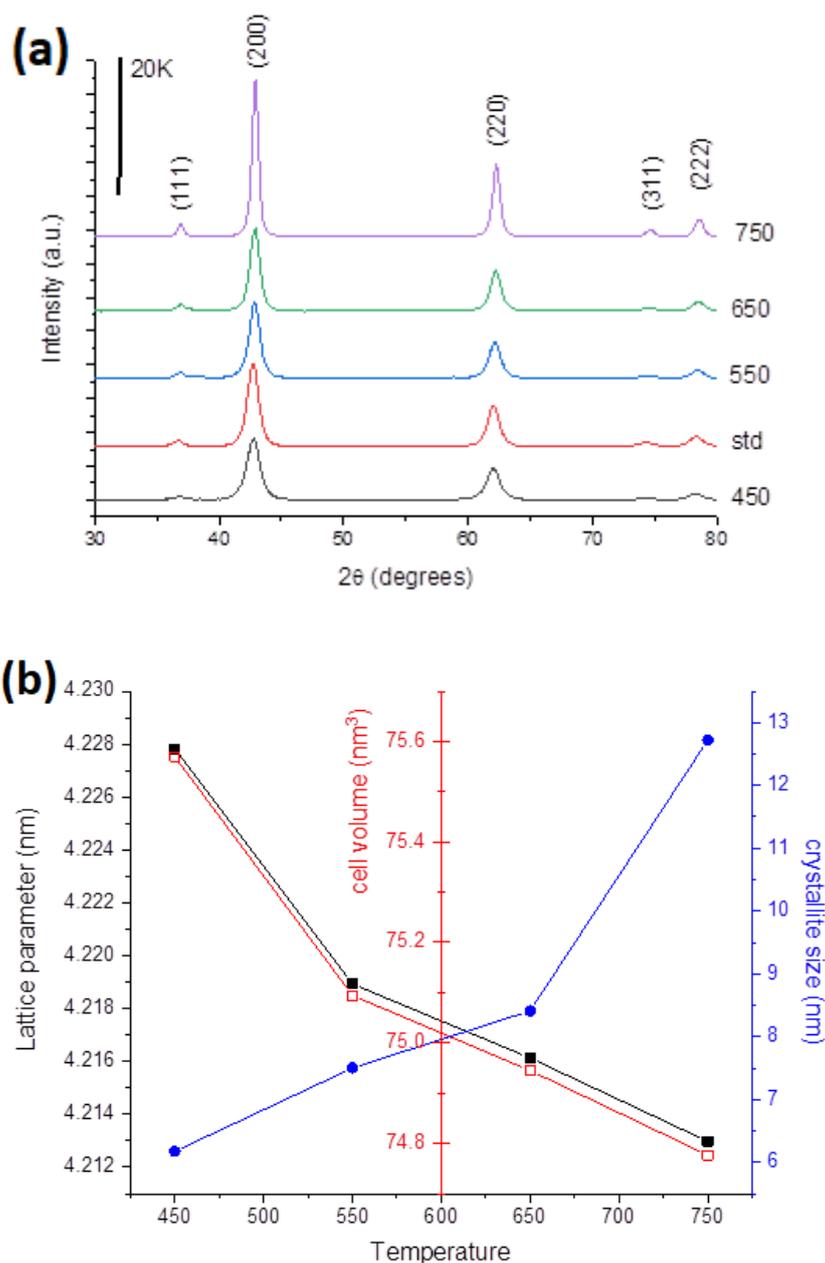
Figure 2. (a) Powder XRD patterns for catalysts MgO_450 (black), MgO_550 (blue), MgO_650 (green), MgO_750 (purple). (b) based on the (200) reflection: Lattice parameter, cell volume and crystallite size a function of heat treatment temperature.

3.2.2 Assessment of the textural properties by N_2 physisorption

3.2.2.1 BET surface area analysis

The textural properties of a solid can have a profound effect on its performance as a catalyst. The aim here was to explore how the heat treatment temperature effects the SA and how this correlates

with the crystallite sizes. The SAs of the synthesised catalysts were therefore assessed from the associated isotherms using a 5-point BET method. This analysis was conducted on a Quadrasorb gas adsorption analyser. The SAs determined were 187, 154, 125 and 74 m^2 g^{-1} for the MgO_450, MgO_550, MgO_650 and MgO_750, respectively (Table 2). This shows a relatively linear decrease in SA with temperature, as highlighted in Figure 3. The reduction in SA correlates with the crystallinity of the materials; crystallinity increases as the SA is reduced (Table 2).

Evidently, increasing the final heat treatment temperature resulted in a relatively proportional decrease in the SA of the material. When higher temperatures are used in the preparation of MgO, OH groups and defects can be removed, leading to a thermodynamically more stable and smoother structure.[10–14] Sintering also has been reported in several studies with MgO previously and is a common occurrence with high SA solid materials.[3,10] Changes in SA with the temperature treatment would be expected to affect trends for other characteristics such as the crystallite size and base site distribution or concentration.[10]

3.2.2.2 Pore size analysis

To investigate the SA further, the pore volume and pore radius of the materials were derived, through re-evaluation of the associated N_2 physisorption isotherms (appendix Figures 8 – 11). The pore data is shown in Table 2 and Figure 3. The volume of pores of the catalyst materials decrease on the increase of the heat treatment temperature. The trend in pore volume was relatively linear until MgO_750, which shows a sharp decrease. Pore volumes for MgO_450, MgO_550 and MgO_650 were determined to be 0.95, 0.89 and 0.83 (cc/g), respectively. However, the pore volume of the MgO_750 sample was determined to be less than half that of the MgO_650 sample; 0.32 (cc/g) This is possibly due to collapse of the pore structure over a certain threshold temperature. A similar sharp collapse with different MgO samples has been observed in previous literature, albeit at a higher temperature of 800 °C.[15]

The pore radius were also derived from the isotherms, but no clear trend with the thermal treatment temperature was established. The MgO_450 sample exhibited a radius of 17.9 Å, which increased to 118.3 Å with MgO_550. This is the highest value for radius, which subsequently decreased to 89.8 Å in the MgO_650 sample and 44.6 Å in the MgO_750. This reinforces the hypothesis that structural and physical changes occur during the final heat treatment under N_2.

Table 2. Surface area analysis parameters. BET m² g, Pore volume cc/g, Pore radius (Å) and XRD diffraction crystallite sizes

Catalyst ID.	BET (m²/g)	Pore volume (cc/g)	Pore radius (Å)	Crystallite sizes nm	Proportional increase in crystallite size
MgO_450	187	0.95	17.9	6.2	/
MgO_550	154	0.89	118.3	7.5	0.2
MgO_650	125	0.83	89.8	8.4	0.1
MgO_750	74	0.31	44.6	12.7	0.5
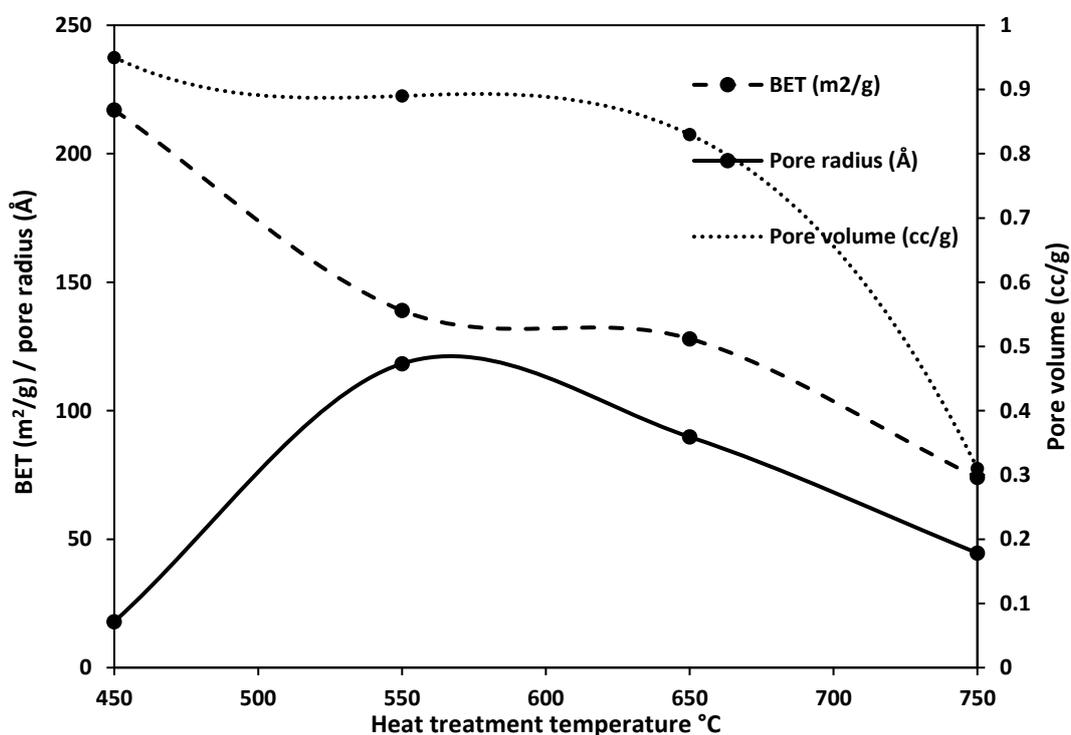
Figure 3. Surface area parameters graph BET m² g, Pore volume cc/g, Pore radius (Å).

3.2.3 Scanning electron microscopy and transmission electron microscopy

So far, the characteristics of the catalyst samples obtained *via* N_2 adsorption techniques and XRD indicate that some unexpected process is occurring on increasing the heat treatment temperature, evidenced by the pore radius and crystallite size. This may be due to an unidentified type of phase change during the heat treatment, but no evidence of this has yet been observed. To try and investigate, the samples were analysed *via* scanning *electron* microscopy (SEM). This allows for the samples to be explored for morphologically differences at microscale or nanoscale. The images for SEM for the series of catalysts are shown in Figure 4.
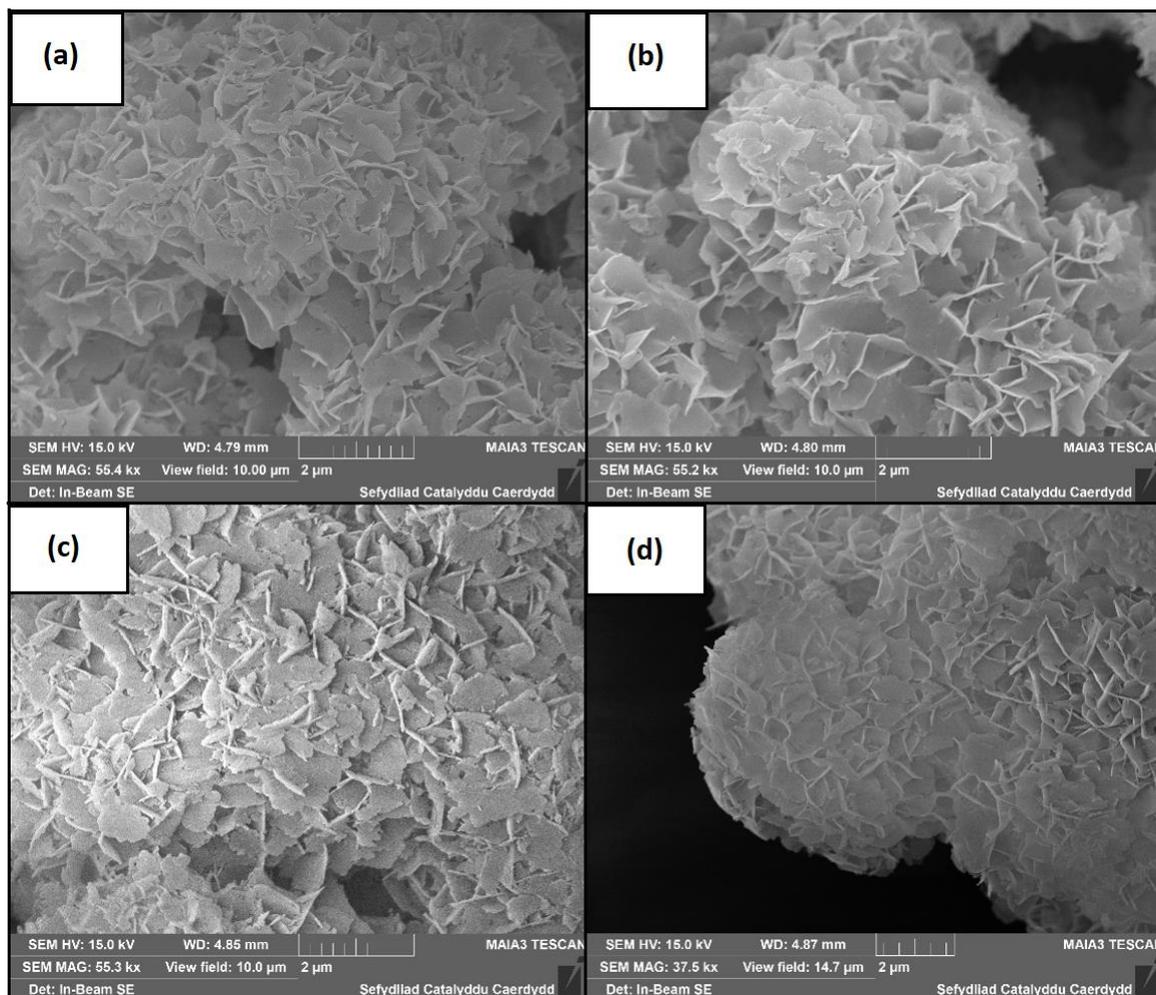
Figure 4. SEM images of powder samples of MgO_450 (a) MgO_550 (b) MgO_650 (c) MgO_750 (d).

As can be seen from the images, these samples resemble an arranged interlocked 'nanoflake' morphology, which is similar to what has been observed previously with MgO.[16] This morphology is considered to form during the reflux step of the preparation, as MgO is rehydrated to $Mg(OH)_2$. It is known that morphology can be retained upon thermal transition back to MgO, when heated anaerobically.[17] The loss of H_2O may create pores and defects as vapor forces itself out of the material bulk.[7] However, overall, the structure seen here at this scale is likely not significantly changed *via* the heat treatment. They may exhibit a slight decrease in definition as the temperature increases. Overall, at the level of magnification possible with SEM there is no distinct morphological differences between the MgO samples at microscale. While the SEM analysis reveals the morphology of the samples, it has not significantly contributed to the understanding of how the materials are different and how this relates to characteristics such as the pore and crystallite size changes. This led to the samples being analysed *via* transmission electron microscopy (TEM) to view the nanostructure. These images are shown in Figure 5.
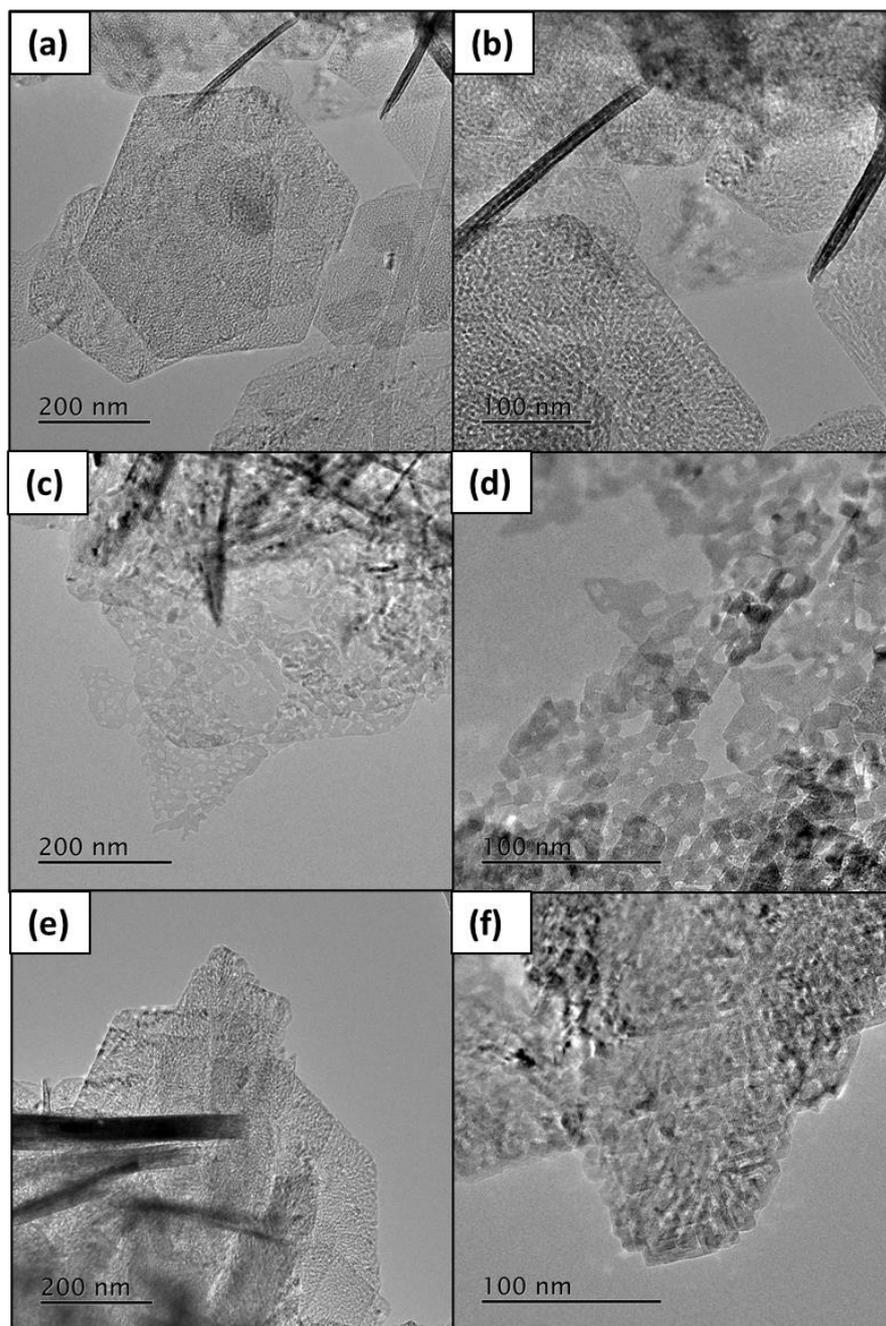
Figure 5. Representative TEM micrographs of the MgO_450 (a) and (b), MgO_650 (c) and (d), MgO_750 (e) and (f)) catalysts

The TEM analysis revealed that a well-defined hexagonal platelet structure is present on MgO_450 and MgO_750. It has shown that these can be produced simply with hydration of MgO with deionised water and that thermal treatment in N_2 can result in the morphology being retained.[18] Similar arrangements of structure at this scale of MgO and $Mg(OH)_2$ has been observed when several preparation strategies have been adopted for MgO synthesis.[16,19–22] Interestingly, a clear lack of this structure was observed in the MgO_650 sample. When increasing the temperature from

450 °C to 650 °C, (MgO_450 to MgO_650) the hexagonal structure appears to degrade, forming an ill-defined globular-like texture. The individual units are more random and visibly larger for MgO_650, there is little evidence of the formation of the larger hexagonal platelets. The material seems to have conglomerated. This can be possibly partially explained due to sintering or degradation; however, this does not explain why MgO_750 does not show this loss of ordered structure. Higher temperatures would be expected to cause a higher degree of sintering. Within the images there also seems to be some thicker nanorod structures that have formed, which can be also observed in other preparations.[23,24] These are more evident, larger, and well defined in MgO_450 and MgO_750. However, these may also be attributed to side-on platelets. MgO_650 does not clearly exhibit these features in a significant quantity or size.

The presence of the ordered structure at the 450 °C and 750 °C but not at 650 °C treated catalysts is unexplained. One possible explanation could be that MgO_650 represents an intermediate stage where the material structure is undergoing rearrangement. This indicates that the structure may begin to re-crystalize at higher temperatures of 750 °C (MgO_750). On increasing the temperature to 650 °C (MgO_650) there is a significant change in the sample's microstructure. MgO_650 retains its periclase crystal structure (Figure 3) but on analysis of the images (Figure 5) seems to possess proportionally large degree of irregular intercrystallite channels. Evidence of this occurring before has led to it being considered to be due to the formation and exfoliation of water molecules from the structure as $Mg(OH)_2$ is dehydrated.[7] Increasing the temperature to 750 °C (MgO_750) results in a similar nanostructure to that observed with MgO_450. The TEM indicates that the crystallites have started to aggregate producing a lamella-like structure. There is also evidence that may suggest that the hexagonal crystallites are reforming, possibly seeded from any remaining original hexagonal crystallites.

3.2.4 Basic site analysis

Many studies have confirmed that the basic properties of metal oxides like MgO govern the substance's reactivity as a catalyst.[10,25–28] These sites are likely to perform an important role in the transformation of glycerol to methanol. Acidic sites have been shown to promote the double dehydration of glycerol to acrolein.[29,30] This led to Haider *et al.*[2] considering the use of basic sites for the dehydration reaction of glycerol which spurred the initial and subsequent investigations.[1] It was proposed that the dehydration would also be accompanied by a separate radical fragmentation pathway promoted by a reductive atmosphere. The steam present under our reaction conditions would provide this.[2] Reaction metrics such as selectivity, conversion/activity and CMB are all thought to be affected by the type and distribution of the basic sites. Varying the heat treatment temperature was proposed to be a simple way of varying the basic site concentration and

distribution on the surface. Higher temperature can cause, annealing, sintering, and smoothing of the surface, resulting in lower SA and active sites. Distribution of types of sites can be affected by higher temperatures due to surface smoothing, where exposed O^{2-} sites on edges and steps may be preferentially removed.[10,12]

The basic site concentration and distribution is expected to correlate with conversion of glycerol *via* processes such as dehydration. Cosimo *et al.*[10] reports that the main types of basic site on MgO are low coordination O^{2-}, the oxygen in Mg^{2+}-O^{2-} pairs and OH. The relative concentrations of these may influence characteristics such as conversion, selectivity and CMB. The large quantity of formyl and unsaturated intermediates which form in this reaction, could serve as platforms for coupling and polymerisation reactions.[1] Condensation reactions are known to occur on MgO, specifically with compounds such as aldehydes or ketones.[1,2] This is a concern as in previous experiments; aldehydes, such as acetaldehyde and acrolein, and ketones such as hydroxyacetone have represented a large portion of the carbon selectivity in the reaction product stream.[1,2]

To define the types of basic sites present in these samples and establish how they were influenced by the final heat treatment temperature, further characterisation of the MgO samples was required. The samples were therefore investigated by CO_2 diffuse reflectance Fourier transform infrared spectroscopy (CO_2-DRIFT) and CO_2-Temperature programmed desorption (CO_2-TPD).

3.2.4.1 Basic site analysis – CO_2 adsorption diffuse reflectance Fourier transform spectroscopy

The series of MgO catalysts were investigated by *in-situ* DRIFTS. In these experiments, CO_2 was used as an acidic probe molecule. The aim of these experiments was to identify the nature of the basic sites, in each of the MgO catalysts. Different geometries of CO_2 bonding should exhibit absorbances at specific wavenumbers within the IR spectrum. These could be compared with literature values identified and defined by other researchers in previous experimental and computational studies. The bonding geometry reveals what kind of site CO_2 would be bonded to on the MgO surface, such as defects or edges. The aim here was to identify the types of site present which could then be quantified with TPD experiments, and thus identify the type and proportion of the basic sites on a sample. This could allow for conclusions to be made on the relationship between different sites, proportions, and the effect on catalytic performance.

CO_2 can form carbonates with the MgO surface. It is noted that the vibrational signal may vary from literature examples, so a best estimate of what they correspond with has been made based on several sources. The DRIFTS spectra (Figure 6) confirm that the temperature of the N_2 heat treatment does indeed influence the proportion of basic sites in the MgO samples. The absorption bands for CO_2 carbonates on the MgO surface are typically located from 1800 cm^{-1} to 1200 cm^-

[1].[10,31,32] On an ideal MgO (100) surface, the terrace situated Mg and O atoms are five coordinated, corner sites are 4 coordinated and edge sites are 3 coordinated.[10] MgO prepared from the precipitation of $Mg(OH)_2$ are known to be highly defective which has been confirmed using high resolution transmission electron microscopy (HRTEM) and therefore likely to exhibit many lower coordinated sites.[17]

On the catalysts prepared for this study, upon adsorption of CO_2 at room temperature, there are three clear adsorption bands present in the spectra in the 1200 – 1800 region (Figure 6, Table 3). These do not correlate exactly with the values reported in previous literature but using the information available an estimation of what these bands represent has been made. Literature values show a wide range of identications for basic sites on MgO *via* DRIFTS (Table 4). This is due to morphology and other features affecting the wavelength of absorbances, but this leads to considerable overlap in the sources. Here a best approximation of what the DRIFT spectra represent is made with reference to this literature. Table 3 shows the general values which have been used to attribute our data with different types of sites, which was based on the data from literature studies shown in Table 4.

Literature reports the bands between approximately 1200 – 1800 cm^{-1} may be attributed to species forming on MgO basic sites. [10,31–34] A symmetric (1360 – 1400 cm^{-1}) and asymmetric (1510 – 1560 cm^{-1}) O-C-O stretch may be attributed to uni-coordinated ions of O^{2-} present on edges.[10] The obtained DRIFTS (Figure 6) show a large absorbance between approximately 1580 –1480 cm^{-1} which has been attributed to these O^{2-} sites. According to literature the bicarbonate species which form on hydroxylated oxygen atoms (OH), can be attributed to a symmetric band at 1480 cm^{-1} and an asymmetric band at 1650 cm^{-1}, with a general range of 1220 – 1660 cm^{-1}.[10,17,32,33] When raising the temperature of the DRIFTS cell, the absorption around 1650 cm^{-1} is significantly reduced for each sample. This led to this band being inferred to likely be the main indicator of the more labile OH groups. The small feature at 1460 cm^{-1} may also be attributed to them. Bi-dentate carbonates form on Lewis acid – Brønsted base pairs (Mg^{2+} -O^2). [10,31,32,34] Literature shows a variety of different cm^{-1} ranges for this which overlap. So as a best approximation, it is proposed that the major absorption between 1440 – 1350 cm^{-1} may be attributed to this due to the relative proportions expected from stability and catalyst treatment temperatures.
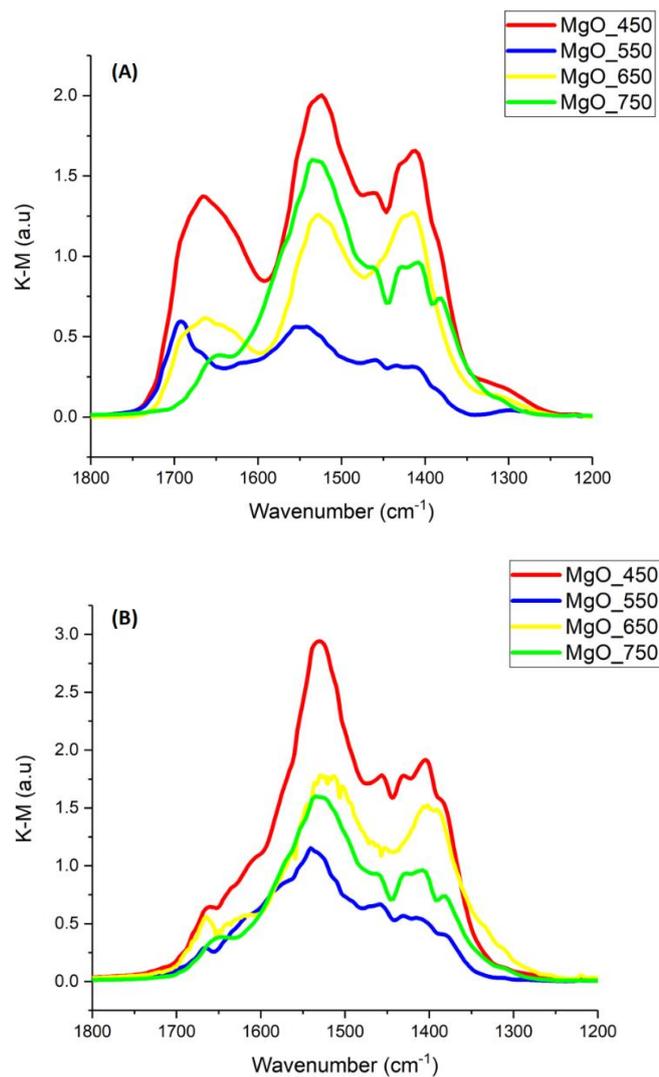
Figure 6. DRIFT spectra of CO₂ adsorbed on MgO_450 -750 catalysts at room temperature (a) and at 200 ˚C (b).

Table 3. Attributed DRIFTS adsorption bands basic sites and CO₂ species.

Site	OH	O^{2-}	Mg^{2+} -O^2
CO_2 adsorption mode	Bicarbonate	Monodentate carbonates	Bidentate carbonates
Main Attributed /cm^{-1}	1700 − 1600	1580 −1480	1440 − 1350

Table 4. Literature values for DRIFTS adsorption bands basic sites and CO_2 species.

	OH	O^{2-}	$Mg^{2+}-O^{2}$
Reference	Bicarbonate / hydrogen carbonates (cm^{-1})	Monodentate carbonates (cm^{-1})	Bidentate & tridentate carbonates (cm^{-1})
[10]	1220 asymmetric 1480 asymmetric 1650 asymmetric	1360–1400 symmetric 1510 – 1560 asymmetric	1610 – 1630 symmetric 1320–1340 symmetric
[31]		1370–1590 general area attributed 1440 v_{3high} DFT (110) 1378 v_{3low} DFT (110)	1270 – 1390 general area attributed 1620 – 1710 general area attributed 1680 v_{3high} Drifts 1650-1730 v_{3high} DFT 1125-1200 v_{3low} DFT 1651 v_{3high} Drifts (tridentate 100) 1304 v_{3low} Drifts (tridentate 100) 1600-1650 v_{3high} DFT (tridentate 100) 1280-1300 v_{3low} DFT (tridentate 100) 1516 v_{3high} Drifts (tridentate 100) 1347 v_{3low} Drifts (tridentate 100) 1560 v_{3high} DFT (tridentate 100) 1330 v_{3low} DFT (tridentate 100)
[33]	1655–1658 v_2 1405–1419 v3 1220–1223 v4	1510–1550 v_{3high} 1390–1410 v_{3low} 1035–1050 v_1	
[32]	1480 v_3 1250 v_4	1590,1510 v_{3high} 1415 v_{3low}	1385,1335 v_{3low}
[17]	1650 v_2 1510,1408 v3 1220 v4		
[35]		1550 v_{3high} 1410 v_{3low} 1050 v_1	
[36]		1520 v_{3high} 1370 v_{3low} 1060 v_1	1670, 1630 v_{3high} 1270 v_1
[34]		1550 v_{3high} 1410 v_{3low} 1050 v_1	1670,1630 v_{3high} 1315,1280 v_{3low} 1000,850 v_1 950,830 v_1

The relative proportion of different basic sites can affect selectivity and activity and thus may be key in explaining differences in behaviour for our catalyst. Di Cosimo *et al.*[10] found this when using MgO for the aldol condensation of citral and acetone to pseudoionone and the synthesis of 4-

methyl-3-penten-2-ol. During the formation of pseudoione the activity decreased with calcination temperature, the opposite was true for 4-methyl-3-penten-2-ol. This was attributed to be due to the change in basic site distribution; strong O^{2-} sites were needed for the formation of pseudoionones while medium strength Mg^{2+}-O^{2-} pairs were needed for the later.

The most prominent bands observed on the MgO_450 and MgO_550 reside between 1480 to 1580 cm^{-1}. According to literature reports, this corresponds to a monodentate species adsorbed to uni-coordinated ions of O^{2-}.[10] The $1360 - 1400$ cm^{-1} adsorption that also relates to these sites reported in the literature is visible on MgO_550, but obscured on MgO_450. Finally, the band between $1380 - 1440$ cm^{-1} could be indicative of bi-dentate carbonate species forming on Lewis acid – Brønsted base pairs (Mg^{2+} -O^{2}). The bands at $1270 - 1390$ cm^{-1} reported in the literature may be equivalent but with a different morphology affecting the adsorption wavenumber.

Evidently, each of the catalysts exhibit different relative proportions of these adsorption bands. This may give some clue to their catalytic function. Firstly, for the MgO_450 catalyst, the signal representing CO_2 adsorbed to O^{2-} exhibits a higher intensity in comparison to the other sites at room temperature. As the temperature of the DRIFT cell is increased, this becomes more significant (Figure 6b). This may be due to the adsorbed CO_2 being removed preferentially from the Mg^{2+} - O^{2-} and OH sites. This is a similar case with the other catalysts, which indicates that O^{2-} more strongly bonds CO_2 than the other sites. For the MgO_550 catalyst, the CO_2 O^{2-} stretch is also significantly prominent at both temperatures, especially when compared to OH which exhibits a weak band in comparison. MgO_650 exhibits relatively equal intensities for these two sites at room temperature. However, once the temperature is increased the signal deemed to represent the CO_2 adduct attached to Mg^{2+} - O^{2-} is reduced slightly, again indicating the CO_2 is slightly less bound than on the O^{2-} sites. MgO_750 shows a high degree of CO_2 on both O^{2-} and OH sites at room temperature. However, the stretch representing CO_2 adsorbed to OH intensity is significantly reduced in comparison once the temperature increases. This indicates that OH only weakly adsorbs CO_2.

The low coordinated O^{2-} anions (resulting in monodentate carbonates) may be the strongest basic sites, due to the persistence of adsorbed CO_2 to them at high temperatures. The OH groups on the surface resulting in bicarbonates are likely to be weaker as are more easily removed. Oxygen in Mg^{2+} - O^{2} is approximated to be stronger, resulting in bidentate carbonates persisting longer than the bicarbonates. Cosimo et al.[10] using similar samples and techniques reports that the order of strength of the basic sites observed was low coordination O^{2} > The oxygen in Mg^{2+} - O^{2-} pairs > OH. (Monodentate carbonates > bidentate carbonates > bicarbonates). Other literature sources come to the same conclusion.[17,37] However, OH groups while relatively weak may be very important to

catalysis and can significantly promote reactions,[37–40] such as the aldol condensation of acetaldehyde.[38]

3.2.4.2 Basic site analysis – CO₂ Temperature programmed desorption

CO_2-TPD experiments were employed, as this technique allows for the quantification of basicity of the sample in terms of μ-moles of CO_2 which adsorb to the MgO surface. From these experiments, the aim was to quantify the relative density and number of basic sites on a samples surface. Different sites can be identified by their desorption temperature, which can be related to the information gained on the nature of the sites from the DRIFTS experiments.

The corresponding desorption patterns of the CO_2-TPD experiments are presented in Figure 7, with μ-moles of CO_2 desorbed reported in Table 5. It is important to note, that a high pre-treatment of 400 °C was first required to ensure any hydroxy and carbonate surface species, which from due to the interaction of MgO with water vapour and CO_2 in air, had been fully removed prior to analysis.[10] This was necessary to achieve as clean surface as possible, while minimising any further structural or chemical changes.
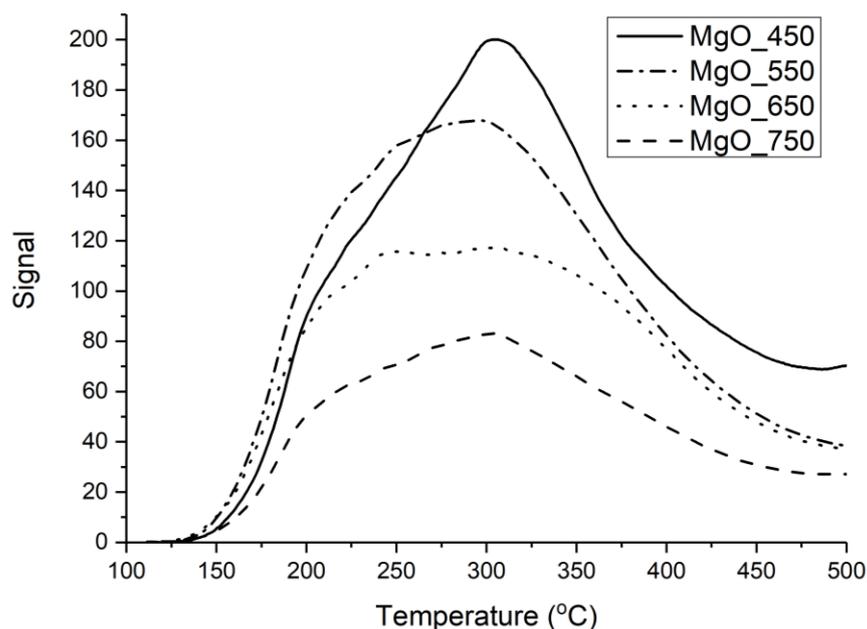
Figure 7. TPD profiles for MgO_450-750, Pre-treatment: He 150 mL min⁻¹ 300 °C 1 hr, CO₂ adsorbed at 25 °C 30 mL min⁻¹, physiosorbed CO₂ removed at 110 °C 1 hr followed by TPD to 400 °C at 15 °C min⁻¹.

Table 5. Characterisation data, BET and TPD for MgO_450 -750

Catalyst ID	Surface area $m^2 g^{-1}$	< 450 °C TPD μ moles CO_2 g^{-1}	< 450 °C TPD μ moles CO_2 m^2
MgO_450	187	1409	8
MgO_550	154	1290	8
MgO_650	125	1022	8
MgO_750	74	642	9

Analysis of CO_2 TPD experiments (Figure 7) show that the signal response at lower temperatures is likely to be attributed to weaker basic sites, with strength increasing as the desorption of the CO_2 temperature increases. The weaker sites would less strongly bind CO_2, releasing it at a lower temperature. Unfortunately, distinct separate peaks corresponding to well defined sites could not be identified. This means that here the different bonding structures could not be determined solely from these experiments. It was thought, based on the literature, the DRIFTS experiments and the identification of possible features on the curve; that it was likely that there were hidden peaks representing different basic sites.[10]

Deconvolution of the TPD curve into contributing peaks was attempted, but there was not adequate confidence in its accuracy. Therefore, in tandem with the DRIFTS, an estimation of the location of the basic sites within the TPD curves was made. The slight feature between 180 – 210 °C was identified as likely to be due to bicarbonate species of CO_2 desorbing as OH species are expected to be most labile. The most dominant peak in the DRIFTS represents O^{2-} , therefore the peak centred between 280 to 340 °C is likely to be unidentate carbonate species decomposing from O^{2-} sites on the surface. Finally, the feature between 230 to 270 °C is approximated to represent bidentate CO_2 species desorbing from Mg^{2+} - O^{2-}. This correlates with the slight features seen in the curves. MgO_650 shows a flatter curve peak, indicating that as with the DRIFTS the proportion of the strong and medium sites may be similar.

While quantitative data on the proportion of the basic sites was not possible. Total basicity per gram and m^2 could be calculated (Table 5). The total basicity, defined as μ-moles CO_2 per gram of material desorbed, decreases as the heat treatment temperature is raised. The basicity, per m^2 however, stays stable. While the signal does not return to baseline, the temperature was not taken higher in these experiments. Above 450 °C, the temperature begins to exceed the minimum heat treatment temperature of the samples were prepared at. This can result in the structural properties

such as the morphology and SA of the material changing. This means that signal obtained at temperatures higher than 450 °C is incomparable between the catalyst samples.

3.2.5. Characterisation summary

In summary, increases of heat treatment temperature in the final stages of the catalyst preparation have several significant effects on the surface species present and catalyst structure. The increase corresponds to a linear decrease in catalyst SA, an increase in crystallite size, especially between the final two temperatures and a decrease in basicity per gram of catalyst. At least two different basic site strengths are observed; likely to represent low coordinated O^{2-} and the oxygen in Mg^{2+}-O^2 pairs. These were attributed to the mono and bi-dentate bonding modes seen *via* DRIFTS. Strong O^{2-} sites seem to be more prevalent over MgO_450, MgO_550 and MgO_750, while MgO_650 may possess a more equal distribution. This may be linked to the morphology; TEM shows that both MgO_450 and MgO_750 exhibit similar nanostructures while MgO_650 does not.

3.3 Catalytic reaction testing – vapour phase catalytic conversion of glycerol over MgO

3.3.1 Influence of MgO catalyst heat treatment temperature. 50 wt.% 360 °C

Introduction

The primary aim of the glycerol valorisation investigations over MgO was to obtain higher reaction selectivity (and thus yields) to methanol. Initially, a series of experiments were conducted under identical conditions using the four MgO samples prepared herein. For this series of experiments, a 50 wt. % glycerol feed was passed over 0.5 g of catalyst at 360 °C. These parameters were chosen for the initial studies, as they are identical to conditions our group have utilized previously.[1,2,13] Catalysts were initially tested at 360 °C 50 wt.% as this allowed for the catalysts to be compared at below full glycerol conversion.

3.1.1.1 Glycerol activation

A reaction pathway network for the reaction of glycerol over MgO and metal oxides was developed in previous studies.[1,2,13] From this previously established understanding there are two main reaction pathways predicted to produce methanol, and a third that would yield primarily acrolein. The activation and dehydration of glycerol through the secondary hydroxyl group is thought to lead to a double dehydration cumulating in acrolein (product 22, Figure 8). Activation of a terminal hydroxyl group is expected to lead to a dehydration/tautomerisation to hydroxyacetone (product 5). This monodehydration is predicted to be twice as likely as the acrolein route due to there being two terminal hydroxyls and only one secondary hydroxyl group. A radical cleavage of a C-C bond can also yield a methanol and ethylene glycol radical. This can result in glyceraldehyde which can undergo another cleavage to give a second methanol and acetyl radical. The conversion of glycerol

is expected to be tightly linked to how well the catalyst promotes the initial glycerol reaction over its surface.
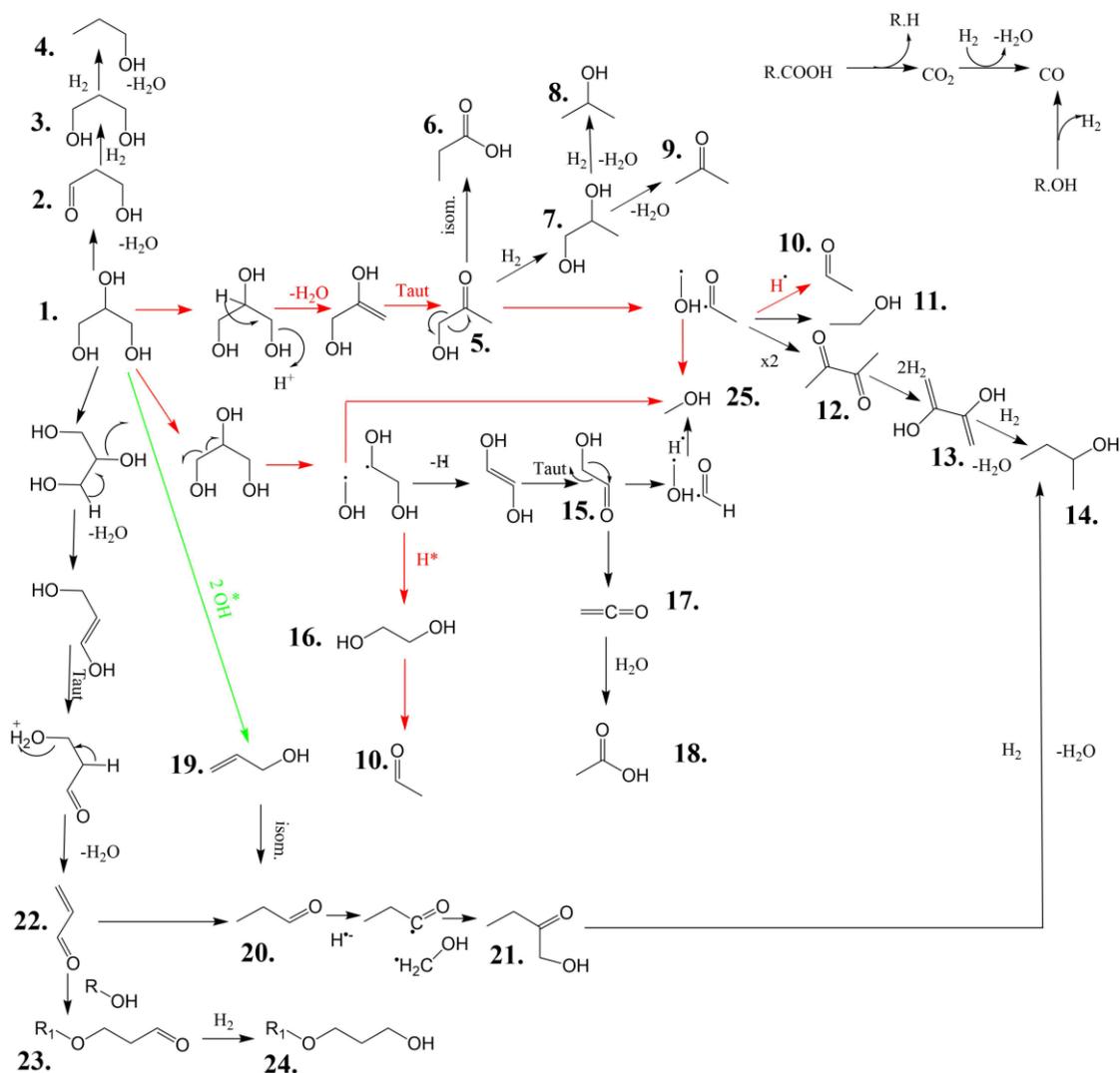
Figure 8. Proposed reaction network for the catalytic transformation of glycerol into a range of different products over MgO. Red arrows correspond to dominant reaction pathways over MgO. The green arrow corresponds to a dominant pathway occurring in the absence of MgO. 1. Glycerol; 2. 3-hydroxypropenal; 3. 1,3-propanediol; 4. 1-propanol; 5. hydroxyacetone; 6. propanoic acid; 7. 1,2-propanediol; 8. 2-propanol; 9. ace- tone; 10. acetaldehyde; 11. ethanol; 12. 2,3-butanedione; 13. 2,3-butandiol; 14. 2-butanol; 15. glycolaldehyde; 16. ethylene glycol; 17. ethenone; 18. acetic acid; 19. allyl alcohol; 20. 1-propanal; 21. 1-hydroxyl-2-butanone; 22. acrolein; 23. 3-alkoxypropanal; 24. 3-alkoxy propanol; 25. Methanol. Reproduced from work presented in L. R. Smith, P. J. Smith, K. S. Mugford, M. Douthwaite, N. F. Dummer, D. J. Willock, M. Howard, D. W. Knight, S. H. Taylor and G. J. Hutchings, Catal. Sci. Technol., 2019, 19–22.[1]

3.3.1.2 Conversion and activity

Distinct differences in catalyst activity were observed over the different MgO samples. As shown in Table 6 and (full selectivity and standard error is shown in Table 8), the activity of the catalyst samples loosely correlated to the temperature they were heat treated at. In general, the conversion of glycerol (C_{gly} (%)) decreased as the temperature of the N_2 heat treatment increased, except for when 750 °C (MgO_750) was used. On increasing the treatment temperature from 450 °C to 550 °C and 650 °C, glycerol conversion decreased from 87 % to 80 % to 75 %, respectively. This is also reflected in the activity in terms of (g_{gly} h^{-1} g_{cat}^{-1}). It was initially postulated that the loss of conversion with increasing heat treatment temperature, may be due to the lower basicity and SA of the higher temperature treated samples. As these characteristics are reduced, naturally, it would be logical to assume that the catalysts become less active. However, this is not observed; the MgO_750 catalyst exhibited a higher glycerol conversion (80 %) than the MgO_650 catalyst. This is surprising, given these materials lower SA, lower total basicity, and higher crystallite size. It is therefore reasonable to suggest that the increased activity is attributed to another factor, such as the proportion of a specific basic site or the samples differing porosity. DRIFTS experiments (Figure 6) indicate that MgO_650 may exhibit a lower proportion of O^{2-} edges. These sites are expected to be the strongest of MgO's basic sites.[10,17,37] The perceived lower proportion of O^{2-} sites may contribute to the catalyst being less able to facilitate the activation of glycerol.

Table 6. Performance of MgO catalysts on the gas phase valorisation of glycerol reaction conditions: Aqueous glycerol solution (50 wt.%; 0.016 mL min^{-1}; Ar (50 mL min^{-1}); catalyst (0.5 g); bed volume (1 mL); GHSV = 4615 h^{-1}; temperature (360 °C).

Acronym: C (conversion); ACE(acetaldehyde), ACR(acrolein); MOH(methanol); HAD(hydroxyacetone); UNK(unknown); EG(ethylene glycol); CMB(carbon mass balance: GC1 + coke carbon moles to carbon moles of glycerol injected into reactor).

***Coke calculated from TGA**

| Catalyst ID | Conversion$_{gly}$ / % (+/-) | Activity (g_{gly} h^{-1} g cat^{-1}) | % Selectivity (**STY** / g h^{-1} kg cat^{-1}) | | | | | | coke* / mg g$_{cat}$$^{-1}$ | Coke % of CMB % | CMB / % (+/-) |
			ACE	ACR	MOH	HAD	UNK	EG			
MgO_450	87 (4.3)	0.93	19.7 (**92**)	13.4 (**53**)	11.9 (**85**)	23.2 (**122**)	8.3 (**NA**)	8.2 (**54**)	89.1	3.0	74 (3.2)
MgO_550	80 (1.8)	0.88	17.4 (**83**)	11.2 (**45**)	10.1 (**74**)	28.3 (**152**)	8.1 (**NA**)	9.3 (**63**)	79.2	2.9	78 (1.3)
MgO_650	75 (1.4)	0.81	20.2 (**118**)	12.7 (**64**)	9.8 (**93**)	23.7 (**173**)	8.4 (**NA**)	9.2 (**71**)	105.5	3.2	98 (1.2)
MgO_750	80 (1.6)	0.86	21.6 (**98**)	12.8 (**49**)	11.4 (**79**)	23.9 (**122**)	7.6 (**NA**)	8.1 (**52**)	43.5	2.1	79 (1.7)

3.3.1.3 Carbon mass balance (CMB) and coke

The CMB is an important factor in our experiments, and measures what percentage of the carbon fed into the reactor is accounted for. Having a relatively low CMB is not desired as indicates a significant proportion of our reaction products are not quantified. In the previous work published by Smith *et al.*[1] this equated for a significant *ca.* 26 % of carbon under these conditions (74 % CMB)(Table 1). A loss of over quarter of the carbon is not ideal and it was hypothesised that the responsible culprit was the formation of heigh weight molecular products (HWMP) which were not detected by GC-FID. Total carbon content analysis and LCMS analysis supported this theory. These HWMP are postulated to result from bimolecular condensation reactions catalysed by basic sites on the MgO,[1] which has been shown to promote bimolecular condensations.[10,25,26,38,41,42] Part of the motivation of altering the catalyst heat treatment temperature was to reduce the basicity thought to be responsible.

As with the conversion, the CMB follows a rough trend up till MgO_650, where higher conversions result in lower CMB. MgO_450 has a CMB of 74 %, increasing to 78 % for MgO_550, 98 % for MgO_650 and decreasing to 79 % for MgO_750 (Table 6). The 98 % CMB obtained for MgO_650 is a significant development for this reaction. A CMB this high had not been previously observed under these conditions for MgO. This is the equivalent to only 1-2 % of carbon proceeding to these higher weight products and fouling, which is a significant improvement on the other samples in the series and that observed in previous works.[1] This result indicates that MgO_650 likely does not produce HWMP's in high concentrations.

To help confirm the high CMB and lack of undetected HWMPs, the product mixture was sent for CHN analysis to determine the Total-Carbon-Content of the liquid fraction (Table 7). This showed that the GC analysis CMB was representative and supported our conclusion. The liquid analysis was in accordance with that observed from GC analysis at 85 %. The remaining 13 % of carbon was assigned to coking (3.2 %) and gas phase products (8.7 %). In conclusion, this experiment shows that is only possible for a small percentage of the carbon to have been used in the formation of HWMP over MgO_650.

Table 7. Total organic carbon CHN analysis – MgO_650. Reaction conditions; 360 °C ,50 % glycerol/water flow 0.016 mL min⁻¹, 0.5 g MgO, 50 mL min⁻¹ Ar, 3 hours

	MgO_650 360 °C
Catalyst coking (TGA)	3.2
Gas analysis (GC)	8.7
Liquid analysis (GC)	85.7
Liquid analysis (CHN)	85.1
Total Carbon (including coke) %	98

When analysing how coke % (Figure 9, Table 7) relates to CMB, MgO_650 exhibits the highest degree of coking and highest CMB. This is unexpected, the catalysts that are thought to produce a higher concentration of high weight products may be expected to coke more as it can form from carbonaceous molecules undergoing cyclization, condensation, and polymerisation.[43]

Figure 9a shows that MgO_650 with the highest mg g⁻¹ cat of coke has the least unquantified coke, Figure 9b and 9c shows that the basicity does not directly correlate with the amount of Coke and unquantified Carbon and thus CMB as would be expected. It is possible that if any HWMPs are formed over MgO_650, they may be less likely to desorb which could result in the formation of coke. This could potentially block the sites responsible for condensation, leading to only a small amount of the higher weight products being produced. Blockage of basic sites could also affect the activity. While something to consider, there is no evidence for this currently and such strong adsorption would be normally attributed to a high basicity sample. Condensation of glycerol and products within the pore structure of metal oxides could also add to coke formation.[44] Diffusion both within and out of pores is likely influenced by the diameter.[44] MgO_750 exhibits a small volume pore structure compared to the other samples, it also has the relatively low pore diameter. The low volume may not allow for a high enough amount of substrate within the pore structure to result in significant coking. However, with our series there isn't a clear trend between the pore diameter and the coking or CMB. It seems that multiple factors may affect this such as the pore size, basicity, SA, morphology and possibly more. At current level of understanding it is difficult to deconvolute these competing factors to draw strong conclusions.

The loss of CMB and coke over MgO_450 and MgO_550 is proposed to be generally due to the HWMP, MgO_650 high CMB is proposed to be due to not forming these products. As these would be usually attributed to basicity the low CMB over MgO_750 is currently unexplained. It could possibly be caused by either something else forming that fouls the reactor, or another important

catalyst characteristic that promotes condensation reactions. The high degree of coking over MgO_650 may indicate that changes to the catalysts basicity occurs *in-situ*, this may result in MgO_650 actually being less basic than MgO_750 due to its high level of coke formed. As currently investigated, the characterisation of the samples reveals the features that match the trend we see with the four catalysts performance is the difference in morphology, large crystallite size (for 750) and possibly O^{2-} prominence. However, if any of these features are responsible or why is not understood or proven yet.

3.3.1.4 Selectivity to methanol and yield

The selectivity observed over the catalysts stays relatively stable over the series, with a few notable changes. The selectivity is calculated from the detected carbon in the products compared to the carbon in the converted glycerol. As discussed previously, it's hypothesised that a significant proportion of HWMPs are formed through various biomolecular reactions. These are not included in the selectivity calculation however which results in the product yields changing more than the selectivity would suggest.

As the N_2 heat treatment temperature was increased, selectivity to methanol decreases slightly. The MgO_450 exhibited the highest methanol selectivity of 11.9 % followed by MgO_750 at 11.4 %. However, a slight increase in methanol yield is observed over the MgO_650 catalyst, due to the increase in its associated CMB. MgO_650 therefore exhibited the highest methanol STY yield (93 g h^{-1} kg cat h^{-1}). This illustrates the importance of achieving a high CMB, or rather, modifying the catalyst to suppress undesirable reactions. While a promising result, this methanol STY is however lower than the space time yield exhibited by the MgO_STD catalyst in our groups previous study, under identical reaction conditions (131 g h^{-1} kg cat h^{-1}).[1] The lower methanol STY obtained by MgO_650 is likely due to the significantly lower methanol selectivity (MgO_650 methanol selectivity was 9.8 %, MgO_STD was 23.4 %).

In summary, it is proposed that the improvement in CMB from increasing the temperature during preparation from 450 °C to 650 °C is linked to the amount of undetected HWMPs produced. This is inferred from the CMB increase, which may be due to decreased biomolecular reactions such as aldol condensations, which are known to occur over MgO. [10,42] Exactly why these products are not produced as much over MgO_650 but are with MgO_750 is not yet understood.
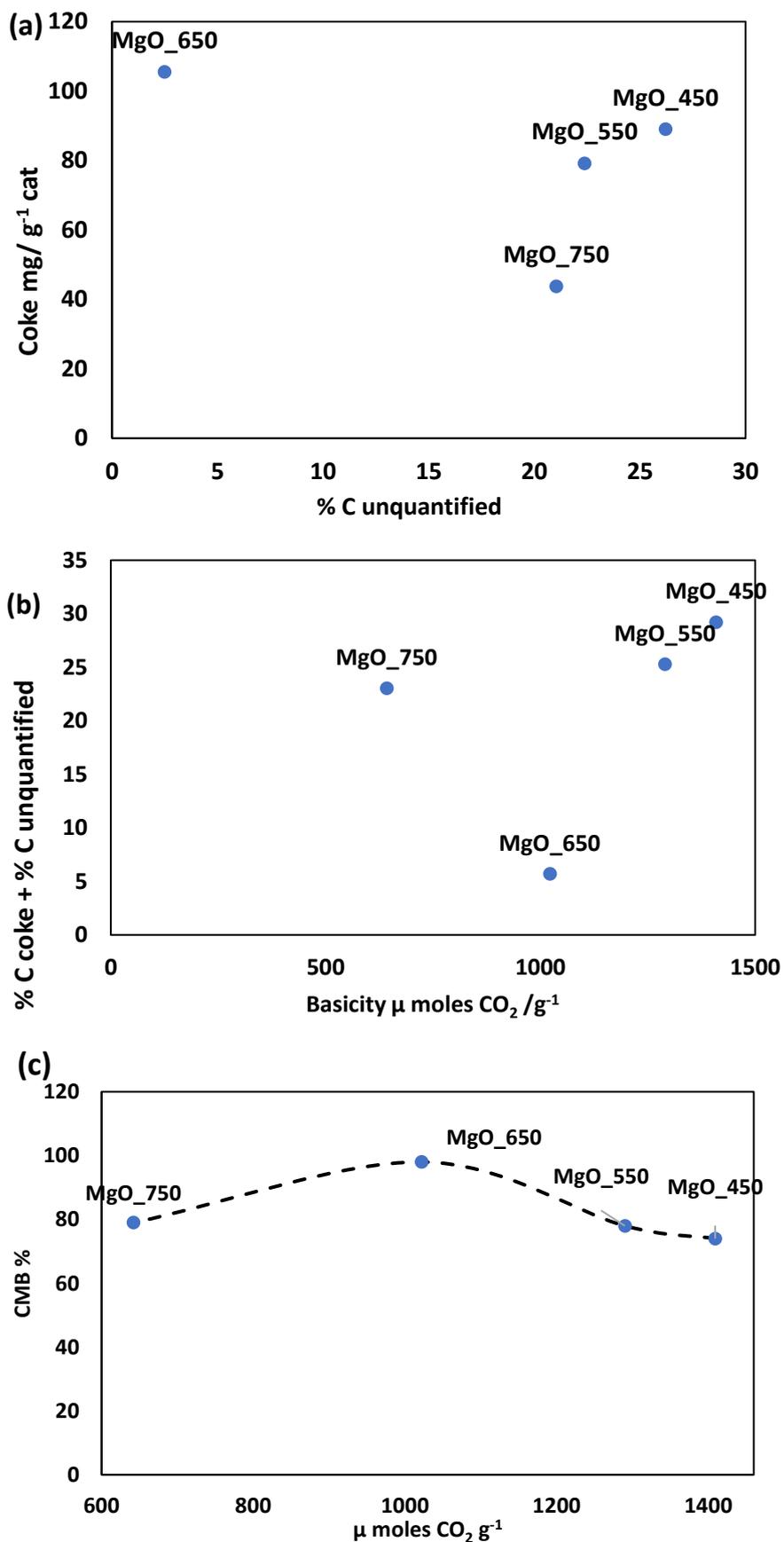
Figure 9. (a) coke mg/ g^{-1} cat vs % C HMWP (b) Coke mg/ g^{-1} cat + % C HMWP vs catalyst basicity in µ moles CO$_2$ /g^{-1}. (c) CMB vs catalyst basicity in µ moles CO$_2$ /g^{-1}

3.3.1.5 Formation of high weight molecular products over MgO

To further validate the hypothesis that HMWPs may be produced in these reactions, it was important to consider how they might form. Presented in Figure 10 is a scheme which proposes how some of these products may start to form. Due to the high variation of products, both known and unknown, in our product stream, it's likely that several combinations of substrates could react to form these species.
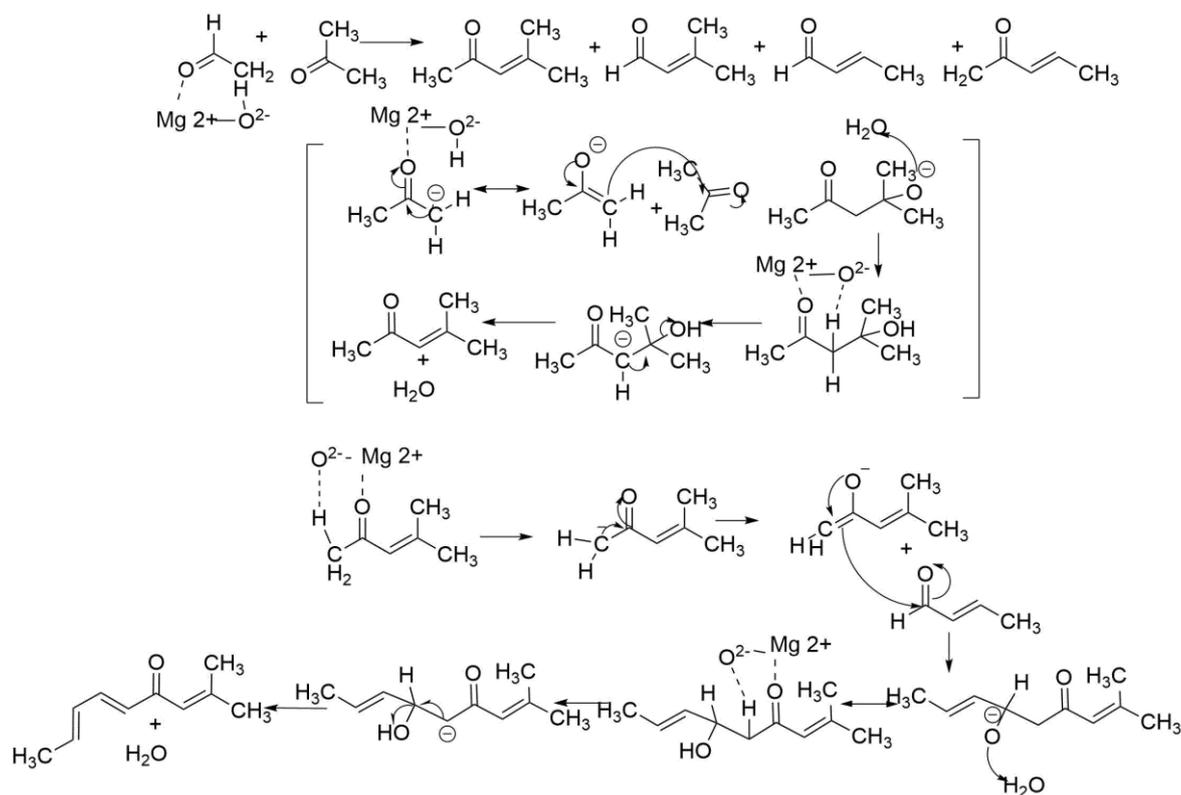
Figure 10. Aldol cross-condensation of acetone and acetaldehyde. Followed by possible cross-condensation of α, β unsaturated ketone (acetone enolate) and acetaldehyde enolate to form precursors to HMWP's.

Ketones and aldehydes are known to undergo cross and self-condensation reactions. [1,10,26,38] Figure 10, as an illustrated example, shows a cross condensation reaction between acetone and acetaldehyde. These two molecules can react and lead to the formation of four different products. These are two forms each of enolate nucleophiles and carbonyl electrophiles. In the event of self-condensation, such as the type which likely occurs with acetone, an α, β-unsaturated ketone will form. Using the classical understanding of the aldol condensation mechanism, the reactions would be catalysed by basic sites on MgO. These sites could remove an alpha proton from a methyl group of a ketone or aldehyde, which would result in the formation of an enolate.[38] This enolate could subsequently initiate a nucleophilic attack on an second substrate molecule; acetaldehyde in this

example. This would be followed by protonation, to yield the aldol addition product. α-Hydrogen and the analogous β-hydroxyl group are then removed by the catalysed elimination of water from the aldol addition product.
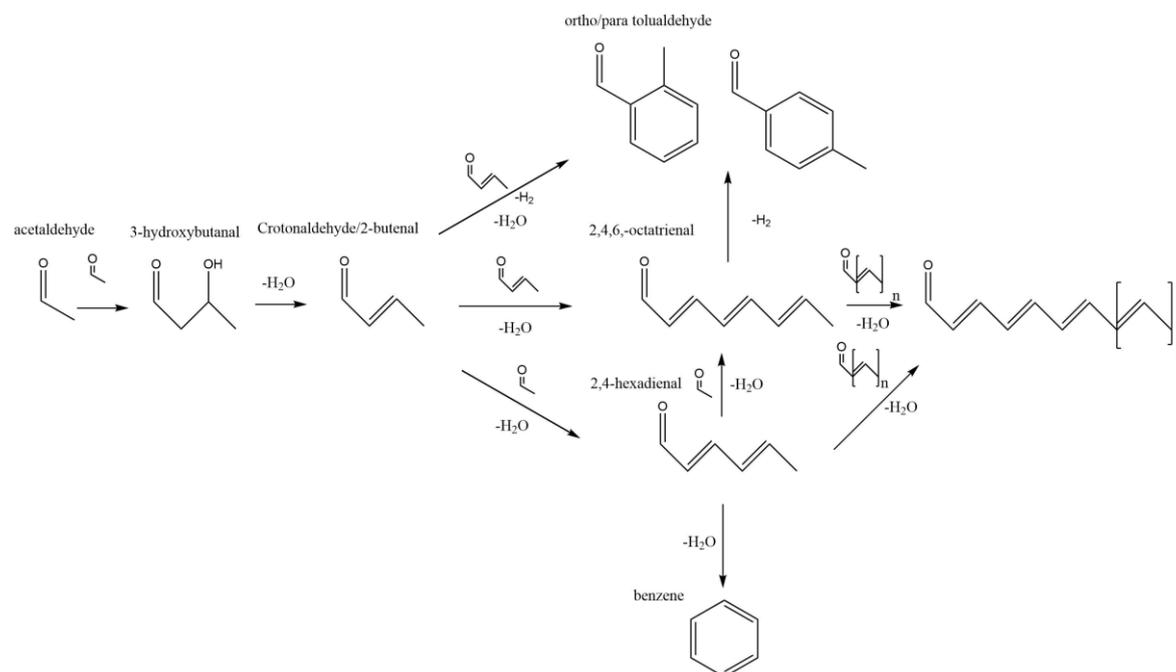
Figure 11. Possible acetaldehyde condensation pathways to precursors to HWMP.[48] **M. Lusardi, T. Struble, A. R. Teixeira and K. F. Jensen, Catal. Sci. Technol., 2020, 10, 536 DOI: 10.1039/C9CY01927H**

In a similar way to this scheme, a possible example of this type of reaction occurring would be the self-condensation of acetaldehyde to 3-hydroxybutanal, which in turn can undergo a dehydration to crotonaldehyde,[38] these reactive products may also be a source of the HWMPs (Figure 11). It is possible that a variety of products can form from acetaldehyde and its condensation products, including aromatic compounds such as benzene and tolualdehydes,[45] this could occur through mechanisms such as Michael additions, dehydrations, electrocyclization and aldol condensation. Some example products could include ortho and para tolualdehyde, 2,4,6-octatrienal and 2,4-hexadienal.[46–48] These may themselves undergo further reaction, resulting in larger products with expected high boiling points that would not be easily analysed *via* GC. For example, tetradecahexenal could form from the condensation of two 2,4,6-octatrienal, or other products. The possible continuation reaction of acetaldehyde and intermediate products such crotonaldehyde could result in HWMP. A relatively high selectivity to acetaldehyde is observed over most conditions and thus it is possible that this may occur to some extent. Figure 11 shows an

example of a possible route to a HWMP *via* the addition of acetaldehydes and crotonaldehydes. There is a complicated mixture of products in our stream however, so this is likely a simplification.

Sainna *et al.*[13] recently demonstrated that water can readily undergo dissociative adsorption over a MgO, under our reaction conditions. Given that the reactions presented herein are run under aqueous conditions, it's important to consider how this might influence reactivity on the catalysts surface. They modelled the expected surface of ideal MgO_450 and how it would interact with water to promote dissociative adsorption. If a large proportion of the MgO surface is hydroxylated, it could influence the catalysts' ability to abstract a proton from a methyl group which, as discussed, is an important step in the aldol condensation mechanism. OH⁻ sites on MgO surfaces are active for some base catalysed reactions and have been shown to enhance activity for certain reactions.[39,40] Previously, OH⁻ species on MgO surfaces have been identified to be the active sites for the aldol addition of acetone.[10,25,49,50] In these experiments reported by Zhang *et al.*[49], the exposure of a water onto clean MgO surface, led to a significant increase in both the catalysts activity and selectivity to the desired diacetone alcohol.
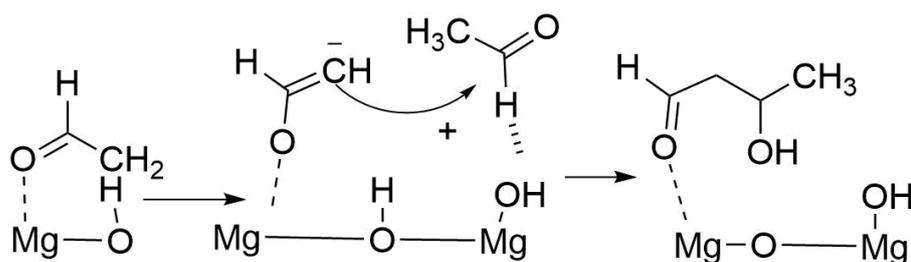
Figure 12. Acetaldehyde self-condensation to 3-hydroyxbutanal, based on the calculations found in Fan et al. A partially hydroxylated surface of MgO would lead to a more active catalyst for this reaction than a clean surface. D. Fan, X. Dong, Y. Yu and M. Zhang, Phys. Chem. Chem. Phys., 2017, 19, 25671–25682.[38]

Other studies, such as DFT studies performed by Fan *et al.*[38] also investigated aldol condensation reactions over OH⁻ sites on MgO. Fan *et al.*[38] deduced that there were two primary types of OH groups on MgO surfaces; those created *via* the protonation of surface O^{2-} groups and those created by the hydroxylation of Mg^{2+}. The authors evidenced that the adsorption of acetaldehyde directly to Mg^{2+} sites was more stable than adsorption onto surface hydroxyl groups. They proposed, illustrated in Figure 12 that this was due to a more favourable adsorption configuration, which involves the oxygen atom of acetaldehyde interacting with Mg^{2+}. Once adsorbed, it was proposed that the acetaldehyde molecule undergoes enolization. Fan *et al.* suggested that the OH groups are important for the second stage of the reaction, where a second acetaldehyde molecule adsorbs onto an adjacent OH site *via* hydrogen bonding. The OH group is relatively weak, thus, the alkoxide

anion is comparatively unstable. The two acetaldehyde molecules react forming a 3-hydroxybutanal molecule, as this is a more energetically favourable configuration. Therefore, it was concluded from their simulation that while OH exhibits a lower protonation ability than Mg^{2+} - O^{2-} sites, the partial hydroxylation of the surface leads to a more reactive catalyst for aldol condensations of acetaldehyde.

Through referring back to the DRIFTS experiments in Figure 6, a higher relative proportion of surface hydroxides was inferred on the MgO_450 and MgO_550 samples, than on the surface of MgO_650. MgO_450, MgO_550 and MgO_750 also have a strong adsorption in the region expected to correspond to monodentate carbonates on uni-coordinated ions of O^{2-} on step edges (thought to be strong sites). MgO_650 on the other hand exhibits a relatively even ratio between O^{2-} and Mg^{2+} -O^2 (medium). It may be possible that the degree of sites being of the O^{2-} type is an important factor in this reaction. These O^{2-} may undergo hydroxylation more freely as well due to their high expected strength, possibly allowing for more energetically favourable dissociation of water. However, the DRIFTS experiments are performed *ex-situ* to our experimental conditions without the presence of water, this means that it cannot be determined from them how hydroxylated the surface actually are in reaction conditions. However, if the surfaces of MgO_450, MgO_550 and MgO_750 are more highly hydroxylated under reaction conditions this would help support the explanation that their lower CMB results from the catalysts promoting self-condensation between reaction products in reference to Fan *et al*. [38]

As highlighted in the full selectivity data in Table 8, a large variety of aldehydes and ketones are formed in the reaction over MgO. Proportionally, a high abundance of acetaldehyde, acrolein and hydroxyacetone are produced. It is therefore likely that the HMWPs formed arise from condensation reactions involving these compounds. The large distribution of HMWPs in the post reaction mixture was evidenced, qualitatively, by LCMS analysis for MgO_450, the signal intensity and number of peaks was significantly lower for MgO_650 (Figure 13). A wide range of different products are clearly observed over LCMS rather than a few distinct peaks. The mass spectrum for the peaks saw a wide range of m/z values (appendix figure 14.)
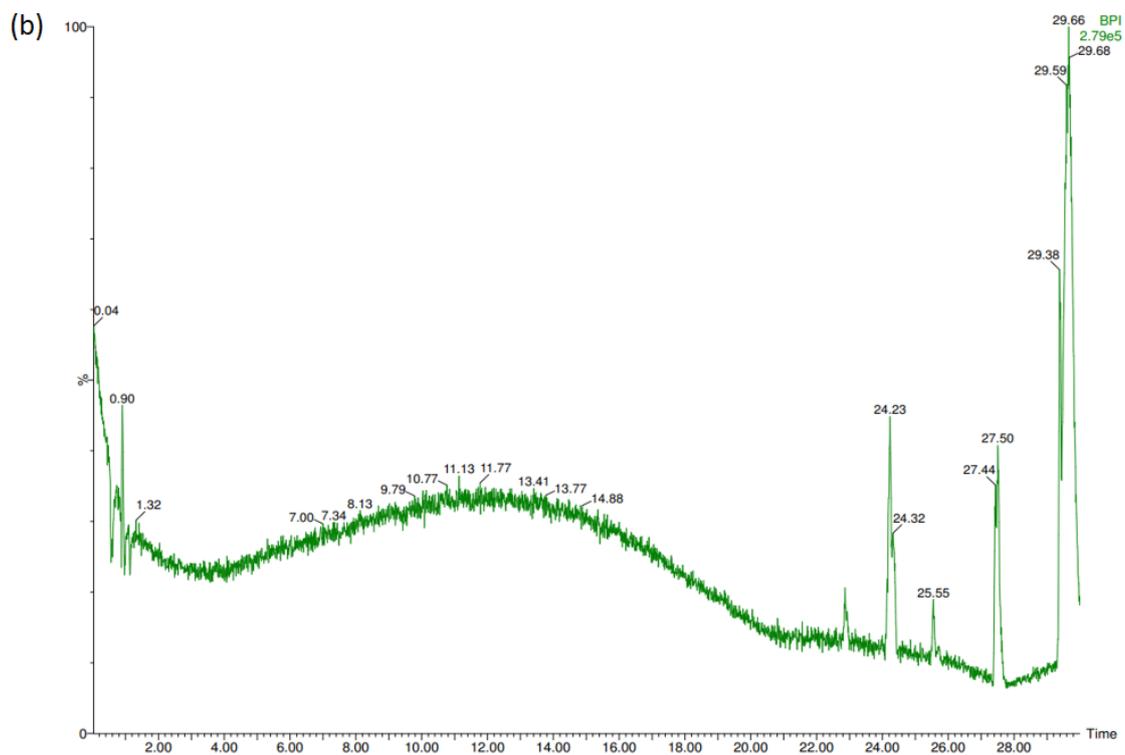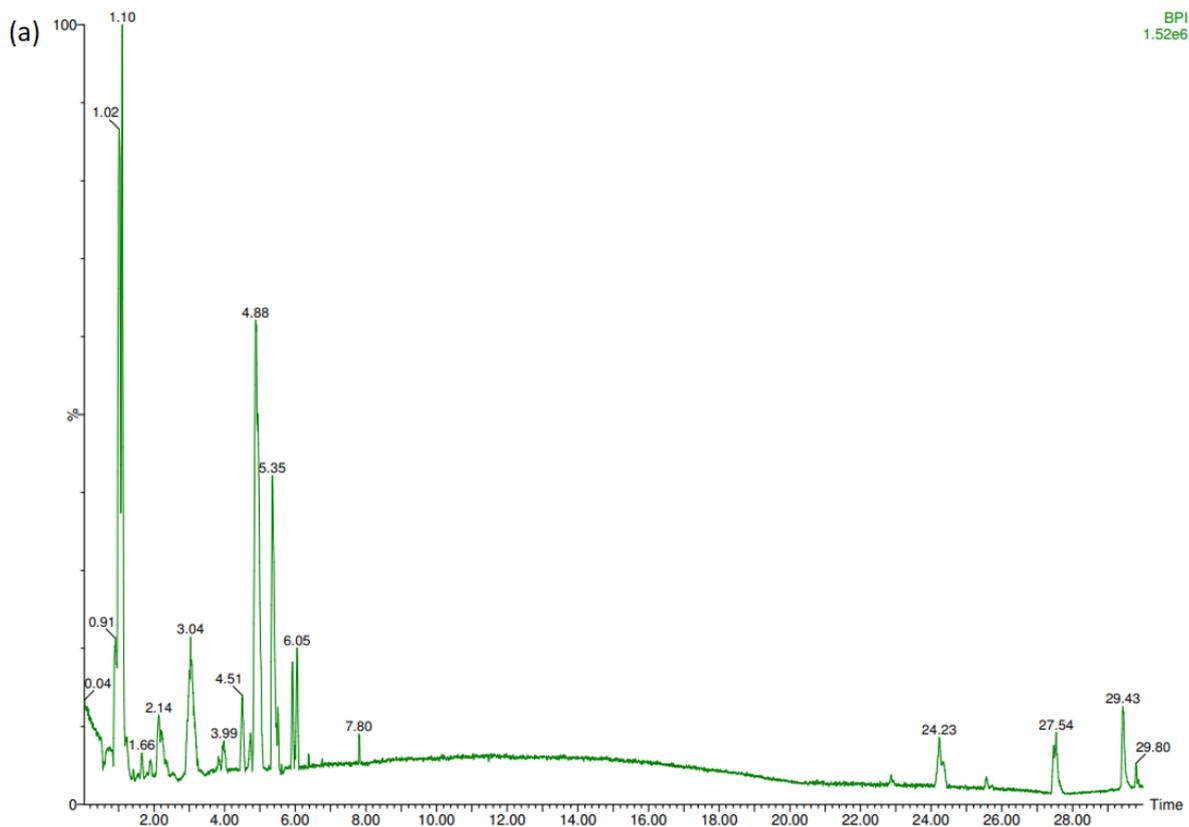
Figure 13. LCMS chromatogram for the reaction mixture of MgO_450 (a) and MgO_650 (b) at 360 C 50 wt. % glycerol.

The overall basicity determined by TPD does not tie well to the activity and CMB. It seems from data obtained from the coking that basicity data obtained from the fresh catalysts is not representative of the basicity of the samples under reaction conditions. Here it seems that is possible the MgO_650 may be less basic than MgO_750, due to whichever process causes it to coke more. This potentially leads to its lower activity and higher CMB. It is not possible however to determine this currently however, basicity would have to be measured in the dynamic *in-situ* conditions.

MgO_750 behaves unexpectedly compared to its identified characteristics, the total SA is relatively low (74 m^2) and is combined with a relatively large crystallite size (12.7 nm). This results in less available area for substrate adsorption. Thus, this should yield an increase in the proximity of the reactants on the catalysts surface. Increased proximity of substrate on the surface may be a factor in promotion of more intermolecular reactions between intermediate products.

3.3.1.6 Summary and conclusion

The results presented in this section provided motivation for the subsequent experiments presented in this thesis. A series of catalyst samples of MgO were prepared by varying the final heat treatment temperature from 450 – 750 °C. Raising the temperature led to a decrease in SA, basic site concentration, pore volume and an increase in crystallite size. MgO_450 and MgO_550 exhibited a hexagonal plate structure, MgO_650 exhibited a degraded structure which seemed to exhibit intercrystallite channels possibly cause by the exfoliation of structural water. MgO_750 in turn showed a microstructure similar to the lower temperature treated samples. The crystallites seemed to begin to aggregate into a lamella like arrangement. When tested for the gas phase conversion of glycerol the samples decreased in conversion and increased in CMB until MgO_650. MgO_650 exhibited a very high CMB of 98% which had not been observed before over MgO for this reaction. It is postulated that this is due to the sample not facilitating the production of HWMPs which are not analysed well by our method. The compounds suspected to be the main contributors for the formation of the HWMPs are likely to be sourced from the aldehyde and ketone groups. Products such as acetaldehyde which is produced in a high selectivity are known to readily undergo condensation reactions over basic catalysts.[10,26,51] The observed selectivity to products stays relatively stable and does not exhibit a clear trend, however the higher CMB exhibited by MgO_650 results in a higher STY for methanol being achieved, even with a lower conversion. This goes to show how important it is to achieve a high CMB in reactions. It is thought that the catalysts' ability to form HWMP products is linked to its proportion of strong basic sites, which may be more likely to dissociate water than coke, and once hydroxylated may stabilise molecules for further reaction.

Table 8. Full selectivity for MgO_450 – 750 at 360 c 50 wt.%

	MgO_(450)	+/-	MgO_(550)	+/-	MgO_(650)	+/-	MgO_(750)	+/-
acetaldehyde	19.7	0.8	17.4	0.4	20.2	1.5	21.6	0.5
propionaldehyde	0.6	0.2	0.1	0.1	0.6	0.1	0.6	0.0
acetone	0.1	0.1	0.3	0.1	0.1	0.1	0.1	0.0
acrolein	13.4	0.6	11.2	0.5	12.7	0.9	12.8	0.6
methanol	11.9	0.3	10.1	0.4	9.8	0.3	11.4	0.3
2-propanol	0.6	0.2	0.0	0.1	0.4	0.1	0.6	0.0
ethanol	0.0	0.2	0.6	0.2	0.1	0.1	0.0	0.0
2,3-butanedione	1.2	0.0	1.4	0.1	1.1	0.1	1.3	0.0
2-butanol	0.1	0.0	0.1	0.0	0.0	0.0	0.1	0.0
1-propanol	0.1	0.0	0.1	0.0	0.1	0.0	0.0	0.0
3-hexanone	0.0	0.1	0.1	0.0	0.0	0.0	0.0	0.0
allyl alcohol	0.8	0.0	0.7	0.0	0.6	0.1	0.8	0.1
cyclopentanone	0.6	0.0	0.7	0.0	0.3	0.1	0.6	0.1
hydroxyacetone	23.2	0.1	28.3	0.9	23.7	1.2	23.9	0.2
3-ethoxy-1-propanol	0.9	0.0	0.7	0.0	0.9	0.1	0.9	0.1
acetic acid	0.5	0.2	1.3	0.2	0.5	0.2	0.4	0.2
Glycidol	1.0	0.1	0.9	0.2	2.9	0.6	1.6	0.2
propionic acid	0.3	0.2	0.9	0.2	0.2	0.2	0.2	0.0
1,2-propanediol	2.1	0.3	2.7	0.0	2.6	0.3	2.2	0.0
unknown(s)	8.3	0.3	8.1	0.1	8.4	0.6	7.6	0.5
ethylene glycol	8.2	0.9	9.3	0.1	9.2	1.4	8.1	0.1
1,3-propanediol	0.8	0.1	0.5	0.0	0.8	0.1	0.6	0.0
phenol	0.1	0.0	0.2	0.0	0.3	0.1	0.0	0.0
CO	2.8	0.1	2.2	0.1	2.7	0.3	2.8	0.0
CO_2	2.7	0.5	1.8	0.2	1.9	0.1	2.0	0.2
Glycerol conversion	87	4.3	80	1.8	75	1.4	80	1.6
Carbon balance	74	3.2	78	1.3	98	1.2	79	1.7
Methanol STY g h^{-1} kg h^{-1}	85	3.6	74	1.4	93	6.0	79	3.2

3.3.2 Influence of heat treatment temperatures on low conversion reactions

To develop a more comprehensive understanding of the processes occurring, investigation focusing on different stages of the reaction was conducted. First low conversion reactions were explored, there has not been significant work on low conversion over MgO reactions, with previously reported reactions exhibiting 70 % + conversion.[1,2] Here, reactions were conducted at lower temperatures, with the aim to only convert a minimal portion of the glycerol fed and isolate a higher degree of intermediate products. This was done with the series of catalysts to better understand how the physicochemical properties such as basicity effect the selectivity in the early stages of the

reaction. The contact time and temperature were adjusted, so that each material was analysed at low conversion (< 10 %). At this level of conversion, products such as methanol, acrolein and acetaldehyde are expected to be in low abundance, as they are not primary reaction products.

To reduce the catalyst contact time, a lower amount of catalyst (0.1 g) was used. The bed was kept at a constant volume of 1 mL using SiC as a diluent). For comparison, in a typical reaction with 0.5 g catalyst the GHMV was 6000 (L h^{-1} Kg^{-1} cat), which would increase to 30000 (L h^{-1} Kg^{-1} cat) if only 0.1 g were to be used. Furthermore, reactions were carried out at 320 °C, to achieve conversions below 10 % (Table 9). The conversions achieved are relatively consistent over each catalyst with CMB of approximately 100 %. On the other hand, there are significant differences in the product distributions between the catalysts under these conditions. This illustrates that the MgO catalysts act differently in the initial stage of the reaction, with a variation in the preferential reaction route evidently dependant on the catalysts surface.

In contrast to the previously discussed experiments carried out at increased catalyst contact and reaction temperature (Table 6, Table 8) (360 °C, 50 wt.% 0.5 g MgO), the selectivity to acrolein was found to be higher than acetaldehyde (Table 8). For these low conversion reactions over MgO_650, the selectivity was 7.0 % to acetaldehyde and 12.6 % to acrolein (Table 10). In contrast, under the standard reaction conditions (Table 8); at high conversion and 360 °C, the selectivity to acetaldehyde was 20.2 % and acrolein was 12.7 %.

This may indicate that the formation of acetaldehyde is promoted more by contact time and higher temperature than acrolein. It seems that the double dehydration may be less temperature dependant than the radical cleavage reactions expected to yield acetaldehyde. Reactions reported in the literature where acrolein is the desired product often use temperatures of the range of 280 °C – 340 °C, over acidic catalysts.[52–56] Titanium dioxide was used as a base for mixed oxides investigated by W.Suprun and co-workers for the conversion of glycerol. The impregnation of Mg resulted in a lowed acidity and low selectivity to acrolein which only increased marginally when taking the temperature from 180 – 330 °C.[57] Previous work on the MgO_STD sample by Smith *et al.*[1] found that on raising the temperature from 360 to 440 °C, along with the accompanied increase in conversion, the selectivity to acetaldehyde increased more than acrolein. The same was observed with ceria where the O^{2-} defect sites can be highly basic,[5] selectivity was also significantly influenced depending on morphology.[4]

Table 9. Influence of catalyst pre-treatment temperatures on reactions carries out at 320 °C

Reaction conditions: Aqueous (H_2O) glycerol solution (50 wt.%); Ar(50 mL min^1); catalyst (0.1 g); (bed volume 1 mL) GHSV = 4615 h^{-1}); temperature (320 °C); pressure (1 atm).

Acronym: C (conversion); ACE(acetaldehyde), ACR(acrolein); MOH(methanol); HAD(hydroxyacetone); UNK(unknown); EG(ethylene glycol); CMB(carbon mass balance).

*Coke calculated from thermogravimetric analysis

Catalyst	C_{gly} (%) (+/-)	Selectivity % (**STY** / gh^{-1} kgcat^{-1})						CMB % (+/-)
		ACE	ACR	MOH	HAD	UNK	EG	
MgO_450	8 (2.6)	7.2 **(12)**	13.8 **(19)**	8.6 **(21)**	26.9 **(49)**	12.1 **(NA)**	14.0 **(33)**	105 (5.6)
MgO_650	5 (2.5)	7.0 **(18)**	12.6 **(28)**	8.1 **(32)**	25.9 **(77)**	20.3 **(NA)**	14.5 **(54)**	102 (3.2)
MgO_750	7 (2.8)	6.2 **(16)**	11.1 **(25)**	8.0 **(32)**	22.2 **(65)**	28.1 **(NA)**	13.4 **(50)**	100 (3.1)

From the proposed scheme (Figure 8) acrolein and acetaldehyde are thought to form through different pathways. Acetaldehyde which proceeds from the fragmentation of both hydroxyacetone and ethylene glycol, may require a higher temperature due to the several reaction steps. The degree of coking may also influence the reaction, a lower reaction temperature may result in the catalyst being less coked. A stabilisation period of 2 hours 15 minutes is used for all reactions run before collection which allows for an initial build-up of coke, this may influence the degree that the samples can catalyse the double dehydration. The formation of acrolein through a double dehydration may be a simpler process occurring over one surface adsorption cycle. The smaller amount of catalyst used in these reactions means that a shorter contact time is available before full desorption. This could result in there not being enough catalyst surface to undergo these multiple adsorption/reaction processes. It would be expected that the decrease in contact time would influence how far along a specific pathway the substrate proceeds. Selectivity to a particular pathway would be expected to be tied to changing reaction conditions or MgO surface characteristics.

On increasing the catalyst heat treatment temperature, the selectivity to detectable unknowns increases; from 12.1 % for MgO_450, to 20.3 % and 28.1 % for MgO_650 and MgO_750, respectively. For MgO_650 and MgO_750 these are significantly higher than seen in other reactions over MgO (9.3 % and 9.2%. respectively under 3.3.1 standard conditions). This is likely due to temperature effecting the rate through which different pathways progress. These may be reaction

intermediates but are not necessarily HWMP precursors. In reference to reaction schemes previously published, there are some intermediates and products in the proposed reaction scheme which have not be quantified, these could include molecules such as glyceraldehyde, ethenone and 3 hydroxy-propenal. MgO_650's lower observed activity and the lower temperature may result in these products, which at higher temperatures would proceed to more terminal products. They could be the precursors to HWMP, for MgO_450 and MgO_550, but this seems unlikely for MgO_650 due to its lack of observed production to HWMP under higher conversion. However, under these reaction conditions the surface of the catalyst is significantly less coked than in section 3.3.1 which may allow this, however this does not explain why MgO_650 exhibits such a high selectivity.

It is possible that some of these products are seen in significant amounts under these conditions. This suggestion is even more pertinent given that over the MgO_450 catalyst, which under higher temperature conditions has a relatively low CMB, exhibits the lowest selectivity to unknowns (12.1 %). Products, such as acetaldehyde which can undergo further bimolecular reactions to HMWP are produced only in minor quantities. This combined with the short contact time results in no discernible loss of CMB from HWMP. On the other hand, if these unknowns are the beginning of the HWMP, there may be a mechanism upon the surface of the MgO_650 that either breaks down larger products or inhibits further growth at higher temperature conversion. From the 3.3.1 section reactions, MgO_650 also seems to be the least active catalyst, while at these low conversion experiments this is not as clear. The low conversion of glycerol is initially expected to be due to basicity and SA, but MgO_750 was lower for both of these characteristics. Other characteristics that may affect its consumption of glycerol may be the higher coking it exhibited at those temperatures, possibly blocking active sites.

In summary, when running reactions at a low temperature and contact time a relatively high concentration of unknown products is observed. These are likely intermediate precursors to quantified products and condensation products. Over MgO_650 which does show a significant selectivity to these unknowns it would be expected that these are the former, or if the later would be broken down at higher temperatures or not formed due to higher coking under different conditions. The more basic catalysts exhibit less unknowns, and more products such as hydroxyacetone. This shows they may react the substrates through more steps than the less basic catalysts, which may have trouble binding before desorption. Negligible HWMP are inferred with full CMB throughout. This is likely due to the products which readily undergo condensation not being produced in significant concentration. Acetaldehyde, which is normally more prevalent than acrolein is less selective here which may be due to shorter contact time and lower temperature.

Hydroxyacetone while still making up a high proportion of the products is unlikely to contribute to HWMPs under these conditions as it is expected to require high temperatures to convert.

Table 10. Product distribution of varied heat treatment temperature catalysts at low conversion. Reaction conditions; 320 °C ,50 wt.% glycerol/water flow 0.016 mL min^{-1}, 0.1 g MgO, 50 mL min^{-1} Ar, 3 hours.

Carbon mole selectivity %	MgO_450	MgO_650	MgO_750
Acetaldehyde	7.2	7.0	6.2
propionaldehyde	0.2	0.0	0.1
acetone	0.1	0.1	0.1
acrolein	13.8	12.6	11.1
methanol	8.6	8.1	8.0
ethanol	0.3	0.3	0.3
2,3-butanedione	0.1	0.1	0.1
1-propanol	0.1	0.0	0.0
allyl alcohol	0.8	0.6	0.6
cyclopentanone	0.1	0.1	0.1
hydroxyacetone	26.9	26.0	22.2
3-ethoxy-1-propanol	3.9	2.1	1.7
acetic acid	0.3	0.2	0.2
Glycidol	0.0	0.1	0.7
propionic acid	4.6	2.6	3.1
1,2-propanediol	2.8	2.7	2.4
unknown(s)	12.1	20.3	28.1
ethylene glycol	14.0	14.5	13.4
1,3-propanediol	2.3	0.8	0.2
phenol	0.3	0.0	0.2
CO	0.4	0.6	0.3
CO2	0.9	0.5	0.0
Glycerol conversion %	8	5	7
Carbon balance %	105	102	100
Methanol STY. g h^{-1} kg h-1	21	32	32
Coke % carbon	<1 %	<1 %	<1 %

3.3.3   Assessing the influence of water in the reactor feed

Water is usually used as a feed diluent, typically accounting for 50 wt.% of the feed. Previously, it was suggested by Haider *et al.*[2] that water could be used as a source of hydrogen for the production of methanol. This was tested in an experiment where the water was replaced with D_2O, which resulted in a significant drop in conversion. This led to the conclusion that water was the source of hydrogen in the reductive process.[2] Smith *et al.*[1] also found that the use of higher concentrations of water in the reactor feed led to a higher CMB, which may be attributed to water preventing condensation reactions.[58] Given that water can readily undergo dissociative adsorption on MgO surfaces,[39,59–63] and that surface hydroxyls can dramatically influence the reactivity of MgO in various reactions,[37–40] it was important that the role of H_2O is understood. The aim was to investigate how this change would affect how the catalyst interacts with the substrate and products. These experiments were initiated by swapping out the water diluent with D_2O in the

feedstock stream. The experiments were run under standard conditions of 360 °C and 50 wt.% glycerol so as to compare the results to those obtained in section 3.3.1.

Previous computational studies carried out in our research group by Sainna et al.[13] demonstrated that the hydrogen from water was energetically unlikely to be a key reductive resource for the last step of the formation of methanol from glycerol, but that MgO would likely be easily hydroxylated via the dissociative adsorption of water on its surface. Therefore, water could be instrumental in the initial phases of the reaction and its dissociation would hydroxylate the surface in-situ. As mentioned, hydroxylation may possibly be an indicator of a catalysts ability to promote bimolecular reactions.

The experiments were performed over the MgO samples, to establish whether the preparation of the catalyst affected its ability requirement for water as a hydrogen source. When avoiding adding H_2 into the feed, water is thought to be able to use as a source of hydrogen for the dehydration of glycerol to 2,3-dihydroxy-propenel and then a enol–keto tautomerism to hydroxyacetone (Figure 14).[2]
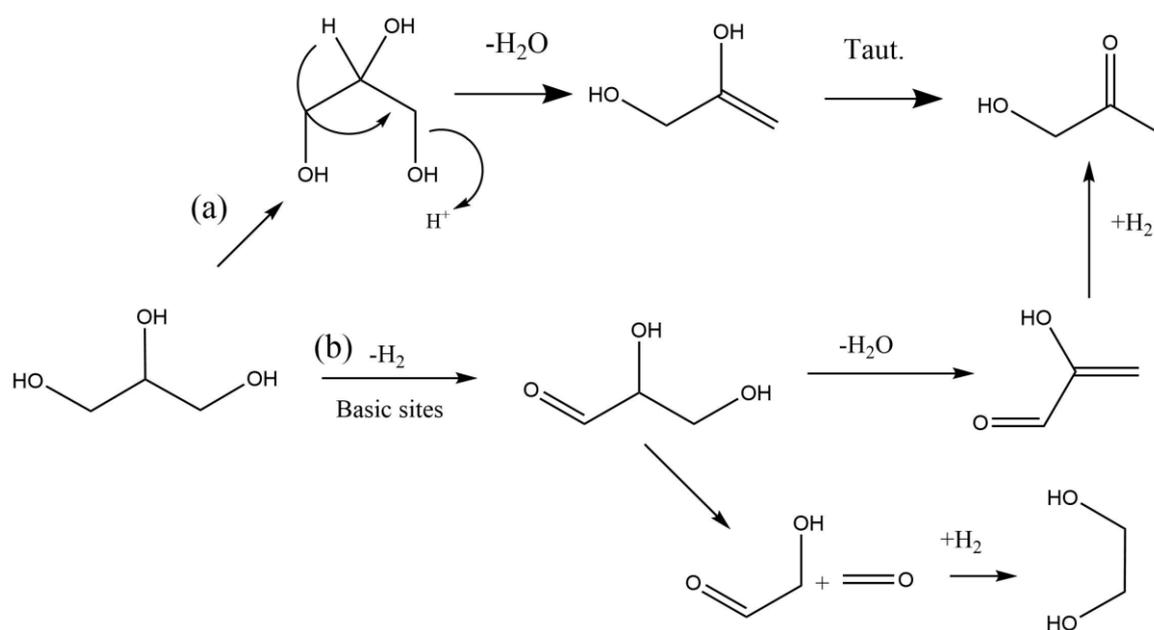
Figure 14. Glycerol activation to hydroxyacetone over basic catalysts pathways (a) Haider et al.[2] (b) Kinage et al.[64] M. H. Haider, N. F. Dummer, D. W. Knight, R. L. Jenkins, M. Howard, J. Moulijn, S. H. Taylor and G. J. Hutchings, Nat. Chem., 2015, 7, 1028–1032. A. K. Kinage, P. P. Upare, P. Kasinathan, Y. K. Hwang and J. S. Chang, Catal. Commun., 2010, 11, 620–623.

A hydrogen source is also proposed to be required for the formation of hydroxyacetone through an alternative route, in which glycerol would undergo a dehydrogenation to 2,3-dihydroxy-propanal

followed by a dehydration and then hydrogenation, or a fragmentation and hydrogenation to ethylene glycol, this was proposed to occur over basic sites by Kinage *et al.*[64] They were however looking at acid/base catalysts, a too high proportion of basic sites was proposed to result in ethylene glycol from 2,3-dihydroxy-propanal. We were interested in seeing if the higher degree of coking and presumed loss of basicity over MgO_650 would mean it activated glycerol by another route.

The results, presented in Table 11 and Table 12, indicate that the use of D_2O can indeed inhibit the conversion of glycerol, to differing degrees, depending on the heat treatment temperature used. With the MgO materials calcined at lower temperatures, a strong kinetic isotopic effect (KIE) was observed on the activity of the catalyst. MgO_ 450 exhibited a KIE of 1.6, MgO_550 that of 1.5. MgO_650 only a showed a negligible decrease of conversion with a KIE of 1.0. However, MgO_750 showed a very strong KIE of 2.1. This is unexpected based on total basicity alone and seems to correlate to the proportion of strong basic sites.

Table 11. Performance of MgO catalysts un the gas phase valorisation of glycerol using D_2O
Reaction conditions: Aqueous (D_2O / H_2O) glycerol solution (50 wt.%); Ar(50 mL min^1); catalyst (0.5 g); (bed volume (1 mL) GHSV 4615 h^{-1}) ; temperature (360 °C); pressure (1 atm).
Acronym: X (conversion); ACE(acetaldehyde), ACR(acrolein); MOH(methanol); HAD(hydroxyacetone); UNK(unknown); EG(ethylene glycol); CMB(carbon mass balance).

Catalyst ID	X glycerol (%) (+/-)	KIE	% Selectivity						CMB (%) (+/-)
			ACE	ACR	MOH	HAD	UNK	EG	
D2O MgO_450	54 (4.4)	1.6	13.8	10.8	9.9	28.6	9.6	12.2	98 (2.4)
H2O MgO_450	87 (4.3)		19.7	13.4	11.9	23.2	8.3	8.2	74 (3.2)
D2O MgO_550	53 (0.3)	1.5	13.0	10.0	10.0	28.6	14.3	11.0	95 (5.2)
H2O MgO_550	80 (1.8)		17.4	11.2	10.1	28.3	8.1	9.3	78 (1.3)
D2O MgO_650	71 (0.9)	1.0	17.0	10.9	10.6	26.7	9.4	10.2	94 (2.2)
H2O MgO_650	75 (1.4)		20.2	12.7	9.8	23.7	8.4	9.2	98 (1.2)
D2O MgO_750	38 (2.3)	2.1	14.6	8.9	9.1	28.7	8.9	14.2	95.1 (1.4)
H2O MgO_750	80 (1.6)		21.6	12.8	11.4	23.9	7.6	8.1	79 (1.7)

The decrease in glycerol conversion supports the changes in selectivity observed. There was a reduction of acetaldehyde (*ca.* - 5 %) selectivity when H_2O was replaced with D_2O, however, the concentration of intermediate products such as hydroxyacetone (*ca*. + 5 %), and ethylene glycol (*ca*. + 3 %) increased.

Interestingly, the CMB increased in reactions carried out over MgO_450 and MgO_550, when D_2O was used. An increase from 74 % to 98 % CMB over MgO_450 and the accompanied drop from 87 % conversion to 54 % was noted with the replacement of H_2O with D_2O. MgO_550 shows an increase in CMB from 78 % to 95 % as the conversion drops from 80 % to 53 %. Naturally, the lower conversion itself would result in there being significantly lower concentration of reactive intermediates. These intermediates would likely have less interaction with each other resulting in HWMPs and thus a higher CMB is observed.

Another possible explanation is that, in the presence of D_2O, the MgO surface is protonated/deuterated to Mg-O(H/D) at a slower rate. Mg-O(H) are thought to be of a lower basic strength than surface Mg^{2+}-O^{2-} and edge O^{-2} sites. However, hydroxyl sites are expected to be important to catalysis, in certain scenarios they have been shown to be very active. Fan *et al.* saw they stabilise substrates on the surface allowing for bimolecular interaction (section 3.3.1.4).[38]

In contrast to the other catalysts, the reactivity of the MgO_650 material is notably only marginally affected using D_2O. This indicates that the first stage of the reaction, the dehydration of glycerol, preferentially uses a proton from a different source with MgO_650. This indicates that over this catalyst the reaction route in the initial stages may be different. Due to their higher degree of basicity per gram, MgO_450 and 550, may be more efficient at dissociating water and use its hydrogen for the dehydration of glycerol. Conversely, over MgO_650, which is less basic, this possibly results in another route being more favourable. The more basic catalysts may not proceed down this route, in the absence of water due to D_2O possibly adsorbing more strongly to the surface potentially blocking the active sites. However, this is not the case with MgO_750 which is significantly affected by D_2O inclusion, indicating that the basic site distribution of O^{2-} is important for water dissociation.

The results of the experiments with D_2O suggest that the dissociative adsorption of water, which form hydroxylated Mg sites *in situ*, must at least be partially responsible for catalysing undesirable side reactions seen over the more basic catalysts. There is a correlation between the catalysts that lose a high degree of CMB and those which exhibit a significant KIE with D_2O. The DRIFTS experiments (Figure 6) indicated that bicarbonate species form on hydroxylated sites are quite prevalent on MgO_450 and MgO_550. If these OH sites are deuterated under reaction conditions, it may affect their reactivity. The deuteriation of the OH basic sites may lead to the reactivity changing, deuterium has twice the mass of hydrogen, this may result in a change in how it would interact and possibly incorporate with the substrates.

MgO_750 is however greatly affected by the change to D_2O, so this cannot just be an effect of basicity. The *ex-situ* investigations of basicity may not show the full picture however, it cannot be determined how basic the samples actually are under reaction conditions.
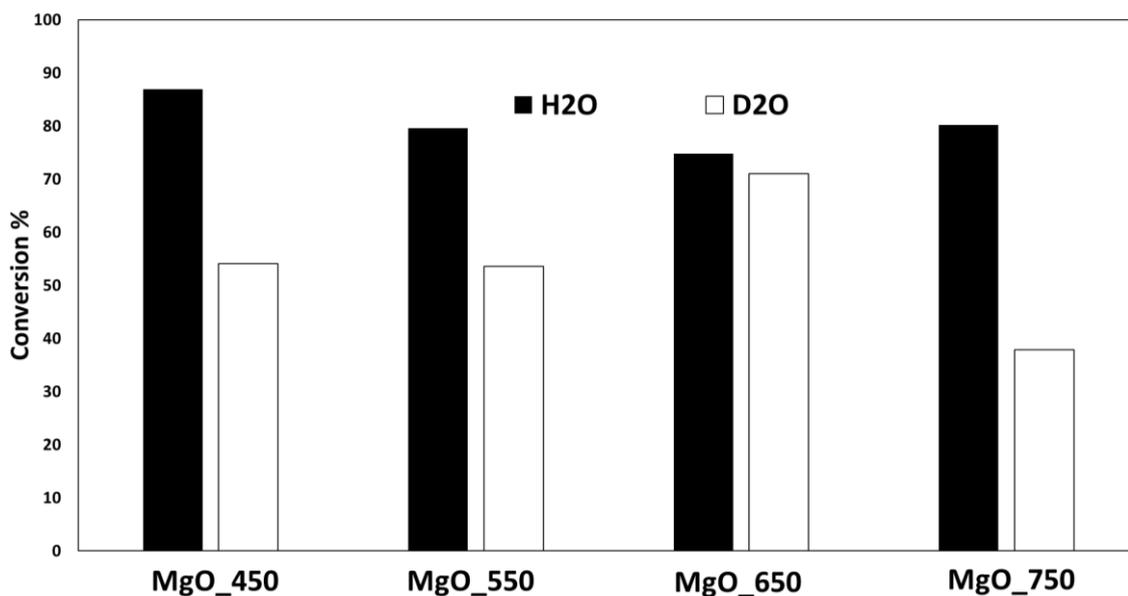
Figure 14. MgO_450 – MgO_750 D_2O and H_2O experiments compared. Reaction conditions; 360 °C ,50 % glycerol / water flow 0.016 mL min^{-1}, 0.5 g MgO, 50 mL min^{-1} Ar, 3 hours.

Based on the evidence so far presented it is hypothesised that the CMB of the glycerol reaction may be based on several parameters, these may include the total concentration and the type of basic sites, and the morphology of the MgO surface. It is also suspected that the ability for the surface to be hydroxylated by H_2O present in the stream is key as removal of water from the stream results in large differences in activity for all the samples apart from MgO_650.

Table 12. Full selectivity MgO_450 – MgO_750 D$_2$O experiments. Reaction conditions; 360 °C ,50 % glycerol / water flow 0.016 mL min^{-1}, 0.5 g MgO, 50 mL min^{-1} Ar, 3 hours.

	MgO_450	(+/-)	MgO_550	(+/-)	MgO_650	(+/-)	MgO_750	(+/-)
Acetaldehyde	13.8	0.4	13.0	0.6	17.0	0.6	14.6	0.5
propionaldehyde	0.5	0.0	0.5	0.0	0.6	0.0	0.2	0.0
acetone	0.2	0.1	0.1	0.0	0.5	0.2	0.2	0.1
acrolein	10.8	0.5	10.0	0.6	10.9	0.2	8.9	0.3
methanol	9.9	0.0	10.0	0.7	10.6	0.7	9.1	0.0
2-propanol	0.0	0.0	0.0	0.0	0.0	0.0	0.0	0.0
ethanol	0.5	0.0	0.5	0.0	0.6	0.0	0.4	0.0
2,3-butanedione	0.8	0.1	0.7	0.0	1.1	0.1	1.1	0.1
1-propanol	0.1	0.0	0.1	0.0	0.1	0.0	0.0	0.0
3-hexanone	0.1	0.0	0.1	0.0	0.0	0.0	0.0	0.0
allyl alcohol	0.7	0.0	0.8	0.0	0.8	0.1	0.6	0.0
cyclopentanone	0.5	0.0	0.5	0.0	0.6	0.0	0.6	0.0
hydroxyacetone	28.6	0.9	28.6	0.1	26.7	0.9	28.7	0.6
3-ethoxy-1-propanol	1.5	0.2	0.7	0.2	1.0	0.2	1.6	0.1
acetic acid	1.0	0.1	0.9	0.1	1.1	0.1	1.1	0.1
Glycidol	0.5	0.1	0.5	0.0	0.6	0.0	0.6	0.1
propionic acid	1.6	0.2	1.2	0.4	1.2	0.2	2.5	0.2
1,2-propanediol	3.0	0.1	3.6	0.4	2.4	0.3	3.6	0.1
unknown(s)	9.6	0.5	14.3	0.4	9.4	0.2	8.9	0.7
ethylene glycol	12.2	0.3	11.0	2.0	10.2	0.4	14.2	0.2
1,3-propanediol	0.8	0.2	0.9	0.4	0.7	0.2	0.4	0.2
phenol	0.2	0.0	0.1	0.0	0.2	0.0	0.2	0.0
CO	1.7	0.1	1.4	0.2	2.1	0.1	1.2	0.1
CO$_2$	1.6	0.0	0.5	0.5	1.5	0.1	1.3	0.0
Glycerol conversion	54	4.4	53	0.3	71.	0.9	38	2.1
Carbon balance	98	2.4	95	5.2	94	2.2	95	2.9
Methanol STY. g h^{-1} kg h^{-1}	65	8.0	66	2.3	81	3.6	55	4.7

3.3.4 Influence of reaction temperature on product distribution

With MgO_650 obtaining a high CMB at 360 °C, the catalyst was tested under varied temperatures to see if the catalyst could maintain high CMB under different conditions and conversion levels. This was also done to tie in with the low conversion results in section 3.3.2. Running reactions at a higher temperature would also be important to try an achieve greater yields of products such as methanol. Increased thermal input should lead to an increase to full conversion and decrease of intermediate products such as hydroxyacetone and ethylene glycol in favour of products such as methanol. Radical reactions which are proposed to be important in our reaction, leading to potentially favourable yields of methanol compared to other pathways would also be expected to be more prominent at higher temperatures over MgO. [1]

The reaction temperature has a pronounced effect on the product distribution seen over MgO for the conversion of glycerol. Reactions were primarily conducted over MgO_650. The conversion increases significantly from 28 % at 320 °C to 75 % at 360 °C, further increases to 400 °C almost reaches full conversion at 96 %. Further increases to 440 °C gives only a marginal increase to 97 %,

however it does still lead to product distribution changes. The catalyst manages to maintain a high CMB throughout of above 90 %. Any loss of CMB at high temperatures is attributed mainly to an increase in reactor fouling and catalyst coking. A significant increase in HWMP does not seem evident at higher temperatures over MgO_650, otherwise it might be expected that the CMB would drop off significantly.

The product selectivity changes significantly as the temperature increases. Selectivity to aldehydes goes up distinctly, especially that for acetaldehyde and acrolein. At 320 °C there is a 10.6 % selectivity towards acetaldehyde and 11.7 % towards acrolein. On increasing the temperature, acetaldehyde quickly becomes the dominant aldehyde, with 20.2 % to 12.7 % at 360 °C and 27.4 % acetaldehyde to 16.4 % acrolein at 440 °C.

The proposed reaction pathways are shown in Figure 8. The double dehydration may be less temperature dependant compared to the radical defragmentation to methanol and acetaldehyde. Reactions in the literature to acrolein often use temperatures of the range of 280 °C – 340 °C, over acidic catalysts.[52–56] This indicates that the high temperatures often used in our reactions (320 °C – 480 °C) are not necessary for high acrolein yields. Table 13 shows that increasing the temperature over 400 °C only marginally increases the selectivity to acrolein to 16.4 % compared to acetaldehyde which reaches 27.4 %. A corresponding decrease in ethylene glycol is observed, with a selectivity of 9.9 % at 320 °C decreasing to 4.8 % at 440 °C.

Methanol does not see a clear trend in selectivity, staying between 9 – 14 % throughout, the output yield of methanol does increase with conversion up to 122 g h^{-1} kg h^{-1} at 400 °C from 35 g h^{-1} kg h^{-1} at 320 °C. However, the increase to 440 °C sees an actual decrease in yield of methanol down to 105 g h^{-1} kg h^{-1} at approximately the same conversion of glycerol. This may be due to methanol being consumed at higher temperatures, this may be related to the decomposition of methanol to give CO and H$_2$.[65,66] The CO increases with temperature which may be partly explained by this. CO$_2$ also increases by temperature which may be produced by the water gas shift reaction (WGS) over MgO.[67]

The selectivity to intermediate products such as: diols, unknowns and hydroxyacetone, which are usually the major product seen over MgO at lower temperatures decrease, as the temperature increases. The unknowns decrease from 11.7 % to 6.1 % between 320 °C - 400 °C but then stabilise at higher temperatures indicating the leftover unknowns are likely not be intermediates.

Compared to previous work in the area the maintenance of high CMB throughout a variance of temperature indicates that this catalyst suppresses the formation of high weight products over a

broad range of conditions and conversion level. The slight decrease in CMB is likely to be attributed to an increase in reactor fouling.

Table 13. Influence of reaction temperature - MgO_650 Reaction conditions; 320 - 440 °C ,50 % glycerol/water flow 0.016 mL min⁻¹, 0.5 g MgO, 50 mL min⁻¹ Ar, 3 hours.

Carbon mole selectivity %	320 °C	360 °C	400 °C	440 °C
Acetaldehyde	10.6	20.2	23.5	27.4
propionaldehyde	0.0	0.6	1.0	1.5
acetone	0.3	0.1	0.2	0.2
acrolein	11.7	12.7	12.6	16.4
butyraldehyde	0.0	0.0	0.0	0.0
methanol	12.4	9.8	13.4	9.7
2-propanol	0.0	0.4	0.0	0.1
ethanol	0.5	0.1	0.9	0.8
2,3-butanedione	0.5	1.1	1.7	1.5
2-butanol	0.0	0.0	0.0	0.0
1-propanol	0.1	0.1	0.1	0.2
3-hexanone	0.1	0.0	0.2	0.2
2-hexanone	0.0	0.0	0.0	0.0
2-methyl-1-propanol	0.0	0.0	0.0	0.0
allyl alcohol	0.8	0.6	1.0	1.1
cyclopentanone	0.5	0.3	0.7	0.5
hydroxyacetone	31.5	23.7	20.8	16.5
3-ethoxy-1-propanol	1.0	0.9	1.1	0.9
acetic acid	0.7	0.5	1.6	1.6
Glycidol	0.4	2.9	0.7	0.5
propionic acid	2.1	0.2	1.2	0.8
1,2-propanediol	2.4	2.6	2.0	1.6
unknown(s)	11.7	8.4	6.1	6.3
ethylene glycol	9.9	9.2	6.4	4.8
1,3-propanediol	0.3	0.8	0.5	1.0
phenol	0.1	0.3	0.1	0.0
CO	1.3	2.7	2.8	3.5
CO_2	1.2	1.9	1.6	2.8
Glycerol conversion %	28	75	96	97
CMB %	96	98	97	94
Methanol STY g h⁻¹ kg h⁻¹	35	90	122	105
coke % carbon	2.27	3.2	4.52	5.41

3.3.5 Pre-treatment and catalyst deactivation analysis – MgO_450 and MgO_650

In this section, the samples of MgO_450 and MgO_650 were tested at 360 °C, 50 wt.% glycerol and varying reaction times. This was conducted to analyse how the catalyst behaves when initially exposed to glycerol. How coke builds up on the surface and the changes to reactivity that may result was a key area of interest. In the glycerol over MgO experiments performed previously, the catalyst undergoes a pre-treatment stabilisation period in which the products are not analysed. For the first 15 minutes 0.1 mL min⁻¹ of 50 wt.% glycerol is flowed over the catalyst. After 15 minutes the flow of glycerol solution is reduced to 0.016 mL min⁻¹ and run for a further 2 hours before collection begins. This follows the method of reaction data collection in previous publications on this reaction.[1,2] The pre-treatment period was determined to be required as the catalyst showed a low

and shifting CMB during the earlier stages, which stabilised by the 2 hours run time point.[1,2] This was determined to be due to *in-situ* changes to the catalyst under reaction conditions, such as a layer of coke forming on the surface. It is important to know what is happening during this time is understood for our catalysts, it may help further explain differences in performance that can't be explained *via* pre-reaction characterisation alone. MgO_450 and MgO_650 were investigated due to their significantly different SA, basicity, and reaction performance. MgO_650 especially was focussed on, this was due to the high degree of coking observed in the reaction from section 3.3.1. The catalyst characteristics during the collection period are thought to be different compared to the fresh samples due to coke build up. This is thought to possibly have an effect on the catalyst's basicity *in-situ* and may have contributed to it obtaining a high CMB.

The reaction samples were collected as separate fractions during the reaction time. These included between 15 minutes to 1 hrs 15 minutes (first half of the pre-treatment period). 15 minutes to 2 hrs 15 mins (full pre-treatment period). These can then be compared to 2.15 hrs 15 mins to 5 hrs 15 mins, which represent the full normal collection time (3.3.1 results). The reaction results for MgO_650 are shown in Table 14 in terms of µmole product hr ^{1}. The conversion shows that the reactivity of the MgO_650 changes over time and needs to stabilise. With MgO_650 there is a clear trend on the increase of CMB over time. With the first hour of reaction after the initial 15 minutes giving a CMB of 75 %, this then increases to 96 % for the second hour, comparable to the value obtained during the full reaction run. MgO_450 (Table 15) behaves quite different, contrary to MgO_650 its glycerol conversion increases at the later collection time. The conversion is 74 % during the pre-treatment and 87 % in the 3-hour standard collection period. In tandem CMB decreases over time. It starts at a high 94 % in the first hour, decreasing to 85 % in the second before settling at 74 % during the full run. The lower conversion observed initially may contribute to the higher CMB seen during the pre-treatment.

To see how the catalyst cokes over time the catalyst samples were removed and investigated by TGA and TPD. The TGA data for carbon deposition in mg g^{-1} is shown in Table 14 and Table 15 for MgO_650 and MgO_450 respectively. Coking of the MgO_650 catalyst is 106 mg g^{-1} when the collected after a full 5.15 hrs. However, it seems that a significant portion of this is obtained in the first 1 hrs and 15 minutes where 64 mg g^{-1} is on the surface increasing to 67 mg g^{-1} at the end of the pre-treatment period. With MgO_450 also exhibits an increase with time, again the majority forms in the first 1 hr and 15 minutes. MgO_450 exhibits 60, 77 and 89 mg g^{-1} of coke at each respective sampling point. Due to its lower SA, MgO_650 has more coke per m^2 of catalyst SA than MgO_450. MgO_650 has 0.5 mg m^2 during the pre-treatment and 0.8 mg m^2 after the full reaction. MgO_450 has 0.3 after the first hour, 0.4 after the pre-treatment and 0.5 mg m^2 after the full run (5.15 hrs,

(pre-treatment + collection run). This would lead to it being expected for MgO_650's surface basicity to be more prominently decreased under reaction conditions.

The coke observed, while the majority is made in the first hour, could possibly lead to deactivation of the catalyst in long run reactions. Some deactivation was observed on reacting MgO_650 for 48 hours where its conversion was reduced to 46 %, CMB remained at 98 % (Table 18). This is observed over heterogeneous catalysts before with the conversion of glycerol.[43,68–71] However with the MgO_STD used for glycerol conversion, it was found to not deactivate significantly. Glycerol conversion was ca. 97 % at 2 hours, decreasing to *ca.* 87 % at 4 hours, where it remained relatively stable for the remaining time of the experiment (48 hours).[1]

To explore how the basicity of the catalysts were affected by undergoing reaction and coking, the post reaction samples were investigated *via* CO_2 TPD. Coking on the active sites of a basic catalyst may lead to deactivation.[70] For this experiment up to 300 °C is analysed by TPD. Higher temperatures cannot be accurately analysed as above 300 °C coke is removed (TGA appendix figure 15 - 18). The unused MgO_650 catalyst desorbs 491 μ moles CO_2 g^{-1} by the time the TPD reaches 300 °C. This decreases to 15 μ moles co_2 g^{-1} after the pre-treatment period. After a full reaction run (5.15 hrs), for MgO_650 a slight increase of CO_2 is seen, 68 μ moles co_2 g^{-1} is desorbed. For MgO_450, as a fresh sample it exhibited 771 μ moles CO_2 g^{-1}. 15 μ moles CO_2 g^{-1} is observed after the pre-treatment period but recovers to 106 μ moles CO_2 g^{-1} after the full run. This indicates that the coke builds up during the pre-treatment blocking basic sites, but if the reaction is run longer some process uncovers a small proportion of the basic sites. This may explain the drop and then recovery of the glycerol conversion observed with MgO_650. The amount of μ moles CO_2 g^{-1} desorbed after the full reaction seems proportional to the original amount of basicity exhibited, with both catalysts exhibiting approximately 14 % of the CO_2 g^{-1} of the fresh catalyst after the full run. MgO_450 still seems to exhibit a higher basicity after the reaction has taken place, but immediately post pre-treatment with initial coking the difference in the catalyst's basicity is removed. Further changes occur during the collection period, the conversion of MgO_450 especially indicates that the catalysts have not yet stabilised.

These results further indicate that the basicity data obtained from the fresh catalysts may not be indicative of their actual characteristics under reaction conditions. For MgO_650 the low CMB observed for the first hour and 15 minutes could be due to the exposed basic sites not yet covered by coke. However, the presence of a high CMB for MgO_450 at the early time intervals is contrary to this conclusion. It could be that the higher coking seen for MgO_650 may preferentially block certain sites, possibly stronger ones, which DRIFTS indicated MgO_650 may have less of. The D_2O

experiments shown indicate that MgO_650 can activate glycerol possibly in a different way than MgO_450.

These experiments have shown us that MgO_450 and MgO_650 behave significantly differently in the early points of the reaction. As seen with other experiments, the correlation between basicity and CMB is not yet clear, there may be several competing factors, which are hard to deconvolute for definite conclusions. Of course, the results for CO_2 TPD presented here are also not obtained during reaction conditions, the samples are cooled and removed where they would be exposed to air. Only a light pre-treatment could be used for the TPD experiments as not to remove the coke we were investigating. There may also be dynamic processes under reaction conditions changing with the catalyst surface. In other words, these results only show the catalyst surface at a specific point and not under reaction conditions, so they may not be representative of its characteristics *in-situ.*

Table 14. MgO_650 Pre-treatment μmole product hr^{-1} - Reaction conditions; 360 °C ,50 % glycerol / water flow 0.016 mL min^{-1}, 0.5 g MgO, 50 mL min^{-1} Ar.

μmole product hr^{-1}	15 mins - 1 hr 15 mins	15 mins - 2 hr 15 mins	2 hrs 15 mins - 5 hrs 15 mins
acetaldehyde	978	1151	1322
propionaldehyde	23	20	22
acetone	3	3	3
acrolein	408	439	552
butyraldehyde	0	1	0
methanol	1405	1217	1263
2-propanol	0	0	22
ethanol	37	31	29
2,3-butanedione	39	41	46
2-butanol	0	0	1
1-propanol	4	3	1
3-hexanone	3	3	0
2-hexanone	0	0	0
2-methyl-1-propanol	0	0	0
allyl alcohol	30	27	28
cyclopentanone	19	17	16
hydroxyacetone	1114	1064	1062
3-ethoxy-1-propanol	20	0	21
acetic acid	82	60	28
Glycidol	52	47	189
propionic acid	56	61	11
1,2-propanediol	108	113	113
unknown(s)	177	226	258
ethylene glycol	557	543	691
1,3-propanediol	20	21	35
phenol	3	3	1
CO	303	281	361
CO2	395	309	231
glycerol conversion %	75	68	75
CMB %	83	96	98
Methanol STY. g h^{-1} kg h^{-1}	96	82	93
carbon deposition mg g^{-1}	64	67	106

Table 15. MgO_450 Pre-treatment μmole product hr⁻¹ - Reaction conditions; 360 °C ,50 % glycerol / water flow 0.016 mL min⁻¹, 0.5 g MgO, 50 mL min⁻¹ Ar.

μmole product hr⁻¹	15 mins - 1 hr 15 mins	15 mins - 2 hr 15 mins	2 hrs 15 mins - 5 hr 15 mins
Acetaldehyde	737	843	1046
propionaldehyde	21	18	20
acetone	3	3	3
acrolein	391	362	472
butyraldehyde	1	0	0
methanol	1566	1276	1259
2-propanol	0	0	21
ethanol	38	31	1
2,3-butanedione	33	28	32
2-butanol	0	0	2
1-propanol	4	3	5
3-hexanone	2	2	0
2-hexanone	0	0	0
2-methyl-1-propanol	0	0	0
allyl alcohol	34	28	28
cyclopentanone	17	13	12
hydroxyacetone	1207	1000	821
3-ethoxy-1-propanol	18	18	19
acetic acid	77	63	25
Glycidol	54	38	52
propionic acid	25	41	9
1,2-propanediol	118	108	76
unknown(s)	180	197	295
ethylene glycol	567	535	436
1,3-propanediol	16	13	28
phenol	2	2	3
CO	229	198	296
CO2	442	183	283
glycerol conversion %	74	74	87
CMB %	94	85	74
Methanol STY g h⁻¹ kg h⁻¹	105	81	85
carbon deposition mg g⁻¹	60	77	89
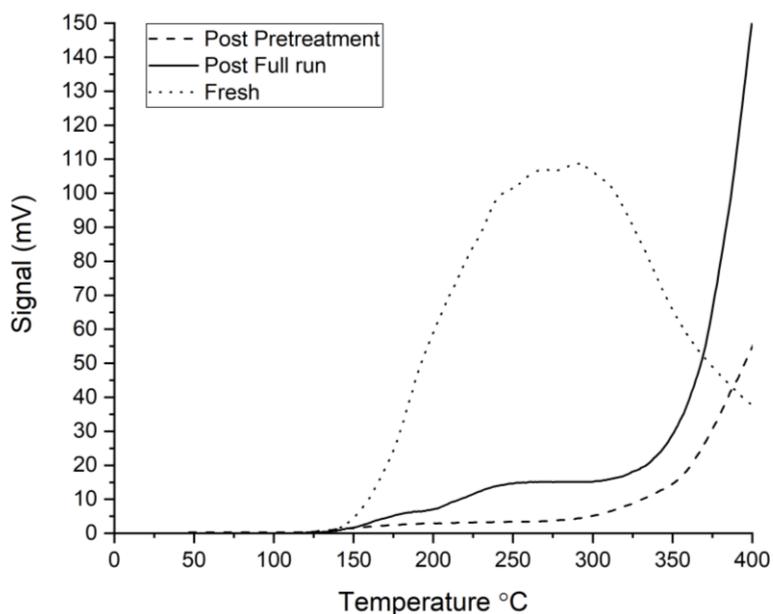
Figure 15. MgO-650 CO_2 TPD Curves- Post Reaction and fresh Catalyst samples: Pre-treatment He 150 mL min^{-1} 300 °C 1 hr, CO_2 adsorbed at 25 °C 30 mL min^{-1}, physisorbed CO_2 removed at 110 °C 1 hr followed by TPD to 400 °C at 15 °C min^{-1} Sample : MgO_650 0.5 g, 50 % . wt glycerol, 360 °C, 50 mL min^{-1} Ar 0.1 mL min^{-1} 15 mins, 0.016 mL min^{-1} after.

Table 16. CO_2 TPD Curves – MgO_650 - Post Reaction and fresh Catalyst samples µmoles CO_2 g^{-1}

Sample	< 300 °C µmoles CO_2 g^{-1}	< 300 °C µmoles CO_2 m^2
Fresh	491	4
Post pre-treatment	15	0
Post full Run	68	1
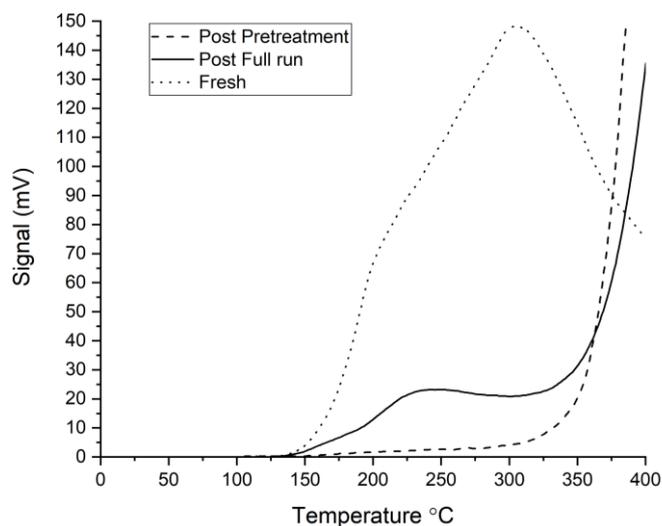
Figure 16. MgO_450 - CO₂ TPD Curves- Post Reaction and fresh Catalyst samples: Pre-treatment He 150 mL min⁻¹ 300 °C 1 hr, CO₂ adsorbed at 25 °C 30 mL min⁻¹, physisorbed CO₂ removed at 110 °C 1 hr followed by TPD to 400 °C at 15 °C min⁻¹ Sample : MgO_450 0.5 g, 50 % . wt glycerol, 360 °C, 50 mL min⁻¹ Ar 0.1 mL min⁻¹ 15 mins, 0.016 mL min⁻¹ after.

Table 17. CO₂ TPD Curves- MgO_450 -Post Reaction and fresh Catalyst samples μmoles CO₂ g⁻¹

Sample	< 300 °C μmoles CO₂ g⁻¹	< 300 °C μmoles CO₂ m²
Fresh	771	4
Post pre-treatment	15	0
Post full Run	106	1

Table 18. Results for glycerol reaction collected between 45-48 hrs. Aqueous glycerol solution (50 wt.%; 0.016 mL min^{-1}; Ar (50 mL min^{-1}); catalyst (0.5 g); bed volume (1 mL); GHSV = 4615 h^{-1}; temperature (360 °C).

	Selectivity %
acetaldehyde	12.4
propionaldehyde	0.2
acetone	0.0
acrolein	13.4
butyraldehyde	0.0
methanol	5.1
ethanol	0.1
2,3-butanedione	0.8
3-hexanone	0.1
allyl alcohol	0.3
cyclopentanone	0.4
hydroxyacetone	31.8
3-ethoxy-1-propanol	1.3
acetic acid	0.9
Glycidol	0.5
propionic acid	1.8
1,2-propanediol	3.2
unknown(s)	12.2
ethylene glycol	12.4
1,3-propanediol	0.4
phenol	0.2
CO	0.7
CO$_2$	1.8
Glycerol conversion %	47
Carbon balance %	98
MeOH STY g h^{-1} kg h^{-1}	27

3.3.6   Influence of catalyst mass to glycerol concentration ratio

3.3.6.1 MgO mass variation - 2g of catalyst 50 % 360 °C

The majority of reactions previously discussed use the same catalyst mass to glycerol ratio and contact time. Exploring the effect of contact time in this reaction is important and there may be unidentified mass transfer limitations present in heterogenous catalytic systems such as our own. This is important as the diffusion of the reagent from bulk gas to the catalysts active site effects the rate of reaction.[72,73] Without adequate diffusion, the reaction will become diffusion limited. The pressure of the gaseous reactants, temperature, velocity, particle size and solubility in the liquid

phase upon the catalyst surface effect the diffusion of the bulk species.[73,74] If an external mass transport limitation, between bulk gas and surface is significantly dominant, the rate of reaction for example may not correlate well with the temperature, catalyst mass and SA. Here we explored different catalyst masses while keeping the temperature constant. This was to see how extending or reducing the contact time would affect the conversion and product distribution. The aim was to see whether the 0.5 g previously used was the optimal amount of catalyst to achieve adequate activity and methanol yield at 360 °C.

Experiments with a higher mass of catalyst were used to increase the conversion without raising the temperature. Achieving relatively high conversions, which should result in less intermediates at relatively low temperatures would be desirable. This is due to smaller energy requirements, lower reactor fouling and lower selectivity to aldehydes.
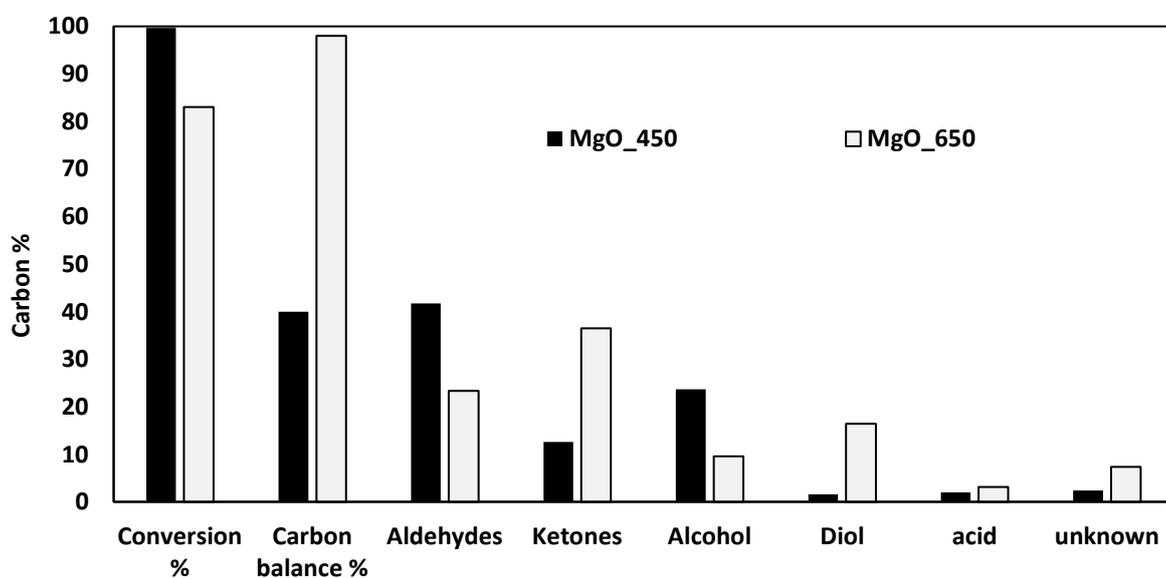
Figure 17. High catalyst mass experiments - MgO_450, MgO_650. Reaction conditions; 360 °C ,50 % glycerol/water flow 0.016 mL min^{-1}, 2 g MgO, 50 mL min^{-1} Ar, 3 hours.

2 g of MgO_450 and MgO_650 were tested under standard reaction conditions of 360 °C and 50 mL min^{-1} Ar. The increase in contact time resulted in a space velocity decrease (from 4615L h^{-1} L^{-1} Cat / to 1154 L h^{-1} L^{-1} Cat. The catalyst bed was made up to 2 mL with SiC. As expected, both catalysts show an increase in conversion. MgO_450 shows almost full conversion of 99 % +, an increase from 87 % when 0.5 g is used. MgO_650 interestingly shows a modest increase of 8 %, increasing from 75 % to 83 %. The increase in conversion is not proportional to the increase in amount of catalyst, with a significant amount of the substrate still failing to react on MgO_650's surface. There may be possible diffusion limitations occurring over the surface, possibly with pore structure of MgO_650

being smaller. For MgO_450, which has a significantly higher SA, larger pores, and more basic sites, this seems to not be as significant under these conditions. However, this may not be the case, the conversion is high, and so the amount of glycerol to react decreases which may lead to this disproportionate conversion.

With 2 g of catalyst a stark decrease in CMB is seen for MgO_450 from 74 % to 40 %. This is one of the lowest CMBs obtained from a glycerol experiment over MgO. Loss of CMB over MgO_450 is postulated from previous experiments to be due to bimolecular condensation reactions resulting in undetected HWMPs. With the significantly higher contact time, active sites, and SA available it is possible these types of reactions become dominant. This may be exacerbated by the increase in selectivity to products such as acetaldehyde. Overall, it seems a longer contact time on the catalyst surface allows for a higher propagation of condensation reactions. This coincides with the results for MgO_650 which as in other reactions does not exhibit a drop in CMB, maintaining a high value of 98 %. This further indicates that MgO_650 does not likely significantly promote those types of reaction.

The product distribution changes significantly for both catalysts. This however materialises in opposite ways. Increasing the catalyst mass for MgO_450 increases the selectivity to end products such as aldehydes, mono-alcohols and presumably HWMPs (inferred from the low CMB). MgO_650 sees an increase in intermediates such as hydroxyacetone. MgO_450 results in a high selectivity to acetaldehyde of 29 %, this is a 10 % increase from the 0.5 g experiment. MgO_650 on the other hand sees a decrease, selectivity is 20.2 % with 0.5 g and 14.8 % with 2 g.

The selectivity to hydroxyacetone decreases by more than half with MgO_450, from 23.2 % to 10.3 %. Hydroxyacetone has been shown to be a consistent intermediate product, even at high temperature and conversion reactions. As an intermediate it is inferred that the decrease in hydroxyacetone would be due to being further converted. The selectivity to products such as 1,2-propanediol, 2-propanol, acetone or unknowns does not increase, and propionic acid only sees a marginal increase. Therefore, the drop in hydroxyacetone selectivity may be linked to the drop in CMB. It is postulated that hydroxyacetone or any acetone produced may possibly be undergoing condensation reactions towards HWMPs. It is known to rapidly undergo aldol condensations in alkaline conditions,[75] and can undergo dimerization.[76] This may be promoted by the elongated contact time. Increasing the mass of MgO_650 produces an increase in hydroxyacetone, from 23.7 % to 33.0 %. This may be due to the increase in conversion producing more hydroxyacetone, however this may accumulate with MgO_650 without extra thermal input. If the condensation theory over MgO_450 is correct, the high selectivity to hydroxyacetone with MgO_650 may be due

to it being stable on its surface, and not promoting condensation reactions resulting in a high CMB. The higher conversion, but lack of temperature to push reactants further through the reaction pathways may result in an accumulation of selectivity to hydroxyacetone at the expense of end products such as acetaldehyde. Ethylene glycol selectivity changes radically over MgO_450. It is reduced from 8.2 % to 0.6 %. This may attribute to the high selectivity to acetaldehyde. MgO_650 sees a slight increase as with hydroxyacetone.

It should be noted that due to the low CMB s the yields are relatively low even for high selectivity products such as methanol for MgO_450. This is clear when comparing to other experiments and MgO_650. MgO_450 at 20 % methanol results in 27 g h^{-1} kg^{-1} cat while MgO_650 with 8% methanol, 29 g h^{-1} kg^{-1} cat. In reality if our theory is correct the major products over MgO_450 here are the breadth of the undetected condensation products that likely make up a significant amount of the 60 % lost carbon. Due to this, the changes in selectivity are easier to understand over MgO_650 as the observed selectivity is responsible for the vast majority of the CMB.

Increasing the catalyst contact time results in significant changes in performance. Conversion increases for both catalysts, but to a higher degree with MgO_450. Selectivity however changes significantly for the catalysts MgO_450 produces more later products in the stream, and less intermediates, MgO_650 does the opposite. A very low CMB is seen with MgO_450 which is thought to be due to condensation reactions, which may be more prominent with longer contact times. MgO_650 retains a high CMB indicating it likely does not promote these reactions to the same degree.

3.3.6.2 MgO mass variation - 0.0125 g – 0.5 g of catalyst 50 % 360 °C
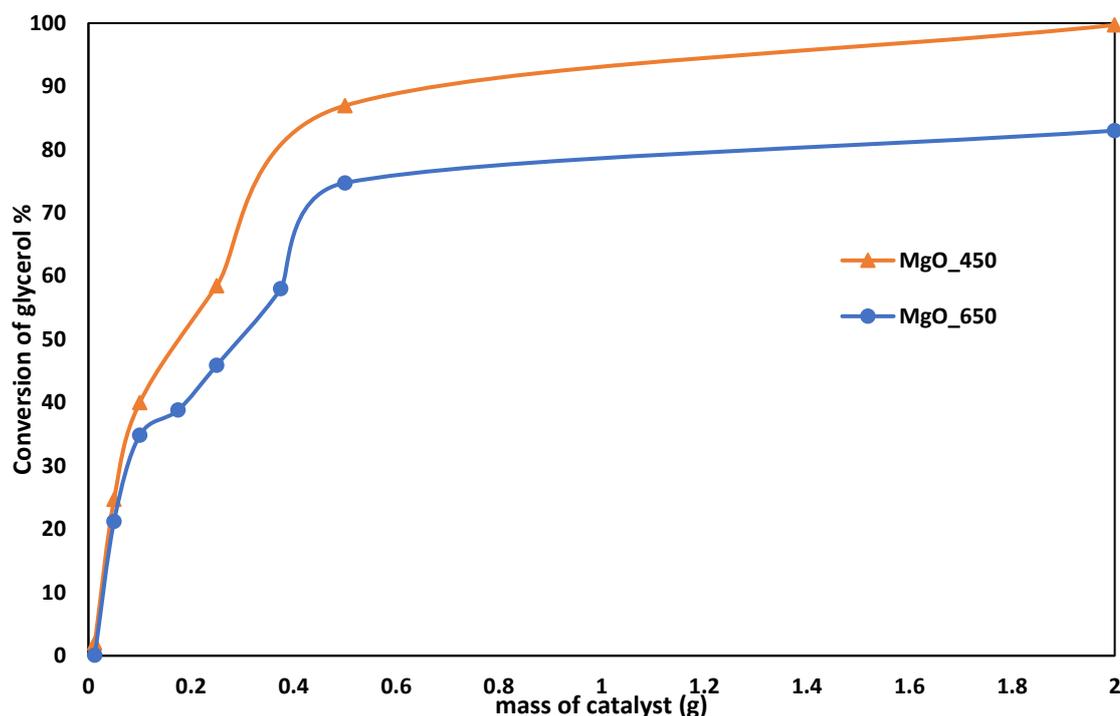
Figure 18. Influence of catalyst mass change – MgO_450, MgO_650. Reaction conditions; 360 °C ,50 % glycerol/water flow 0.016 mL min^{-1}, 0.0125 – 2 g MgO, 50 mL min^{-1} Ar, 3 hours.

To further investigate the effect of catalyst mass, a series of experiments using less than 0.5 g were conducted. Here we kept the bed at a volume at 1 ml using SiC as a diluent. The aim was to explore the minimum amount of catalyst needed for adequate conversion and yields. The previous reaction with 2 g of catalyst (3.3.6.1) did not result in a proportional increase in conversion when the catalyst mass was increased from 0.5 g to 2 g with MgO_650. This may indicate diffusion limitations from the vapour phase fluid bulk to the catalyst surface, or the high conversion decreasing the glycerol concentration enough to slow activity. If this was the case a non-linear trend of mass to conversion may be expected.

Results are shown in (Table, Table 20 and Table 21). Using 0.0125 g of catalyst results in almost inactivity, the results are only slightly more active than seen in catalyst free experiments.[1] MgO_450 shows 2 % conversion while MgO_650 exhibits a negligible conversion . The catalyst mass is very small and thus does not promote significant levels of conversion. In the previously reported catalyst free reactions with just SiC in the reactor bed a significant selectivity of allyl alcohol was seen of 37.3 %.[1] However, here we see 1.0 % with MgO_450 and 2.5 % for MgO_650. This indicates that even with the very small amount of conversion and catalyst, the MgO is still controlling the selectivity, thus likely responsible for the conversion that is seen.

On increasing the catalyst to 0.05 g we see a sharp increase in conversion. 0.05 g is approximately the minimum amount needed to initiate effective catalysis. The conversion of glycerol here was 25 % and 21 % for MgO_450 and MgO_650. When compared to reactions in 3.3.2 the temperature is very important for conversion. 0.1 g of catalyst used at 320 °C resulted in less than 10 % conversion. 320 °C likely does not provide enough thermal energy above the vaporisation temperature of glycerol to efficiently activate the MgO surface for dehydration. 360 °C gives a significantly higher conversion and different product distribution even with less catalyst.

Shown in (Table 19), a small amount of catalyst can promote the conversion of glycerol quite efficiently. The 0.5 g reactions use 10x the catalyst, but only result in approximately 4 x the conversion. Further increases in conversion are observed as you increase the catalyst mass. Generally, the conversion observed above 0.0125 g of catalyst and 0.25 g of catalyst is disproportionally high compared to what is seen with higher loadings. Small amounts of catalyst can promote significantly more conversion than would be expected and under these conditions increasing the mass results in a lower efficiency. This becomes increasing evident when using more than 0.5 g of catalyst. This is further illustrated in terms of activity of grams of glycerol converted per hour per g catalyst (g_{gly} h^{-1} g cat^{-1}). 0.05 g of catalyst gives the highest activity for MgO_450 of 3.31 g_{gly} h^{-1} g cat^{-1} while 0.05 – 0.1 g is highly active with 2.84 and 2.73 g_{gly} h^{-1} g cat^{-1}. This sharply decreases up to 0.25 g followed by a tapering gradual decrease to 2 g of 0.31 and 0.23 g_{gly} h^{-1} g cat^{-1} for MgO_450 and MgO_650 respectively. An identical trend is seen when looking at activity per m^2 of catalyst (Table 20 ,Table 21).

This indicates when a small amount of catalyst is used in the bed the majority of its surface may be more saturated. At higher amounts of catalyst, a smaller proportion of the catalyst surface may be saturated at any given point. This is indicated with a higher efficiency per gram of catalyst with the low mass experiments. This may indicate that the reaction is somewhat mass transfer limited. The reaction may be partially controlled by the rate at which the substrate can diffuse to the reactor bed surface. When taking the reaction to 2 g, even with the bed size increase, the reactant cannot diffuse quick enough to make full efficient use of the whole MgO surface. The changes in activity may alternatively be due to the concentration of glycerol decreasing, resulting in less for the catalyst surface to convert at any given point.

Table 19. Mass and conversion compared to 0.5 g experiment - Influence of catalyst mass change – MgO_450, MgO_650. Reaction conditions; 360 °C ,50 % glycerol/water flow 0.016 mL min^{-1}, 0.0125 – 2 g MgO, 50 mL min^{-1} Ar, 3 hours.

	Catalyst mass (g)	0.0125	0.05	0.1	0.175	0.25	0.375	0.5	2
MgO_450	mass % of 0.5g	2.5	10	20	n/a	50	n/a	100	400
	conversion % of 0.5g	2	28	37	n/a	56	n/a	100	115
MgO_650	mass % of 0.5g	2.5	10	20	35	50	75	100	400
	conversion % of 0.5g	0	28	47	52	61	78	100	126

When discussing the CMB for these reactions, MgO_450 shows a general decrease as the catalyst mass is increased. This relates to the increasing conversion and the available SA for bi-molecular reactions to take place. MgO_650 shows a relatively high CMB throughout with no clear trend. This indicates again that it may not promote reactions that lead to undetected heavy products.

Shown in figure 19, the selectivity observed in the reactions is generally attributed to be a product of the conversion. With MgO_450, on increasing the catalyst mass and hence conversion we see a significant increase in acetaldehyde, from approximately 10 % to 20 – 30 % at high conversion. Methanol selectivity also increase steadily with mass increases. 5 % increases up to 11 % with 0.5 g. Acrolein sees a slight decrease here for both MgO_450 and MgO_650 as conversion increases. Hydroxyacetone trends downwards with MgO_450, likely due to its further conversion. Over MgO_650 it also trends down slightly, but with 2 g of catalyst increases, indicating here the catalyst may be producing a significant amount of hydroxyacetone but not efficiently converting it.

Overall, from the catalyst variation experiments it can be seen that the activity of the catalyst per gram decreases as the mass passes 0.05 g. An explanation may be due to limitations in the transport of glycerol from the bulk fluid to the surface of the catalyst bed, but this is likely mainly to do with decreasing glycerol concentration as conversion increases. When little catalyst is used this is not a problem as the amount that reaches it is enough to saturate and the concentration is high. CMBs are relatively stable throughout for both catalysts. However, for MgO_450 a sharp drop at 2 g indicates prolonged exposure and large available surface may lead to undesirable side reactions. This does seem to occur over MgO_650. Previous evidence has indicated it does not promote the formation of HWMPs.

(a) MgO_450
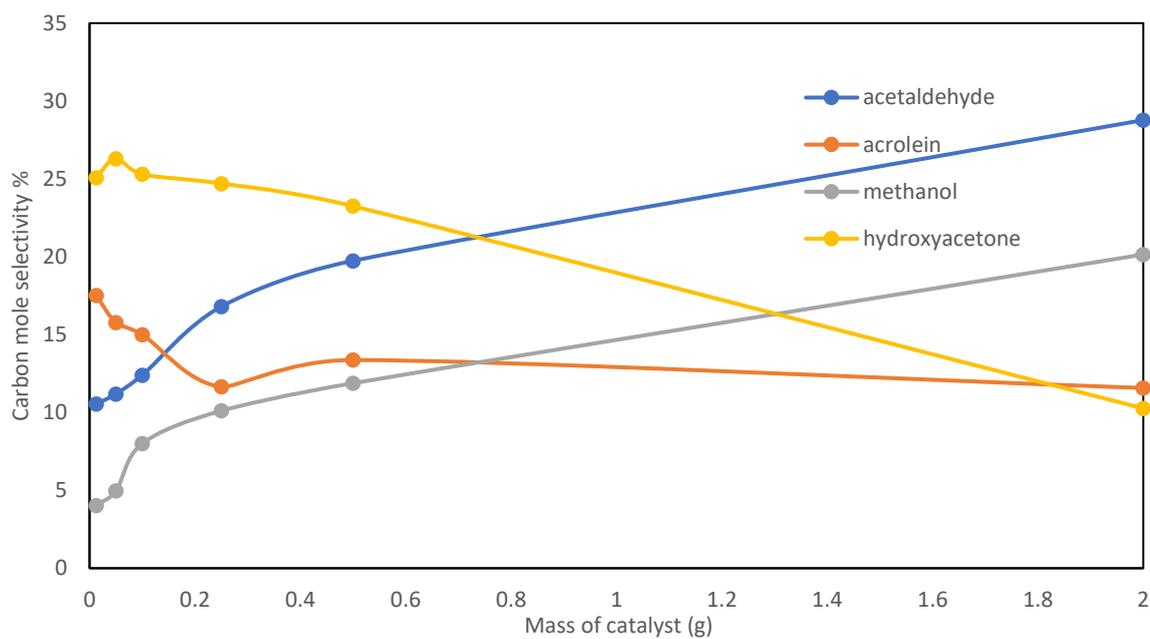
(b) MgO_650
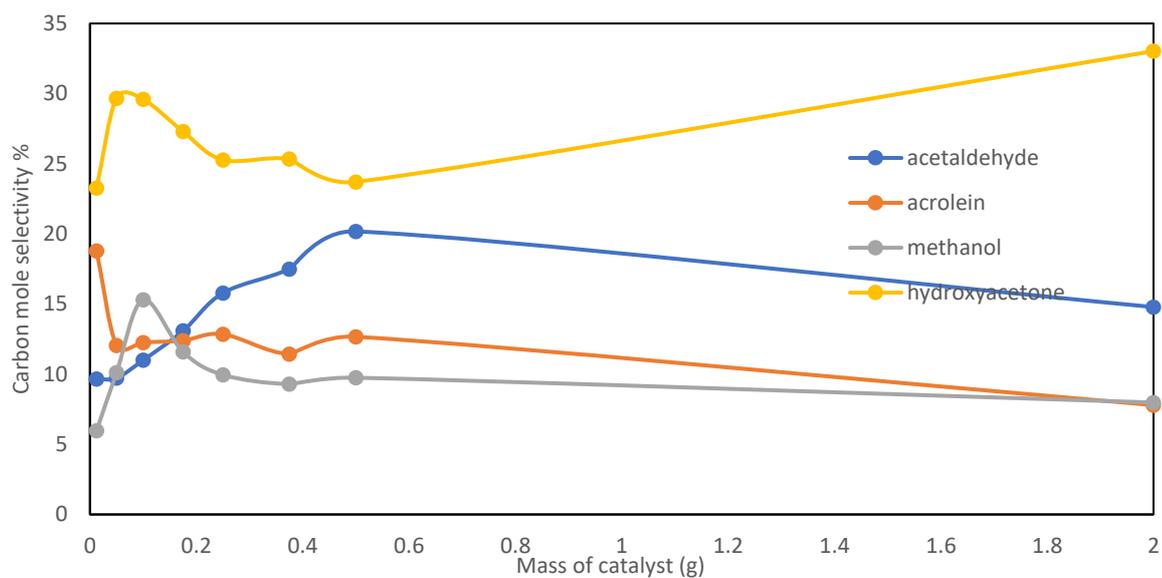
Figure 19. Selectivity - influence of catalyst mass change – MgO_450 (a), MgO_650 (b). Reaction conditions; 360 °C ,50 % glycerol/water flow 0.016 mL min^{-1}, 0.0125 – 2 g MgO, 50 mL min^{-1} Ar, 3 hours.

Table 20. Influence of catalyst mass change – MgO_450. Reaction conditions; 360 °C ,50 % glycerol/water flow 0.016 mL min^{-1}, 0.0125 – 2 g MgO, 50 mL min^{-1} Ar, 3 hours.

MgO_450	0.0125	0.05	0.1	0.25	0.5	2
acetaldehyde	10.5	11.2	12.4	16.8	19.7	28.8
propionaldehyde	0.3	0.2	0.1	0.4	0.6	1.4
acetone	0.0	0.0	0.2	0.0	0.1	0.2
acrolein	17.5	15.8	15.0	11.6	13.4	11.6
butyraldehyde	0.0	0.0	0.0	0.0	0.0	0.0
methanol	4.0	5.0	8.0	10.1	11.9	20.1
2-propanol	0.0	0.0	0.0	0.0	0.6	0.0
ethanol	0.0	0.2	0.2	0.5	0.0	1.6
2,3-butanedione	0.0	0.2	0.1	0.8	1.2	1.2
2-butanol	0.0	0.0	0.0	0.0	0.1	0.0
1-propanol	0.0	0.0	0.0	0.1	0.1	0.3
3-hexanone	0.0	0.0	0.0	0.1	0.0	0.2
2-hexanone	0.0	0.0	0.0	0.0	0.0	0.0
2-methyl-1-propanol	0.0	0.0	0.0	0.0	0.0	0.0
allyl alcohol	1.0	0.7	1.0	0.9	0.8	1.6
cyclopentanone	0.2	0.2	0.1	0.4	0.6	0.7
hydroxyacetone	25.1	26.3	25.3	24.7	23.2	10.3
3-ethoxy-1-propanol	5.5	5.4	1.5	0.0	0.9	0.0
acetic acid	0.2	0.3	0.3	0.7	0.5	1.2
Glycidol	0.0	0.4	0.0	0.4	1.0	0.6
propionic acid	6.3	5.5	5.0	2.8	0.3	0.7
1,2-propanediol	0.0	3.0	1.9	2.8	2.1	0.6
unknown(s)	10.5	10.3	10.5	10.6	8.3	2.4
ethylene glycol	18.9	15.5	14.6	13.1	8.2	0.6
1,3-propanediol	0.0	0.1	0.3	0.3	0.8	0.3
phenol	0.0	0.0	0.0	0.0	0.1	0.0
CO	0.0	0.0	1.5	1.6	2.8	6.0
Co2	0.0	0.0	1.9	1.3	2.7	9.5
Glycerol conversion	2	25	32	48	87	100
CMB %	102	84	84	89	74	40
Methanol g h^{-1} kg^{-1}	77	64	187	45	80	27
Activity g$_{gly}$ h^{-1} g$_{cat}$$^{-1}$	0.85	3.31	1.72	1.04	0.93	0.31
Activity (μmol$_{gly}$ h^{-1} m^2$_{cat}$$^{-1}$	50	192	100	60	54	18

Table 21. Influence of catalyst mass change – MgO_650. Reaction conditions; 360 °C ,50 % glycerol/water flow 0.016 mL min⁻¹, 0.0125 – 2 g MgO, 50 mL min⁻¹ Ar, 3 hours.

MgO_650	0.0125	0.05	0.1	0.175	0.25	0.375	0.5	2
acetaldehyde	9.7	9.7	11.0	13.1	15.8	17.5	20.2	14.8
propionaldehyde	0.3	0.2	1.8	0.4	0.4	0.7	0.6	0.7
acetone	0.0	0.0	0.0	0.0	0.0	0.0	0.1	0.1
acrolein	18.8	12.1	12.3	12.4	12.9	11.4	12.7	7.8
butyraldehyde	0.0	0.0	0.0	0.0	0.0	0.0	0.0	0.0
methanol	6.0	10.1	15.3	11.6	10.0	9.3	9.8	8.0
2-propanol	0.0	0.0	0.0	0.0	0.0	0.0	0.4	0.0
ethanol	0.3	0.5	0.6	0.6	0.5	0.5	0.1	0.5
2,3-butanedione	0.0	0.2	0.0	0.5	0.8	0.8	1.1	2.2
2-butanol	0.0	0.0	0.0	0.0	0.0	0.0	0.0	0.0
1-propanol	0.0	0.0	0.0	0.0	0.1	0.1	0.1	0.1
3-hexanone	0.0	0.0	0.0	0.0	0.1	0.1	0.0	0.2
2-hexanone	0.0	0.0	0.0	0.0	0.0	0.0	0.0	0.0
2-methyl-1-propanol	0.0	0.0	0.0	0.0	0.0	0.0	0.0	0.0
allyl alcohol	2.5	1.2	1.3	1.1	0.8	0.8	0.6	0.7
cyclopentanone	0.0	0.2	0.3	0.3	0.4	0.4	0.3	1.0
hydroxyacetone	23.3	29.7	29.6	27.3	25.3	25.3	23.7	33.0
3-ethoxy-1-propanol	5.5	6.6	2.2	3.3	2.0	1.6	0.9	0.1
acetic acid	0.0	0.4	0.6	0.5	0.7	0.9	0.5	1.9
Glycidol	0.0	0.2	0.0	0.3	0.4	0.5	2.9	1.0
propionic acid	5.9	4.2	4.1	4.4	2.4	0.3	0.2	1.2
1,2-propanediol	3.0	2.9	2.2	2.7	2.7	3.0	2.6	4.4
unknown(s)	11.3	6.1	6.3	5.9	9.6	10.9	8.4	7.4
ethylene glycol	12.6	15.8	11.0	14.9	13.1	11.5	9.2	10.8
1,3-propanediol	1.0	0.1	0.1	0.1	0.3	0.3	0.8	1.3
phenol	0.0	0.0	0.0	0.0	0.0	0.1	0.3	0.2
CO	0.0	0.0	0.6	0.3	1.0	2.4	2.7	1.4
CO_2	0.0	0.0	0.8	0.3	1.0	1.6	1.9	1.3
Glycerol conversion %	0	21	35	39	46	58	75	83
CMB %	100	97	96	97	96	95	98	98
Methanol g h⁻¹ kg⁻¹	115	175	247	104	111	67	90	29
Activity g_{gly} h⁻¹ g_{cat}⁻¹	0.12	2.84	2.73	1.49	1.12	0.86	0.81	0.23
Activity (μmol_{gly} h⁻¹ m²$_{cat}$⁻¹)	10	247	237	129	97	74	70	20

3.3.7   Low feed substrate reaction 10 % wt. glycerol - MgO_450 and MgO_650

Previous research has shown that changing the glycerol and water concentration may have a significant effect on reaction results.[1] The majority of previous investigation is with 50 wt.% glycerol feedstocks, it was hoped this would allow for high yields comparable to what would be seen for a commercial process, as well as reduce the amount of water and energy required.[77] However, previous literature examples of glycerol conversion tend to use more dilute feedstocks and different carrier gas flow, this makes it hard to compare yields.[78,79]

Smith *et al.*[1] has previously shown that the concentration of water to glycerol in the feed stream can have a prominent effect on reaction results. A higher concentration of water seemed to help inhibit condensation reactions over MgO leading to a higher CMB. Water acting as an inhibiting source for the formation of HWMPs has been seen before.[58] The increase in water concentration leads to a lower glycerol concentration and thus a lower concentration of reactive intermediates, this can help inhibit unwanted side reactions. These may be prominent at high concentration due to their functionality and proximity.[80] Large intermolecular condensation reaction products are caused by a multitude of chain reactions with a variety of substrates. As such they will often depend on the concentration of more than one substrate and have a reaction order of ≥1.5.[81]

In the previous reactions with MgO_STD, a 10 wt.% reaction at 400 °C in comparison to 50 wt.% increased conversion from 90 % to 100 %, and CMB from 77 % to 84 %. Selectivity to alcohols, and aldehydes increased, and ketones and diols decreased. Experiments were performed with a 10 wt.% glycerol feed at 400 °C. High temperatures were used to try and convert intermediates such as hydroxyacetone. Contact time is kept the same but catalyst mass to feed concentration ratio increases. This was conducted by keeping the catalyst mass the standard 0.5 g but changing the wt.% of the glycerol feed. Here the feed was changed to a 10 % glycerol by wt.% solution, a decrease in concentration of 5 x. The partial pressure also changes, at 50 wt.% reactions glycerol is 0.14 mbar, this decreases to 0.026 mbar at 10 wt.%. Water has 0.18 mbar at 50 wt.% which increases to 0.29 mbar at 10 wt.% glycerol.

MgO_450 and MgO_650 show significant difference when water is changed to D_2O and clear differences in characteristics, thus were chosen for this investigation. The results are presented in Figure 20 and Table 22. First, looking at the reactions done at 400 °C, high conversion is seen with 90 % + for both catalysts. MgO_450 achieves 99.5% and MgO_650 93 %. While the difference is smaller it still illustrates how MgO_650 is a less active catalyst. A higher CMB is achieved for MgO_450 with 10 wt.% glycerol feed than the 50 wt.% reactions. As expected, this indicates that a decrease in reactant concentration and increase in water produces a higher CMB, this is proposed to be due to it inhibiting the formation of condensation products.
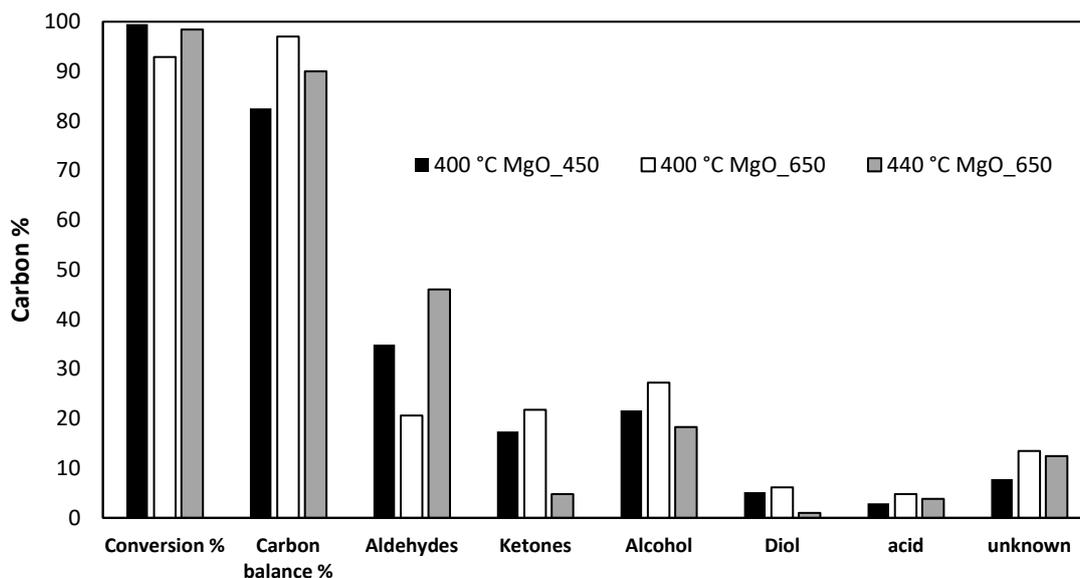
Figure 20. Low glycerol feed concentration experiments (10 %) – MgO_450, MgO_650. Reaction conditions; 400 -440 °C ,10 % glycerol/water flow 0.016 mL min⁻¹, 0.5 g MgO, 50 mL min⁻¹ Ar, 3 hours.

Differences in selectivity between the samples is quite prominent under these conditions. At 400 °C a high selectivity to aldehydes is seen with MgO_450. Acetaldehyde is observed with MgO_450 of 26.0 %, MgO_650 exhibits 16.3 %. Acrolein is 7.1 % with MgO_450 and 2.1 % with MgO_650. Generally, products identified as intermediates are lower over MgO_450. Hydroxyacetone is 13.0 % on MgO_450 and 15.7 % over MgO_650, unknowns are 7.8 % and 13.5 % respectively. These differences are likely mainly a product of conversion. However, a higher selectivity is seen with MgO_650. The selectivity to methanol is higher for both catalysts compared to the 50 % experiments. Here 17.7 % and 21.7 % were observed over MgO_450 and MgO_650 respectively. This gave a yield of 31.4 and 39.4 g⁻¹ kg⁻¹. Which compares well with that seen in the higher concentration experiments, which used a 5x more glycerol.

MgO_650 was also tested at 440 °C at this wt.%, this was to see if its high CMB would persist, and if an even higher selectivity and yield to methanol could be obtained. Conversion increases to 98 %, still lower than MgO_450 at 400 °C. Here a decrease in CMB is observed, possibly due to more reactor fouling. Interestingly at 440 °C MgO_650 has a very high selectivity to acetaldehyde of 36 % and a lower selectivity to methanol of 14.7 %, this is similar to what was seen in section 3.3.4 with 50 wt.% glycerol, where it was concluded that due to the increase in CO this may due decomposition of methanol to give CO and H_2.[65,66] which can proceed to give CO_2 (WGS).[67]

Overall, it seems that the addition of high concentrations of water can help improve the CMB for MgO_450, likely due to the reduction of intermolecular condensation reactions. The benefit of more water is less with MgO_650 which previous evidence indicated does not produce HWMPs in significant concentrations.

Table 22. Low glycerol feed concentration experiments (10 %) – MgO_450, MgO_650. Reaction conditions; 400 -440 °C ,10 % glycerol/water flow 0.016 mL min^{-1}, 0.5 g MgO, 50 mL min^{-1} Ar, 3 hours.

	400 °C	400 °C	440 °C
	MgO_450	MgO_650	MgO_650
acetaldehyde	26.0	16.3	36.0
propionaldehyde	1.8	2.2	3.1
acetone	0.4	0.5	0.8
acrolein	7.1	2.1	6.9
butyraldehyde	0.0	0.0	0.0
methanol	17.7	21.7	14.7
2-propanol	0.0	0.0	0.0
ethanol	2.0	2.8	1.8
2,3-butanedione	2.3	3.2	1.6
2-butanol	0.0	0.0	0.0
1-propanol	0.5	0.7	0.4
3-hexanone	0.4	0.5	0.3
2-hexanone	0.0	0.0	0.0
2-methyl-1-propanol	0.0	0.0	0.0
allyl alcohol	1.4	1.9	1.1
cyclopentanone	1.3	2.0	0.3
hydroxyacetone	13.0	15.7	1.8
3-ethoxy-1-propanol	0.2	0.2	0.1
acetic acid	1.9	2.7	1.8
Glycidol	0.5	0.5	0.4
propionic acid	1.0	2.0	2.1
1,2-propanediol	1.5	1.8	0.4
unknown(s)	7.8	13.5	12.4
ethylene glycol	3.1	3.4	0.5
1,3-propanediol	0.6	0.9	0.1
phenol	0.0	0.0	0.2
CO	2.0	3.0	8.1
CO$_2$	7.6	2.5	5.1
Glycerol conversion %	100	93	98
CMB %	83	97	93
Methanol g h^{-1} kg^{-1}	31	39	35

3.3.8 Influence of initial calcination time on basicity and reaction

This study investigates how the calcination time of a catalyst would affect its characteristics and performance. This was to try and deconvolute some of the differences between MgO_450 and MgO_STD, where the only difference of preparation was the duration of the initial calcination.

New MgO samples were prepared by calcining commercial Mg (OH)$_2$ at 450 °C for 2 hours and 24 hours. Results presented in Table 23. Characterisation results presented in Figure 21 and Table 24. This preparation resulted in catalysts both with a SA of approximately 24 m^2 g^{-1}. Analysed *via* TPD, the samples exhibited significantly different basicity. This was also the case even when normalised to SA – which was not the case with our temperature varied samples. MgO_2hr, exhibits a significantly higher basicity of 309 μ moles co$_2$ g^{-1} and 13 μ moles co$_2$ m^2 compared to the longer calcined MgO_24hr of 186 μ moles co$_2$ g^{-1} and 8 μ moles co$_2$ m^2. The 13 μ moles co$_2$ m^2 shown for the MgO_2hr samples are comparable to the 12.5 μ moles co$_2$ m^2 exhibited for the temperature varied samples, which final heat treatment times were only 1 hour longer. On increasing the calcination time, the basicity per gram clearly decreases. However, increasing the calcination time does not affect the SA, this is affected by temperature as shown in 3.2.2. This results in increasing the temperature time also resulting in a decrease in basicity intensity per m^2.

Reaction results are presented in Table 23. MgO_24hr results in a higher CMB of 99 % compared to MgO_2hr's 76 %. There is a significant difference in conversion though, which may be linked to the basicity, as the SA of the two catalysts is the same. The more basic catalyst MgO_24hr exhibits a conversion of 48 % while MgO_2hr only shows 24 %. The decrease in CMB and increase in conversion with constant SA in these two catalysts show that basicity is an important characteristic for MgO. Here again it is likely that at least some of this decrease in CMB between the two catalysts is due to the production of HWMP *via* aldol condensation reactions occurring with the more basic catalyst. Selectivity can be explained mainly by the difference in conversion. More aldehydes and alcohols are made over MgO_2hr, this is likely due to its higher basicity per m^2. MgO_2hr produces 13.8 % acetaldehyde, 14.8 % acrolein and 15.4 % methanol. MgO_24hr produces 10.9 %, 12.6% and 8.5 % respectively. Conversely MgO_24hr has a higher selectivity to intermediate products such as hydroxyacetone (25.9 %), ethylene glycol (14.4 %) and detected unknowns (12.3 %). MgO_2hr respectively yields 24.1 %, 12.2 % and 6.2 %. While glycerol conversion and methanol selectivity are higher over MgO_2hr, due to its low CMB the yield of methanol is only around 25 % higher with 41 g h^{-1} kg^{-1} achieved compared to MgO_24hr 31 g h^{-1} kg^{-1}.

Changing catalyst preparation parameters as simple as the time of calcination can clearly lead to differences in catalyst characteristics and performance. Higher basicity per m^2 or g^{-1} can help drive the glycerol to methanol reaction but may also contribute to a decrease in CMB.

Table 23. Influence of calcination time – MgO_2hr, MgO_24hr. Reaction conditions; 360 °C ,50 % glycerol/water flow 0.016 mL min^{-1}, 0.5 g MgO, 50 mL min^{-1} Ar, 3 hours.

	2hr	24hr
acetaldehyde	13.8	10.9
propionaldehyde	0.0	0.3
acetone	0.1	0.1
acrolein	14.8	12.6
butyraldehyde	0.0	0.0
methanol	15.4	8.5
2-propanol	0.2	0.2
ethanol	0.3	0.4
2,3-butanedione	0.3	0.2
2-butanol	0.0	0.0
1-propanol	0.0	0.0
3-hexanone	0.0	0.0
2-hexanone	0.0	0.0
2-methyl-1-propanol	0.0	0.0
allyl alcohol	1.1	0.7
cyclopentanone	0.3	0.2
hydroxyacetone	24.1	25.9
3-ethoxy-1-propanol	2.3	2.5
acetic acid	0.3	0.3
Glycidol	1.5	1.6
propionic acid	1.7	2.9
1,2-propanediol	1.6	2.6
unknown(s)	6.2	12.3
ethylene glycol	12.2	14.4
1,3-propanediol	1.3	0.7
phenol	0.1	0.4
CO	1.4	1.2
CO$_2$	0.8	1.1
Glycerol conversion %	48	24
CMB %	76	99
Methanol g h^{-1} kg^{-1}	41	31
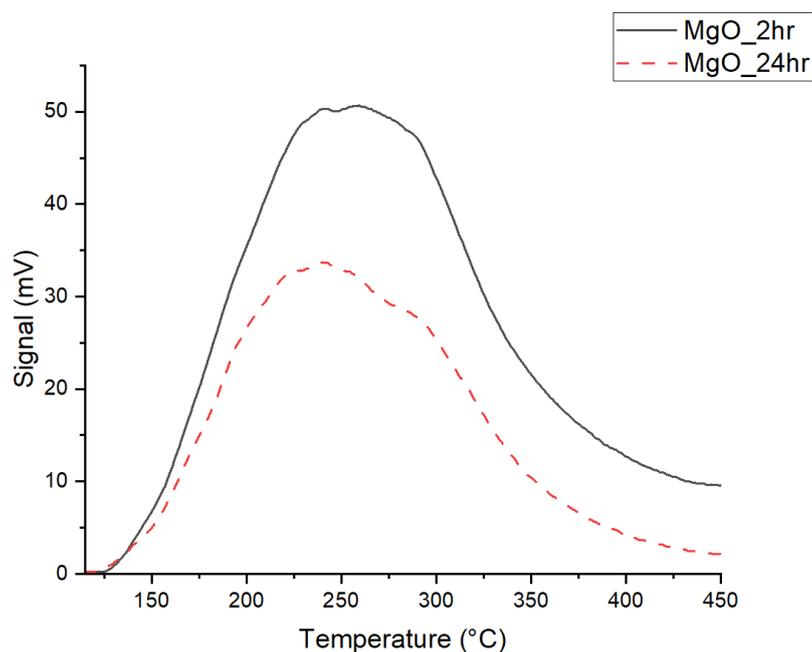
Figure 21. MgO_2-24 hr - CO_2 TPD Curves- Post Reaction and fresh catalyst samples: Pre-treatment He 150 mL min^{-1} 300 °C 1 hr, CO_2 adsorbed at 25 °C 30 mL min^{-1}, physisorbed CO_2 removed at 110 °C 1 hr followed by TPD to 400 °C at 15 °C min^{-1}.

Table 24. MgO_2-24 hr - CO_2 TPD μmoles $CO_2\,g^{-1}$

Catalyst ID	μ moles co_2 /g^{-1}	μ moles co_2 /m^2
MgO 2 hr	309	12.9
MgO 24 hr	186	8.1

3.4 Conclusions and summary

A series of MgO samples were prepared. Preparation involved calcining $Mg(OH)_2$ at 450 °C, refluxed in H_2O at 110 °C followed by subsequent heat treatment in N_2 at 450/550/650/750 °C. The samples were termed MgO_x50 respectively. The samples were characterised by a variety of techniques which identified trends in the physiochemical characteristics. Basicity per gram, porosity and SA were reduced as the heat treatment temperature was increased. Surface morphology of the samples exhibited hexagonal formations for all the catalysts apart from MgO_650. The formation of a distinct morphology on all but the MgO_650 catalyst is not yet understood. The loss of structure is however hypothesised to be due to the formation of intercrystallite channels releasing water at 550 - 650 °C. Above this temperature its believed that the morphology begins to reform, possibly

seeded by any remaining hexagonal crystallites. The proportion of O^{2-} strong basic sites analysed by DRIFTS correlates with the morphology changes, so these factors may be linked.

To investigate how the differing catalyst preparation and characteristics effect catalytic performance, the samples of MgO were tested for the gas phase conversion of glycerol in water. This was conducted in a fixed bed flow reactor under a variety of conditions. It was found that MgO_650 exhibited a high CMB under all conditions. Evidence points toward lower CMB s for the other samples being linked to the formation of higher weight products over MgO. This is expected to be prominent to higher basicity samples such as MgO_450. But also occurs over lower basicity samples such as MgO_750. This high CMB of MgO_650 is attributed to this catalyst not forming these products, but why it doesn't and MgO_750 does is not fully understood. Experiments using D_2O suggest that MgO_450, MgO_650 and MgO_750 all rely on the dissociative adsorption of H_2O to maintain high activity for the activation of glycerol.

Loss of CMB may be linked to the catalysis of condensation reactions between products in the reactant feed. Primarily attributed to aldehydes. This is thought to be promoted by the right mix of basic site distribution and morphology. Maintaining a high CMB is important for several reasons. A high CMB results in a higher yield of the detected products, selectivity is only a measure of the detected carbon, so products not quantified are not included in this. In this way high selectivity but low CMB will result in worse yields than reactions obtaining average selectivity but high CMB. Obtaining a high CMB means the majority of the carbon fed into the reactor is accounted for and quantified. This makes the selectivity more accurate, resulting in a better understanding of what is occurring on the catalysts surface and higher yields.

Reactions changing the experimental conditions such as the temperature and glycerol feed concentration were found to have significant effects on the catalyst activity. Higher conversions lead to a higher selectivity of products such as methanol, acetaldehyde, acrolein, while lower conversions result in more detected unknowns, ethylene glycol and hydroxyacetone. MgO_650 manages to maintain high CMB with high conversion and temperature reactions, while MgO_450 prone to losing considerable CMB when obtaining more conversion. This indicates that MgO_650 is not active for further reactions of products such as acetaldehyde, even under volatile conditions. Investigations into catalyst mass to feed ratio indicated that activity per g decreased with catalyst mass and conversion increases, indicating diffusion limitations or lack of glycerol to further react, this results in nonlinear increases in conversion on increasing catalyst surface. Calcination time was also found to be important in effecting catalyst characteristics and performance, longer calcination times resulted in the same SA but lower basicity, which correlated in an increase in CMB.

Overall, it's clear that the catalyst preparation and characteristics can affect the conversion of glycerol and resulting product distribution markedly. However, the picture is complicated with many competing factors resulting in unexpected results and non-linear trends. It is therefore important that a better understanding of the reaction pathways that can occur over the surface are investigated.

3.5 References

(1) Smith, L. R.; Smith, P. J.; Mugford, K. S.; Douthwaite, M.; Dummer, N. F.; Willock, D. J.; Howard, M.; Knight, D. W.; Taylor, S. H.; Hutchings, G. J. New Insights for the Valorisation of Glycerol over MgO Catalysts in the Gas-Phase. *Catal. Sci. Technol.* **2019**, 19–22. https://doi.org/10.1039/C8CY02214C.

(2) Haider, M. H.; Dummer, N. F.; Knight, D. W.; Jenkins, R. L.; Howard, M.; Moulijn, J.; Taylor, S. H.; Hutchings, G. J. Efficient Green Methanol Synthesis from Glycerol. *Nat. Chem.* **2015**, *7* (12), 1028–1032. https://doi.org/10.1038/nchem.2345.

(3) Bartley, J. K.; Xu, C.; Lloyd, R.; Enache, D. I.; Knight, D. W.; Hutchings, G. J. Simple Method to Synthesize High Surface Area Magnesium Oxide and Its Use as a Heterogeneous Base Catalyst. *Appl. Catal. B Environ.* **2012**, *128*, 31–38. https://doi.org/10.1016/j.apcatb.2012.03.036.

(4) Smith, L. R.; Sainna, M. A.; Douthwaite, M.; Davies, T. E.; Dummer, N. F.; Willock, D. J.; Knight, D. W.; Catlow, C. R. A.; Taylor, S. H.; Hutchings, G. J. Gas Phase Glycerol Valorization over Ceria Nanostructures with Well-Defined Morphologies. *ACS Catal.* **2021**, *11* (8), 4893–4907. https://doi.org/10.1021/acscatal.0c05606.

(5) Smith, P. J.; Smith, L.; Dummer, N. F.; Douthwaite, M.; Willock, D. J.; Howard, M.; Knight, D. W.; Taylor, S. H.; Hutchings, G. J. Investigating the Influence of Reaction Conditions and the Properties of Ceria for the Valorisation of Glycerol. *Energies* **2019**, *12* (7), 1359. https://doi.org/10.3390/en12071359.

(6) Xu, C.; Bartley, J. K.; Enache, D. I.; Knight, D. W.; Hutchings, G. J. High Surface Area MgO as a Highly Effective Heterogeneous Base Catalyst for Michael Addition and Knoevenagel Condensation Reactions. *Synthesis (Stuttg).* **2005**. https://doi.org/10.1055/s-2005-918467.

(7) Ding, Y.; Zhang, G.; Wu, H.; Hai, B.; Wang, L.; Qian, Y. Nanoscale Magnesium Hydroxide and Magnesium Oxide Powders: Control over Size, Shape, and Structure via Hydrothermal Synthesis. *Chem. Mater.* **2001**, *13* (2), 435–440. https://doi.org/10.1021/cm000607e.

(8) Smith, L. R. Gas-Phase Conversions of Glycerol to Methanol Over Ceria-Based Catalysts, Cardiff University, 2020.

(9) *International Centre for Diffraction Data.* https://www.icdd.com.

(10) Di Cosimo, J. I.; Díez, V. K.; Ferretti, C.; Apesteguía, C. R. Basic Catalysis on MgO: Generation, Characterization and Catalytic Properties of Active Sites. *Catalysis* **2014**, *26* (3000), 1–28. https://doi.org/10.1039/9781782620037-00001.

(11) Morterra, C.; Ghiotti, G.; Boccuzi, F.; Coluccia, S. An Infrared Spectroscopic Investigation of the Surface Properties of Magnesium Aluminate Spinel. *J. Catal.* **1978**. https://doi.org/10.1016/0021-9517(78)90268-3.

(12) Evans, J. V.; Whateley, T. L. Infra-Red Study of Adsorption of Carbon Dioxide and Water on Magnesium Oxide. *Trans. Faraday Soc.* **1967**, *63*, 2769–2777. https://doi.org/10.1039/tf9676302769.

(13) Sainna, M. A.; Nanavati, S.; Black, C.; Smith, L.; Mugford, K.; Jenkins, H.; Douthwaite, M.; Dummer, N. F.; Catlow, C. R. A.; Hutchings, G. J.; Taylor, S. H.; Logsdail, A. J.; Willock, D. J. A Combined Periodic DFT and QM/MM Approach to Understand the Radical Mechanism of the Catalytic Production of

Methanol from Glycerol. *Faraday Discuss.* **2020**, *34* (4), 240–241. https://doi.org/10.19009/jjacg.34.4_240.

(14)   Chizallet, C.; Costentin, G.; Che, M.; Delbecq, F.; Sautet, P. Revisiting Acido-Basicity of the MgO Surface by Periodic Density Functional Theory Calculations: Role of Surface Topology and Ion Coordination on Water Dissociation. *J. Phys. Chem. B* **2006**, *110* (32), 15878–15886. https://doi.org/10.1021/jp060840l.

(15)   Xu, C.; Enache, D. I.; Lloyd, R.; Knight, D. W.; Bartley, J. K.; Hutchings, G. J. Mgo Catalysed Triglyceride Transesterification for Biodiesel Synthesis. *Catal. Letters* **2010**. https://doi.org/10.1007/s10562-010-0365-5.

(16)   Sutradhar, N.; Sinhamahapatra, A.; Pahari, S. K.; Pal, P.; Bajaj, H. C.; Mukhopadhyay, I.; Panda, A. B. Controlled Synthesis of Different Morphologies of MgO and Their Use as Solid Base Catalysts. *J. Phys. Chem. C* **2011**, *115* (25), 12308–12316. https://doi.org/10.1021/jp2022314.

(17)   Menezes, A. O.; Silva, P. S.; Hernández, E. P.; Borges, L. E. P.; Fraga, M. A. Tuning Surface Basic Properties of Nanocrystalline MgO by Controlling the Preparation Conditions. *Langmuir* **2010**, *26* (5), 3382–3387. https://doi.org/10.1021/la903149y.

(18)   Hanlon, J. M.; Bravo Diaz, L.; Balducci, G.; Stobbs, B. A.; Bielewski, M.; Chung, P.; MacLaren, I.; Gregory, D. H. Rapid Surfactant-Free Synthesis of Mg(OH)2 Nanoplates and Pseudomorphic Dehydration to MgO. *CrystEngComm* **2015**, *17* (30), 5672–5679. https://doi.org/10.1039/C5CE00595G.

(19)   Devi, S. Synthesis and Characterization of Magnesium Oxide Nanoparticles. *Elixir Nanotechnol.* **2012**, *50*, 10618–10620.

(20)   Mortazavi, G.; Mobasherpour, I.; Rad, E. M. Synthesis of Cubic MgO Nanostructure by an Easy Hydrothermal-Calcinations Method. *J. Ceram. Process. Res.* **2014**, *15* (2), 88–92. https://doi.org/10.1073/pnas.1204514109.

(21)   Dong, H.; Du, Z.; Zhao, Y.; Zhou, D. Preparation of Surface Modified Nano-Mg(OH)2 via Precipitation Method. *Powder Technol.* **2010**, *198* (3), 325–329. https://doi.org/10.1016/j.powtec.2009.11.014.

(22)   Klabunde, K. J.; Stark, J.; Koper, O.; Mohs, C.; Park, D. G.; Decker, S.; Jiang, Y.; Lagadic, I.; Zhang, D. Nanocrystals as Stoichiometric Reagents with Unique Surface Chemistry. *J. Phys. Chem.* **1996**. https://doi.org/10.1021/jp960224x.

(23)   Cui, Z.; Meng, G. W.; Huang, W. D.; Wang, G. Z.; Zhang, L. D. Preparation and Characterization of MgO Nanorods. *Mater. Res. Bull.* **2000**, *35* (10), 1653–1659. https://doi.org/10.1016/S0025-5408(00)00369-X.

(24)   Sutradhar, N.; Sinhamahapatra, A.; Roy, B.; Bajaj, H. C.; Mukhopadhyay, I.; Panda, A. B. Preparation of MgO Nano-Rods with Strong Catalytic Activity via Hydrated Basic Magnesium Carbonates. *Mater. Res. Bull.* **2011**, *46* (11), 2163–2167. https://doi.org/10.1016/j.materresbull.2011.02.024.

(25)   Di Cosimo, J. I.; Dïez, V. K.; Apesteguía, C. R. Base Catalysis for the Synthesis of α,β-Unsaturated Ketones from the Vapor-Phase Aldol Condensation of Acetone. *Appl. Catal. A Gen.* **1996**. https://doi.org/10.1016/0926-860X(95)00289-8.

(26)   Khalaf, A. J.; Hargreaves, J.; David, J. S. Base Catalysis with Metal Oxides. In Metal Oxide Catalysis. *Met. Oxide Catal.* **2009**. https://doi.org/doi:10.1002/9783527626113.ch21.

(27)   Hattori, H. Solid Base Catalysts: Generation, Characterization, and Catalytic Behavior of Basic Sites. *J. Japan Pet. Inst.* **2004**, *47* (2), 67–81. https://doi.org/10.1627/jpi.47.67.

(28)   Busca, G. Bases and Basic Materials in Chemical and Environmental Processes. Liquid versus Solid Basicity. *Chem. Rev.* **2010**, *110* (4), 2217–2249. https://doi.org/10.1021/cr9000989.

(29)   Haider, M. H.; Dummer, N. F.; Zhang, D.; Miedziak, P.; Davies, T. E.; Taylor, S. H.; Willock, D. J.; Knight, D. W.; Chadwick, D.; Hutchings, G. J. Rubidium- and Caesium-Doped Silicotungstic Acid

Catalysts Supported on Alumina for the Catalytic Dehydration of Glycerol to Acrolein. *J. Catal.* **2012**, *286*, 206–213. https://doi.org/10.1016/j.jcat.2011.11.004.

(30)   Haider, M. H.; D'Agostino, C.; Dummer, N. F.; Mantle, M. D.; Gladden, L. F.; Knight, D. W.; Willock, D. J.; Morgan, D. J.; Taylor, S. H.; Hutchings, G. J. The Effect of Grafting Zirconia and Ceria onto Alumina as a Support for Silicotungstic Acid for the Catalytic Dehydration of Glycerol to Acrolein. *Chem. - A Eur. J.* **2014**, *20* (6), 1743–1752. https://doi.org/10.1002/chem.201302348.

(31)   Cornu, D.; Guesmi, H.; Krafft, J. M.; Lauron-Pernot, H. Lewis Acido-Basic Interactions between CO 2 and MgO Surface: DFT and DRIFT Approaches. *J. Phys. Chem. C* **2012**, *116* (11), 6645–6654. https://doi.org/10.1021/jp211171t.

(32)   V. Stark, J.; G. Park, D.; Lagadic, I.; J. Klabunde, K. Nanoscale Metal Oxide Particles/Clusters as Chemical Reagents. Unique Surface Chemistry on Magnesium Oxide As Shown by Enhanced Adsorption of Acid Gases (Sulfur Dioxide and Carbon Dioxide) and Pressure Dependence. *Chem. Mater.* **1996**, *8* (8), 1904–1912. https://doi.org/10.1021/cm950583p.

(33)   Kwon, H. H.-K.; Park, D.-G. G. Infra-Red Study of Surface Carbonation on Polycrystalline Magnesium Hydroxide. *Bull. Korean Chem. Soc.* **2009**, *30* (11), 2567–2573. https://doi.org/10.5012/BKCS.2009.30.11.2567.

(34)   Yanagisawa, Y.; Takaoka, K.; Yamabe, S.; Ito, T. Interaction of CO2 with Magnesium Oxide Surfaces: A TPD, FTIR, and Cluster-Model Calculation Study. *J. Phys. Chem.* **2002**, *99* (11), 3704–3710. https://doi.org/10.1021/j100011a043.

(35)   Yang, J.; Li, Y.; Zhao, X.; Fan, W. Critical Role of Water and Oxygen Defects in C–O Scission during CO2 Reduction on Zn2GeO4(010). *Langmuir* **2018**, *34* (12), 3742–3754. https://doi.org/10.1021/acs.langmuir.7b03360.

(36)   Lind, A.; Thorshaug, K.; Anne Andreassen, K.; Blom, R.; Arstad, B. The Role of Water during CO2 Adsorption by Ca-Based Sorbents at High Temperature. *Ind. & Eng. Chem. Res.* **2018**, *57* (8), 2829–2837. https://doi.org/10.1021/acs.iecr.7b04052.

(37)   Hu, J.; Zhu, K.; Chen, L.; Kübel, C.; Richards, R. MgO(111) Nanosheets with Unusual Surface Activity. *J. Phys. Chem. C* **2007**, *111* (32), 12038–12044. https://doi.org/10.1021/jp073383x.

(38)   Fan, D.; Dong, X.; Yu, Y.; Zhang, M. A DFT Study on the Aldol Condensation Reaction on MgO in the Process of Ethanol to 1,3-Butadiene: Understanding the Structure-Activity Relationship. *Phys. Chem. Chem. Phys.* **2017**, *19* (37), 25671–25682. https://doi.org/10.1039/c7cp04502f.

(39)   Chizallet, C.; Costentin, G.; Lauron-Pernot, H.; Krafft, J. M.; Bazin, P.; Saussey, J.; Delbecq, F.; Saufet, P.; Che, M. Role of Hydroxyl Groups in the Basic Reactivity of MgO: A Theoretical and Experimental Study. *Oil Gas Sci. Technol.* **2006**, *61* (4), 479–488. https://doi.org/10.2516/ogst:2006023a.

(40)   Petitjean, H.; Guesmi, H.; Lauron-Pernot, H.; Costentin, G.; Loffreda, D.; Sautet, P.; Delbecq, F. How Surface Hydroxyls Enhance MgO Reactivity in Basic Catalysis: The Case of Methylbutynol Conversion. *ACS Catal.* **2014**. https://doi.org/10.1021/cs5010807.

(41)   Xu, C.; Bartley, J. K.; Enache, D. I.; Knight, D. W.; Hutchings, G. J. High Surface Area MgO as a Highly Effective Heterogeneous Base Catalyst for Michael Addition and Knoevenagel Condensation Reactions. *Synthesis (Stuttg).* **2005**, No. 19, 3468–3476. https://doi.org/10.1055/s-2005-918467.

(42)   Díez, V. K.; Apesteguía, C. R.; Di Cosimo, J. I. Aldol Condensation of Citral with Acetone on MgO and Alkali-Promoted MgO Catalysts. *J. Catal.* **2006**, *240* (2), 235–244. https://doi.org/10.1016/j.jcat.2006.04.003.

(43)   Jiang, X. C.; Zhou, C. H.; Tesser, R.; Di Serio, M.; Tong, D. S.; Zhang, J. R. Coking of Catalysts in Catalytic Glycerol Dehydration to Acrolein. *Ind. Eng. Chem. Res.* **2018**, *57* (32), 10736–10753. https://doi.org/10.1021/acs.iecr.8b01776.

(44)   Hulteberg, C.; Leveau, A.; Brandin, J. G. M. Pore Condensation in Glycerol Dehydration: Modification of a Mixed Oxide Catalyst. *Top. Catal.* **2017**, *60* (17), 1462–1472. https://doi.org/10.1007/s11244-

017-0827-8.

(45)   Kurokawa, H.; Yanai, M.; Ohshima, M.; Miura, H. Cyclodimerization of Crotonaldehyde to Form
         Cyclohexadienecarbaldehydes and Tolaldehydes over Solid Base Catalysts. *React. Kinet. Mech.
         Catal.* **2012**, *105* (2), 401–412. https://doi.org/10.1007/s11144-011-0381-5.

(46)   Moteki, T.; Rowley, A. T.; Bregante, D. T.; Flaherty, D. W. Formation Pathways toward 2- and 4-
         Methylbenzaldehyde via Sequential Reactions from Acetaldehyde over Hydroxyapatite Catalyst.
         ChemCatChem **2017**, *9* (11), 1921–1929. https://doi.org/https://doi.org/10.1002/cctc.201700151.

(47)   Chang, Y.-C.; Ko, A.-N. Vapor Phase Reactions of Acetaldehyde over Type X Zeolites. *Appl. Catal. A
         Gen.* **2000**, *190* (1), 149–155. https://doi.org/https://doi.org/10.1016/S0926-860X(99)00293-8.

(48)   Lusardi, M.; Struble, T.; Teixeira, A. R.; Jensen, K. F. Identifying the Roles of Acid–Base Sites in
         Formation Pathways of Tolualdehydes from Acetaldehyde over MgO-Based Catalysts. *Catal. Sci.
         Technol.* **2020**, *10* (2), 536–548. https://doi.org/10.1039/C9CY01927H.

(49)   Zhang, G.; Hattori, H.; Tanabe, K. Aldol Addition of Acetone, Catalyzed by Solid Base Catalysts:
         Magnesium Oxide, Calcium Oxide, Strontium Oxide, Barium Oxide, Lanthanum (III) Oxide and
         Zirconium Oxide. *Appl. Catal.* **1988**. https://doi.org/10.1016/S0166-9834(00)80114-1.

(50)   Bennici, S.; León, M.; Ordóñez, S.; Vega, A.; Auroux, A.; Faba, L.; Díaz, E. Consequences of MgO
         Activation Procedures on Its Catalytic Performance for Acetone Self-Condensation. *Appl. Catal. B
         Environ.* **2013**, *147*, 796–804. https://doi.org/10.1016/j.apcatb.2013.10.014.

(51)   Quesada, J.; Faba, L.; Díaz, E.; Ordóñez, S. Role of the Surface Intermediates in the Stability of Basic
         Mixed Oxides as Catalyst for Ethanol Condensation. *Appl. Catal. A Gen.* **2017**, *542* (June), 271–281.
         https://doi.org/10.1016/j.apcata.2017.06.001.

(52)   Bagheri, S.; Julkapli, N. M.; Yehye, W. A. Catalytic Conversion of Biodiesel Derived Raw Glycerol to
         Value Added Products. *Renew. Sustain. Energy Rev.* **2015**.
         https://doi.org/10.1016/j.rser.2014.08.031.

(53)   Pagliaro, M.; Ciriminna, R.; Kimura, H.; Rossi, M.; Della Pina, C. From Glycerol to Value-Added
         Products. *Angew. Chemie - Int. Ed.* **2007**, *46* (24), 4434–4440.
         https://doi.org/10.1002/anie.200604694.

(54)   de Oliveira, A. S.; Vasconcelos, S. J. S.; de Sousa, J. R.; de Sousa, F. F.; Filho, J. M.; Oliveira, A. C.
         Catalytic Conversion of Glycerol to Acrolein over Modified Molecular Sieves: Activity and
         Deactivation Studies. *Chem. Eng. J.* **2011**, *168* (2), 765–774.
         https://doi.org/10.1016/j.cej.2010.09.029.

(55)   Tsukuda, E.; Sato, S.; Takahashi, R.; Sodesawa, T. Production of Acrolein from Glycerol over Silica-
         Supported Heteropoly Acids. *Catal. Commun.* **2007**, *8* (9), 1349–1353.
         https://doi.org/10.1016/j.catcom.2006.12.006.

(56)   Ulgen, A.; Hoelderich, W. F. Conversion of Glycerol to Acrolein in the Presence of WO 3/TiO 2
         Catalysts. *Appl. Catal. A Gen.* **2011**, *400* (1–2), 34–38. https://doi.org/10.1016/j.apcata.2011.04.005.

(57)   Suprun, W.; Gläser, R.; Papp, H. Reaction Pathways for Catalytic Gas-Phase Oxidation of Glycerol
         over Mixed Metal Oxides. *DGMK Int. Conf. Catal. - Innov. Appl. Petrochemistry Refin.* **2011**, 253–
         260.

(58)   Liu, C.; Liu, R.; Wang, T. Glycerol Dehydration to Acrolein: Selectivity Control over CsPW/Nb2O5
         Catalyst. *Can. J. Chem. Eng.* **2015**, *93* (12), 2177–2183.
         https://doi.org/https://doi.org/10.1002/cjce.22339.

(59)   Odelius, M. Mixed Molecular and Dissociative Water Adsorption on MgO[100]. *Phys. Rev. Lett.*
         1999. https://doi.org/10.1103/PhysRevLett.82.3919.

(60)   Kim, Y. D.; Stultz, J.; Goodman, D. W. Dissociation of Water on MgO(100). *J. Phys. Chem. B* **2002**.
         https://doi.org/10.1021/jp012306d.

(61)   Kim, Y. D.; Lynden-Bell, R. M.; Alavi, A.; Stulz, J.; Goodman, D. W. Evidence for Partial Dissociation of Water on Flat MgO(100) Surfaces. *Chem. Phys. Lett.* **2002**. https://doi.org/10.1016/S0009-2614(02)00009-X.

(62)   Costa, D.; Chizallet, C.; Ealet, B.; Goniakowski, J.; Finocchi, F. Water on Extended and Point Defects at MgO Surfaces. *J. Chem. Phys.* **2006**, *125* (5). https://doi.org/10.1063/1.2212407.

(63)   De Leeuw, N. H.; Watson, G. W.; Parker, S. C. Atomistic Simulation of the Effect of Dissociative Adsorption of Water on the Surface Structure and Stability of Calcium and Magnesium Oxide. *J. Phys. Chem.* **1995**, *99* (47), 17219–17225. https://doi.org/10.1021/j100047a028.

(64)   Kinage, A. K.; Upare, P. P.; Kasinathan, P.; Hwang, Y. K.; Chang, J. S. Selective Conversion of Glycerol to Acetol over Sodium-Doped Metal Oxide Catalysts. *Catal. Commun.* **2010**, *11* (7), 620–623. https://doi.org/10.1016/j.catcom.2010.01.008.

(65)   Foyt, D. C.; White, J. M. Thermal Decomposition of Methanol Adsorbed on Magnesia. *J. Catal.* **1977**, *47* (2), 260–268. https://doi.org/https://doi.org/10.1016/0021-9517(77)90173-7.

(66)   Liang, S. H.; Gay, I. D. Adsorption and Thermal Decomposition of Methanol on Magnesium Oxide. Carbon-13 NMR Studies. *Langmuir* **1985**, *1* (5), 593–599. https://doi.org/10.1021/la00065a014.

(67)   Shido, T.; Asakura, K.; Iwasawa, Y. Reactant-Promoted Reaction Mechanism for Catalytic Water-Gas Shift Reaction on MgO. *J. Catal.* **1990**, *122* (1), 55–67. https://doi.org/https://doi.org/10.1016/0021-9517(90)90261-H.

(68)   Suprun, W.; Lutecki, M.; Haber, T.; Papp, H. Acidic Catalysts for the Dehydration of Glycerol: Activity and Deactivation. *J. Mol. Catal. A Chem.* **2009**, *309* (1–2), 71–78. https://doi.org/10.1016/j.molcata.2009.04.017.

(69)   Kong, P. S.; Aroua, M. K.; Daud, W. M. A. W. Conversion of Crude and Pure Glycerol into Derivatives: A Feasibility Evaluation. *Renew. Sustain. Energy Rev.* **2016**, *63*, 533–555. https://doi.org/10.1016/j.rser.2016.05.054.

(70)   Hernandez, D.; Velasquez, M.; Ayrault, P.; Lopez, D.; Fernandez, J. J.; Santamaria, A.; Batiot-Dupeyrat, C. Gas Phase Glycerol Conversion over Lanthanum Based Catalysts: LaNiO3and La2O3. *Appl. Catal. A Gen.* **2013**, *467*, 315–324. https://doi.org/10.1016/j.apcata.2013.07.016.

(71)   Checa, M.; Nogales-Delgado, S.; Montes, V.; Encinar, J. M. Recent Advances in Glycerol Catalytic Valorization: A Review. *Catalysts* **2020**, *10* (11), 1–41. https://doi.org/10.3390/catal10111279.

(72)   Ertl, G.; Knözinger, H.; Weitkamp, J. *Handbook of Heterogeneous Catalysis*; 2008. https://doi.org/10.1524/zpch.1999.208.part_1_2.274.

(73)   Klaewkla, R.; Arend, M.; F., W. A Review of Mass Transfer Controlling the Reaction Rate in Heterogeneous Catalytic Systems. In *Mass Transfer - Advanced Aspects*; 2011. https://doi.org/10.5772/22962.

(74)   Fogler, S. External Diffusion Effects on Heterogeneous Reactions. In *Elements of Chemical Reaction Engineering*; Pearson, 2008; pp 757–811.

(75)   Chavan, R. B. 3 - Indigo Dye and Reduction Techniques. In *Denim*; Paul, R., Ed.; Woodhead Publishing Series in Textiles; Woodhead Publishing, 2015; pp 37–67. https://doi.org/https://doi.org/10.1016/B978-0-85709-843-6.00003-2.

(76)   Koichumanova, K.; Vikla, A. K. K.; Cortese, R.; Ferrante, F.; Seshan, K.; Duca, D.; Lefferts, L. In Situ ATR-IR Studies in Aqueous Phase Reforming of Hydroxyacetone on Pt/ZrO2 and Pt/AlO(OH) Catalysts: The Role of Aldol Condensation. *Appl. Catal. B Environ.* **2018**, *232* (January), 454–463. https://doi.org/10.1016/j.apcatb.2018.03.090.

(77)   Yan, W.; Suppes, G. J. Low-Pressure Packed-Bed Gas-Phase Dehydration of Glycerol to Acrolein. *Ind. Eng. Chem. Res.* **2009**, *48* (7), 3279–3283. https://doi.org/10.1021/ie801200p.

(78)   Katryniok, B.; Paul, S.; Bellière-Baca, V.; Rey, P.; Dumeignil, F. Glycerol Dehydration to Acrolein in

the Context of New Uses of Glycerol. *Green Chem.* **2010**, *12* (12), 2079–2098. https://doi.org/10.1039/C0GC00307G.

(79)   Katryniok, B.; Paul, S.; Capron, M.; Dumeignil, F. Towards the Sustainable Production of Acrolein by Glycerol Dehydration. *ChemSusChem* **2009**, *2* (8), 719–730. https://doi.org/10.1002/cssc.200900134.

(80)   Mane, R. B.; Rode, C. V. Continuous Dehydration and Hydrogenolysis of Glycerol over Non-Chromium Copper Catalyst: Laboratory-Scale Process Studies. *Org. Process Res. Dev.* **2012**, *16* (5), 1043–1052. https://doi.org/10.1021/op200383r.

(81)   Doering, F. J.; Schaefer, G. F. Reaction Kinetics of the Aldol Condensation of Mixed C7 Aldehydes. *J. Mol. Catal.* **1987**, *41* (3), 313–328. https://doi.org/10.1016/0304-5102(87)80109-8.

Chapter 4

## Mechanistic studies using intermediate products of the valorisation of glycerol over MgO

4.1 Introduction

From the previous published literature,[1–3] and the work performed in chapter 3, it has been shown that there is more than one possible reaction pathway for the conversion of glycerol over MgO (Figure 1). This was originally deduced in the seminal work, where it was identified that there were at least two main routes which could lead to methanol production and another significant route leading to acrolein.[1,2] One of the more dominant proposed routes proceeds through the intermediate hydroxyacetone. This is identified by a high selectivity to hydroxyacetone under all conditions with MgO, it is routinely the most dominant product. Hydroxyacetone usually accounts for 18 – 30 % of the overall selectivity (chapter 3) this means that the glycerol dehydration to it is a major pathway. There are also several products that are likely directly derived from hydroxyacetone such as propanoic acid, 1,2-propanediol and acetone. However, while this route can produce methanol it is assumed not to be the optimal pathway. It is postulated to likely yield one molecule of methanol from glycerol, while C-C cleavage routes could potentially yield two. It also seems to exhibit a relatively stable nature. Previous experiments show a lack of a significant increase in methanol selectivity as hydroxyacetone selectivity is reduced at high temperatures. (Chapter 3).

The other identified route to methanol from glycerol, involves the C-C cleavage to an ethylene glycol radical as an intermediate. Ethylene glycol is seen with typically 8 – 15 % selectivity over most reaction conditions. It is thought *via* the proposed mechanistic understanding that the C-C cleavage pathway could produce a higher yield of methanol than the hydroxyacetone route. Two molecules of methanol are possible, one from the fragmentation of glycerol and a second from glycolaldehyde fragmentation. Glyceraldehyde has a similar structure and undergoes an analogous fragmentation to hydroxyacetone.

A third identified route results in acrolein *via* a double dehydration of glycerol. The conversion of glycerol to acrolein has been the focus of considerable research efforts,[4,5] Typically the production of acrolein is done using acidic catalysts, such as silico-tungstic acid. [6,7] Haider *et al,* considered that acrolein production could be base catalysed, however this led to the discovery that routes to methanol were more prominent in base conditions.[1] For the production of methanol of acrolein is

not considered favourable due to its toxicity and as there is no expected route between the products.

Figure 1. Proposed reaction network for the catalytic transformation of glycerol into a range of different products over MgO. Red arrows correspond to dominant reaction pathways over MgO. The green arrow corresponds to a dominant pathway occurring in the absence of MgO. 1. Glycerol; 2. 3-hydroxypropenal; 3. 1,3-propanediol; 4. 1-propanol; 5. hydroxyacetone; 6. propanoic acid; 7. 1,2-propanediol; 8. 2-propanol; 9. acetone; 10. acetaldehyde; 11. ethanol; 12. 2,3-butanedione; 13. 2,3-butandiol; 14. 2-butanol; 15. glycolaldehyde; 16. ethylene glycol; 17. ethenone; 18. acetic acid; 19. allyl alcohol; 20. 1-propanal; 21. 1-hydroxyl-2-butanone; 22. acrolein; 23. 3-alkoxypropanal; 24. 3-alkoxy propanol; 25. Methanol. Reproduced from work presented in L. R. Smith, P. J. Smith, K. S. Mugford, M. Douthwaite, N. F. Dummer, D. J. Willock, M. Howard, D. W. Knight, S. H. Taylor and G. J. Hutchings, Catal. Sci. Technol., 2019, 19–22.[2]

The mentioned mechanistic routes were proposed originally in the 2015 nature chemistry paper by Haider *et al.*[1] and were based on how the different intermediates and products from methanol could relate and react with each other. Further work investigating this reaction with MgO, experimentally and computationally have been undertaken,[2,3] and over ceria as a catalyst.[8–10] It was discovered through improvement of the analysis method that there was several side reactions and products that were unaccounted for in the original 2015 paper. This has led to the proposal of a more complex reaction mechanism shown in Figure 1. It was also identified that there was a gap in the carbon mass (CMB), which was proposed to be due to the formation of high weight molecular products (HWMP). This led to a revaluation of the methanol selectivity.

4.2 Studies using intermediate substrates.

### 4.2.1 Reactions from hydroxyacetone as a feed substrate

4.2.1.1 Introduction

A series of experimental reactions using hydroxyacetone as a substrate feed were performed. This was to investigate the specific products that are obtained directly from converting hydroxyacetone. Identifying the products of hydroxyacetone conversion could allow for confirmation of proposed mechanistic routes and whether hydroxyacetone conversion is desirable for methanol production. Hydroxyacetone is a key product over MgO from glycerol. It is also often seen as a major product of the conversion of glycerol under a variety of conditions.[8,11–15] The conversion of hydroxyacetone to a number of products has been demonstrated, including methylglyoxal *via* oxidation with OH radicals,[16] and 1,2-propanediol through hydrogenation reactions.[17,18] The key area of interest was the methanol yield, as well as that of reducing undesirable products such as acetaldehyde and acrolein. The proposed hydroxyacetone route of glycerol to methanol is initiated *via* glycerol dehydration at the terminal position, followed by a rapid tautomerisation step to yield hydroxyacetone (Figure 2).[1,2] A radical fragmentation similar to the Norrish type-1 process result in a hydroxymethyl radical methanol precursor and acetyl radical. The Norrish type-1 processes involves aldehyde or ketone undergoing a photochemical promoted C-C bond cleavage between the α-carbon and the carbonyl group (Appendix Section 6.1).[19,20] The radical precursors from hydroxyacetone fragmentation can be reduced to methanol, ethanol and acetaldehyde, respectively. The acetyl radical can react with itself to result in 2,3 butanedione, which is observed in small amounts.
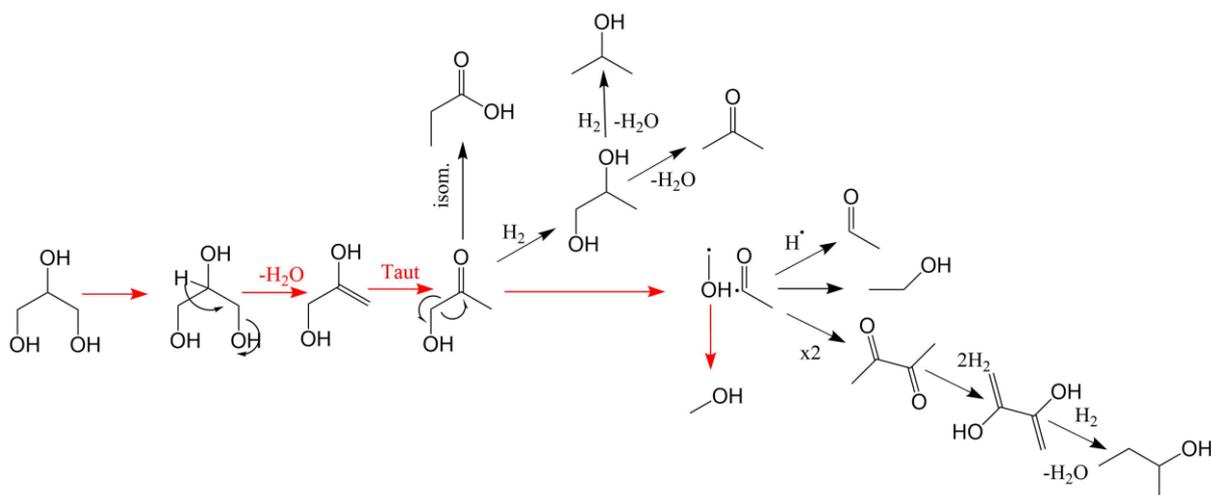
Figure 2. Glycerol to methanol through dehydration to hydroxyacetone proposed pathway. Red arrows: route to methanol. Black arrows: side reactions.

To better understand the reaction pathways, one step would be to identify what products the intermediates result in, and the catalysts propensity to convert the intermediate substrate. It is therefore important that we investigate the different catalysts activity for the conversion of the various intermediates. Furthermore, it is hoped that these experiments can help elucidate further understanding for the catalyst samples performance for the conversion of glycerol.

4.2.1.2 50 % feed conversion

Initially, a 50 wt.% hydroxyacetone feed was reacted over MgO_450, MgO_650 and MgO_750, at temperatures of 320 °C, 360 °C and 400 °C. Results are shown in Table 1, Table 2, and Table 3 for MgO_450, 650 and 750, respectively. The conversion of hydroxyacetone was quantified to try and understand the stability of the formed hydroxyacetone on the catalysts.

4.2.1.2.1 Conversion

At 320 °C, MgO_450 exhibited a low conversion of around 16 %, which did not noticeably change on the increase to 360 °C. With MgO_650, negligible conversion was observed with less than 1 % at 320 °C and 1 % at 360 °C. In this temperature range that MgO_650 is not significantly active for the conversion of hydroxyacetone. MgO_750 exhibited the highest conversion at 360 °C, indicating that similarly to the conversion of glycerol, the basicity and surface area are not the most important factors in determining conversion. When the reaction temperature is bought up to 400 °C the activity for all catalysts increases significantly, with conversions of 33 %, 21 %, and 64 % over MgO_450, MgO_650 and MgO_750, respectively. This demonstrates that the low surface area and total basicity of MgO_750 does not impede its ability to react hydroxyacetone.

Table 1. Hydroxyacetone reactions over MgO_450. Product selectivity - Reaction conditions: 320 - 400 °C, 50 wt.% hydroxyacetone, 0.016 mL min^{-1}, 0.5 g catalyst, 50 mL min^{-1} Ar. 3 hours.

Carbon mole selectivity %	Blank 50% 360°C	MgO_450 50 % 320 °C	MgO_450 50 % 360 °C	MgO 450 50 % 400 °C
acetaldehyde	0.0	12.2	20.3	45.4
propionaldehyde	0.0	0.0	0.3	0.5
acetone	0.0	1.2	1.4	0.9
methanol	0.0	1.3	1.3	1.4
2-propanol	0.0	0.0	0.0	0.1
ethanol	0.0	0.2	0.2	0.1
2,3-butanedione	0.0	2.7	2.3	1.4
1-propanol	0.0	0.3	0.2	0.0
3-hexanone	0.0	1.2	1.8	1.0
allyl alcohol	0.0	0.4	0.0	0.1
cyclopentanone	0.0	3.9	3.3	3.1
3-ethoxy-1-propanol	5.9	2.0	1.4	0.8
acetic acid	0.0	6.2	8.0	5.1
Glycidol	10.5	4.4	5.2	2.9
propionic acid	5.6	4.4	4.0	5.4
1,2-propanediol	0.0	4.5	8.8	5.8
unknown(s)	0.0	44.9	34.7	18.6
ethylene glycol	78.1	0.7	0.5	3.3
1,3-propanediol	0.0	2.4	2.4	2.0
CO	0.0	1.0	0.5	1.0
CO$_2$	0.0	6.3	3.3	1.1
Hydroxyacetone conversion %	1	16	16	33
CMB %	100	89	84	78
Methanol STY g h^{-1} kg^{-1}	0	1	1	4
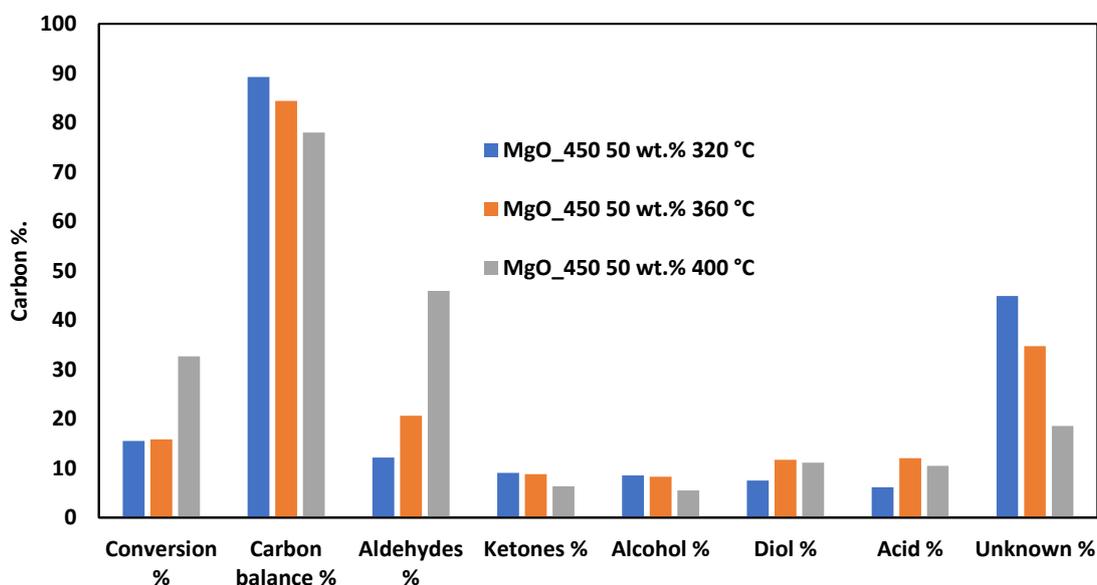
Figure 3. Hydroxyacetone reactions over MgO_450 - Reaction conditions: 320 - 400 °C, 50 wt.% hydroxyacetone, 0.016 mL min^{-1}, 0.5 g catalyst, 50 mL min^{-1} Ar. 3 hours.

Table 2. Hydroxyacetone reactions over MgO_650. Product selectivity - Reaction conditions: 320 - 400 °C , 50 wt.% hydroxyacetone, 0.016 mL min^{-1}, 0.5 g catalyst, 50 mL min^{-1} Ar. 3 hours.

Carbon mole selectivity %	Blank 50% 360 °C	MgO_650 50 % 320 °C	MgO_650 50 % 360 °C	MgO_650 50 % 400 °C
acetaldehyde	0.0	21.3	26.5	46.9
propionaldehyde	0.0	0.0	0.4	0.6
acetone	0.0	1.8	1.6	1.5
methanol	0.0	1.4	1.2	1.7
2,3-butanedione	0.0	3.8	2.0	1.7
3-hexanone	0.0	1.6	1.9	1.6
2-hexanone	0.0	0.0	0.0	0.0
allyl alcohol	0.0	0.0	0.0	0.0
cyclopentanone	0.0	3.1	2.6	2.0
3-ethoxy-1-propanol	5.9	1.6	1.1	1.3
acetic acid	0.0	9.5	9.2	7.8
Glycidol	10.5	2.4	8.0	4.3
propionic acid	5.6	4.2	4.7	3.5
1,2-propanediol	0.0	11.8	13.5	7.2
unknown(s)	0.0	24.8	14.4	13.4
ethylene glycol	78.1	0.0	0.6	2.3
1,3-propanediol	0.0	3.4	2.9	2.0
CO	0.0	1.4	3.3	0.9
CO_2	0.0	8.1	6.2	1.2
Hydroxyacetone conversion %	1	0	1	21
CMB %	100	100	99	98
Methanol STY g h^{-1} kg^{-1}	0	1	1	6
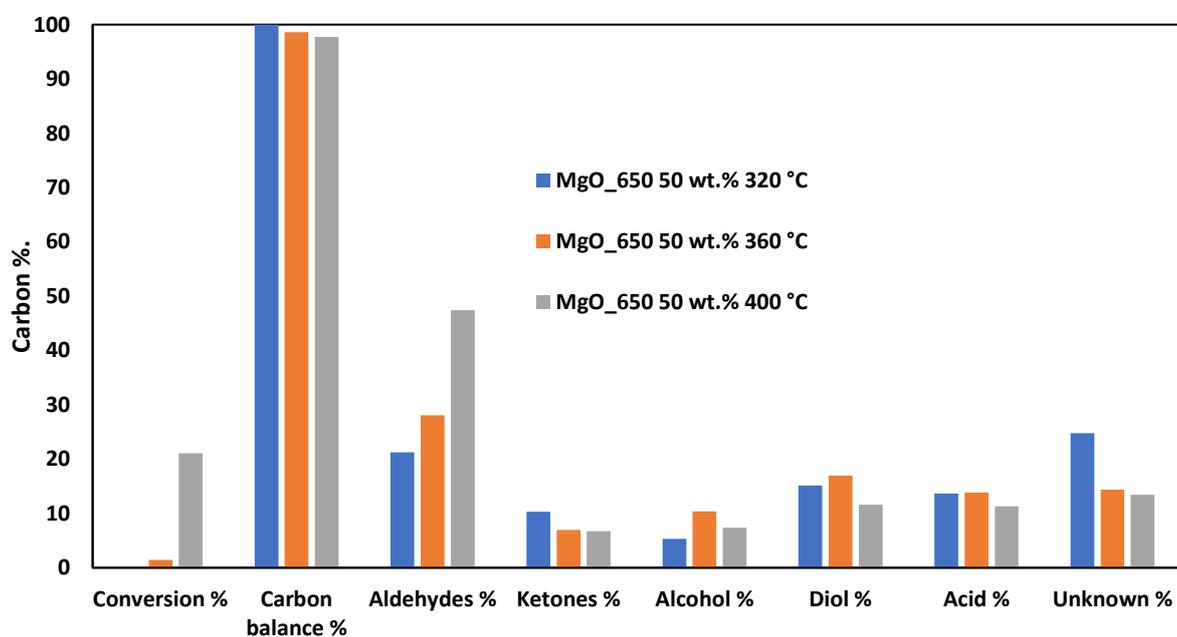
Figure 4. Hydroxyacetone reactions over MgO_650 - Reaction conditions: 320 - 400 °C, 50 wt.% hydroxyacetone, 0.016 mL min^{-1}, 0.5 g catalyst, 50 mL min^{-1} Ar. 3 hours.

Table 3. Hydroxyacetone reactions over MgO_750. Product selectivity - Reaction conditions: 320 - 400 °C , 50 wt.% hydroxyacetone, 0.016 mL min^{-1}, 0.5 g catalyst, 50 mL min^{-1} Ar. 3 hours.

Carbon mole selectivity %	Blank 50% 360 °C	MgO_750 50 % 360 °C	MgO_750 50 % 400 °C
acetaldehyde	0.0	24.4	47.0
propionaldehyde	0.0	0.0	2.1
acetone	0.0	2.1	3.6
methanol	0.0	2.0	2.0
ethanol	0.0	2.2	0.8
2,3-butanedione	0.0	3.2	2.0
1-propanol	0.0	0.0	0.2
3-hexanone	0.0	0.0	2.3
allyl alcohol	0.0	0.0	0.1
cyclopentanone	0.0	4.5	1.8
3-ethoxy-1-propanol	5.9	1.7	1.9
acetic acid	0.0	10.3	5.8
Glycidol	10.5	7.5	3.0
propionic acid	5.6	2.5	1.3
1,2-propanediol	0.0	11.7	7.1
unknown(s)	0.0	24.1	14.9
ethylene glycol	78.1	0.6	0.1
1,3-propanediol	0.0	3.2	1.6
CO	0.0	0.0	1.1
CO$_2$	0.0	0.0	1.3
Hydroxyacetone conversion %	1	18	64
CMB %	100	92	70
Methanol STY g h^{-1} kg^{-1}	0	3	9

4.2.1.2.2 CMB

As shown in Figure 3, a general downwards trend is observed for the CMB of MgO_450 as the reaction temperature increases. This is negligible over MgO_650 which maintains an almost full CMB throughout (Figure 4). This is expected at the lower temperatures, where little to almost no conversion is achieved. MgO_650 still achieves a CMB of 98 %, at 400 °C, despite a significant hydroxyacetone conversion (21 %). This indicates that it may not be active for formation of significant quantities of HWMP produced from products of hydroxyacetone at these temperatures. This was in agreement with the results observed in the glycerol experiments, discussed in chapter 3 (3.3.1). In these experiments and previous publications in the group,[2,10] a decrease in CMB was attributed to be due to HWMP forming, which are not quantified by the analysis method. MgO_650 showed potential with obtaining significantly high CMB over a range of conditions. (Up to 94 % - 98 %). This was attributed to lack of formation of the HWMP. Evidence from using LCMS and CHN analysis indicated these may be produced from MgO_STD and MgO_450.

MgO_450 shows a more pronounced downwards trend, with the CMB decreasing from 89 % to 84 % and 79 % over the temperature range. MgO_450 exhibits a significantly higher conversion at each temperature than MgO_650. The conversion is slightly lower over MgO_450 than MgO_750 at 400

°C (*ca.* 16 *vs.* 21 %), yet a lower CMB was obtained over MgO_450. A drop is observed upon increasing the temperature to 360 °C, despite no enhancement in the conversion of hydroxyacetone. A further drop in CMB is seen with an increase in conversion at 400 °C. This indicates that as with the glycerol experiments, MgO_450 may result in a higher degree of unquantified products when converting hydroxyacetone than MgO_650. Raising the temperature increases the quantity of unquantified products even when the conversion doesn't increase. So, it is not likely only an effect of increased conversion. MgO_750 likewise sees a trend between increase in temperature, conversion, and CMB. On increasing the temperature from 360 °C to 400 °C the CMB decreases from 92 % to 70 %. MgO_750 is the most active catalyst for this reaction but obtains a fairly good CMB over 360 °C in comparison to MgO_450 with a similar conversion. However, on increasing the temperature the CMB drops to the lowest obtained with the catalysts at 400 °C, but the conversion observed for MgO_750 at this temperature is significantly higher.

Selectivity

The selectivity to the different products was analysed to determine which products could originate from hydroxyacetone at varying temperature. The catalysts MgO_450 and MgO_650 were compared, but it must be noted that the conversions obtained over these catalysts was significantly different. This means the main differences in selectivity may just be due to the different levels of hydroxyacetone conversion.

4.2.1.2.3 Unknown selectivity

A change in selectivity is observed with reaction temperature change. An interesting point from this experiment is the high selectivity to unknowns observed. These unknowns are products which are detected by GC-FID but not yet identified. Identification of reaction products was carried out *via* the GC-FID analysis of expected compounds and comparison to reaction chromatograms and *via* GC-MS (supplementary material Haider *et al.*[1]). Further products have been identified from the unknowns detected since this publication leading to a more complete analysis and reaction scheme. These include products such as acetaldehyde, 1,2-propanediol, 1,3-propanediol, cyclopentanone, acetic acid, propanoic acid and CO.

Up to 45 % selectivity to unknown products is seen at low temperatures. It is possible that these hydroxyacetone derived unknown products are a source of some of the unknowns exhibited in the glycerol reaction, in which selectivity in the range of 10 – 20 % are usually seen. With glycerol, higher selectivity to unknowns was seen at lower conversion. MgO_450 exhibits the highest selectivity of unknowns in general, especially at lower temperatures with it exhibiting 45 % selectivity at 320 °C. MgO_450 also shows the lowest CMB here and in the glycerol experiments. It

may be the case that the proliferation of these hydroxyacetone sourced unknown products on its surface may be a factor in explaining the lower CMB.

There is a correlation between reaction temperature and unknown selectivity (Figure 5). Over MgO_450, 320 °C reaction conditions result in 44.9 % selectivity to unknowns, decreasing to 34.7 % at 360 °C. MgO_650 shows a similar trend, but exhibits lower unknown selectivity overall, probably due to its insufficient conversion, proceeding from 24.8 % to 14.4 % as the reaction temperature was increased from 320 °C to 360 °C. MgO_750 shows also shows a decrease from 21.8 % to 14.9 % on increasing temperature from 360 °C to 400 °C. At 400 °C MgO_750 has a similar selectivity to unknowns as the other catalysts, but a significantly higher conversion. This may indicate that the unknowns representing intermediates are reduced, and the ones seen here are terminal products. The number of individual unknown peaks change with temperature (appendix Table 1), they increase from 320 °C to 360 °C and then decrease at 400 °C, showing the makeup the unknown species changes with temperature. Detected unknown products are a significantly dominant under these conditions along with acetaldehyde. This indicates there is significant chemistry occurring which is not yet understood.
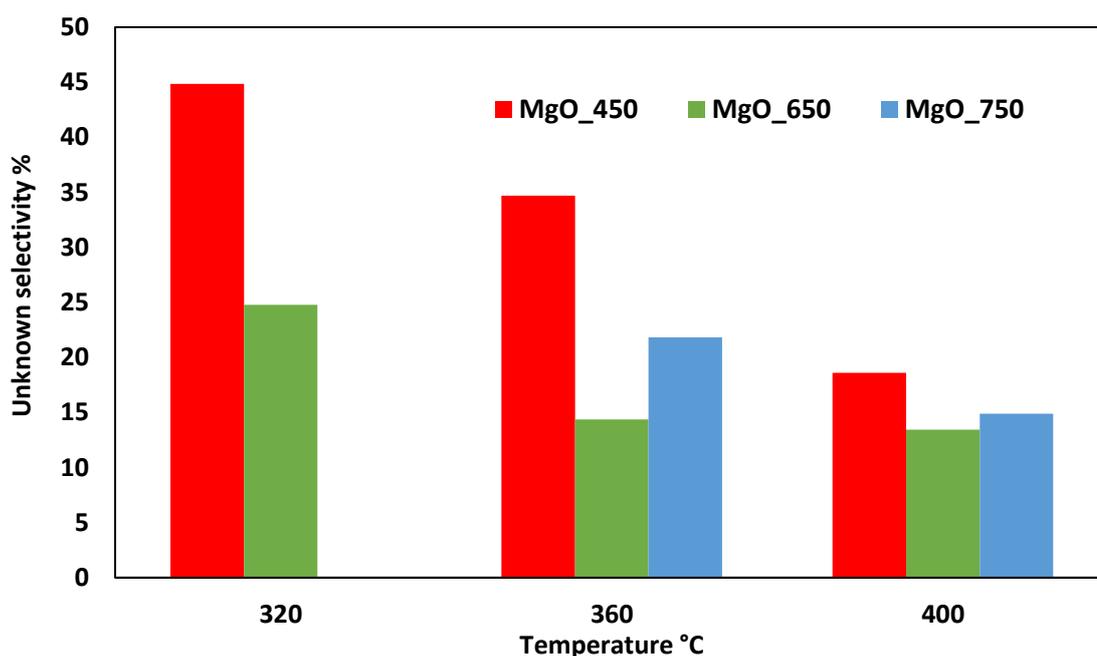
Figure 5. Hydroxyacetone reactions over MgO_450, 650, 750. Detected unknown selectivity - Reaction conditions: 320 - 400 °C, 50 wt.% hydroxyacetone, 0.016 mL min^{-1}, 0.5 g catalyst, 50 mL min^{-1} Ar. 3 hours.

It is suspected that the unknowns formed over MgO could partially be attributed to the precursors to heavier products forming, possibly related to acetaldehyde. The almost inert nature of MgO_650 for the conversion of hydroxyacetone may help explain why it exhibits such a high CMB. Very high

temperatures, or a low concentration of hydroxyacetone is needed to give a noticeable conversion of hydroxyacetone over MgO_650. From this it can be inferred that anything seen to originate from it is likely to be only produced in negligible amounts under glycerol reaction conditions. However, this may lead to an underestimation of its performance, as radical species sourced from the C-C cleavage of glycerol may influence the reactivity of other species such as hydroxyacetone.

4.2.1.2.4 1,2 propanediol selectivity

1,2-propanediol can form when hydroxyacetone reacts with H_2. Significant selectivity to 1,2-propanediol is observed, especially over MgO_650. An increase from 4.5 % to 8.8 % is seen on increasing the temperature from 320 °C to 360 °C with MgO_450. 11.8 % to 13.5 % is observed with MgO_650. With the increase to 400 °C a slight decrease is seen to 5.8 % for MgO_450 and 7.2 % with MgO_650. MgO_750 exhibits 11.7 % decreasing to 7.1 % as temperature rises from 360 °C to 400 °C.

However, MgO_650 only manages to convert a very small amount of hydroxyacetone so the actual yield is low. 1,2-propanediol is not seen in the catalyst free reaction, suggesting that a catalyst is crucial for its formation. The formation of 1,2-propaendiol from hydroxyacetone is a hydrogenation reaction which was demonstrated efficiently by Akiyama *et al.*[18] with ambient hydrogen pressure. The reactions discussed in this thesis involve low partial pressures of hydrogen with no added H_2 stream. Conversion of glycerol selectively to 1,2-propanediol in the absence of added hydrogen has been achieved over Pt impregnated NaY zeolite catalysts.[21] Here it was thought that the reducing environment for the hydrogenation was produced from water steam reforming. Another example where 1,2-propanediol is prepared from glycerol with *in-situ* generated H_2 include over Pd/Fe_2O_3 where the hydrogen was provided by dehydrogenation of the 2-propanol or ethanol solvent.[22] Further work investigated the aqueous phase reforming generation of *in-situ* hydrogen for hydrogenation over Pt-Ni bimetallic catalysts supported on γ-Al_2O_3.[23] The high concentration of water in our feed may act as a source.

4.2.1.2.5 Acetaldehyde selectivity

As the reaction temperature increases, an increase in acetaldehyde selectivity is observed over all catalysts. Acetaldehyde increases significantly with increasing reaction temperature, becoming the major product at 400 °C. With MgO_450 it increases from 12.2 % to 20.3 % to 45.4 % at 320, 360 and 400 °C, respectively. This concurs with a drop in the CMB with MgO_450 indicating a possible link to condensation reactions. Condensation reactions may yield heavy products that are not quantified *via* GC-FID leading to lower CMB. Acetaldehyde is a reactive species which can undergo condensation reactions catalysed by basic catalysts such as MgO.[24–26] Acetaldehyde can result in 3-

hydroxybutanal *via* aldol condensation and crotonaldehyde *via* subsequent dehydration.[26] These species can further react giving larger products such as ortho and para tolualdehyde, 2,4,6 octatrienal and 2,4 hexadienal.[27] Which may possibly further react to form HWMP. MgO_650 sees a similar trend in selectivity, starting higher at 21.3 % it increases to 26.5 % and 46.9 % respectively over the temperature increase. This is not met with a corresponding drop in CMB however, reinforcing the theory MgO_650 does not promote bimolecular reactions (section 3.3.1.5). MgO_750 shows a similar jump between 360 to 400 °C of 24.4 to 47 % with a corresponding drop in CMB, showing similarities to MgO_450's behaviour.

4.2.1.2.6 Acrolein selectivity

No acrolein is observed to be produced from the conversion of hydroxyacetone, this is expected as was postulated to proceed *via a* separate pathway. The proposed reaction scheme indicates that acrolein production involves a double dehydration reaction.[1,2] Initial dehydration at the secondary position leads to the formation of 3-hydroxypropanal, which can either react with H_2 to yield 1,3 propanediol and or dehydrate further to acrolein. Interestingly a small selectivity to 1,3 propanediol is observed, the route to this from hydroxyacetone is not yet clear, but under these conditions it is not observed to dehydrate to acrolein itself.

4.2.1.2.7 Acetic acid selectivity

There is a relatively high selectivity of acetic acid (6 % - 10 %) compared to the glycerol reactions (3 % - 4 %). Acetic acid in the proposed scheme forms from the hydration of ketene, which itself forms from the dehydration of glycolaldehyde. Glycolaldehyde is an expected intermediate in the fragmentation to ethylene glycol pathway but has not been quantified. It is however highly reactive, so a significant portion is not expected to exist in reaction mixture. In aqueous solutions glycolaldehyde rapidly interconverts between four different species, the aldehyde only accounting for a minor portion, this would make it difficult to accurately quantify.[28] It is likely that the acetic acid obtained using hydroxyacetone as a substrate is produced *via* a different route. There is a significant selectivity to acetaldehyde which itself can undergo oxidation to acetic acid. This can occur non catalytically in presence of oxygen or water and is likely driven by radical species.[29] The water diluent used in the feed stream may allow for oxidation of acetaldehyde explaining the acetic acid seen here.

4.2.1.2.8 2,3 butanedione selectivity

2,3 butanedione is observed and decreases as the temperature increases. It is however only seen in small quantities accounting for less than 4 % of the selectivity. This decreases slightly with temperature. MgO_450 decreases from 2.7 % to 1.4 % and MgO_650 3.8 % to 1.7 % over the

temperature range. This is expected to form *via* the hydroxyacetone route, by the radical combination of two acetyl radical molecules sourced from the fragmentation of hydroxyacetone. However, the selectivity here is comparable to that seen from glycerol. If it was produced solely from the hydroxyacetone scheme, then it would be expected to exhibit a higher selectivity with hydroxyacetone substrate than in the glycerol reactions, due to the higher concentration of its substrate. It seems though that under these conditions the formation of acetaldehyde is significantly more favourable, competing processes and significantly different conditions can affect this. Radical reactions may be more prominent from glycerol than hydroxyacetone, but further evidence to back this up is needed.

4.2.1.2.9 Cyclopentanone selectivity

Cyclopentanone is also seen to be produced from hydroxyacetone. The selectivity to cyclopentanone is about 4 % and decreases to 3 % on the temperature change from 320 °C to 360 °C with MgO_450. MgO_650 exhibits a slightly lower selectivity – decreasing from 3 – 2 %. It is not clear how cyclopentanone, a C_5 product is made from glycerol a C_3 product. This product is seen reliably in both with glycerol reactions and hydroxyacetone. In the reactions with glycerol cyclopentanone is proportionally only seen in very small amounts compared to here at less than 0.5 % selectivity. This significant increase with hydroxyacetone as a pure substrate suggests that it formed after the formation of hydroxyacetone in the scheme.

4.2.1.2.10 Glycidol selectivity

Glycidol is present in a relatively high selectivity compared to glycerol reactions. Especially under catalyst free 360 °C conditions where 10.5 % is observed. The selectivity to glycidol for MgO_450 and MgO_650 represent a volcano-like plot with temperature. At 320 °C 4.4 % and 2.4 % selectivity is seen over MgO_450 and MgO_650 respectively. This increases to 5.2 % and 8.0 % at 360 °C followed by a drop to 2.9 % and 4.3 %. Glycidol can form from glycerol carbonate, which itself can result from a reaction with glycerol and CO_2.[30] Glycidol can also originate from glycerol *via* a direct 1,2 elimination of water.[13,31,32] Allyl alcohol can be epoxidized to glycidol under differing conditions,[33] but itself is not seen from hydroxyacetone here regardless. The pathway to glycidol is not directly clear when using hydroxyacetone as a substrate.

4.2.1.2.11 Propionic acid selectivity

Propionic acid is a structural isomer of hydroxyacetone and is seen a significant amounts. Over MgO_450 a general increase in propionic acid is observed as the temperature and conversion increase, it increases slightly from 4.4 % to 5.4 % over the temperature range. MgO_650 sees a slight decrease, with 4.2 %, 4.7 % and 3.5 % seen over the temperature range. This may be skewed

somewhat by the very low conversion observed, with some production and low conversion may be non-catalytic isomerisation in the feed.

4.2.1.2.12 COx selectivity

COx selectivity varies with temperature. The selectivity to CO_2 decreases with the increase in reaction temperature. This may be due to a higher degree of the reverse water gas shift reaction,[34] however there is no clear increase in CO selectivity. With MgO_450 CO_2 decreases from 6.3 % to 3.3 % to 1.07 % over the 320 °C to 400 °C range. MgO_650 sees a more dramatic decrease in CO_2 selectivity with temperature increase. 6.2 % is observed at 320 °C which decreases to 1.2 % and 0.2 % at 360 °C and 400 °C respectively. MgO_750 on the other hand shows a selectivity of 0.2 % at 360 °C but sees an increase to 1.3 % at 400 °C.

CO stays relatively stable over MgO_450, staying between 1.0- 0.5 %. Over MgO_650, CO decreases with temperature 3.3 % to 0.9 % and 0.3 % from 320 °C- 400 °C. MgO_750 also increases here from 0.2 % to 1.3 %. The increases in selectivity to CO_x with MgO_750 with the increase in temperature is contrary to the other catalysts, but the conversion is significantly higher at 400 °C. It also experiences a much larger increase in conversion from 360 °C than observed with the other catalysts.

4.2.1.2.13 Methanol selectivity.

Methanol was not produced in high quantities or selectivity when using hydroxyacetone as a feed substrate. Selectivity was generally below 3 % which is significantly lower than the 10 % + often observed with glycerol as a source substrate. This combined with the low conversion of hydroxyacetone achieved by the catalysts results in very low STY of methanol. This does not significantly improve at higher temperatures. Selectivity does not increase with temperature and relatively low increases in conversion for the catalysts results in low STY across the board.

It may be inferred from this data, that it is likely that hydroxyacetone conversion is not a significant contributor to methanol production when glycerol is used as a feed substrate. Methanol yields under glycerol reaction conditions are 70 – 130 g h^{-1} kg^{-1} typically. Here, using a pure feed of hydroxyacetone, yields of less than 10 g h^{-1} kg^{-1} methanol is achieved. In the glycerol reactions the concentration of hydroxyacetone on the catalyst surface would be significantly lower, so the yield of methanol from hydroxyacetone would be even lower than that seen here. This means it the amount of hydroxyacetone that converts to methanol is likely to be negligible when using glycerol as a feed substrate. However, due to the removal of the other routes seen from glycerol, certain interactions which promote methanol production from hydroxyacetone *in-situ* may not occur under these conditions.

4.2.1.3 10 % reactions with hydroxyacetone.

Reactions were carried out with a 10 wt.% hydroxyacetone feed in order to explore how a high catalyst mass to substrate concentration ratio would affect the product distribution. In previous results using glycerol, reducing the wt.% to 10 % led to a significant increase in substrate conversion. This was accompanied by a relatively high CMB retention, particularly when compared to the reactions with higher substrate concentration, whereby an increase in lost carbon was observed as the reaction temperature was increased. This was not the case with the MgO_650 catalyst which maintains a high CMB over nearly all conditions including high temperature. Typically, with a 50 wt.% feedstock, hydroxyacetone conversion was low. Thus, it was considered important to explore the product distribution at a high level of hydroxyacetone conversion, in order to help identify and confirm intermediates and terminal products. It is expected that a significant increase in catalyst volume and surface area ratio to hydroxyacetone would lead to pronounced increase in conversion. This is expected due to the lower concentration of hydroxyacetone to react over the same surface with a consistent contact time.

4.2.1.3.1 Conversion

As can be seen in Table 4, the conversion is significantly higher for both catalyst samples. However, this is not relatively proportional to the increase in catalyst mass to substrate ratio. Experiments at 400 °C with 50 wt.% weight glycerol did not achieve significantly higher conversions. Changing the feedstock to 10 wt.% at 400 °C did result in significantly higher conversions. Upon reducing the hydroxyacetone concentration from 50 to 10 wt.%, an increase in hydroxyacetone conversion was observed. At a reaction temperature of 400 °C, conversion of 64 % and 34% were observed over MgO_450 and MgO_650, respectively. Similarly, to the experiments performed with 50 wt.% hydroxyacetone, MgO_650 was shown to be inefficient at converting hydroxyacetone. Both lowering the feedstock concentration and increasing the reaction temperatures resulted in only small increases in conversion. Linking this with the glycerol experiments, where high selectivity to hydroxyacetone was observed, even at high reaction temperatures and glycerol conversions, indicates that hydroxyacetone is reasonably stable over MgO_650 under reaction conditions.

4.2.1.3.2 Selectivity

A high selectivity to unknowns were seen compared to the same temperature reactions at 50 wt.%. This is likely due to the increase in conversion resulting in more unknown intermediates and potentially detectable HWMP precursors. Lower CMB may indicate here that the high conversion of hydroxyacetone predominantly leads to more of these products. This is unexpected though as water is expected to inhibit the condensation reactions. Interestingly there was a substantial increase from the 50 wt.% reactions CO_2 selectivity, here with the higher conversion the CO_2

selectivity has increased, when at 50 wt.% increasing the conversion decreased CO_2 selectivity. The presence of CO_2 in the glycerol over MgO reaction was also proposed to be due to organic acid decarboxylation.[2,35,36] MgO_450 had a selectivity to CO_2 of 14.8 % and MgO_650 11 % this is likely a function of conversion with MgO_450 having almost double the conversion of hydroxyacetone as MgO_650. This would be explained as CO_2 is not thought of to exist as an intermediate product.

Table 4. Hydroxyacetone reactions over MgO_450 and 650. Product selectivity - Reaction conditions: 400 °C, 10 wt.% hydroxyacetone, 0.016 mL min^{-1}, 0.5 g catalyst, 50 mL min^{-1} Ar. 3 hours.

Carbon mole selectivity %	MgO_450 10 % 400 °C	MgO 650 10 % 400 °C
acetaldehyde	20.8	24.6
propionaldehyde	1.9	1.6
acetone	2.2	1.4
butyraldehyde	0.1	0.0
methanol	2.3	5.3
2-propanol	0.0	1.1
ethanol	2.4	1.3
2,3-butanedione	1.5	0.0
1-propanol	1.2	0.7
3-hexanone	0.0	1.8
allyl alcohol	2.0	0.3
cyclopentanone	2.6	2.0
3-ethoxy-1-propanol	0.1	1.8
acetic acid	5.2	4.4
Glycidol	0.0	1.8
propionic acid	4.3	3.6
1,2-propanediol	15.6	19.0
unknown(s)	22.0	16.9
ethylene glycol	0.3	0.3
1,3-propanediol	0.3	0.6
phenol	0.3	0.5
CO	0.0	0.0
CO_2	14.8	11.0
Hydroxyacetone conversion %	64	34
CMB %	64	84
Methanol STY g h^{-1} kg^{-1}	2	3

Selectivity to methanol was slightly higher here for both catalysts. MgO_450 exhibited 2.3 % an increase from approximately 1 %. MgO_650 increased to 5.3 % from 1.7 %, both approximately doubling. This again may likely be linked to conversion, as methanol is a mainly terminal product.

Acetaldehyde selectivity is significantly lower than that seen at 50 wt.%. This seems to be counteracted by a preference to unknowns and 1,2-propanediol. As already stipulated hydroxyacetone is not indicated by these experiments as a main source of methanol. Forcing more aggressive conditions upon HA does increase conversion and methanol yield, but only by a negligible amount. The chemistry resulting from glycerol is likely more complicated and could lead

to a higher degree of methanol sourced from hydroxyacetone than seen here due to radical moieties obtained from glycerol C-C cleavage. There is likely competing and more active routes for the production of the methanol observed in the glycerol experiments. The next key candidate to investigate was the intermediate ethylene glycol.

4.2.2 Ethylene glycol reactions

4.2.2.1 Introduction

Reactions using ethylene glycol as a feed substrate were performed to investigate the products that could be sourced *via* its reaction over MgO and the catalysts activity for its conversion. Ethylene glycol is also a major intermediate in the conversion of glycerol accounting for approximately 8 – 15 % selectivity depending on conditions/catalysts. Theoretically the reaction which proceeds through the proposed C-C cleavage if glycerol should be preferable compared to dehydration to hydroxyacetone. The hypothesised route allows for two molecules of methanol to be produced (Figure 6).
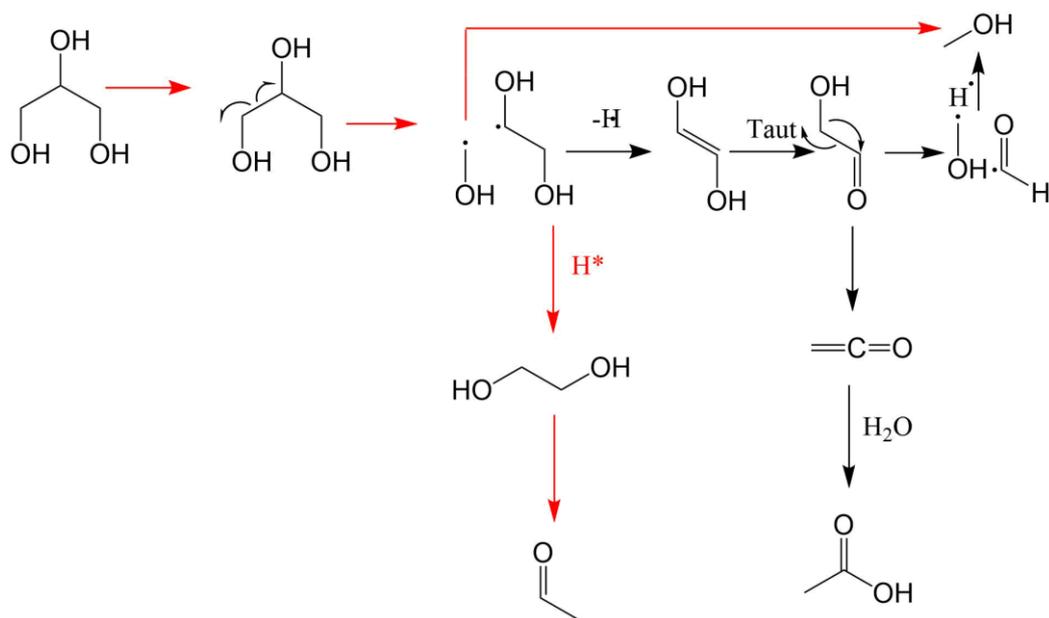
Figure 6. Glycerol to methanol radical fragmentation to ethylene glycol proposed pathway

One from the C-C cleavage fragmentation of glycerol to a methanol and ethylene glycol radical, and secondly the fragmentation related to a Norrish type-1 process of glycolaldehyde (Appendix section 6.1). Of course, it is not possible to isolate the methanol from the first fragmentation of glycerol here, as starting from ethylene glycol misses out this step and does not involve the C_3 source of carbon in the environment. However, if ethylene glycol directly still individually exhibits a high yield of methanol, it would be likely mean it is a major pathway compared to the hydroxyacetone mono-dehydration. However, isolating a pathway and remaining representative is difficult, it could result

in possible interactions between different pathway products not accounted for. It is also possible that not as much radical ethylene glycol will result from reacting ethylene glycol compared to glycerol. The results for the ethylene glycol experiments are shown in detail in Table 5 and Figure 7. These reactions were carried out with a 50 wt.% solution of ethylene glycol in water at temperatures of 320 – 440 °C.

Table 5. **Ethylene glycol reactions over MgO_450, MgO_650 and MgO_750. Reaction conditions: 50 wt.% ethylene glycol in water, 320 °C - 440 °C with 0.5 g catalyst. 0.1 mL min^{-1} 15 mins, 0.016 mL min^{-1} 2 hours, 0.016 mL min^{-1} 3 hours collect. 50 mL min^{-1} Ar flow.**

|	Blank 360 °C	MgO_450 320 °C	MgO_450 360 °C	MgO_450 400 °C	MgO_450 440 °C	MgO_650 320 °C	MgO_650 360 °C	MgO_650 400 °C	MgO_650 440 °C	MgO_750 360 °C	MgO_750 400 °C
acetaldehyde	34.2	22.7	25.6	22.4	18.4	16.5	20.1	21.2	22.7	37.2	20.4
propionaldehyde	0.0	0.0	0.6	0.4	1.5	0.0	0.2	0.8	1.0	0.2	0.5
acetone	0.0	0.0	0.2	0.1	0.4	0.0	0.0	0.2	0.2	0.0	0.1
acrolein	0.0	0.0	0.0	0.0	0.1	0.0	0.0	0.0	0.1	0.0	0.0
butyraldehyde	0.0	0.0	0.0	0.1	0.2	0.0	0.0	0.1	0.1	0.0	0.0
methanol	0.8	9.5	11.6	11.4	14.2	14.7	18.5	14.4	11.8	9.5	14.3
ethanol	2.1	21.3	31.1	23.8	16.2	25.9	24.5	18.7	14.6	17.4	22.2
2,3-butanedione	0.0	0.0	0.1	0.2	0.4	0.0	0.4	0.4	0.5	0.3	0.4
1-propanol	0.0	0.1	0.4	1.2	2.4	0.6	1.0	2.2	1.7	0.2	1.6
3-hexanone	0.0	0.0	0.0	0.1	0.1	0.0	0.0	0.1	0.1	0.0	0.1
allyl alcohol	0.0	0.0	0.0	0.3	0.1	0.2	0.2	0.3	0.2	0.2	0.1
cyclopentanone	0.0	0.6	0.3	0.5	0.6	0.7	0.6	0.6	0.7	0.5	0.7
hydroxyacetone	6.4	8.4	10.1	12.4	13.2	12.4	12.2	14.1	15.6	9.5	13.8
3-ethoxy-1-propanol	0.0	8.1	1.1	0.9	0.9	4.7	2.5	2.2	1.7	2.8	2.7
acetic acid	4.2	1.9	5.2	6.0	6.5	2.0	2.8	2.7	3.0	1.7	2.6
Glycidol	0.0	0.0	0.0	0.3	0.4	0.0	0.2	0.4	0.5	0.2	0.4
propionic acid	0.0	0.1	0.0	0.1	1.4	0.2	0.4	0.8	1.5	0.5	1.0
1,2-propanediol	27.9	14.3	5.0	8.2	3.5	13.2	7.0	6.7	5.6	8.9	9.2
unknown(s)	20.1	7.3	3.7	6.2	14.8	5.5	4.1	7.3	10.2	6.7	7.3
1,3-propanediol	1.2	0.2	0.1	0.2	0.2	0.2	0.1	0.2	0.3	0.3	0.2
phenol	3.0	0.9	0.0	0.0	0.0	0.0	0.0	0.0	0.2	0.7	0.1
CO	0	1.6	2.0	2.3	0.4	1.0	2.7	3.1	0.7	1.4	1.1
CO_2	0	3.2	2.8	3.0	4.0	2.1	2.7	3.5	7.0	1.8	1.3
Ethylene glycol conversion %	2	4.	31	40	78	4	36	47	68	23	51
CMB %	98	99	76	75	74	100	95	94	93	88	77
Methanol STY g h^{-1} kg^{-1}	0	4	9	28	115	10	38	72	86	14	57

(a)

(b)
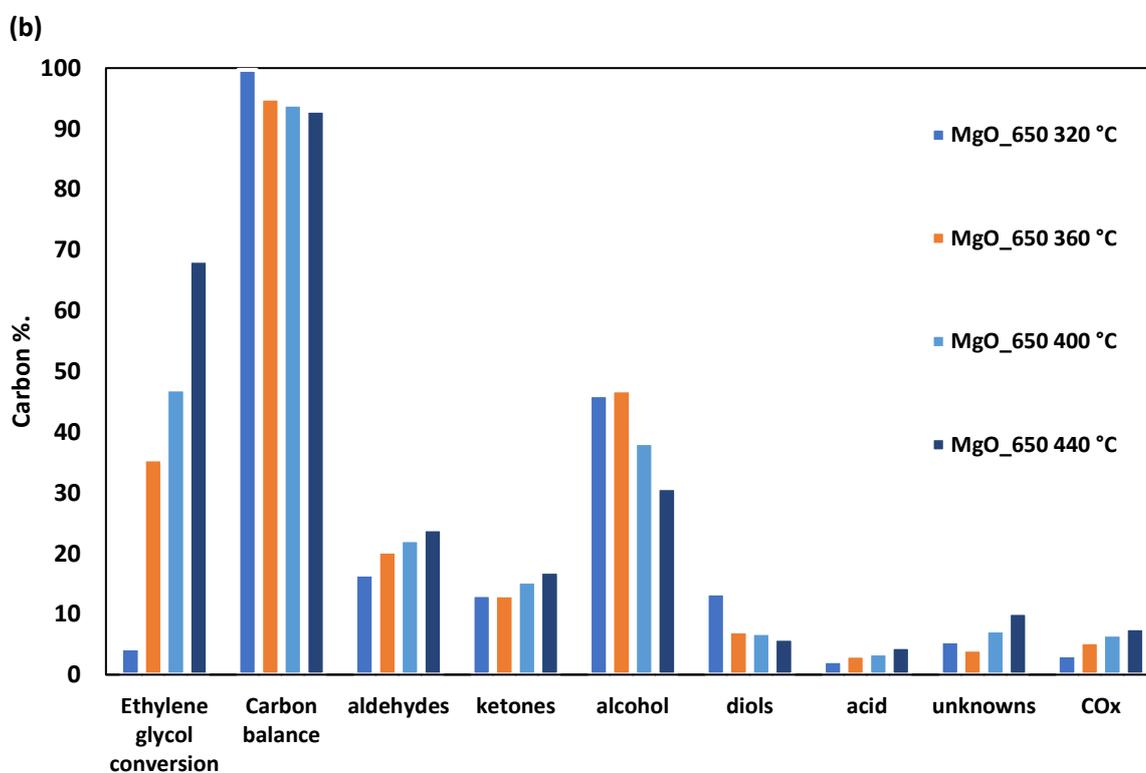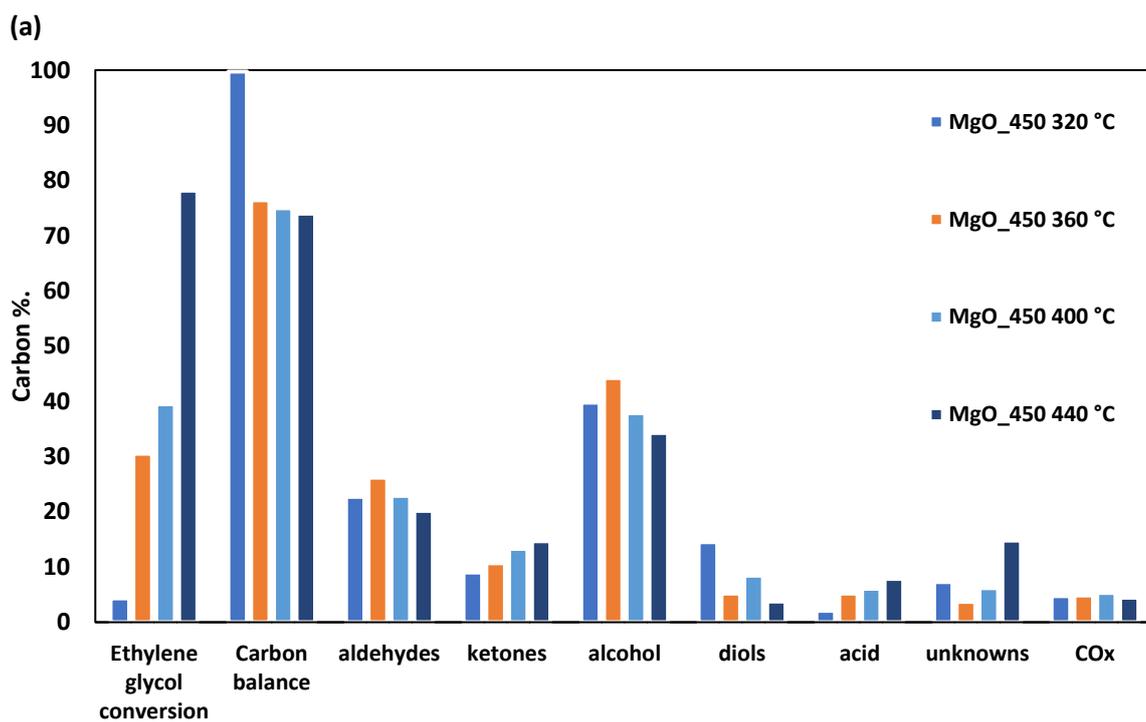
Figure 7. Ethylene glycol reactions over MgO_450 (a) and MgO_650 (b). Reaction conditions: 50 wt.% ethylene glycol in water, 320 °C - 440 °C with 0.5 g catalyst. 0.1 mL min^{-1} 15 mins, 0.016 mL min^{-1} 2 hours, 0.016 mL min^{-1} 3 hours collect. 50 mL min^{-1} Ar flow.

4.2.2.2 Conversion

The conversion of ethylene glycol achieved could not be correlated to either the basicity of the catalysts, or the surface area. (Figure 8) MgO_450 shows the lowest conversion of 31 % at 360 °C this increases to 40 % at 400 °C. MgO_650 shows 36 % at 360 °C increasing to 47 % at 400 °C. MgO_750 exhibits a low conversion of 22.7 %, at 360 °C but results in the highest conversion at 400 °C of 51 %. It seems that for the conversion of ethylene glycol, the surface area and basic site concentration are not the most important factors due to no clear trend. The characteristic which promotes this behaviour is however unclear.
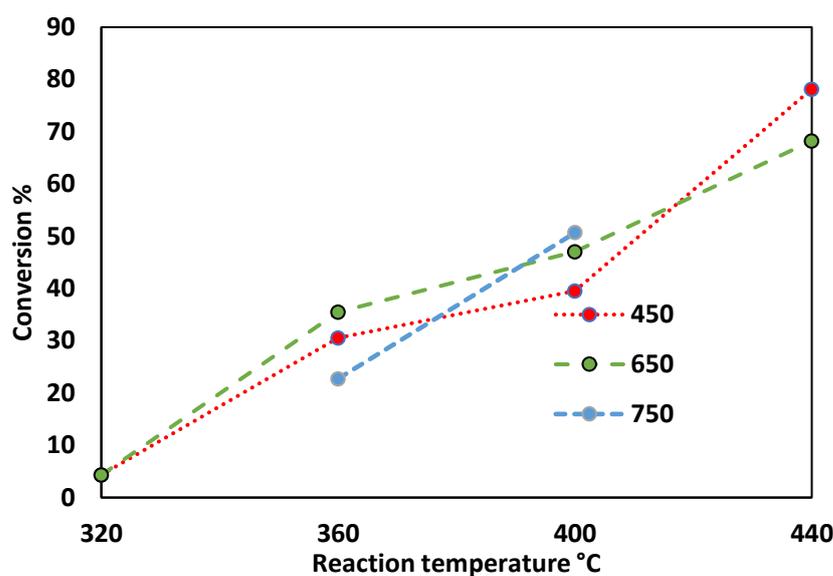
Figure 8. Ethylene glycol reactions over MgO_450 (red), MgO_650 (green) and MgO_750 (blue) – Conversion to reaction temperature - Reaction conditions: 50 wt.% ethylene glycol in water, 320 °C - 440 °C with 0.5 g catalyst. 0.1 mL min^{-1} 15 mins, 0.016 mL min^{-1} 2 hours, 0.016 mL min^{-1} 3 hours collect. 50 mL min^{-1} Ar flow.

4.2.2.3 CMB

At the low temperature of 320 °C the samples exhibit a high CMB in excess of 99 % (Figure 9). This decreases steadily as the reaction temperature, and consequently, ethylene glycol conversion, increases. MgO_450 exhibits a large decrease in CMB to 76 % followed by a gradual decrease beyond this temperature. MgO_650 on the other hand decreases more steadily, with only a drop of almost 5 % to 95 % initially, followed by a similar gradual decrease at further temperature increases. The initial larger drop in CMB on increasing the temperature from 320 °C to 360 °C is likely caused by the large jump in conversion seen in tandem. Interestingly while the conversion increases significantly with higher reaction temperature only small drops in CMB are observed.

167
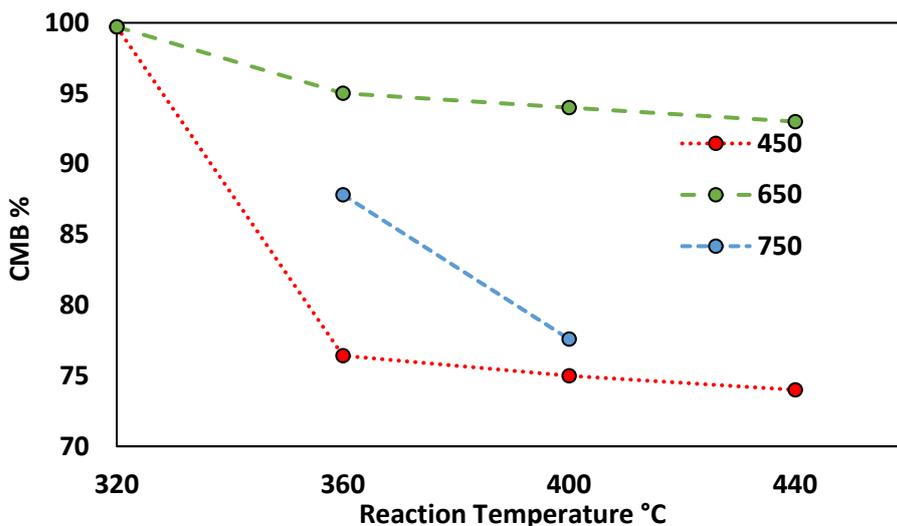
Figure 9. Ethylene glycol reactions MgO_450 (red), MgO_650 (green) and MgO_750 (blue) – CMB to reaction temperature- Reaction conditions: 50 wt.% ethylene glycol in water, 320 °C - 440 °C with 0.5 g catalyst. 0.1 mL min⁻¹ 15 mins, 0.016 mL min⁻¹ 2 hours, 0.016 mL min⁻¹ 3 hours collect. 50 mL min⁻¹ Ar flow.

4.2.2.4 Hydroxyacetone selectivity

A notable result was that hydroxyacetone was observed as a major product. However, hydroxyacetone is a C3 molecule, with the substrate, ethylene glycol, a C2 molecule. MgO under these conditions, seems to be catalysing C-C bond formation between products in the reactant effluent. There are examples of MgO catalysts promoting C-C bond formation in the literature, especially in the area of oxidative methane coupling where Li/MgO based catalysts are known to be one of the most investigated for this reaction.[37–40] Another examples of MgO promoting this type of reaction includes transition metal cation activated MgO, which have been used for selective catalytic C-C bond formation with methanol as a methylenating agent to produce vinyl groups from saturated ketones esters and nitriles.[41] Hydroxyacetone also occurs from ethylene glycol under the catalyst free conditions at a low selectivity of 6.4 %, indicating this can occur to an extent without MgO.

Hydroxyacetone is seen in relatively high selectivity under most conditions. The production *via* ethylene glycol, accompanied by the dehydration of glycerol and the catalyst's low ability to convert it help explain hydroxyacetone ubiquitous presence in glycerol feed reactions. However, this behaviour is not wholly unprecedented over MgO. As shown in previous chapters, products such as cyclopentanone (C5) and phenol (C6) are also produced over MgO from glycerol. It is also expected

that HWMP form through condensation reactions occur.[2] LCMS and CHN analysis has helped support this assumption. (Section 3.3.1.3)

Hydroxyacetone selectivity tends to trend upwards as the reaction temperature and conversion increases (Figure 10). The increase of selectivity is only marginal though and does not correspond with the large jumps in conversion. MgO_650, interestingly results in a higher selectivity across the experiments to hydroxyacetone than the other samples. It exhibits; 12.4 % at 320 °C which stays stable on increase to 360 °C – selectivity then increases to 14.1 % to and 15.6 % when reaching 400 °C and 440 °C respectively. MgO_450 exhibits a similar trend but with a consistently lower selectivity to hydroxyacetone. 8.4 % selectivity is witnessed at 320 °C increasing to 10.1 %, 12.4 % and 13.2 % as the temperature increases to 360 °C, 400 °C and 440 °C respectively. MgO_750 shows as sharper jump of 9.5 % to 13.8 % on increasing the temperature from 360 °C to 400 °C, this is in conjunction to a steeper jump in conversion than seen with the other samples. Hydroxyacetone selectivity is correlated to the conversion with it generally increasing in tandem. MgO_650 is not necessarily more selective for hydroxyacetone production. Once hydroxyacetone is formed on MgO_650 it seems to remain relatively stable. This is indicated by its ubiquitous presence and MgO_650's very low rate of conversion when hydroxyacetone is used as a substrate molecule (section 4.2.1).
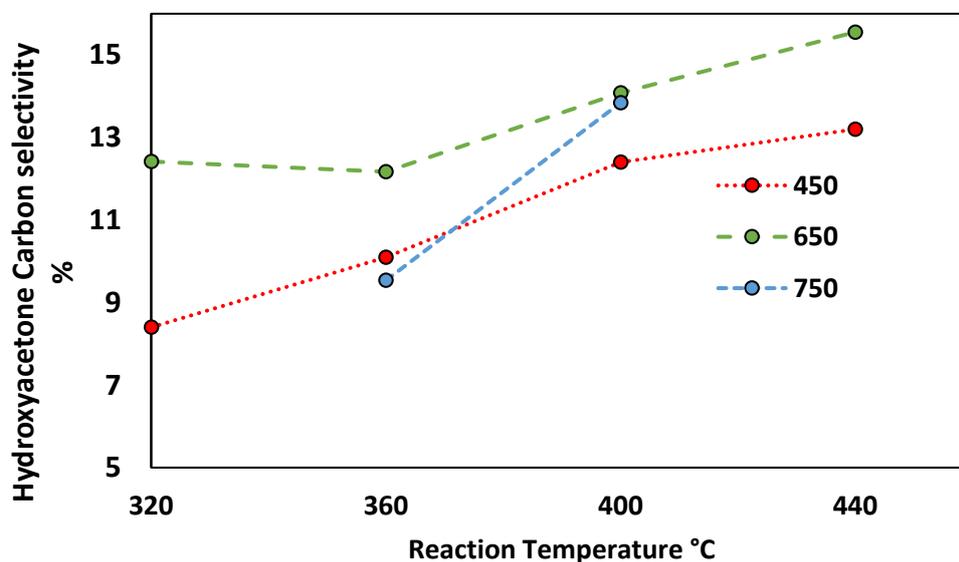
Figure 10. Ethylene glycol reactions over MgO_450 (red), MgO_650 (green) and MgO_750 (blue) – Hydroxyacetone carbon selectivity % - Reaction conditions: 50 wt.% ethylene glycol in water, 320 °C- 440 °C with 0.5 g catalyst. 0.1 mL min^{-1} 15 mins, 0.016 mL min^{-1} 2 hours, 0.016 mL min^{-1} 3 hours collect. 50 mL min^{-1} Ar flow.

4.2.2.5 Ethanol selectivity

Unlike the reactions performed with glycerol whereby a low selectivity to ethanol (< 1 %) was observed, when using ethylene glycol, it is a major product, accounting for between 14.6 % to 31.1 %. It is also not seen in the hydroxyacetone feed experiments, it seems to be sourced primarily from the ethylene glycol route under these conditions. The direct conversion of ethylene glycol to ethanol could involve a hydrogenolysis reaction, which would require a source of hydrogen. H_2 could possibly be sourced *in-situ* from aqueous phase reforming,[21,23] or methanol decomposition.[42,43] The route to ethanol proposed in the previous work would see it sourced from the acetaldehyde radical *via* a reduction (Figure 11).[1,2] However we do not see a significant selectivity to ethanol in hydroxyacetone or glycerol feed experiments, indicating that something else is responsible for the selectivity to ethanol from ethylene glycol.
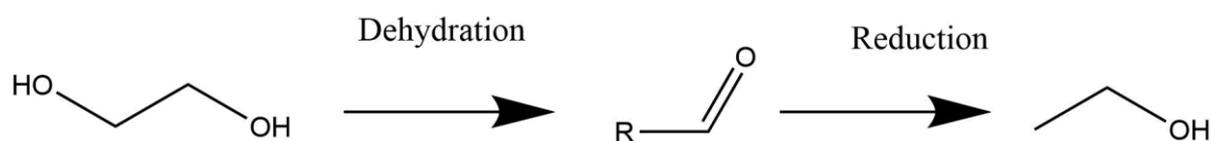
Figure 11. Reaction pathway -ethylene glycol to ethanol

It is possible that when ethylene glycol is used in high concentration as seen here, the most competitive route is the hydrogenolysis reaction to ethanol leading to the high selectivity. When glycerol is used it seem this reaction becomes uncompetitive with almost no ethanol produced, the hydrogen is likely to be used elsewhere.

The experiments using intermediates from the conversion of glycerol as the feedstock substrate were performed to try and isolate and gain better insight into individual pathways. However, it is important to note that it is fundamentally changing the reaction product stream. Products that are obtained only from glycerol, are mostly removed from the equation. This means that the chemistry and interactions between species sourced from those pathways are mostly absent. This evidently results in significantly different changes in product selectivity as other unexpected pathways are now more favourable. This is likely important for understanding the unexpected results such as the ethanol abundance.

Shown in Figure 12, MgO_450 starts with a selectivity of 21.3 % to ethanol at 320 °C, this increases to 31.1 % at 360 °C before decreasing to 23.8 % and 16.2 % at the higher temperatures of 400 °C and 440 °C. MgO_650 shows a more linear trend with the highest selectivity to ethanol obtained at 320 °C of 25.9 % which subsequently decreases to 24.5 %, 18.7 % and 14.6 % at 360, 400 and 440 °C respectively. Inversely MgO_750 sees a slight increase in selectivity to ethanol from 17.4 % to 22.2 % in the increase from 360 °C to 400 °C. Conversion did not directly correlate with ethanol

selectivity, for MgO_450 it exhibited a volcano distribution with selectivity peaking at 30 % conversion and then decreasing, while MgO_650 generally decreased with increasing conversion and MgO_750 increasing. The reactions at 320 °C and 360 °C are the most comparable for MgO_450 and MgO_650 with relatively close conversions. At approximately 4 % conversion MgO_650 exhibits more ethanol, but at 30 – 35 % conversion the samples perform very similarly.

With MgO_450 and MgO_650 there is tendency for a reduction of ethanol selectivity in the favour of other products when increasing the temperature. In the environment of high temperatures, a larger mix of products and higher conversion results with less ethylene glycol present, this is closer to the reaction conditions seen with glycerol. So, interactions between the products may be more favourable resulting in less hydrogen available for ethanol production.
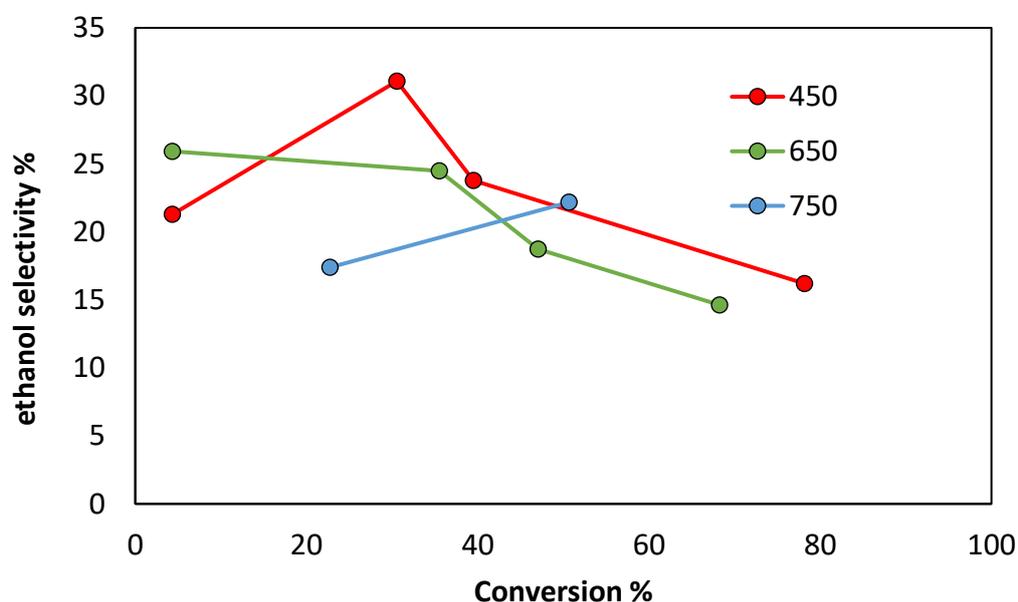
Figure 12. Ethylene glycol reactions over MgO_450 (red), MgO_650 (green) and MgO_750 (blue) – ethanol selectivity % - Reaction conditions: 50 wt.% ethylene glycol in water, 320 °C- 440 °C with 0.5 g catalyst. 0.1 mL min⁻¹ 15 mins, 0.016 mL min⁻¹ 2 hours, 0.016 mL min⁻¹ 3 hours collect. 50 mL min⁻¹ Ar flow.

4.2.2.6 Acetaldehyde selectivity

Acetaldehyde selectivity is thought to be important, as previously discussed it is suspected to self-condense and is a major product over MgO in most situations. MgO_650 shows a gradual increase with temperature proceeding from a selectivity of 16.5 %, 20.1 %, 21.2 % and 22.7 % to acetaldehyde over temperatures of 320 °C, 360 °C, 400 °C and 440 °C respectively. Of course, the conversion is increasing so the yield is increasing proportionally. Ethylene glycol can lose water to form acetaldehyde through a dehydration reaction.

MgO_450 in contrast does not show a clear trend with the temperature of reaction. In a similar way to its ethanol selectivity, on increasing from 320 °C, 360 °C, 400 °C and 440 °C the selectivity to acetaldehyde changes from 22.7 %, 25.6 %, 22.4 % and down to 18.4 % respectively. This may be due to the condensation of acetaldehyde. Theoretically changes in acetaldehyde selectivity may be masked by conversion of produced acetaldehyde by aforementioned condensation reactions. The increase in temperature may produce more acetaldehyde over MgO_450, which allows for a higher degree of condensation reactions occurring. This could result in lower observed selectivity to acetaldehyde as it is removed from the stream. There is no evidence for this as of yet, but acetaldehyde over the catalysts is explored in section 4.4.3.

At 360 °C MgO_750 has a very high selectivity to acetaldehyde of 37.2 %, but only a low conversion of ethylene glycol of 22.7%. On increasing the temperature to 400 °C this decreases significantly to 20.4 % with an accompanied conversion increase and CMB drop. This may also indicate that at these higher temperatures more of the acetaldehyde is forming HWMP in conjunction with preferential selectivity to products such as methanol and hydroxyacetone.

4.2.2.7 Acetic acid selectivity

Acetic acid increases in selectivity with increases in reaction temperature, this is expected as takes several stages to reach and is seen as a terminal product. Conversion and temperature increasing results in an increase in acetic acid selectivity with an individual catalyst. However, there is overlapping effects of catalyst and conversion, for example MgO_450 is the most selective even with it being the generally least active for ethylene glycol conversion. As ethylene glycol converts to glycolaldehyde and then dehydrates to ketene, this can react further with the addition of water to give acetic acid.

4.2.2.8 1,2-propanediol selectivity

The previously established mechanical route to 1,2-propanediol is the reduction of hydroxyacetone. A relatively high selectivity is seen here with ethylene glycol, especially when compared to the hydroxyacetone feed experiments. However, conversions are significantly different. 1,2-propanediol, like hydroxyacetone was originally unexpected to be sourced from the ethylene glycol pathway. But like discussed for hydroxyacetone it may be formed through a C-C coupling reaction. There is possibly an interaction between the relative selectivity of these two products. It is not yet determined how hydroxyacetone or 1,2-propanediol are produced from the conversion of ethylene glycol. 1,2-propanediol could be produced from the hydrogenation to hydroxyacetone, or conversely hydroxyacetone from the dehydrogenation of 1,2-propanediol. They may both be produced simultaneously and interconvert.

The relatively high selectivity to 1,2-propanediol compared to hydroxyacetone may imply hydroxyacetone converts more easily than we thought from other results, or that there is an alternative route to 1,2-propanediol. The dehydration product of 1,2-propanediol, acetone is only seen in negligible amounts as with other reactions. As hydroxyacetone increases in selectivity as the temperature increases, 1,2-propanediol decreases its selectivity share, this indicates that 1,2-propanediol may be the source to convert to hydroxyacetone (Figure 13). Interestingly 1,2-propanediol is a major product in the catalyst free reaction at 4 % conversion and 29.1 % selectivity indicating that MgO directs other pathways preferentially.
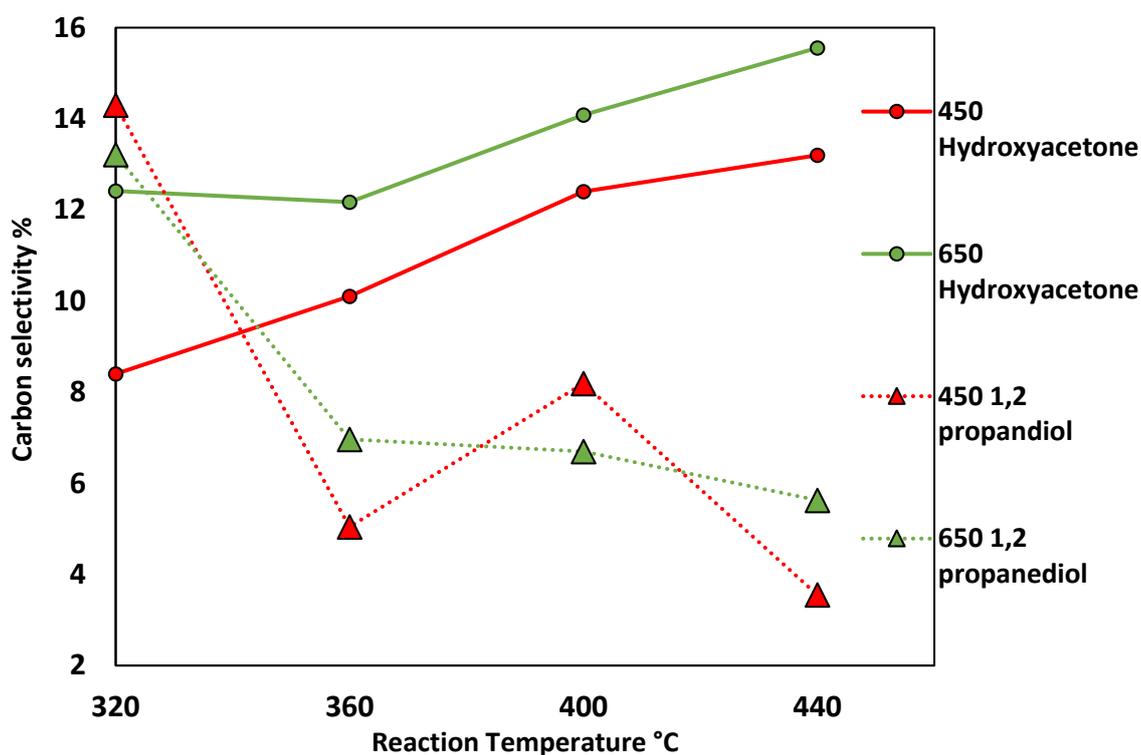
Figure 13. Ethylene glycol reactions over MgO_450 (red), MgO_650 (green) – Hydroxyacetone (circles) and 1,2-propanediol (triangles) selectivity - Reaction conditions: 50 wt.% ethylene glycol in water, 320 °C-440 °C with MgO_450/650 0.5 g catalyst. 0.1 mL min^{-1} 15 mins, 0.016 mL min^{-1} 2 hours, 0.016 mL min^{-1} 3 hours collect. 50 mL min^{-1} Ar flow.

4.2.2.9 Methanol selectivity

The selectivity to methanol changes over reaction temperature for each catalyst. With MgO_450, it sees a general upwards trend as the temperature increases. 9.5 % at 320 °C, 11.6 % at 360 °C, selectivity doesn't significantly change at 400 °C, but conversion increases resulting in a higher yield. Selectivity to methanol peaks at 440 °C for MgO_450 at 14.2 %. The STY of methanol increases

steadily as the conversion and selectivity increase with temperature for MgO_450. 4 to 9 g h^{-1} kg^{-1}, followed by 28 and 115 g h^{-1} kg^{-1} at 320 – 440 °C.

Selectivity to methanol for MgO_650 is 14.7 % at 320 °C increasing to 18.5 % at 360 °C, followed by a decrease to 14.4 % and 11.8 % at 400 °C and 440 °C respectively. A similar situation is seen with glycerol methanol selectivity at higher temperatures (chapter 3). This is accompanied by the significant jumps in conversion. With MgO_650, we see a higher selectivity to methanol, a higher conversion, and a higher CMB at reaction temperatures of 320 °C to 400 °C. These factors lead to a higher STY to methanol at these temperatures than with MgO_450. However, at 440 °C the conversion and selectivity to methanol is higher with MgO_450. This results in a significantly lower STY over MgO_650 at 440 °C of 86 g h^{-1} kg^{-1} compared with 115 g h^{-1} kg^{-1}, despite the noticeably higher CMB over MgO_650.

At 360 °C and 36 % conversion the increase in thermal energy results in a higher yield of methanol. However, when using higher temperatures, the competition from increases in acetaldehyde, hydroxyacetone, unknowns and 1,2-propanediol selectivity leads to a decrease in the selectivity of methanol obtained. However as with MgO_450, the increases in conversion result in significant increases in the STY of methanol. With 10, 38, 72 and 86 g h^{-1} kg^{-1} obtained at the increasing temperatures. MgO_750 shows an increase in selectivity with the increase of temperature of 360 °C to 400 °C and 22.7 to 50.7 % conversion. The selectivity increases from 9.5 % to 14.3 % methanol, which corresponds to a significant jump in STY due to the increase in conversion. Despite the drop in CMB the STY increases from 14 to 57 g h^{-1} kg^{-1}. This is lower than the other catalysts due to the difference in conversion and CMB.

These results show a similar methanol selectivity to that which is seen with the pure glycerol feed. At first this would indicate this may not be the dominant pathway, but when reacting glycerol, an ethylene glycol radical and a methanol radical form first before ethylene glycol. This ethylene glycol radical is likely to be more reactive than ethylene glycol and possibly produced in greater amounts from glycerol. Of course, as mentioned, only one molecule of methanol is expected to be obtained from ethylene glycol, while with glycerol as a source one could result from the radical produced in the C-C cleavage of glycerol. The radical ethylene glycol molecule itself may result in chemistry not seen represented in the results and it is not determined yet exactly how MgO activates ethylene glycol. The formation of glycolaldehyde from the ethylene glycol radical and its subsequent radical cleavage may be more preferential under glycerol reaction conditions.

4.2.2.10 Unknowns' selectivity

The observed selectivity to detected unknown products changes with the reaction temperature (Figure 14). At the low temperature of 320 °C a low selectivity to unknowns of 7.3 % and 5.5 % for MgO_450 and MgO_650 respectively is present. This decreases marginally to 3.7 % and 4.1 % at 360 °C for MgO_450 and MgO_650. On increasing to higher temperatures, MgO_450 increases to 6.2 % at 400 °C and then more than doubles to 14.8 % at 440 °C. MgO_650 also increases significantly first to 7.3 % at 400 °C and then to 10.2 % at 440 °C. As shown at both high and low temperature MgO_450 presents more unknowns, while at middling temperatures MgO_650 produces a higher proportion. This may be due to the type of unknowns changing throughout the reaction temperatures. A relatively high selectivity is seen at low temperatures, as with other reactions as they are likely intermediary species due to the low conversion and thermal energy.

Increasing the temperature pushes these further along the reaction scheme, shifting the selectivity to identified products, especially species that are thought of as being relatively stable. However, on further increases of temperature it seems that this promotes the formation of more unknowns, possibly the precursor to undetectable heavier species. Some evidence of this is seen in the chromatograms, whereas the temperature increases the number of unidentified peaks also increases for both catalysts, with some major ones forming in the mid to late parts of the run (Appendix Table 2).
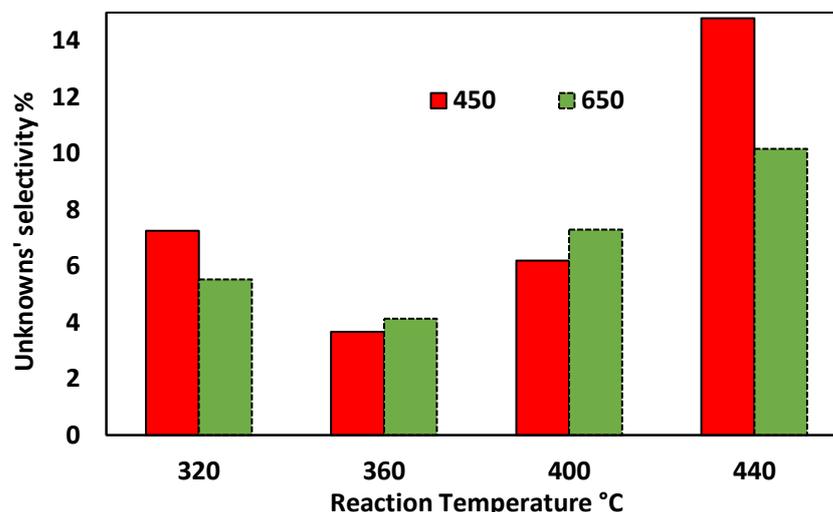
Figure 14. **Ethylene glycol reactions over MgO_450 (red) and MgO_650 (green) Unknown selectivity % - Reaction conditions: 50 wt.% ethylene glycol in water, 320 °C - 40 °C with MgO_450/650 0.5 g catalyst. 0.1 mL min^{-1} 15 mins, 0.016 mL min^{-1} 2 hours, 0.016 mL min^{-1} 3 hours collect. 50 mL min^{-1} Ar flow.**

However, the CMB does stay relatively stable for MgO_450 at temperatures above 320 °C after the initial drop off. MgO_750 only shows a minor change in selectivity to unknowns between 360 °C and 400 °C. of 8.9 to 9.2 %, likely as with other samples further temperature reactions would have to be explored to see more distinct changes.

4.2.2.11 COx Selectivity

Both catalysts see an increase in CO selectivity up to a 400 °C followed by a decrease at 440 °C. The yield stays relatively stable overall. MgO_450 sees 1.6 % increasing to 2.0 % and 2.3 % with a large dip to 0.4 % at 440 °C. MgO_650 exhibits a similar trend with 1.0 %, 2.1 %, 3.1, and 0.7 %. This is accompanied with a general trend upwards for CO_2 selectivity. Increasing from 3.2 %, 2.81 % to 4.0 % with MgO_450 and 2.1 %, 2.7 %, 3.5 % and 7.0 % with MgO_650.

The ethylene glycol reactions have yielded several important results, but it is not clear still if it is a major pathway to methanol. It seems to be more prevalent the hydroxyacetone but there are possibly other pathways. The results of high selectivity to ethanol indicate that the reaction over glycerol has interactions between the different identified pathways and trying to isolate these removes some of the chemistry resulting in results not aligning with the glycerol experimentation.

4.3.1   4.3 Co-feeding experiments.

4.3.2   Ethylene glycol / glycerol co-feed

Experiments with ethylene glycol (4.2.2) produce a higher selectivity and yield to methanol than reactions using hydroxyacetone as a substrate. However, the chemistry was altered and resulted in high selectivity to products not observed in the glycerol experiments such as ethanol. This indicated that the experiment was not representative of the chemistry of ethylene glycol under glycerol reaction conditions. To try and account for this, cofeeding experiments involving the addition of ethylene glycol to the substrate feed were conducted. This was to investigate the effect of increasing ethylene glycol partial pressure in the presence of glycerol and its reactants. Increasing the ethylene glycol pressure was expected to result in an increase in the concentration of hydroxymethyl radical moieties. These can be obtained from glycolaldehyde undergoing the Norrish type-1 like fragmentation (Appendix Section 6.1). It was expected that this may result in a higher yield of methanol. The transformation of the radical species to methanol also requires a source of hydrogen which itself could possibly be sourced from ethylene glycol.

Reactions were performed at 400 °C with 45 wt.% glycerol with 5 wt. % ethylene glycol. The results are shown in Table 6. Ethylene glycol addition resulted in a slightly higher conversion (99 %) than observed with MgO_650 over that seen with just glycerol (96 %) at 400 °C. This is likely due to the slight decrease in original glycerol concentration, with slightly less fed in, a higher proportion of it

is converted. There is overall however a slight decrease in catalyst activity 0.95 g h^{-1} g cat^{-1} to 1.03 g h^{-1} g cat^{-1} glycerol converted.

Extra ethanol was not made with the addition of 5 wt.% ethylene glycol (< 1 %). The ethanol selectivity seen is analogous to the pure glycerol experiments. Competing reaction routes for any abstracted hydrogen may result in uncompetitive hydrogenolysis of ethylene glycol to ethanol unless the feed is predominantly ethylene glycol. An experiment was performed using 25 wt.%/25 wt.% Ethylene glycol/ glycerol which only saw 1.55 % ethanol (appendix Table 3).

The two catalysts used for this reaction showed several principal differences. MgO_650 – like in the previous pure ethylene glycol experiments exhibits as higher conversion of ethylene glycol. The summation of both the ethylene glycol produced in the conversion of glycerol and unconverted feedstock amounted to less moles than was fed into the reaction. The amount of ethylene glycol seen in the product stream amounted 68 % of that fed in. MgO_450 showed an opposite effect, it was significantly less active for the conversion of the fed in ethylene glycol, resulted in a higher concentration than the feedstock. It seems that MgO_450 may produce enough ethylene glycol from the glycerol to counteract the catalyst ability to convert both the fed in and produced ethylene glycol. This resulted in 151 % of the starting concentration in the collection. This further shows that the basicity and surface area are not the integral parameter for the conversion of the intermediate ethylene glycol into further products.

There is a slight increase in observed acetaldehyde selectivity on the addition, increasing to 26.6 % from 23.5 % with MgO_650. Methanol however remains unchanged at 13-14 %. When presented with 5 wt.% ethylene glycol, the route through to acetaldehyde, which can proceed via a hydride shift and dehydration or a catalysed reaction through an intermediate enol, appears more dominant.[44] The route to further methanol after the initial cleavage of glycerol proceeds through the intermediate glycolaldehyde and then a radical fragmentation to the hydroxymethyl precursor, the lack of increase in methanol selectivity shows that this reaction pathway does not become more preferential on increasing the concentration of ethylene glycol. An excess of these ethylene glycol derived substrates may override the catalysts usually low activity for condensation routes. MgO_450 may not see this subsequent reduction of its CMB due to hydroxyacetone and acetaldehyde proportionally having a lower concentration.

Table 6. Ethylene glycol and glycerol cofeed reaction over MgO_450 and MgO_650 - Product selectivity - Reaction conditions: MgO_450 – MgO_650, 45 % Glycerol - 5 % EG, MgO_650 50 % glycerol 400 °C, 50 mL min⁻¹ Ar, 0.1 mL min⁻¹ 15 mins, 0.016 mL min⁻¹ after. 3 hours.

Carbon mole selectivity %	MgO_450 400°C EG cofeed 5 % EG - 45 % glycerol	MgO_650 400 °C EG cofeed 5 % EG - 45 % glycerol	MgO_450 400°C 50 % glycerol	MgO_650 400°C 50 % glycerol
acetaldehyde	20.5	26.6	25.3	23.5
propionaldehyde	0.7	0.8	3.0	1.0
acetone	0.1	0.1	0.6	0.2
acrolein	12.2	12.3	12.4	12.6
butyraldehyde	0.0	0.0	0.1	0.0
methanol	10.4	14.1	9.8	13.4
2-propanol	0.0	0.0	0.1	0.0
ethanol	0.7	0.9	0.9	0.9
2,3-butanedione	1.2	1.4	2.2	1.7
1-propanol	0.1	0.1	0.3	0.1
3-hexanone	0.1	0.2	0.3	0.2
allyl alcohol	0.8	1.0	1.1	1.0
cyclopentanone	0.4	0.6	0.6	0.7
hydroxyacetone	18.5	17.1	17.2	20.8
3-ethoxy-1-propanol	0.0	1.1	0.3	1.1
acetic acid	1.7	0.8	1.8	1.6
Glycidol	0.5	0.6	0.5	0.7
propionic acid	0.7	0.7	1.3	1.2
1,2-propanediol	2.3	1.5	0.9	2.0
unknown(s)	5.3	3.8	6.6	6.1
ethylene glycol	n.a	n.a	7.0	6.4
1,3-propanediol	0.7	0.5	0.9	0.5
phenol	0.1	0.0	0.0	0.1
CO	2.3	3.4	3.6	2.8
CO_2	2.5	3.0	3.2	1.6
glycerol conversion %	92	99	99.7	96
Ethylene glycol conversion %	32	- 49	n.a	n.a
CMB %	88	89	84	91
Methanol STY g h⁻¹ kg h⁻¹	98	118	116	122

This cofeeding experiment was performed to tie in with computational modelling undertaken by the computational side of the research group, where they explored the final stage of the glycerol reaction over the MgO catalysts. Sainna *et al*, used DFT and QM/MM techniques were used to model the radical mechanism of the catalytic production of methanol from glycerol.[3] The various calculated results are shown in Table 7, Table 8 and Table 9. The study primarily focussed on deducing what would be the most likely mechanism of the formation of methanol from its precursor. This precursor is the radical hydroxymethyl species which can result through several pathways. First glycerol can undergo a C-C cleavage resulting in an ethylene glycol radical and the hydroxymethyl species. The intermediates; hydroxyacetone and glycolaldehyde can also undergo a fragmentation *via* a C-C bond cleavage between the α-carbon and the carbonyl group of the

molecule.[19,20] This yields the methanol precursor and an acetyl radical from hydroxyacetone and the methanol precursor and a formyl radical *via* glycolaldehyde. It has been theorised that the hydroxy methyl radical can abstract a H atom from another species to produce a methanol molecule such as in Figure 15. In the reaction environment atmospheric H_2 should only be present in negligible amounts as the reaction is carried out in an argon flow.
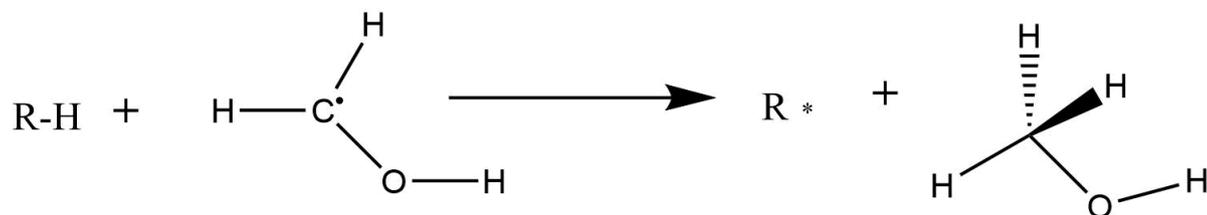
Figure 15. **Hydrogen transfer to produce methanol from a hydroxymethyl radical reproduced from M. A. Sainna, S. Nanavati, C. Black, L. Smith, K. Mugford, H. Jenkins, M. Douthwaite, N. F. Dummer, C. R. A. Catlow, G. J. Hutchings, S. H. Taylor, A. J. Logsdail and D. J. Willock, Faraday Discuss., 2020, 34, 240–241.**

Water makes up for 50 wt.% of the reactor feed, so it was investigated as a hydrogen source. This was done by modelling a lone single water molecules non-dissociative adsorption on the MgO (100) surface. Idealised (100) MgO planes were used for simplicity. This is as they are described as the most common, stable, and characterised exposed termination plane for MgO and alkaline earth oxides in general. [45,46] Thermal decomposition of $Mg(OH)_2$ is shown to yield these planes.[47] This makes it likely that (100) planes are prevalent on the MgO samples prepared for this thesis.

The interactions between the magnesium 5 coordinate (Mg_{5c}) cation and the oxygen coordinate (O_{5c}) anions with the H atoms of water can result in adsorption. When water is co-adsorbed with a dissociated hydroxymethyl radical it gives an energy of adsorption of water of -89 kJ mol^{-1}.[3] When in proximity with the hydroxymethyl radical, bonding of water coordinates through the O of H_2O to the Mg_{5C} site. The cost of the H proceeding to the radical anion is 108 kJ mol^{-1}, resulting in a methoxy anion precursor to methanol. These values were deemed not particularly favourable, water was found to be an energetically unlikely source of the hydrogen in this stage of the reaction. This was backed up with the low glycerol conversion data for MgO (thesis section 3.3.2) in which exhibited a hydrogen balance of 100.6 % from the data. This calculation did not include the diluent water in the final products, this indicated hydrogen from water was not involved in the radical mechanism.

Table 7. Adsorption energies for key molecules on MgO(100) comparing periodic and QM/MM approaches. Data reproduced from M. A. Sainna, S. Nanavati, C. Black, L. Smith, K. Mugford, H. Jenkins, M. Douthwaite, N. F. Dummer, C. R. A. Catlow, G. J. Hutchings, S. H. Taylor, A. J. Logsdail and D. J. Willock, Faraday Discuss., 2020, 34, 240–241.

Molecule	PBEsol (periodic)/kJ mol^{-1}	PBEsol+D3 (periodic)/kJ mol^{-1}	PBEsol (QM/MM)/kJ mol^{-1}	PBE0 (QM/MM)/kJ mol^{-1}
Water	−60	−82	−65	−59
Methanol	−61	−93	−60	−52
$^{\cdot}CH_2OH$	−32	−59	—	—
$^{\cdot}CH_2O^{-}\cdots H^{+}$	−73	−105	−81	−57
Ethylene glycol 1[a]	−61	−109	−65	−45
Ethylene glycol 2[b]	−90	−136	−89	−63

a Ethylene glycol with an OH group interacting with the surface. b Ethylene glycol in a conformation with both OH groups interacting with the surface. In both cases the same gas phase reference conformation is used for calculation of the adsorption energy.

Table 8. Calculated bond dissociation energies for various reactant species (Labels in Figure 16). Data reproduced from M. A. Sainna, S. Nanavati, C. Black, L. Smith, K. Mugford, H. Jenkins, M. Douthwaite, N. F. Dummer, C. R. A. Catlow, G. J. Hutchings, S. H. Taylor, A. J. Logsdail and D. J. Willock, Faraday Discuss., 2020, 34, 240–241.

Molecule/ bond	BDE PBEsol kJ mol^{-1}	BDE PBE0 kJ mol^{-1}	BDE PBE0/PBEsol kJ mol^{-1}	D_{298} expt. kJ mol^{-1}
Glycerol C_1O-H	456	447	455	
Glycerol C_2O-H	443	460	462	
Glycerol C_1-H	418	409	410	
Glycerol C_2-H	405	404	401	
Hydroxyacetone C_1O-H	477	474	477	
Hydroxyacetone C_1-H	339	339	341	
Hydroxyacetone C_2-H	426	415	416	
Ethylene glycol O-H	462	444	445	
Ethylene glycol C-H	413	409	408	
Methanol C-H	426	414	414	402
Methanol O-H	467	447	447	438
*CH_2O-H	163	161	161	126
Water HO-H	563	508	508	497
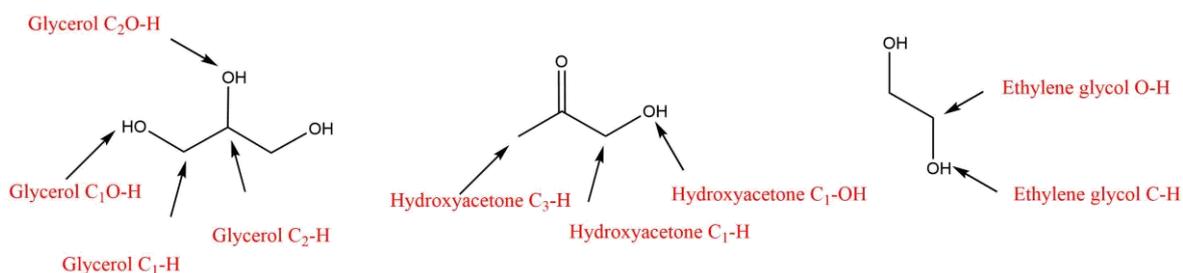
Figure 16. Labelled molecules in relation to Table 8.

Table 9. Calculated H-transfer energies for the various H sources, to form CH$_3$OH(ads) from $^{\cdot}$CH$_2$O$^-$(ads) on MgO steps. Data reproduced from M. A. Sainna, S. Nanavati, C. Black, L. Smith, K. Mugford, H. Jenkins, M. Douthwaite, N. F. Dummer, C. R. A. Catlow, G. J. Hutchings, S. H. Taylor, A. J. Logsdail and D. J. Willock, Faraday Discuss., 2020, 34, 240–241.

Molecule/bond	PBEsol+D3 (periodic)/kJ mol^{-1}	PBE0 (QM/MM)/kJ mol^{-1}	ΔBDE, PBE0 (QM)/kJ mol^{-1}
Water HO–H	105	89	94
E-glycol[a] C–H	—	19	−4
E-glycol[b] C–H	−23	−63	−4
CH$_2$O–H	−223	−192	−254
a End point with neutral ethylene glycol radical. b End point with deprotonation of ethylene glycol radical.			

With water ruled out, how favourably glycerol, hydroxyacetone and ethylene glycol would dissociate on MgO was investigated. The dissociation energies for the X-H cleavage step for were calculated in isolation to the catalysts surface (Table 8). Using PBEsol at BPE0 level the values for C$_2$ and C$_3$ molecules result in significantly energetically favourable values of at nearly 100 kJ mol^{-1} more favourable than the value calculated for water. Using DFT calculations, the lowest energy for the required hydrogen transfer from glycerol was investigated. The abstraction from C$_2$ results in a carbon centred radical 13 kJ mol^{-1} lower than if the same occurred at its C$_1$ site. Thus, a secondary carbon gives a more stable radical than a primary.

Calculations were also performed investigating how methanol adsorbs onto the surface. Methanol interacts with the (100) plane in a way that results in the OH interacting with the O atom at a Mg$_{5c}$ site while the H atom interacts with the basic O$_{5c}$ sites on the surface.[48] It was found that energetically methanol would reform or vaporise rather than stay dissociated upon the MgO (100) surface. Hence it is likely that MgO (100) is not basic enough to heterolytically dissociate methyl from the alcohol group of methanol.[3] Further calculations found that while this was the case for methanol, the energy to abstract a proton from absorbed hydroxymethyl radicals (from the C-C homolytic cleavage of C-C bonds of glycerol or hydroxyacetone) was relatively low and easy for MgO (100) to perform. This led to investigations into a possible disproportionation mechanism.

The bond dissociation energy for the hydroxymethyl alcohol group was found to be low which led to the consideration of a reaction which two -CH$_2$OH moieties combine. They would undergo a disproportionation and result in methanol and formaldehyde, giving a theoretical favourable reaction energy of -254 kJ mol^{-1}. Evidence of formaldehyde formation backs this up. Formaldehyde has not been analytically quantified, but it has been detected in reactions with MgO and glycerol *via* HPLC by using a LpDNPH cartridge to form formaldehyde-DNPH adducts.[3]

This mechanism would proceed *via* the adsorption of two hydroxy methyl radical species, the second which would donate a proton to the surface anion. This results in formaldehyde and a surface methoxy anion, respectively. The mechanism for this process was considered using PBEsol +D3 theory. A dissociated radical on a clean surface followed by a second hydroxymethyl radical both adsorb readily with similar energy, -105 and -107 kJ mol^{-1}, respectively. The H atom is transferred to form a methyl group which immediately takes up another proton from a surface OH group to result in methanol. This reaction is likely to be highly energetically favourable as it indicated a termination of a radical reaction sequence, rather than further radical products with the alternative routes.[3]

The calculations were also performed with QM/MM PBE0 theory. These were generally in accordance with the previous results but with slightly different steps. Water again shows a low reduction in energy on absorption with the radical and proton of -54 compared to -59 kJ mol^{-1} as with a clean surface. With ethylene glycol the adsorption energy was -75 kJ mol^{-1} compared to -63 kJ mol^{-1} with a clean surface. For the disproportionation reaction, the adsorption of a second hydroxymethyl radical is -76 kJ mol^{-1}. Co-adsorption was determined to be more favourable as the energy was 19 kJ mol^{-1} lower than when the second radical adsorbed elsewhere.

When compared to ethylene glycol, the adsorption was only 1 kJ mol^{-1} so only a negligible difference. However, the hydrogen transfer process from the ethylene glycol to the radical, resulting in formation of methanol, led to an energy increase. On the other hand, with the end point of the reaction being a deprotonation of ethylene glycol radical the value was negative, -23 kJ mol^{-1} (periodic), -63 kJ mol^{-1} (QM/MM). The disproportionation H-transfer energies however were significantly more negative at -233 and -192 kJ mol^{-1} respectively showing that this route was still the most energetically favourable route for methanol production.

The data obtained from the cofeeding experiment showed that increasing the pressure of ethylene glycol did not result in a higher yield of methanol. This indicates that ethylene glycol is likely not used for the hydrogen transfer, agreeing with the energy values calculated. Also, while MgO_650 converted much of the extra ethylene glycol, the lack of methanol increase indicates the extra

ethylene glycol did not predominantly proceed to glycolaldehyde and undergo the subsequent fragmentation. Increased conversion of ethylene glycol this way would be expected to result in more hydroxymethyl radicals. These would have been able to undergo disproportionation, yielding a higher degree of methanol and formaldehyde. Formaldehyde is highly reactive as a gas and may be expected to undergo further reaction in our product steam, potentially through condensation reactions with other aldehydes.[49] Due to this high production of formaldehyde may be expected to be evident in a loss of CMB or increase of unknowns. However, with the catalysts a higher CMB and decrease in unknown selectivity was observed with the addition of ethylene glycol. This indicates that there was not an increase in the disproportionation reaction occurring on addition of ethylene glycol.

4.3.3 Acetaldehyde reactions

Acetaldehyde experiments were carried out over MgO_450 and MgO_650. It had been previously hypothesised that acetaldehyde is a significantly undesirable product, which for the purposes of producing methanol for a fuel blend would not be suitable for a mixture due to its high reactivity. It has also been suspected of being linked to condensation reactions leading to reduction of CMB. (Section 3.3) This was due to its expected tendency to undergo bimolecular condensation reactions over the basic sites on MgO's surface. This was expected to result in HWMP which were not detectable *via* our GC analysis method and thus result in a lower CMB and yields for useful products for the reaction. Acetaldehyde is produced in a relatively high selectivity over most of our catalysts, approximately around 20 % depending on the catalyst and reaction conditions, but it is always relatively prevalent. In this experiment a flow of gaseous acetaldehyde in helium was mixed with water and passed over a MgO catalyst at 360 °C. Only a very low concentration of acetaldehyde was used to try and mimic the concentration seen in the 360 °C 50 wt.% glycerol reactions. The main goal was to see if there was a difference between MgO_450 and MgO_650 conversion of acetaldehyde and wherether the CMB dropped with conversion.

4.3.3.1 Conversion and CMB

(Table 10) MgO_450 converts significantly more of the acetaldehyde of 30 % of the feed compared to 1 % MgO_650. It seems that MgO_650 is essentially unreactive for this reaction. Conversion of acetaldehyde results in a corresponding drop in CMB. MgO_450 results in 71% and MgO_650 99 %. This drop in CMB is essentially proportional to the conversion. Very little in the way of detected products are observed.

4.3.3.2 Selectivity

The selectivity to the identified and quantified products results in a different product distribution than seen with other substrates. Very low yields are actually achieved as nearly all carbon from converted acetaldehyde is not observed. So, it must be noted that the high selectivity's are misleading here. For example, methanol is 59.2 % for MgO_450, however this only results in a very low STY of 4.2 g h^{-1} kg^{-1}. MgO_650 shows a much lower selectivity to methanol than MgO_450 at 9.6 %, but due to its almost inactivity only a negligible 0.2 g h^{-1} kg^{-1} of methanol is achieved. MgO_450 achieves high selectivity to ethanol of 22.7 % and 1 – propanol of 6.3 %, compared to none over MgO_650, which exhibits mainly unknown products at 71.8 %.

Table 10. Acetaldehyde feed reaction over MgO_450 and MgO_650 – Product selectivity - Reaction conditions: MgO_450, 50 % H$_2$O – 360 °C, 50 mL min^{-1} Ar, 1 ml min 1000 ppm acetaldehyde in Ar. H$_2$O 0.1 mL min^{-1} 15 mins, 0.016 mL min^{-1} after. 3 hours.

	MgO_450	MgO_650
Methanol	59.2	9.6
Ethanol	22.7	0.0
1-propanol	6.3	0.0
unknown(s)	11.8	71.8
ethylene glycol	0.0	18.6
acetaldehyde conversion	30	1
CMB %	71	99
Methanol STY g h^{-1} kg^{-1}	4	0

4.3.3.3 Conclusion

MgO_450 converts 30 % of the acetaldehyde, this leads to a corresponding decrease in CMB of 30 %. This is thought to be due to it catalysing condensation reactions and leading to products not detected by GC-FID. This means that the product selectivity calculated by GC-FID for MgO_450 only accounts for a small percentage of the overall CMB.

The vast majority of the true selectivity is to undetected unknown products, postulated to be higher weight molecular products originating from self-condensation reactions of acetaldehyde. This shows that MgO_450's loss of CMB in glycerol feed reactions is likely at least partially influenced by the formation of these acetaldehyde sourced condensation products. On the other hand, it seems MgO_650 is unreactive for this process and as such does not make many undetected products resulting in its high CMB. This may help explain MgO_650's repeated high CMBs over a variety of reaction conditions and feed substrates.

4.4 Conclusions and future work

This chapter has explored the gas phase conversion of identified intermediates and products from the conversion of glycerol. Co-feeding experiments were also performed with mixed substrate feed streams. These reactions have been performed over the MgO catalysts produced and characterised in chapter 3 and performed over a range of temperatures from 320 °C to 440 °C. Reactions have been explored using hydroxyacetone as a substrate and ethylene glycol and acetaldehyde. Hydroxyacetone experiments were carried out using either a 50 wt.% or 10 wt.% feedstock diluted by water. Ethylene glycol experiments used 50 wt.% feedstocks. Co-feeding experiments explored 5 wt.% ethylene glycol, 45 wt.% glycerol feeds. Acetaldehyde experiments used 1000 ppm in He cylinders co-fed with water.

4.4.1 Hydroxyacetone

Reactions run with hydroxyacetone yielded only low conversions with the MgO catalysts. Increase of reaction temperature from 320 °C to 400 °C only leads to small increases in conversion of hydroxyacetone with MgO_450, proceeding from 16 % to 33 %. The MgO_650 the catalyst is very lowly active for the conversion of glycerol under each temperature, it exhibits 0 % at 320 °C 1 % at 360 °C and needs at least 400 °C needed for non-negligible hydroxyacetone conversion of 21 %. MgO_750 responds more to increases with temperature from 360 °C where it increases from 18 % to 64 % at 400 °C.

While the selectivity reveals interesting knowledge about the pathway with hydroxyacetone the difference between catalyst samples is mainly attributed to their conversion of the substrate. Selectivity to unknowns is high at low temperatures especially with MgO_450 exhibiting 44.9 % and decreases as the temperature increases. Acetaldehyde is a very dominant product from the conversion of hydroxyacetone reaching 45- 47 % over the catalysts at 400 °C. The propensity to unknowns and acetaldehyde selectivity seems to be more directly affected by temperature than actual conversion, as similar selectivity is seen with MgO_750 at 400 °C to the other catalysts even with more than double the conversion.

Catalyst selectivity is consistently low to methanol under these conditions at less than 2 %, this results in low STY to methanol of less than 10 g h^{-1} kg^{-1}. Under glycerol reaction conditions the methanol yield sourced from hydroxyacetone would be expected to be lower due to hydroxyacetone making up less of the substrate on the catalyst surface. From these results it indicates that the hydroxyacetone route may not be a significant contributor to the methanol we see with glycerol. However, these experiments only observe hydroxyacetone in isolation. In a glycerol feed experiment the different competing pathways and their products may result in

hydroxyacetone behaving differently. The presence of more reactive radical species may affect the substrate and its products in ways which can't be predicted from these results. So hydroxyacetone route as a significant pathway to methanol cannot yet be fully ruled out.

However, it can still be supposed that there are other major pathways for the glycerol to methanol yield. Based on our proposed scheme, a primary route was suspected to be through the glycerol defragmentation pathway yielding ethylene glycol. There however may be other unrealised product routes to methanol occurring simultaneously.

In conclusion, with hydroxyacetone as a substrate there have been several factors identified in relation to the catalyst's performance with MgO. Firstly, hydroxyacetone is relatively stable and once formed is difficult to further convert. This is especially true for the catalyst MgO_650. Over other catalysts it sees significantly higher but still relatively low conversion. This can increase dramatically with temperature. The temperature used also significantly effects the product distribution. Hydroxyacetone produces a lot of detected unknowns, especially at lower temperatures as well as acetaldehyde. As the temperatures increase the selectivity to the unknowns decrease along with the CMB. Acetaldehyde is especially prominent and increases with temperature. It may be linked to CMB and the loss in the glycerol reactions.

4.4.2 Ethylene glycol

Reactions were run with a 50 wt.% ethylene glycol feed over a temperature range of 320 °C to 440 °C. Several significant products were seen which were originally not expected. Ethanol was a major product accounting for up to 31 % selectivity. This does not occur in significant amounts in the glycerol experiments and is thought to be sourced from reduction of the acetyl radical. 1,2-propanediol and hydroxyacetone are also seen to be present. Indicating that C-C coupling reactions are catalysed under these conditions. 1,2-propanediol was thought to form from a hydrogenation of hydroxyacetone, but itself can form from dehydrogenation of hydroxyacetone. However, under these conditions it is not clear whether 1,2-propanediol or hydroxyacetone are produced first or simultaneously. But the increase in hydroxyacetone paired with a 1,2-propanediol decrease may indicate 1,2-propanediol forms first.

Reaction temperature increase exhibits an effect on the product distribution, with a similar trend seen between the catalysts. On increasing the reaction temperature, generally the selectivity to ethanol and 1,2-propanediol decreases significantly. This is accompanied by a general increase in unknown products, hydroxyacetone, acids and CO_2. With these ethylene glycol substrate experiments there does seem to be an effect with the radical chemistry stage of the reaction, the methanol selectivity, at least with MgO_650 is higher with this substrate than with glycerol, but

other radical products such as 2,3 butanediol are less prevalent. 2,3 butanediol occurs via the reaction between two acetyl radical fragments, which appears to be not as dominant compared to the reduction to acetaldehyde.

As shown, hydroxyacetone is a much more stable molecule than ethylene glycol, under the given reaction conditions. Ethylene glycol therefore under these reaction conditions used results in both a higher selectivity and yield to methanol. However, it is important to consider in these experiments the side reactions of the different pathway from glycerol have been removed. This has led to unexpected chemistry such as the production of ethanol and makes it unclear which under glycerol conditions is the major pathway to methanol. Due to the observed selectivity and yields the process of elimination indicates it is the initial homolytic cleavage of glycerol unless there is other unaccounted for routes.

4.4.3 Cofeeding

Co-feeding of multiple substrates was also performed. It was found that using 5 % or 25 % ethylene glycol with glycerol did not result in significant amounts of ethanol. Ethanol was only observed when using the pure ethylene glycol feed. No increase in methanol yield was observed either compared to glycerol reactions. Indicating having a higher concentration of ethylene glycol does not promote the formation of methanol. MgO_450 seemed to produce more ethylene glycol from glycerol than it converted, resulting in more ethylene glycol in the product stream than was fed in.

Some limited tested was performed with acetaldehyde fed into the reactor over the catalysts with water at a partial pressure meant to mimic the concentration observed in 360 °C 50 wt.% glycerol reactions. Here MgO_450 converted 30 % of acetaldehyde with a corresponding drop in CMB of 30 %. MgO_650 however did not a significant conversion and maintained a high CMB. This indicates that conversion of acetaldehyde is undesirable and leads to a loss in CMB, possibly due to higher molecular weight products not detected easily by GC-FID. MgO_650 does not seem under these conditions to be active for that reaction. This could help explain its high CMB observed in most reactions.

4.5.4 Further work

The insight gained from the previous experiments can be further developed. To further investigate the mechanism of our reaction an important next step could involve the use of labelled compounds. Use of substrates such as different positioned ^{13}C labelled glycerol could help elucidate the pathway of individual C atoms in glycerol when identifying them in the products. It should be possible to identify whether methanol is produced preferentially from the C_1 or C_2 position. The hydroxyacetone pathway may be expected to produce preferentially from a C_1 position.

Fragmentation to ethylene glycol may produce one methanol from a C_1 position, the subsequent glycolaldehyde fragmentation to give a C_2 labelled methanol. Using labelled hydroxyacetone it may be possible to confirm the proposed mechanism to 2,3 butanedione by level of incorporation of ^{13}C.

4.6   References

(1)   Haider, M. H.; Dummer, N. F.; Knight, D. W.; Jenkins, R. L.; Howard, M.; Moulijn, J.; Taylor, S. H.; Hutchings, G. J. Efficient Green Methanol Synthesis from Glycerol. *Nat. Chem.* **2015**, *7* (12), 1028–1032. https://doi.org/10.1038/nchem.2345.

(2)   Smith, L. R.; Smith, P. J.; Mugford, K. S.; Douthwaite, M.; Dummer, N. F.; Willock, D. J.; Howard, M.; Knight, D. W.; Taylor, S. H.; Hutchings, G. J. New Insights for the Valorisation of Glycerol over MgO Catalysts in the Gas-Phase. *Catal. Sci. Technol.* **2019**, 19–22. https://doi.org/10.1039/C8CY02214C.

(3)   Sainna, M. A.; Nanavati, S.; Black, C.; Smith, L.; Mugford, K.; Jenkins, H.; Douthwaite, M.; Dummer, N. F.; Catlow, C. R. A.; Hutchings, G. J.; Taylor, S. H.; Logsdail, A. J.; Willock, D. J. A Combined Periodic DFT and QM/MM Approach to Understand the Radical Mechanism of the Catalytic Production of Methanol from Glycerol. *Faraday Discuss.* **2020**, *34* (4), 240–241. https://doi.org/10.19009/jjacg.34.4_240.

(4)   Katryniok, B.; Paul, S.; Bellière-Baca, V.; Rey, P.; Dumeignil, F. Glycerol Dehydration to Acrolein in the Context of New Uses of Glycerol. *Green Chem.* **2010**, *12* (12), 2079–2098. https://doi.org/10.1039/C0GC00307G.

(5)   Talebian-Kiakalaieh, A.; Amin, N. A. S.; Hezaveh, H. Glycerol for Renewable Acrolein Production by Catalytic Dehydration. *Renew. Sustain. Energy Rev.* **2014**, *40*, 28–59. https://doi.org/10.1016/j.rser.2014.07.168.

(6)   Haider, M. H.; D'Agostino, C.; Dummer, N. F.; Mantle, M. D.; Gladden, L. F.; Knight, D. W.; Willock, D. J.; Morgan, D. J.; Taylor, S. H.; Hutchings, G. J. The Effect of Grafting Zirconia and Ceria onto Alumina as a Support for Silicotungstic Acid for the Catalytic Dehydration of Glycerol to Acrolein. *Chem. - A Eur. J.* **2014**, *20* (6), 1743–1752. https://doi.org/10.1002/chem.201302348.

(7)   Haider, M. H.; Dummer, N. F.; Zhang, D.; Miedziak, P.; Davies, T. E.; Taylor, S. H.; Willock, D. J.; Knight, D. W.; Chadwick, D.; Hutchings, G. J. Rubidium- and Caesium-Doped Silicotungstic Acid Catalysts Supported on Alumina for the Catalytic Dehydration of Glycerol to Acrolein. *J. Catal.* **2012**, *286*, 206–213. https://doi.org/10.1016/j.jcat.2011.11.004.

(8)   Smith, P. J.; Smith, L.; Dummer, N. F.; Douthwaite, M.; Willock, D. J.; Howard, M.; Knight, D. W.; Taylor, S. H.; Hutchings, G. J. Investigating the Influence of Reaction Conditions and the Properties of Ceria for the Valorisation of Glycerol. *Energies* **2019**, *12* (7), 1359. https://doi.org/10.3390/en12071359.

(9)   Devlia, J.; Smith, L.; Douthwaite, M.; Taylor, S. H.; Willock, D. J.; Hutchings, G. J.; Dummer, N. F. The Formation of Methanol from Glycerol Bio-Waste over Doped Ceria-Based Catalysts: Doped Ceria Based Catalysts. *Philos. Trans. R. Soc. A Math. Phys. Eng. Sci.* **2020**, *378* (2176). https://doi.org/10.1098/rsta.2020.0059.

(10)   Smith, L. R.; Sainna, M. A.; Douthwaite, M.; Davies, T. E.; Dummer, N. F.; Willock, D. J.; Knight, D. W.; Catlow, C. R. A.; Taylor, S. H.; Hutchings, G. J. Gas Phase Glycerol Valorization over Ceria Nanostructures with Well-Defined Morphologies. *ACS Catal.* **2021**, *11* (8), 4893–4907. https://doi.org/10.1021/acscatal.0c05606.

(11)   Sato, S.; Sakai, D.; Sato, F.; Yamada, Y. Vapor-Phase Dehydration of Glycerol into Hydroxyacetone over Silver Catalyst. *Chem. Lett.* **2012**, *41* (9), 965–966. https://doi.org/10.1246/cl.2012.965.

(12)   Vasconcelos, S. J. S.; Lima, C. L.; Filho, J. M.; Oliveira, A. C.; Barros, E. B.; de Sousa, F. F.; Rocha, M. G. C.; Bargiela, P.; Oliveira, A. C. Activity of Nanocasted Oxides for Gas-Phase Dehydration of Glycerol. *Chem. Eng. J.* **2011**, *168* (2), 656–664. https://doi.org/10.1016/j.cej.2011.01.053.

(13)   Hernandez, D.; Velasquez, M.; Ayrault, P.; Lopez, D.; Fernandez, J. J.; Santamaria, A.; Batiot-Dupeyrat, C. Gas Phase Glycerol Conversion over Lanthanum Based Catalysts: LaNiO3and La2O3. *Appl. Catal. A Gen.* **2013**, *467*, 315–324. https://doi.org/10.1016/j.apcata.2013.07.016.

(14)   Pathak, K.; Reddy, K. M.; Bakhshi, N. N.; Dalai, A. K. Catalytic Conversion of Glycerol to Value Added Liquid Products. *Appl. Catal. A Gen.* **2010**. https://doi.org/10.1016/j.apcata.2009.10.036.

(15)   Lima, C. L.; Vasconcelos, S. J. S.; Filho, J. M.; Neto, B. C.; Rocha, M. G. C.; Bargiela, P.; Oliveira, A. C. Nanocasted Oxides for Gas Phase Glycerol Conversion. *Appl. Catal. A Gen.* **2011**, *399* (1–2), 50–62. https://doi.org/10.1016/j.apcata.2011.03.036.

(16)   Butkovskaya, N. I.; Pouvesle, N.; Kukui, A.; Mu, Y.; Bras, G. Le. Mechanism of the OH-Initiated Oxidation of Hydroxyacetone over the Temperature Range 236-298 K. *J. Phys. Chem. A* **2006**, *110* (21), 6833–6843. https://doi.org/10.1021/jp056345r.

(17)   Sato, S.; Akiyama, M.; Inui, K.; Yokota, M. Selective Conversion of Glycerol into 1,2-Propanediol at Ambient Hydrogen Pressure. *Chem. Lett.* **2009**, *38* (6), 560–561. https://doi.org/10.1246/cl.2009.560.

(18)   Akiyama, M.; Sato, S.; Takahashi, R.; Inui, K.; Yokota, M. Dehydration-Hydrogenation of Glycerol into 1,2-Propanediol at Ambient Hydrogen Pressure. *Appl. Catal. A Gen.* **2009**, *371* (1–2), 60–66. https://doi.org/10.1016/j.apcata.2009.09.029.

(19)   Bamford, C. H.; Norrish, R. G. W. Photodecomposition of Aldehydes and Ketones. *Nature* **1936**, *874* (1934), 1016.

(20)   Norrish Type I Reaction. In *Comprehensive Organic Name Reactions and Reagents*; John Wiley & Sons, Ltd, 2010; pp 2062–2066. https://doi.org/https://doi.org/10.1002/9780470638859.conrr464.

(21)   D'Hondt, E.; de Vyver, S.; Sels, B. F.; Jacobs, P. A. Catalytic Glycerol Conversion into 1,2-Propanediol in Absence of Added Hydrogen. *Chem. Commun.* **2008**, No. 45, 6011–6012. https://doi.org/10.1039/B812886C.

(22)   Musolino, M. G.; Scarpino, L. A.; Mauriello, F.; Pietropaolo, R. Selective Transfer Hydrogenolysis of Glycerol Promoted by Palladium Catalysts in Absence of Hydrogen. *Green Chem.* **2009**, *11* (10), 1511–1513. https://doi.org/10.1039/B915745J.

(23)   Yan, Y.; Zhang, Y.; Jiang, T.; Xiao, T.; Edwards, P. P.; Cao, F. Glycerol Hydrogenolysis over a Pt–Ni Bimetallic Catalyst with Hydrogen Generated in Situ. *RSC Adv.* **2017**, *7* (61), 38251–38256. https://doi.org/10.1039/C7RA05814D.

(24)   Ji, W.; Chen, Y.; Kung, H. H. Vapor Phase Aldol Condensation of Acetaldehyde on Metal Oxide Catalysts. *Appl. Catal. A Gen.* **1997**. https://doi.org/10.1016/S0926-860X(96)00390-0.

(25)   Young, Z. D.; Hanspal, S.; Davis, R. J. Aldol Condensation of Acetaldehyde over Titania, Hydroxyapatite, and Magnesia. *ACS Catal.* **2016**, *6* (5), 3193–3202. https://doi.org/10.1021/acscatal.6b00264.

(26)   Fan, D.; Dong, X.; Yu, Y.; Zhang, M. A DFT Study on the Aldol Condensation Reaction on MgO in the Process of Ethanol to 1,3-Butadiene: Understanding the Structure-Activity Relationship. *Phys. Chem. Chem. Phys.* **2017**, *19* (37), 25671–25682. https://doi.org/10.1039/c7cp04502f.

(27)   Lusardi, M.; Struble, T.; Teixeira, A. R.; Jensen, K. F. Identifying the Roles of Acid–Base Sites in Formation Pathways of Tolualdehydes from Acetaldehyde over MgO-Based Catalysts. *Catal. Sci. Technol.* **2020**, *10* (2), 536–548. https://doi.org/10.1039/C9CY01927H.

(28)   Yaylayan, V. A.; Harty-Majors, S.; Ismail, A. A. Investigation of the Mechanism of Dissociation of Glycolaldehyde Dimer (2,5-Dihydroxy-1,4-Dioxane) by FTIR Spectroscopy. *Carbohydr. Res.* **1998**, *309* (1), 31–38. https://doi.org/https://doi.org/10.1016/S0008-6215(98)00129-3.

(29)   Mostrou, S.; Nagl, A.; Ranocchiari, M.; Föttinger, K.; van Bokhoven, J. A. The Catalytic and Radical Mechanism for Ethanol Oxidation to Acetic Acid. *Chem. Commun.* **2019**, *55* (79), 11833–11836.

https://doi.org/10.1039/C9CC05813C.

(30)　Behr, A.; Eilting, J.; Irawadi, K.; Leschinski, J.; Lindner, F. Improved Utilisation of Renewable Resources: New Important Derivatives of Glycerol. *Green Chem.* **2008**, *10* (1), 13–30. https://doi.org/10.1039/b710561d.

(31)　Sun, W.; Liu, J.; Chu, X.; Zhang, C.; Liu, C. Theoretical Study of the Dynamics and Thermal Mechanisms of the Reaction: Dehydration of Glycerol to Glycidol. *J. Mol. Struct. THEOCHEM* **2010**, *942* (1), 38–42. https://doi.org/https://doi.org/10.1016/j.theochem.2009.11.030.

(32)　Nimlos, M. R.; Blanksby, S. J.; Qian, X.; Himmel, M. E.; Johnson, D. K. Mechanisms of Glycerol Dehydration. *J. Phys. Chem. A* **2006**, *110* (18), 6145–6156. https://doi.org/10.1021/jp060597q.

(33)　Sienel, G.; Rieth, R.; Rowbottom, K. T. Epoxides. In *Ullmann's Encyclopedia of Industrial Chemistry*; American Cancer Society, 2000. https://doi.org/https://doi.org/10.1002/14356007.a09_531.

(34)　González-Castaño, M.; Dorneanu, B.; Arellano-García, H. The Reverse Water Gas Shift Reaction: A Process Systems Engineering Perspective. *React. Chem. Eng.* **2021**, *6* (6), 954–976. https://doi.org/10.1039/D0RE00478B.

(35)　Akiya, N.; Savage, P. E. Role of Water in Formic Acid Decomposition. *AIChE J.* **1998**, *44* (2), 405–415. https://doi.org/https://doi.org/10.1002/aic.690440217.

(36)　Francisco, J. S. A Comprehensive Theoretical Examination of Primary Dissociation Pathways of Formic Acid. *J. Chem. Phys.* **1992**, *96* (2), 1167–1175. https://doi.org/10.1063/1.462204.

(37)　Arndt, S.; Laugel, G.; Levchenko, S.; Horn, R.; Baerns, M.; Scheffler, M.; Schlögl, R.; Schomäcker, R. A Critical Assessment of Li/MgO-Based Catalysts for the Oxidative Coupling of Methane. *Catal. Rev. - Sci. Eng.* **2011**, *53* (4), 424–514. https://doi.org/10.1080/01614940.2011.613330.

(38)　Nibbelke, R. H.; Scheerova, J.; Decroon, M. H. J. M.; Marin, G. B. The Oxidative Coupling of Methane over MgO-Based Catalysts: A Steady-State Isotope Transient Kinetic Analysis. *J. Catal.* **1995**, *156* (1), 106–119. https://doi.org/https://doi.org/10.1006/jcat.1995.1236.

(39)　Mallens, E. P. J.; Hoebink, J. H. B. J.; Marin, G. B. An Investigation of the Oxygen Pathways in the Oxidative Coupling of Methane over MgO-Based Catalysts. *J. Catal.* **1996**, *160* (2), 222–234. https://doi.org/10.1006/jcat.1996.0141.

(40)　Schwach, P.; Frandsen, W.; Willinger, M.-G.; Schlögl, R.; Trunschke, A. Structure Sensitivity of the Oxidative Activation of Methane over MgO Model Catalysts: I. Kinetic Study. *J. Catal.* **2015**, *329*, 560–573. https://doi.org/10.1016/j.jcat.2015.05.007.

(41)　Kurokawa, H.; Ueda, W.; Moro-Oka, Y.; Ikawa, T. *Selective Catalytic C-C Bond Formation on Magnesium Oxide to Produce α,β-Unsaturated Compounds*; 1988; Vol. 41. https://doi.org/10.1016/S0167-2991(09)60827-2.

(42)　Foyt, D. C.; White, J. M. Thermal Decomposition of Methanol Adsorbed on Magnesia. *J. Catal.* **1977**, *47* (2), 260–268. https://doi.org/https://doi.org/10.1016/0021-9517(77)90173-7.

(43)　Liang, S. H.; Gay, I. D. Adsorption and Thermal Decomposition of Methanol on Magnesium Oxide. Carbon-13 NMR Studies. *Langmuir* **1985**, *1* (5), 593–599. https://doi.org/10.1021/la00065a014.

(44)　Smith, W. B. Ethylene Glycol to Acetaldehyde-Dehydration or a Concerted Mechanism. *Tetrahedron* **2002**. https://doi.org/10.1016/S0040-4020(02)00103-5.

(45)　Chizallet, C.; Costentin, G.; Lauron-Pernot, H.; Krafft, J. M.; Bazin, P.; Saussey, J.; Delbecq, F.; Saufet, P.; Che, M. Role of Hydroxyl Groups in the Basic Reactivity of MgO: A Theoretical and Experimental Study. *Oil Gas Sci. Technol.* **2006**, *61* (4), 479–488. https://doi.org/10.2516/ogst:2006023a.

(46)　Khalaf, A. J.; Hargreaves, J.; David, J. S. Base Catalysis with Metal Oxides. In Metal Oxide Catalysis. *Met. Oxide Catal.* **2009**. https://doi.org/doi:10.1002/9783527626113.ch21.

(47)　Hargreaves, J. S. J.; Hutchings, G. J.; Joyner, R. W.; Kiely, C. J. The Relationship between Catalyst

Morphology and Performance in the Oxidative Coupling of Methane. *J. Catal.* **1992**, *135* (2), 576–595. https://doi.org/https://doi.org/10.1016/0021-9517(92)90055-M.

(48)   Petitjean, H.; Tarasov, K.; Delbecq, F.; Sautet, P.; Krafft, J. M.; Bazin, P.; Paganini, M. C.; Giamello, E.; Che, M.; Lauron-Pernot, H.; Costentin, G. Quantitative Investigation of MgO Brønsted Basicity: DFT, IR, and Calorimetry Study of Methanol Adsorption. *J. Phys. Chem. C* **2010**, *114* (7), 3008–3016. https://doi.org/10.1021/jp909354p.

(49)   Cobzaru, C.; Oprea, S.; Dumitriu, E.; Hulea, V. Gas Phase Aldol Condensation of Lower Aldehydes over Clinoptilolite Rich Natural Zeolites. *Appl. Catal. A Gen.* **2008**, *351* (2), 253–258. https://doi.org/https://doi.org/10.1016/j.apcata.2008.09.024.

Chapter 5

Conclusions and further work

5.1 conclusions

The principal objective of this thesis was to develop a greater understanding of how gas phase conversion of glycerol to methanol proceeds over MgO. Specific attention was focused on how the properties of MgO influenced the reaction, and to establish whether they could be modified to obtain higher methanol yields. Strategies for the synthesis of sustainable, 'green' methanol are required. Methanol is a commodity chemical with a variety of uses and itself is used in the production of biodiesel.[1] Producing green methanol could help improve the sustainability of such processes. Commercially, methanol is predominantly produced *via* syngas, derived from fossil fuels. This proceeds through the hydrogenation of CO/CO_2 and the water gas shift reaction,[2] in the presence of a $CuO/ZnO/Al_2O_3$ based catalyst.[3] There is a societal drive to move away from fossil fuels and therefore, producing methanol directly from a renewable source would be beneficial.

In 2015 it was discovered by Haider *et al.*[4] that methanol could be produced from waste glycerol in a one step process at atmospheric pressure and temperatures of ≥ 320 °C. It was envisaged that the methanol produced from waste glycerol could be recycled back into the production of biodiesel resulting in both an economically and environmentally beneficial cycle. There are other methods of producing 'green' methanol such as CO_2 hydrogenation,[5–7] however these often use intensive conditions under high pressure of H_2. Hydrogen is generally sourced from steam methane reforming,[8] or electrolysis of water. In Haider *et al,*[4] the conversion of gaseous glycerol at atmospheric pressure and no added hydrogen was investigated over MgO and CeO_2 catalysts. The process exhibited promising yields of methanol, but it also produced a variety of side products such as acetaldehyde, hydroxyacetone, acrolein, ethylene glycol, 1,2 and 1,3 propanediol. However, a limitation with this initial work was that it predominantly used low concentration glycerol feeds. To obtain higher yields of methanol further work by Smith *et al,*[9] explored using higher concentration of glycerol up to 50 wt.%. The analysis procedure was also improved reporting a larger range of products. This led to a reevaluation of the selectivity to methanol, where up to 27.9 % was achieved with 50 wt.% glycerol feed over MgO. However, an incomplete carbon mass balance (CMB) was observed. 23 % of the glycerol carbon moles, fed into the reactor, were not accounted for in products or coking. It was concluded that this was likely due to bimolecular reactions occurring between reaction products, which were not sufficiently volatile to be vaporized in the GC. This

ultimately provided further motivation for exploring this work. It was important to establish what physicochemical properties influenced the formation of these undesirable products. If these could be identified, the potential for significant increases in methanol space time yield (STY) could be achieved. This is explored in chapter 3. It was also shown in *Smith et al.*[9] that the product distribution was significantly more complex than Haider *et al.*[4] had originally identified. Many more products were identified, and a large range of unknowns detected. This led to a more complete reaction scheme proposed. This was investigated in chapter 4 *via* feeding in intermediate substrates over the various catalysts in hope of seeing how methanol yield correlated with substrate and catalyst properties. From the scheme it was inferred that the radical fragmentation of glycerol should result in a higher yield of methanol than *via* the dehydration route. If this was true, there may be catalyst characteristics or reaction conditions that promote this route. There are three main ways for methanol to form from glycerol proposed. First is the initial homolytic cleavage of glycerol, secondly the cleavage of glyceraldehyde which results from the glycerol cleavage route, and thirdly the cleavage of hydroxyacetone. The source of hydrogen for formation of methanol from its radical was also investigated *via* cofeeding experiments, this was to confer with previous computational studies conducted in the group where it was proposed the hydroxymethyl radical undergoes a disproportionation.

5.1.1 Chapter 3: Reactions of vaporized glycerol over different temperature treated MgO catalysts.

The aim of Chapter 3 was to investigate how changing the physiochemical characteristics of MgO would affect the performance in the gas phase conversion of glycerol. This was done by altering the preparation procedure of the samples, namely, changing the heat treatment temperature in N_2, prior to its application as a catalyst. Initially, a series of MgO catalysts were prepared whereby the temperature of the final N_2 heat treatment was varied from 450, to 550, to 650 and finally to 750 °C. These samples were termed MgO_450, MgO_550, MgO_650 and MgO_750 respectively.

The fresh catalysts were then characterized using a variety of techniques. CO_2 temperature programmed desorption (TPD) was used to quantify the basicity of the samples. The basic site concentration (per g) decreased with an increasing N_2 preparation temperature. However, the basic site density (per m^2) stayed relatively stable due to the proportional decrease in surface area; Surface area decreased from 187 m^2 (with MgO_450) to 74 m^2 (with MgO_750). From the curve observed from the TPD experiments, it was evident that there were multiple peaks present, which were attributed to different strength basic sites. To further probe this and determine the type and distribution of basic sites on the samples surface, CO_2 adsorption diffuse reflectance infrared Fourier transform spectroscopy (DRIFTS) was employed. Upon CO_2 adsorption, the bonding

geometries of the formed adducts could be determined. This would allow for an estimation of the relative proportion of basic sites. It was deduced from the experiments, and through reference to previous literature on the subject, that there were three primary types of basic sites on MgO's surface. [10–12] The strongest sites were attributed to be low coordinate O^{2-} ions, potentially on edges, vacancies, and corners. The medium-strength sites were proposed to be O^{2-} in Mg^{2+}-O^{2-} pairs, whilst the weakest sites were hydroxylated sites of OH^{-}. It was estimated that the MgO_450, MgO_550 and MgO_750 had a higher proportion of the strong O^{2-} sites exposed, while MgO_650 had a more equal distribution between the strong and medium sites. This conclusion is limited however as a qualitative analysis. The amount of CO_2 absorbed or desorbed was not quantified, only the relative size of absorbances were analyzed. Further work could be done to obtain quantified results by calibrating the CO_2 absorption intensity to known amounts.

Next, the samples were analyzed by powder X-ray diffraction (XRD). This was used to determine the MgO phase had been successfully formed and determine crystallite size. In each of the samples, it was confirmed that MgO existed in a periclase phase. The crystallite sizes increased with temperature, relatively linearly, until a large size increase was observed of 8.4 to 12.7 nm, when proceeding from 650 °C to 750 °C. Simultaneously, pore volume decreased with the N_2 treatment temperature and interestingly, a significant drop was observed between the MgO_650 and MgO_750 catalysts. This was hypothesized to be attributed to the pore system collapsing at higher temperatures, which had been observed previously. [13] However, there was no clear trend between the N_2 treatment temperature and average pore radius. SEM investigations revealed that a flake like morphology existed for all the samples, however, under more resolute inspection *via* TEM, it was revealed that the samples treated at 450 °C, 550 °C and 750 °C exhibited an ordered hexagonal structure. The MgO_650 sample did not, however, exhibit this well-defined structure, the cause for this was not confirmed. However, through reference to literature, it was suggested that MgO_650 could undergo exfoliation of water from deep within its structure, resulting in intercrystallite channels forming. [14] MgO_750 exhibited a similar structure to MgO_450 and MgO_550. This indicates that the hexagonal formations somehow reform at higher temperatures, possibly seeded from remaining crystallites after exfoliation.

The material characterization demonstrated that simply varying the N_2 treatment temperature did indeed influence the MgO properties. To evaluate how these different characteristics influenced catalyst performance, the samples were examined for the gas phase conversion of glycerol. Each of the samples were initially tested using a 50 wt. % glycerol feed at 360 °C with 0.5 g of catalyst. It was observed that the catalysts exhibited a decrease in conversion as the treatment temperature

was increased until 650 °C (MgO_650). However, on proceeding to 750 °C (MgO_750), conversion increased. The observed conversion was 87 %, 80 %, 75 % and 80 % for the catalysts, respectively. Conversely, the opposite trend was observed with the associated CMBs. The CMB increased to MgO_650 (74 % - 78 % - 98 %) and the decreased with 750 °C (79 %). These trends may be related to the SA and basic site concentration. However, the behavior of MgO_750 indicated that other factors must be involved. Possibly linked to the proportion of strong sites evidenced by DRIFTS. Other changes to the catalyst surface (such as the possible exfoliation and recrystallization) are seen from proceeding to MgO_750 from MgO_650.

The high CMB observed in the reaction over the MgO_650 catalyst is an important result; the carbon mass balance obtained (98 %) is the highest seen for this reaction when using 50 wt. % glycerol feeds. Further total organic carbon (TOC) and liquid chromatography mass spectrometry (LCMS) analysis was performed. This indicated that the lost carbon mass balance over MgO_450 may be due to the formation of HWMP. Evidence indicated that MgO_650 did not produce significant amount of these products. Incomplete CMB due to HWMP formation was first proposed in Smith *et al.*[9] It is thought that these large molecules form from sequential condensations of different products formed. This would likely involve condensation reactions of ketones and/or aldehydes. The condensation of acetaldehyde with itself can produce 3-hydroxy-propenal which can dehydrate to crotonaldehyde.[15] Crotonaldehyde can undergo further condensations, with itself, acetaldehyde, or other molecules to produce a broad range of larger products.[16–18] The high CMB obtained over MgO_650 highlights that for some reason, these undesirable side products are suppressed. Suppressing these undesirable side reactions seems to result in a higher STY to methanol and other main products. The series sees a similar selectivity to methanol between catalysts. MgO_650 exhibiting the lowest selectivity and conversion, but the highest methanol STY. Methanol STY of 85, 74, 93 and 79 g h^{-1} kg cat^{-1} are obtained for MgO_450, MgO_550, MgO_650 and MgO_750 respectively. This shows that higher CMB can yield higher STY with similar selectivity.

However, while this is promising, the methanol STY achieved by Smith *et al,* was significantly higher at 131 g h^{-1} kg cat^{-1}, 23.4 % selectivity and 74 % conversion under the same conditions. The selectivity for MgO_650 was only 9.8 %. This indicates that high selectivity and CMB is crucial for high methanol yields. High selectivity seems to be linked here to the calcination time, the only difference between MgO_STD and the MgO_450 preparation is that the calcination for MgO_STD is 24 hrs rather than 2 hrs. This may result in structural changes that are intrinsic to obtaining high selectivity. Further research and characterisation are needed. Producing an equivalent of MgO_650

but with the initial calcination time increased to 24 hrs may produce a more selective to methanol catalyst.

It seems that if the production of HWMP is linked to basicity, the distribution of site type is likely more important than the basic site distribution per gram. This may help explain why MgO_750 exhibits a lower CMB than MgO_650. It is noted that the catalyst characteristics and properties obtained for the catalyst samples are obtained *ex-situ* and not under reaction conditions. This means that the catalysts may likely undergo structural and surface changes when under reaction. This could influence parameters such as the basicity, particularly given that coking is known to occur in the reaction. Given that under reaction conditions 50 wt.% of the substrate feed is water, it could induce a degree of rehydration of the catalysts surface to produce OH^- groups. Hydroxylation of oxide catalysts is commonly investigated as it can affect basic catalysts activity.[19] Hydroxyl groups on MgO are can occur *via* the heterolytic dissociation on low coordinate Mg^{2+} - O^{2-} pairs by protonating the O^{2-} and hydroxylating the Mg^{2+}.[19] MgO(100) faces are not expected to dissociate water,[20–22] corner and edge O^{2-} sites are more likely.[21] MgO_650 may exhibit less easily hydroxylated sites due to its differing morphology, this is also indicated by DRIFTS which show a lower proportion of strong sites (attributed to low coordinated corner and edge sites). Hydroxylated sites are important as can influence the stabilization of molecules on the catalyst surface and promote condensation.[15]. To investigate which catalysts dissociate water readily upon their surface, reactions were conducted using D_2O rather than H_2O as a feed diluent. Interestingly, a large kinetic isotopic effect (KIE) was observed over the MgO_450, MgO_550 and MgO_750 catalysts. MgO_650 was only marginally affected. Evidently, water was important for the activation of glycerol over the MgO catalysts, where KIE were observed. It was hypothesized that this could be attributed to the ease by which water is dissociated over these catalysts, under reaction conditions. This may be due to the base site distribution observed *via* DRIFTS. There seemed to be a trend between the samples affected by the presence of D_2O, morphology, higher proportion of strong sites on the fresh catalyst and the lower CMBs observed. It is also proposed that OH- species formed *in-situ* influence glycerol activation and condensation reactions, possibly by stabilizing reactants upon the surface.

Coking may also play a part, MgO_650 exhibited a higher degree of coking at 360 °C. Coking may influence the basicity by blocking sites. During the pre-treatment stage of the reaction MgO_650 coke and CMB increased over time. MgO_450 however saw decrease in CMB with increasing coke. This may indicate that the sites preferentially blocked over the catalysts vary. Carbon, in the form of coke, can potentially block basic active sites which in turn, can influence the catalyst surface *in-*

situ.[23] MgO_650 exhibited a higher degree of coking, which was determined by analysis of the post reaction catalyst by TGA. The blocking of sites by coke could affect the site distribution and result in MgO_650 having a lower total basicity under reaction conditions than MgO_750. This could help explain its lower activity and higher CMB. How coke builds up during the reaction and if it blocks basic sites was investigated. Analysis of MgO_450 and MgO_650 during the first 2 hrs 15 mins was undertaken. It was found with analysis of the post reaction catalysts, that after the pretreatment, the main CO_2 TPD peak indicating basicity was almost entirely removed. This is likely due to formation of coke on the surface. After the full reaction run a small peak had recovered. This indicates that the basicity observed in CO_2 TPD and DRIFTS is likely not representative of the *in-situ* conditions during collection. The reason for the higher coking, however, remains unclear. It is expected that higher initial basicity samples would coke more, especially if they promote condensation reactions. A higher number of strong sites would more strongly chemisorb constituents onto it; however, the proposed hydroxylation of the strong sites may inhibit this. It may be a combination of initial basicity and the morphological differences that cause this. However, none of this is currently confirmed, further investigation into these characteristics is needed. *In-situ* reaction analysis of MgO basic sites would be highly desirable but potentially difficult to perform.

Following this insight, the experimental conditions were changed to analyze the catalysts performance at different stages of the reaction. Parameters such as temperature and contact time were changed. The early stage of the reaction was first investigated to see how the intermediate product distribution varied over the catalysts. Selectivity at low conversion could be important in understanding why the catalyst behave differently at higher conversion, high levels of certain products and intermediates may explain why catalyst produce HWMP. Reactions were performed over the catalyst with a low temperature of 320 °C and 0.1 g of catalyst to try and achieve a low conversion. The decrease in contact time and reduction of temperature resulted in conversions below 10 %. MgO_650 exhibited the lowest of only 5 %. Under these conditions there was not a noticeable difference in CMB. All achieved 100 %, this indicates that higher temperatures, contact time and conversion may be needed for the promotion of condensation reactions. Interestingly the product distributions of the samples were significantly different even with similar conversions. This shows that the samples direct the reaction in different ways. Unknowns were more prominent over the higher temperature treated catalysts. These are thought to be both a mixture of intermediates to quantified products and possibly the initial condensation products, before undergoing several subsequent additions.

Further reactions investigating catalyst mass and contact time were conducted at 360 °C for both catalysts. Increasing the contact time with 2 g of catalyst led to a very low CMB with MgO_450 of 40 %, whereas the CMB observed over the MgO_650 catalyst was maintained at 98 %. This indicates that high contact times are likely to further promote condensation reactions over the MgO_450 catalyst. Evidently, the MgO_650 catalyst does not possess the properties which facilitate these transformations. Further reactions investigated small amounts of catalyst. It seems that changes in catalyst mass were not linear with conversion; the conversion of glycerol per gram of catalyst was the highest at 0.05 g of catalyst. Further increases in catalyst mass increased the conversion but resulted in a lower efficiency per gram. This could be due to the concentration of glycerol decreasing as the conversion goes up, this can result in rate of conversion decreasing as there is less glycerol to convert. Other issues such as with substrate diffusion onto and across the surface of the catalyst could explain this, but this is difficult to evaluate under the conditions used here, typically below 30 % conversion would be needed. Other reactions investigating a low wt.% of glycerol found that water and low concentration of substrate helped inhibit production of HWMP over the catalysts. MgO_450 achieved a higher CMB (83 %) even with a higher conversion and temperature used. However, this was still significantly lower than MgO_650.

To see how the MgO_650 product distribution changes with temperature and conversion, reactions were performed over MgO_650 at a range of temperatures. Temperatures used were 320, 360, 400 and 440 °C. A main aim was to see if MgO_650 could achieve a high CMB through a range of conditions. This could deduce whether the high CMB was a consistent characteristic of the catalyst or condition specific. CMB remained high, there was a small drop at 440 °C to 94 % which may be due to increased fouling. Products changed with temperature. Acetaldehyde increased from 10.6 % to 27.4 % over the range. Acrolein also increased to 16.4 % from 11.7 %. Intermediates decreased with temperature increase. Hydroxyacetone selectivity decreased from 31.5 % to 16.5 %. Interestingly methanol gave the best yield and selectivity of 13.4 % and 122 g h^{-1} kg h^{-1} at 400 °C. This decreased at 440 °C to 9.7 % and 105 g h^{-1} kg h^{-1}. Potentially due to decomposition over MgO.[24,25]

Ultimately, the MgO_650 exhibited higher product yields (including methanol) compared to the other catalysts in the series. This indicates that higher yields to useful products can be obtained by improving the CMB. While the STY to methanol is not as high as previous experiments using MgO, the overall yield of all useful products is high. The removal of catalyst features that promote the unwanted side reactions does not detrimentally impact the methanol yield. It is thought that this is likely related to the distribution of basic sites on the fresh MgO surface and their preference for

coking or hydroxylation under reaction conditions. Catalysts that initially exhibit a higher proportion of strong sites seem to dissociate water more prominently. This may result in more hydroxylated sites. Hydroxylated sites may help stabilize reactants leading to higher activity and condensation promotion as Fan *et al,* suggests.[15] Hydroxylation of the stronger sites may lead to them not coking as much . More coking also seems to lead to a decrease in sites that promote condensation reactions. The responsible initial basic site distribution seems to be linked to morphology, the samples with the hexagonal platelets yielded a higher degree of initial strong sites, possibly due to less exposed (100) plane on the surface.

5.1.2 Chapter 4 Mechanistic studies using intermediate products of the valorisation of glycerol over MgO

The primary aim of Chapter 4 was to explore the different reaction pathways which occur over MgO. This was done by conducting reactions from significant reaction intermediates which are formed in the reaction from glycerol. It was thought that to achieve higher yields of useful products such as methanol, a better understanding of the reaction pathways was required. Understanding which characteristics favored the promotion of certain routes could lead to improved catalyst design. From our previous work, several primary reactions pathways have been confirmed over MgO catalysts.[4,9] The double dehydration of glycerol can lead to acrolein. Two routes have been proposed which can yield methanol. Firstly, dehydration followed by a tautomerization to hydroxyacetone, followed by a subsequent radical fragmentation (Figure 1). This may be significant as hydroxyacetone is a major product, usually seen with 20 – 30 % selectivity in reactions from methanol.
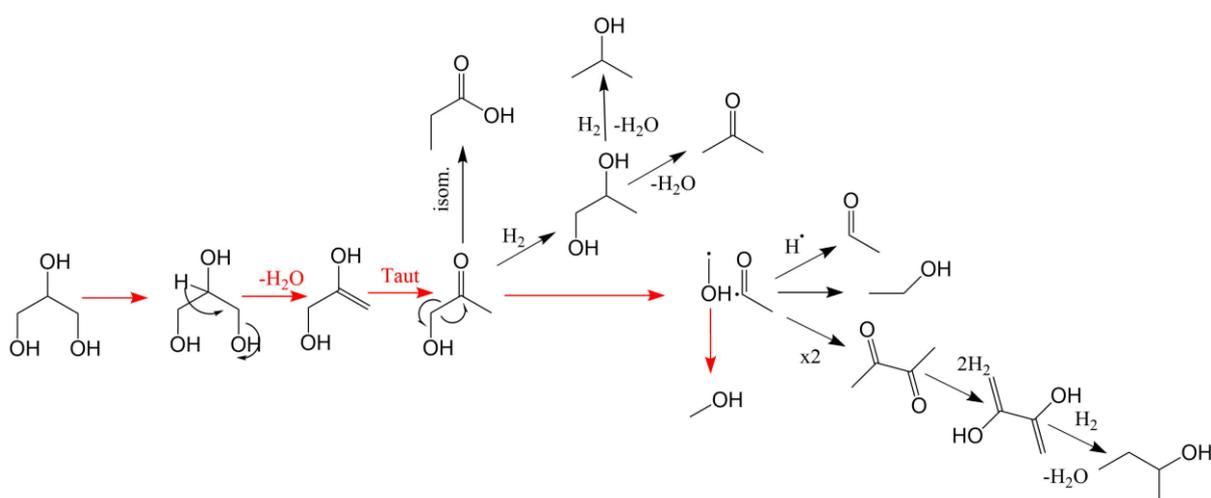
Figure 1. Glycerol to methanol through dehydration to hydroxyacetone proposed pathway. Red arrows: route to methanol. Black arrows: side reactions.

The second primary route is more direct and proceeds through the C-C cleavage of glycerol, resulting in the formation of a methanol radical and an ethylene glycol radical (Figure 2). The latter can proceed *via* loss of a hydrogen atom, resulting in enediol and its tautomeric pair; glycolaldehyde. Glycolaldehyde can undergo fragmentation to an acetyl and another methanol radical. Therefore, this route could lead to the formation of two methanol radicals. Therefore, understanding how this second homolytic C-C cleavage occurs, has the potential to significantly impact the yield of methanol which can be produced from glycerol.
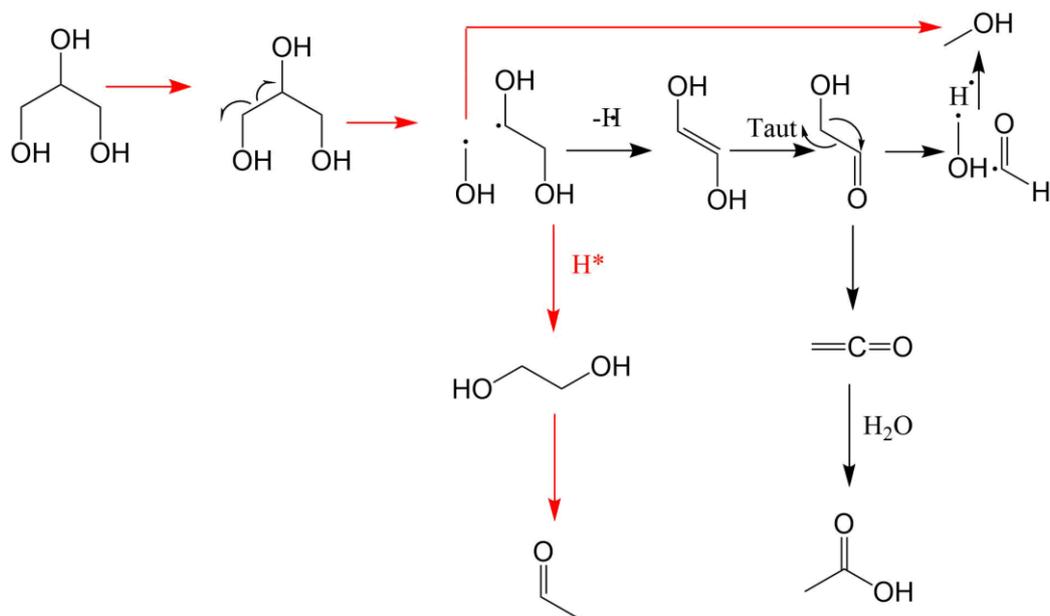
Figure 2. Glycerol to methanol radical fragmentation to ethylene glycol proposed pathway

For this reason, hydroxyacetone and ethylene glycol were used as substrates in reactions over MgO. The catalysts used for these experiments, were the same as those produced and characterized in the previous results chapter (Chapter 3). The reactions were carried out with 10 – 50 wt.% of the substrate in water, under comparable reaction conditions.

Firstly, experiments were conducted using hydroxyacetone as an intermediate. Previous work, presented in Chapter 3, indicated that hydroxyacetone was relatively stable. At 50 wt.%, 440 °C, there was still a selectivity of 16.5 % to hydroxyacetone over 0.5 g MgO_650. This was only reduced to low levels when using a low concentration of glycerol of 10 wt.% and 440 °C to give 1.8 %. When using 50 wt.% hydroxyacetone over the MgO_450 catalyst, the conversion was higher (16 % - 33 %). In the contrary, the MgO_650 catalyst was far less active; it converted less than 1 % of the feed at 320 °C, 1 % at 360 °C and only 21 % at 400 °C. Of the catalysts tested, the MgO_750 catalyst was the most active overall; it achieved hydroxyacetone conversions of 18 % at 360 °C and 64 % at 400 °C. There was no trend between hydroxyacetone conversion and basic site concentration, or SA

observed. In all reactions, acetaldehyde was determined to be the most dominant product. The catalysts exhibited 45 – 47 % selectivity to it at 400 °C. Unknowns were also very prominent at low temperatures, with the MgO_450 catalyst exhibiting a selectivity to unknowns of ca. 44.9 %. Selectivity to methanol was negligible remaining below 2 %. This indicated that the formation of methanol from hydroxyacetone was unlikely to be a prominent pathway for methanol formation from glycerol. Interestingly, a similar trend in the CMB over the different catalysts was observed in these reactions, compared to the reactions conducted from glycerol. The MgO_450 catalyst exhibited the lowest CMB, which decreased with temperature. In the contrary, over the MgO_650 catalyst, a CMB of 98 % was observed at 400 °C. This could suggest that the losses in CMB, observed in the reactions from glycerol, could originate from the formation of hydroxyacetone, and the subsequent reactions it undergoes.

Acetaldehyde has been a suspect for undergoing the proposed condensation reactions to HWMP which can result in loss of CMB. It was the dominant product in the hydroxyacetone experiments and high selectivity was associated with low CMB. To investigate this acetaldehyde in He was tested in the presence of water over MgO_450 and MgO_650. The key parameter here was the CMB. The partial pressure of acetaldehyde was made up to be representative of the concentration observed in typical 360 °C 50 wt.% glycerol reactions. MgO_450 exhibited a CMB of 70 % and conversion of 30 %. MgO_650's activity was negligible with no drop in CMB. Under these circumstances this may indicate that MgO_450 can produce at least some of its condensation HWMP from acetaldehyde self-condensation. This further indicates that MgO_650 is inactive for this kind of reaction. Of course, again this is an extreme simplification, a significantly lower concentration and restricted range of chemicals are present compared to the glycerol reactions.

To see if ethylene glycol would preferentially convert to glycolaldehyde and undergo fragmentation, reactions using Ethylene glycol as the substrate were subsequently conducted. This was done at temperatures between 320 °C to 440 °C. The conversion of ethylene glycol was generally higher than that observed for hydroxyacetone. Again however, there was not a clear trend between substrate conversion and catalyst properties. At lower temperatures of 320 - 360 °C, the MgO_650 catalyst exhibited the highest activity. However, at 400 °C and 440 °C, the MgO_750 and MgO_450 were determined to be the most active, respectively. Conversion was low at 320 °C but increased to 31 – 36 % over the MgO_450 and MgO_650 at 360 °C. At 400 °C, a marginal increase in activity to 40 % and 47 % was observed. Further increases in conversions are occurred at 440 °C, where 78 % and 68 % were observed over the MgO_450 and MgO_650 catalysts, respectively. The observed CMBs in these reactions was determined to correlate with reaction temperature. At 320 °C the MgO_450 and MgO_650 both exhibit a CMB of 99 % +. This decreased

significantly to 76 % over the MgO_450 catalyst but was less influenced by the MgO_650 catalyst (95 %). Conversion of ethylene glycol can be associated with drop in CMB. This may be due to the higher production, and subsequent reaction, of its products such as acetaldehyde.

There were also several unexpected products in the ethylene glycol reactions. Ethanol was a significant product. Selectivity was 14.6 % - 31.1 % over the catalysts. This was unexpected as ethanol is only seen in negligible quantities from glycerol. Ethanol may form through hydrogenolysis. This would require a source of H_2, possibly from *in-situ* from aqueous phase reforming,[26,27] or methanol decomposition.[24,25] Hydroxyacetone and 1,2-propanediol were also produced. This would require a C-C coupling reaction. The selectivity to methanol increased from 9.5 % - 14.2 % with MgO_450 and decreases from 14.7 % to 11.8 % with MgO_650 over the temperature range. This selectivity was significantly higher than with hydroxyacetone and comparable to glycerol experiments. However, if this was the primary route to methanol it would be expected to be significantly higher. The STY is also still low compared to the glycerol experiments. This indicates that it is also not the primary route to methanol. Therefore, the initial homolytic cleavage of glycerol is expected to yield the majority of the methanol.

5.2 Further work

Insight on the complex chemistry that takes place in the gas phase valorisation of glycerol has been achieved. It has been deduced that decreases in CMB are likely due to formation of HWMP. It is proposed that this is due to the basic site distribution effecting things such as *in-situ* hydroxylation and coking. Coking seems to block sites responsible for HWMP formation. It is theorized that hydroxylation seems to help promote glycerol activation, prevent coking, and stabilize potential bi-molecular reactions. This hydroxylation may occur more prevalently over strong edge and corner sites which are expected to be basic enough to dissociate water. Avoiding these HWMP forming condensation reactions to obtain high CMB is of paramount importance; as the results for MgO_650 indicate; that high CMB results in higher yields over the range of products. It is also proposed from the experiments using intermediate substrates that the preferential route to methanol is likely the initial cleavage of glycerol more so than the cleavage of glycolaldehyde. Hydroxyacetone cleavage is not expected to be responsible for significant amounts of the obtained methanol over MgO.

Despite this, much more development is still required if the glycerol to methanol process is to be considered viable at an industrial level. The conversion of gaseous glycerol to methanol over MgO is a complex reaction. It requires several steps and can proceed down multiple pathways; this results in many opportunities for side reactions and by-products. One of the primary undesirable side reactions is the formation of HWMP through condensation reactions. While some progress has

been made on suppressing these reactions, a more detailed understanding of the catalysts physicochemical properties which promote these are required. A priority going forward would be develop a further understanding of what the currently detected unknown products are. A first step here is investigating possible candidates of early-stage condensation reactions. These could include initial molecules from acetaldehyde or aldol condensation discussed in chapter 3, that would be detectable *via* our GC method. Acetaldehyde self-condensation is expected to yield initial products such as 3-hydroxybutanal, crotonaldehyde, 2,4 hexadienal, 2,4,6 octatrienal and tolualdehyde. These could be injected into GC and/or GCMS and compared to the chromatograms to see if they match any of the unknown peaks. Solutions of known quantities could then be used to calibrate for them. If these are a significant proportion of the detected unknowns at low conversion reactions, it may help reinforce that condensation reactions are responsible for HWMP. For larger potential products further analysis of the mass spectrum from LCMS could be performed to try and identify major constituents.

The selectivity and STY to methanol is still fairly low and there is significant room for improvement. Currently the product range is extensive, consisting of many identified and unidentified products. On an industrial scale, this would make separation and purification difficult and likely costly. If the products could be concentrated into a few major desirable compounds such as lower alcohols, the reaction mixture could possibly be used as a fuel blend.[28] Of the catalysts prepared in the study, the MgO_650 catalysts achieved a higher CMB and higher yields of methanol. Despite this, it still compares poorly, in terms of methanol STY, to the previously established MgO and CeO$_2$ catalysts.[9,29–32] Further work should focus on improving the methanol STY while maintaining the high CMB. While not explored within this thesis, significant work has been performed on the use of CeO$_2$ as a catalyst within the research group.[29–32] The best performing CeO$_2$ was found to yield up to 201 g h^{-1} kg^{-1}, at 400 °C and 15 mL^{-1} min^{-1} Ar.[29] The CeO$_2$ sample exhibited a polyhedral hydrothermally produced nanostructure quite different to what we have seen with MgO. However, it only exhibited a CMB of 67 %. The MgO_STD used 400 °C and 50 mL^{-1} min^{-1} Ar gave 205 g h^{-1} kg^{-1} with 77 % CMB.[9] This is significantly higher than seen with the MgO catalysts that have been discussed here. When using 0.5 g, up to 122 g h^{-1} kg^{-1} at 400 °C and 50 mL^{-1} min^{-1} Ar was achieved but with 98 % CMB. It would be interesting to investigate into mixing the polyhedral CeO$_2$ or MgO catalysts with high CMB achieving MgO_650 or producing mixed metal oxides. MgO_STD is made similarly to MgO_450 but with a 24 hr initial calcination. This produces a catalyst that is significantly more selective to methanol resulting high yields. An important step would be to make this catalyst but with a higher heat treatment temperature of 650 °C. This would hopefully combine properties

obtained from the long calcination time with the properties obtained from a 650 °C treatment temperature.

Other preparations of MgO could be explored, heat treating at 650 °C but changing the initial steps could be experimented with. As mentioned, it has been demonstrated by Smith *et al.*[29] that the morphology of CeO_2 was important and could significantly change catalyst performance for this reaction. Previously discussed in Chapter 1 there is a variety of established ways to produce morphological controlled samples of MgO such as nanorods,[33] cubes,[34] and trapezoid samples.[35] There are many different techniques to explore with MgO synthesis such as sol gel,[36] hydrothermal surfactant controlled,[37,38] supercritical methods.[34] and simple decomposition of different precursors.[39] Changing the morphology can affect the reaction in many ways, for example it could change the degree of different crystal planes exposed. As mentioned, the MgO (100) plane is unlikely to be dissociate water compared to edges and corners, which can influence the activity. This may be tuned by trying different morphologies. This wide range of ways to produce MgO means that other characteristics such as basic site distribution and porosity could potentially be significantly changed and investigated.

Characterization of the catalyst and product analysis under reaction conditions is likely hugely important for development of this process. As demonstrated catalyst characteristics can change under reaction conditions but are only analyzed *ex -situ* and as such much of the characterization performed may not be representative of the catalysts in the reaction. This has resulted in difficulty defining direct trends between the physiochemical properties of the catalysts and the reaction results. *In-situ* analysis would be crucial to define definitive trends. It is noted in previous chapters that basicity is important, but it is indicated from coking results, D_2O experiments and post reaction TPD that the basicity of the samples change under reaction conditions. However, it is difficult to perform *in-situ* analysis of the catalyst surface due to the reaction conditions and products. *In-situ* XRD could potentially be used. Analysis of diffraction peaks under reaction conditions could potentially reveal if the catalyst is hydroxylated to a high degree and how coking changes over time. The changes of diffraction peak intensity may show on what planes the coke may preferentially adsorb to.[40] Post reaction catalyst coking could be further investigated by Raman spectroscopy.[41] Solid state nuclear magnetic resonance (SSNMR) spectroscopy has applications in acidic and basic site analysis as well.[42] With use of the right apparatus, *in-situ* continuous flow conditions can be performed in SSNMR with probe molecules under temperature. Organic species can be differentiated by their characteristic resonances. [13]C magic angle spinning (MAS) spectra has a large chemical shift range of more than 300 ppm.[43] This allows for many species to be identified. Klinowski *et al.*[44] investigated the methanol to gasoline reaction and identified 29 species and

monitored their progress on ZSM-5 surfaces. NMR can be used quantitatively so the concentrations of compounds throughout the reaction period can be determined.[45] This process does require ^{13}C enriched reagents however.

The analysis of products in this thesis was done post reaction and collection. It could be possible to arrange onstream analysis of products, where samples could be taken directly from the reactor periodically during reaction and analyzed by GC. Online mass spectrometry could also be employed to analyze HWMP in the reaction stream. This would allow for a better understanding of the chemistry and how it changes over time.

Chapter 4 helped elucidate how the different intermediates may react over MgO, it indicated that the ethylene glycol pathway *via* C-C cleavage may result in more methanol than they dehydration to hydroxyacetone route. However, it also showed how complex the reaction is, there is likely interchange between the pathways and unexpected interactions. Carbon labelling experiments could play a role in further elucidation of the mechanism. Use of substrates such as different positioned ^{13}C labelled glycerol could help analyze the pathway of individual C atoms in glycerol when identifying them in the products. It should be possible to identify whether methanol is produced preferentially from the C1 or C2 position. The hydroxyacetone pathway may be expected to produce preferentially from a C1 position. The homolytic fragmentation to ethylene glycol may produce one methanol from a C1 position, the subsequent glycolaldehyde fragmentation to give a C2 labelled methanol. Using labelled hydroxyacetone it may be possible to confirm the proposed mechanism to 2,3 butanedione by level of incorporation of ^{13}C. As the conversion of ethylene glycol and hydroxyacetone only yielded low amounts of methanol, glycolaldehyde cleavage is not expected to be the primary route. Therefore, in accordance with our reaction scheme it is likely obtained through the initial homolytic cleavage of glycerol which would appear as C1 labelled. If this is the case designing catalysts that could promote this type of reaction may be the next step. The use of cracking catalysts could be used, however in previous studies this has not yielded methanol from glycerol. Primarily acetaldehyde and acrolein are produced from acidic zeolite catalysts.[46]

The results presented in this thesis and other work within the research group indicate that glycerol to methanol over MgO is a highly complex process. The reaction mechanism exhibits a wide range of possible side products. MgO catalyst characteristics have been shown to be very important in directing the reaction. However, there is many competing factors, with basicity, conversion, morphology, and crystallinity possibly producing different effects. This makes it difficult to discern the exact properties that are desirable for productive catalysis. The ability of MgO_650 to obtain a

high CMB is of significant benefit, it reduces the production of unusable side reactions significantly compared to other catalysts. This behavior is observed over a wide range of reaction conditions. The ability for a catalyst to obtain a high CMB over all conditions is a significant advance in this reaction over MgO. This is crucial and results in an overall high yield of usable products such as methanol, acetaldehyde and 1,2-propanediol and hydroxyacetone compared to reactions which obtain a lower CMB. These could possibly be separated for use. Reaction conditions can have significant impact on catalysis results and are key along with catalyst characteristics to obtain high yields. The results may be of use in understanding the chemistry that occurs with glycerol over other catalysts and how other polyols may interact with MgO.

5.3 References

(1)   Dalena, F.; Senatore, A.; Marino, A.; Gordano, A.; Basile, M.; Basile, A. Chapter 1 - Methanol Production and Applications: An Overview. In *Methanol*; Basile, A., Dalena, F., Eds.; Elsevier, 2018; pp 3–28. https://doi.org/https://doi.org/10.1016/B978-0-444-63903-5.00001-7.

(2)   Sheldon, D. Methanol Production - A Technical History. *Johnson Matthey Technol. Rev.* **2017**, *61* (3), 172–182. https://doi.org/10.1595/205651317X695622.

(3)   Balopi, B.; Agachi, P.; Danha. Methanol Synthesis Chemistry and Process Engineering Aspects- A Review with Consequence to Botswana Chemical Industries. *Procedia Manuf.* **2019**, *35*, 367–376. https://doi.org/https://doi.org/10.1016/j.promfg.2019.05.054.

(4)   Haider, M. H.; Dummer, N. F.; Knight, D. W.; Jenkins, R. L.; Howard, M.; Moulijn, J.; Taylor, S. H.; Hutchings, G. J. Efficient Green Methanol Synthesis from Glycerol. *Nat. Chem.* **2015**, *7* (12), 1028–1032. https://doi.org/10.1038/nchem.2345.

(5)   Jiang, X.; Nie, X.; Guo, X.; Song, C.; Chen, J. G. Recent Advances in Carbon Dioxide Hydrogenation to Methanol via Heterogeneous Catalysis. *Chem. Rev.* **2020**, *120* (15), 7984–8034. https://doi.org/10.1021/acs.chemrev.9b00723.

(6)   Bowker, M. Methanol Synthesis from CO2 Hydrogenation. *ChemCatChem* **2019**, *11* (17), 4238–4246. https://doi.org/https://doi.org/10.1002/cctc.201900401.

(7)   Hayward, J. S.; Smith, P. J.; Kondrat, S. A.; Bowker, M.; Hutchings, G. J. The Effects of Secondary Oxides on Copper-Based Catalysts for Green Methanol Synthesis. *ChemCatChem* **2017**, *9* (9), 1655–1662. https://doi.org/10.1002/cctc.201601692.

(8)   Basile, A.; Liguori, S.; Iulianelli, A. 2 - Membrane Reactors for Methane Steam Reforming (MSR). In *Membrane Reactors for Energy Applications and Basic Chemical Production*; Basile, A., Di Paola, L., l. Hai, F., Piemonte, V., Eds.; Woodhead Publishing Series in Energy; Woodhead Publishing, 2015; pp 31–59. https://doi.org/https://doi.org/10.1016/B978-1-78242-223-5.00002-9.

(9)   Smith, L. R.; Smith, P. J.; Mugford, K. S.; Douthwaite, M.; Dummer, N. F.; Willock, D. J.; Howard, M.; Knight, D. W.; Taylor, S. H.; Hutchings, G. J. New Insights for the Valorisation of Glycerol over MgO Catalysts in the Gas-Phase. *Catal. Sci. Technol.* **2019**, 19–22. https://doi.org/10.1039/C8CY02214C.

(10)   Di Cosimo, J. I.; Díez, V. K.; Ferretti, C.; Apesteguía, C. R. Basic Catalysis on MgO: Generation, Characterization and Catalytic Properties of Active Sites. *Catalysis* **2014**, *26* (3000), 1–28. https://doi.org/10.1039/9781782620037-00001.

(11)   Menezes, A. O.; Silva, P. S.; Hernández, E. P.; Borges, L. E. P.; Fraga, M. A. Tuning Surface Basic Properties of Nanocrystalline MgO by Controlling the Preparation Conditions. *Langmuir* **2010**, *26* (5), 3382–3387. https://doi.org/10.1021/la903149y.

(12)   Hu, J.; Zhu, K.; Chen, L.; Kübel, C.; Richards, R. MgO(111) Nanosheets with Unusual Surface Activity. *J. Phys. Chem. C* **2007**, *111* (32), 12038–12044. https://doi.org/10.1021/jp073383x.

(13)   Xu, C.; Enache, D. I.; Lloyd, R.; Knight, D. W.; Bartley, J. K.; Hutchings, G. J. Mgo Catalysed Triglyceride Transesterification for Biodiesel Synthesis. *Catal. Letters* **2010**. https://doi.org/10.1007/s10562-010-0365-5.

(14)   Ding, Y.; Zhang, G.; Wu, H.; Hai, B.; Wang, L.; Qian, Y. Nanoscale Magnesium Hydroxide and Magnesium Oxide Powders: Control over Size, Shape, and Structure via Hydrothermal Synthesis. *Chem. Mater.* **2001**, *13* (2), 435–440. https://doi.org/10.1021/cm000607e.

(15)   Fan, D.; Dong, X.; Yu, Y.; Zhang, M. A DFT Study on the Aldol Condensation Reaction on MgO in the Process of Ethanol to 1,3-Butadiene: Understanding the Structure-Activity Relationship. *Phys. Chem. Chem. Phys.* **2017**, *19* (37), 25671–25682. https://doi.org/10.1039/c7cp04502f.

(16)   Moteki, T.; Rowley, A. T.; Bregante, D. T.; Flaherty, D. W. Formation Pathways toward 2- and 4-Methylbenzaldehyde via Sequential Reactions from Acetaldehyde over Hydroxyapatite Catalyst. *ChemCatChem* **2017**, *9* (11), 1921–1929. https://doi.org/https://doi.org/10.1002/cctc.201700151.

(17)   Chang, Y.-C.; Ko, A.-N. Vapor Phase Reactions of Acetaldehyde over Type X Zeolites. *Appl. Catal. A Gen.* **2000**, *190* (1), 149–155. https://doi.org/https://doi.org/10.1016/S0926-860X(99)00293-8.

(18)   Lusardi, M.; Struble, T.; Teixeira, A. R.; Jensen, K. F. Identifying the Roles of Acid–Base Sites in Formation Pathways of Tolualdehydes from Acetaldehyde over MgO-Based Catalysts. *Catal. Sci. Technol.* **2020**, *10* (2), 536–548. https://doi.org/10.1039/C9CY01927H.

(19)   Chizallet, C.; Costentin, G.; Che, M.; Delbecq, F.; Sautet, P. Infrared Characterization of Hydroxyl Groups on MgO: A Periodic and Cluster Density Functional Theory Study. *J. Am. Chem. Soc.* **2007**, *129* (20), 6442–6452. https://doi.org/10.1021/ja068720e.

(20)   Sainna, M. A.; Nanavati, S.; Black, C.; Smith, L.; Mugford, K.; Jenkins, H.; Douthwaite, M.; Dummer, N. F.; Catlow, C. R. A.; Hutchings, G. J.; Taylor, S. H.; Logsdail, A. J.; Willock, D. J. A Combined Periodic DFT and QM/MM Approach to Understand the Radical Mechanism of the Catalytic Production of Methanol from Glycerol. *Faraday Discuss.* **2020**, *34* (4), 240–241. https://doi.org/10.19009/jjacg.34.4_240.

(21)   Coluccia, S.; Lavagnino, S.; Marchese, L. The Hydroxylated Surface of MgO Powders and the Formation of Surface Sites. *Mater. Chem. Phys.* **1988**, *18* (5), 445–464. https://doi.org/https://doi.org/10.1016/0254-0584(88)90016-8.

(22)   Abriou, D.; Jupille, J. Self-Inhibition of Water Dissociation on Magnesium Oxide Surfaces. *Surf. Sci.* **1999**, *430* (1), L527–L532. https://doi.org/https://doi.org/10.1016/S0039-6028(99)00410-0.

(23)   Hernandez, D.; Velasquez, M.; Ayrault, P.; Lopez, D.; Fernandez, J. J.; Santamaria, A.; Batiot-Dupeyrat, C. Gas Phase Glycerol Conversion over Lanthanum Based Catalysts: LaNiO3and La2O3. *Appl. Catal. A Gen.* **2013**, *467*, 315–324. https://doi.org/10.1016/j.apcata.2013.07.016.

(24)   Foyt, D. C.; White, J. M. Thermal Decomposition of Methanol Adsorbed on Magnesia. *J. Catal.* **1977**, *47* (2), 260–268. https://doi.org/https://doi.org/10.1016/0021-9517(77)90173-7.

(25)   Liang, S. H.; Gay, I. D. Adsorption and Thermal Decomposition of Methanol on Magnesium Oxide. Carbon-13 NMR Studies. *Langmuir* **1985**, *1* (5), 593–599. https://doi.org/10.1021/la00065a014.

(26)   Yan, Y.; Zhang, Y.; Jiang, T.; Xiao, T.; Edwards, P. P.; Cao, F. Glycerol Hydrogenolysis over a Pt–Ni Bimetallic Catalyst with Hydrogen Generated in Situ. *RSC Adv.* **2017**, *7* (61), 38251–38256. https://doi.org/10.1039/C7RA05814D.

(27)   D'Hondt, E.; de Vyver, S.; Sels, B. F.; Jacobs, P. A. Catalytic Glycerol Conversion into 1,2-Propanediol in Absence of Added Hydrogen. *Chem. Commun.* **2008**, No. 45, 6011–6012. https://doi.org/10.1039/B812886C.

(28)   Rahmat, N.; Abdullah, A. Z.; Mohamed, A. R. Recent Progress on Innovative and Potential

Technologies for Glycerol Transformation into Fuel Additives: A Critical Review. *Renew. Sustain. Energy Rev.* **2010**, *14* (3), 987–1000. https://doi.org/https://doi.org/10.1016/j.rser.2009.11.010.

(29)   Smith, L. R.; Sainna, M. A.; Douthwaite, M.; Davies, T. E.; Dummer, N. F.; Willock, D. J.; Knight, D. W.; Catlow, C. R. A.; Taylor, S. H.; Hutchings, G. J. Gas Phase Glycerol Valorization over Ceria Nanostructures with Well-Defined Morphologies. *ACS Catal.* **2021**, *11* (8), 4893–4907. https://doi.org/10.1021/acscatal.0c05606.

(30)   Smith, P. J.; Smith, L.; Dummer, N. F.; Douthwaite, M.; Willock, D. J.; Howard, M.; Knight, D. W.; Taylor, S. H.; Hutchings, G. J. Investigating the Influence of Reaction Conditions and the Properties of Ceria for the Valorisation of Glycerol. *Energies* **2019**, *12* (7), 1359. https://doi.org/10.3390/en12071359.

(31)   Devlia, J.; Smith, L.; Douthwaite, M.; Taylor, S. H.; Willock, D. J.; Hutchings, G. J.; Dummer, N. F. The Formation of Methanol from Glycerol Bio-Waste over Doped Ceria-Based Catalysts: Doped Ceria Based Catalysts. *Philos. Trans. R. Soc. A Math. Phys. Eng. Sci.* **2020**, *378* (2176). https://doi.org/10.1098/rsta.2020.0059.

(32)   Smith, L. R. Gas-Phase Conversions of Glycerol to Methanol Over Ceria-Based Catalysts, Cardiff University, **2020**.

(33)   Sutradhar, N.; Sinhamahapatra, A.; Roy, B.; Bajaj, H. C.; Mukhopadhyay, I.; Panda, A. B. Preparation of MgO Nano-Rods with Strong Catalytic Activity via Hydrated Basic Magnesium Carbonates. *Mater. Res. Bull.* **2011**, *46* (11), 2163–2167. https://doi.org/10.1016/j.materresbull.2011.02.024.

(34)   Sutradhar, N.; Sinhamahapatra, A.; Pahari, S. K.; Pal, P.; Bajaj, H. C.; Mukhopadhyay, I.; Panda, A. B. Controlled Synthesis of Different Morphologies of MgO and Their Use as Solid Base Catalysts. *J. Phys. Chem. C* **2011**, *115* (25), 12308–12316. https://doi.org/10.1021/jp2022314.

(35)   Zhang, X.; Zheng, Y.; Feng, X.; Han, X.; Bai, Z.; Zhang, Z. Calcination Temperature-Dependent Surface Structure and Physicochemical Properties of Magnesium Oxide. *RSC Adv.* **2015**, *5* (105), 86102–86112. https://doi.org/10.1039/c5ra17031a.

(36)   Aramendía, M. A.; Borau, V.; Jiménez, C.; Marinas, J. M.; Ruiz, J. R.; Urbano, F. J. Influence of the Preparation Method on the Structural and Surface Properties of Various Magnesium Oxides and Their Catalytic Activity in the Meerwein-Ponndorf-Verley Reaction. *Appl. Catal. A Gen.* **2003**, *244* (2), 207–215. https://doi.org/10.1016/S0926-860X(02)00213-2.

(37)   Khairallah, F.; Glisenti, A. Synthesis, Characterization and Reactivity Study of Nanoscale Magnesium Oxide. *J. Mol. Catal. A Chem.* **2007**, *274* (1–2), 137–147. https://doi.org/10.1016/j.molcata.2007.04.039.

(38)   Dummer, N. F.; Joyce, L.; Ellicott, H.; Jiang, Y. Surfactant Controlled Magnesium Oxide Synthesis for Base Catalysis. *Catal. Sci. Technol.* **2016**, *6* (6), 1903–1912. https://doi.org/10.1039/c5cy01107h.

(39)   Ruckenstein, E.; Hu, Y. H. The Effect of Precursor and Preparation Conditions of MgO on the CO2 Reforming of CH4 over NiO/MgO Catalysts. *Appl. Catal. A Gen.* **1997**, *154* (1–2), 185–205. https://doi.org/10.1016/S0926-860X(96)00372-9.

(40)   Hargreaves, J. S. J. Powder X-Ray Diffraction and Heterogeneous Catalysis. *Crystallogr. Rev.* **2005**, *11* (1), 21–34. https://doi.org/10.1080/08893110500078324.

(41)   Jang, W. J.; Kim, H. M.; Shim, J. O.; Yoo, S. Y.; Jeon, K. W.; Na, H. S.; Lee, Y. L.; Jeong, D. W.; Bae, J. W.; Nah, I. W.; Roh, H. S. Key Properties of Ni-MgO-CeO2, Ni-MgO-ZrO2, and Ni-MgO-Ce(1-x)Zr(x)O2 Catalysts for the Reforming of Methane with Carbon Dioxide. *Green Chem.* **2018**, *20* (7), 1621–1633. https://doi.org/10.1039/c7gc03605a.

(42)   Fu, Y.; Zhang, L.; Yue, B.; Chen, X.; He, H. Simultaneous Characterization of Solid Acidity and Basicity of Metal Oxide Catalysts via the Solid-State NMR Technique. *J. Phys. Chem. C* **2018**, *122* (42), 24094–24102. https://doi.org/10.1021/acs.jpcc.8b06827.

(43)   Deng, F.; Yang, J.; Ye, C. Solid State NMR Characterization of Solid Surface of Heterogeneous

Catalysts. *Mod. Magn. Reson.* **2008**, 205–211.

(44)   Mirth, G.; Lercher, J. A.; Anderson, M. W.; Klinowski, J. Adsorption Complexes of Methanol on Zeolite ZSM-5. *J. Chem. Soc. Faraday Trans.* **1990**, *86* (17), 3039–3044. https://doi.org/10.1039/FT9908603039.

(45)   Zhang, W.; Xu, S.; Han, X.; Bao, X. In Situ Solid-State NMR for Heterogeneous Catalysis: A Joint Experimental and Theoretical Approach. *Chem. Soc. Rev.* **2012**, *41* (1), 192–210. https://doi.org/10.1039/C1CS15009J.

(46)   Naik, D. V; Singh, K. K.; Kumar, V.; Prasad, B.; Behera, B.; Bangwal, D. P.; Atheya, N.; Garg, M. O. Catalytic Cracking of Glycerol to Fine Chemicals over Equilibrium Fluid Catalytic Cracking Catalyst. *Energy Procedia* **2014**, *54*, 593–598. https://doi.org/https://doi.org/10.1016/j.egypro.2014.07.300.

Chapter 6

Appendix

6.1 Norrish type 1 like radical fragmentation

Haider *et al,* stated that the type of radical fragmentation hydroxyacetone and glycolaldehyde can undergo are similar to a Norrish type 1 process. This reaction involves a C-C bond cleavage between the α carbon of either ketones or aldehydes. [1–3]

6.1.1 Hydroxyacetone
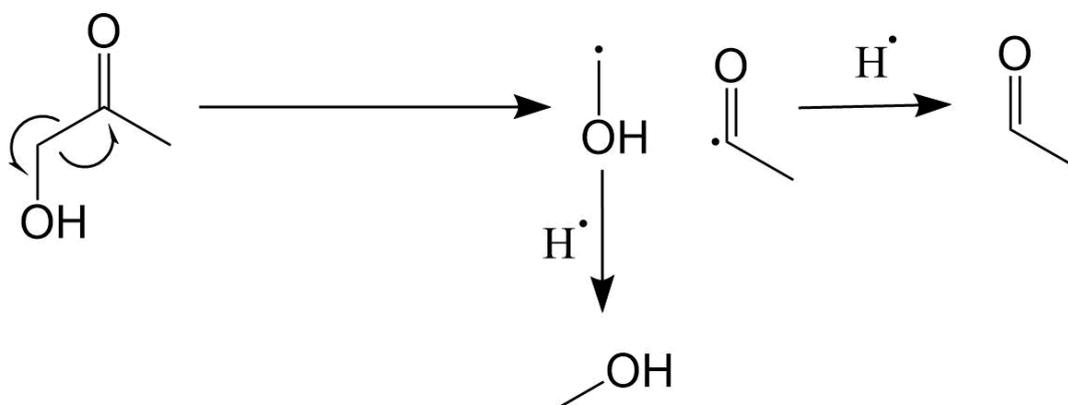
6.1.2 Glycolaldehyde
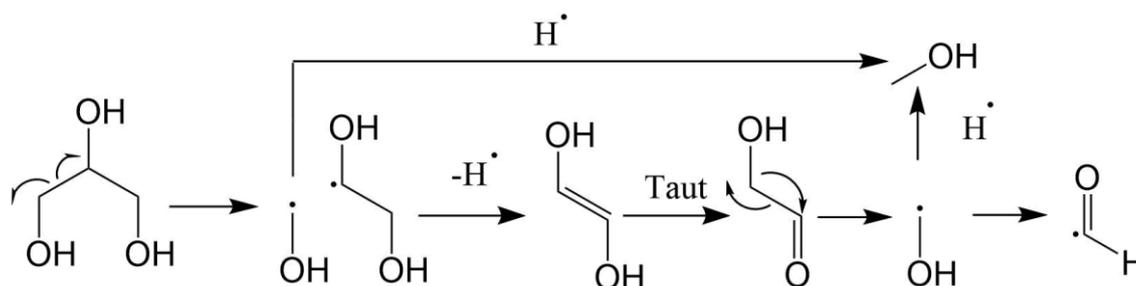
6. 2 Chapter 2

6.2.1 GC organic species example calibration curves

Examples of GC calibration curves are shown below. All analytes were calibrated for using the same method.
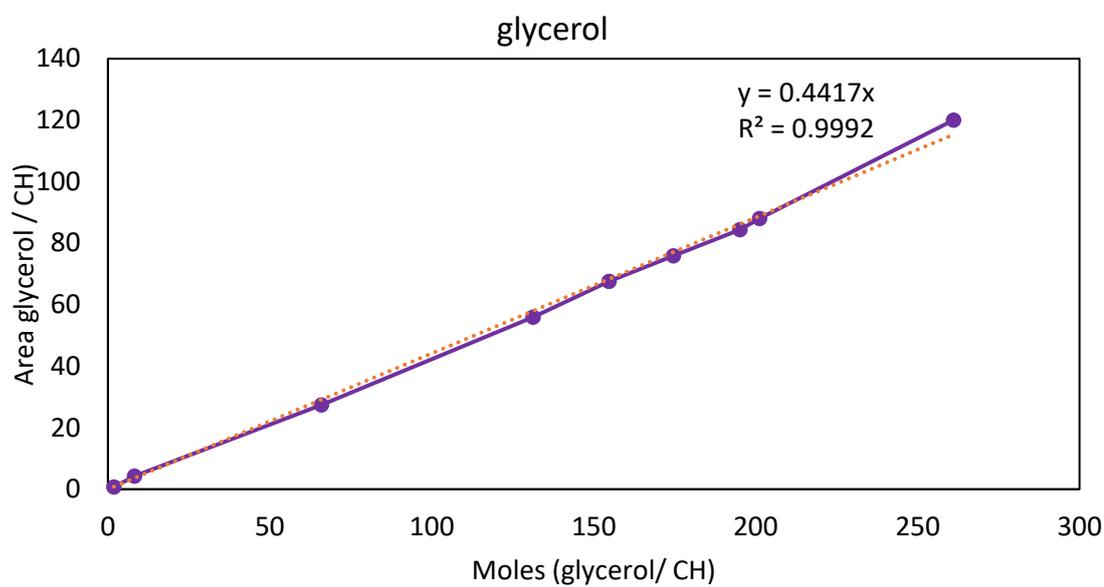
Figure 1. GC calibration for glycerol using cyclohexanol as an external standard.
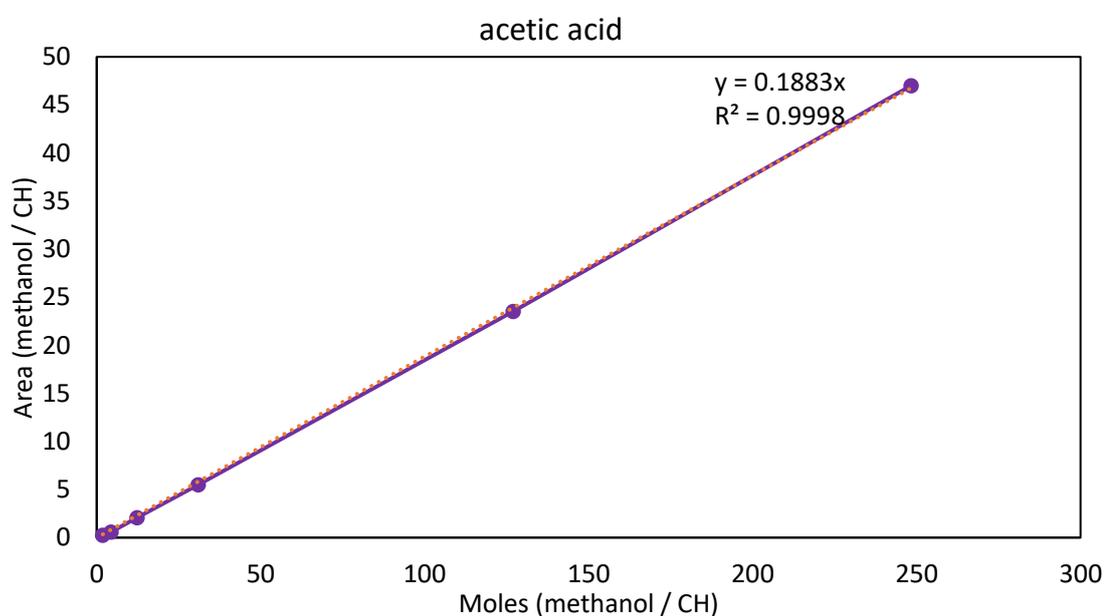
Figure 2. GC calibration for acetic acid glycerol using cyclohexanol as an external standard.
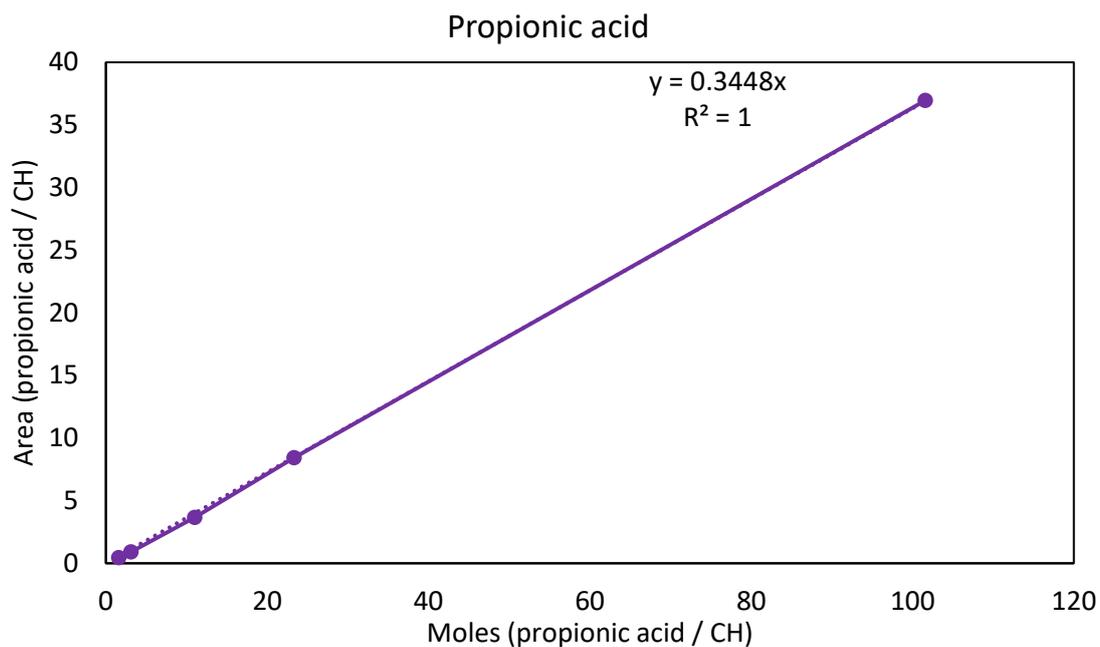
Figure 3. GC calibration for propionic acid using cyclohexanol as an external standard.
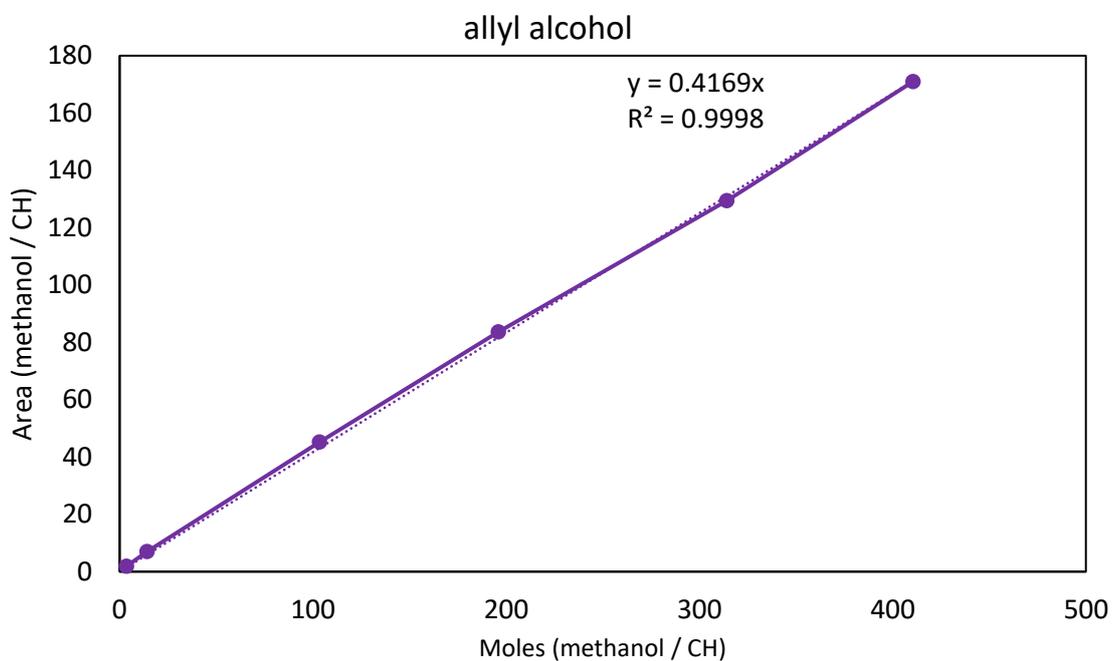
Figure 4. GC calibration for allyl alcohol using cyclohexanol as an external standard.
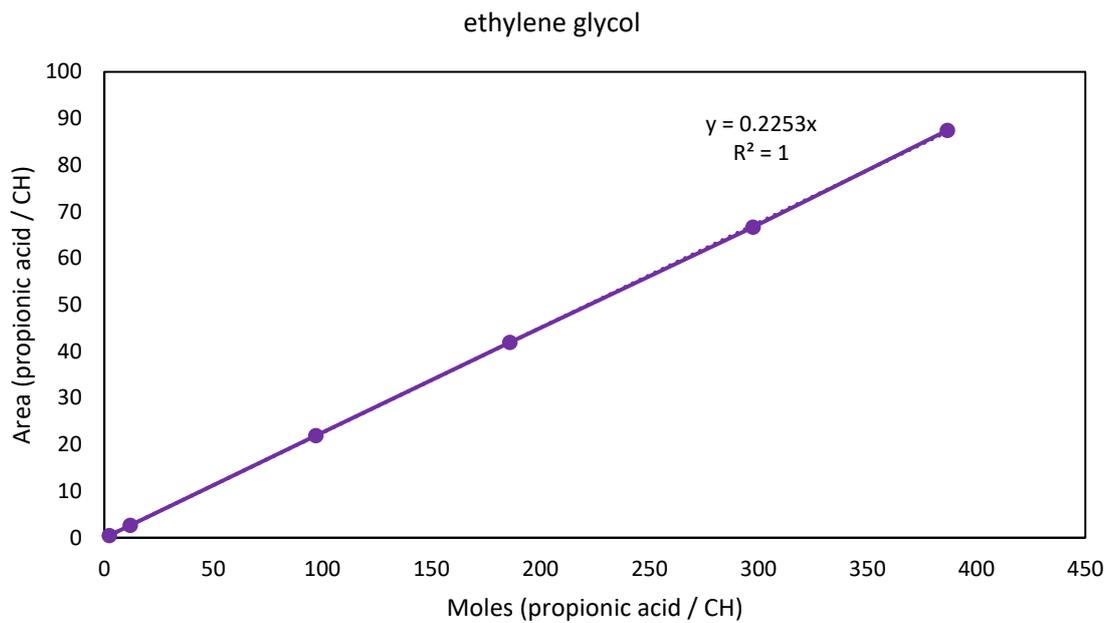
Figure 5. GC calibration for ethylene glycol using cyclohexanol as an external standard.
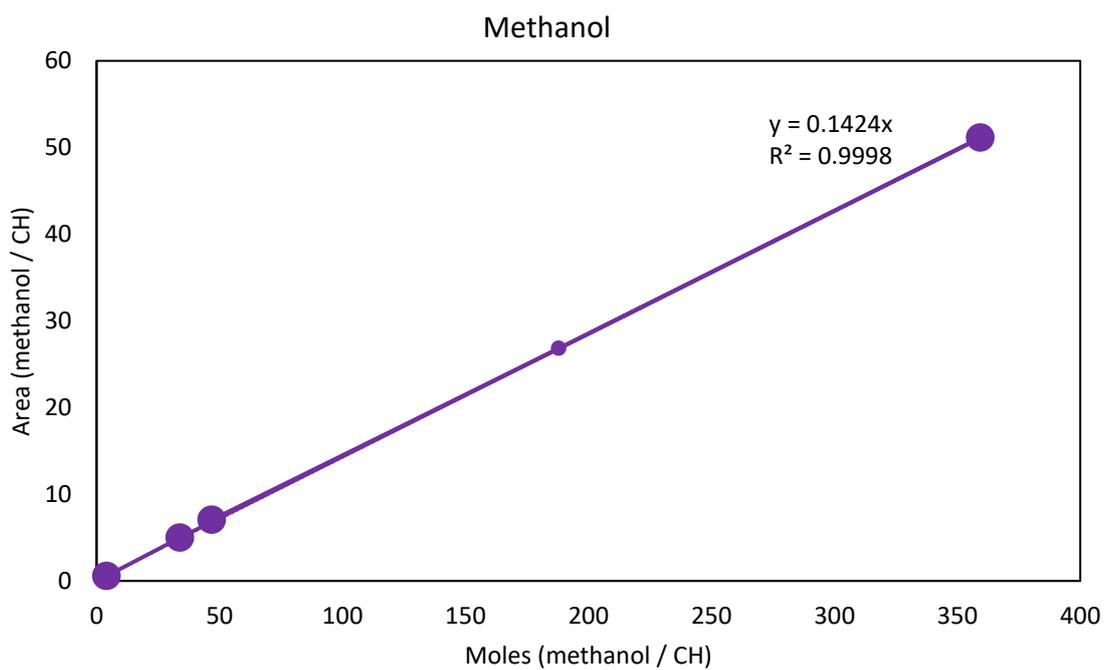
Figure 6. GC calibration for methanol using cyclohexanol as an external standard.

6.1.2 CO$_2$ TPD calibration curve

y = 274.65x
R^2 = 0.9999
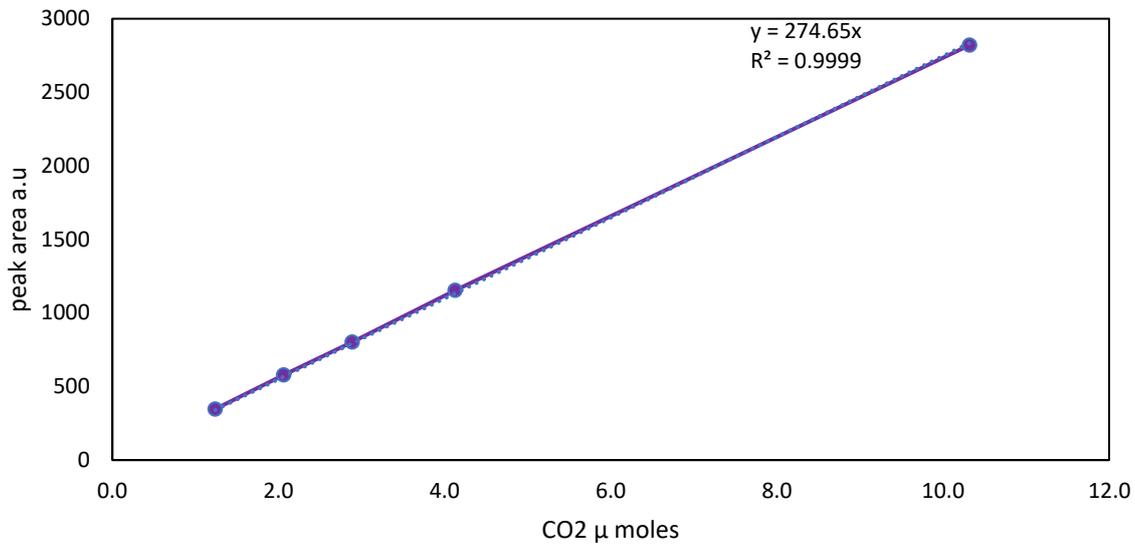
Figure 7. CO$_2$ calibration curve for TPD experiments. Peak areas obtained by injecting different quantities of reactant gas. TCD set to 180 mV.

6.3 Chapter 3

6.3.1 Isotherms of Heat treatment temperature varied MgO.

MgO_450
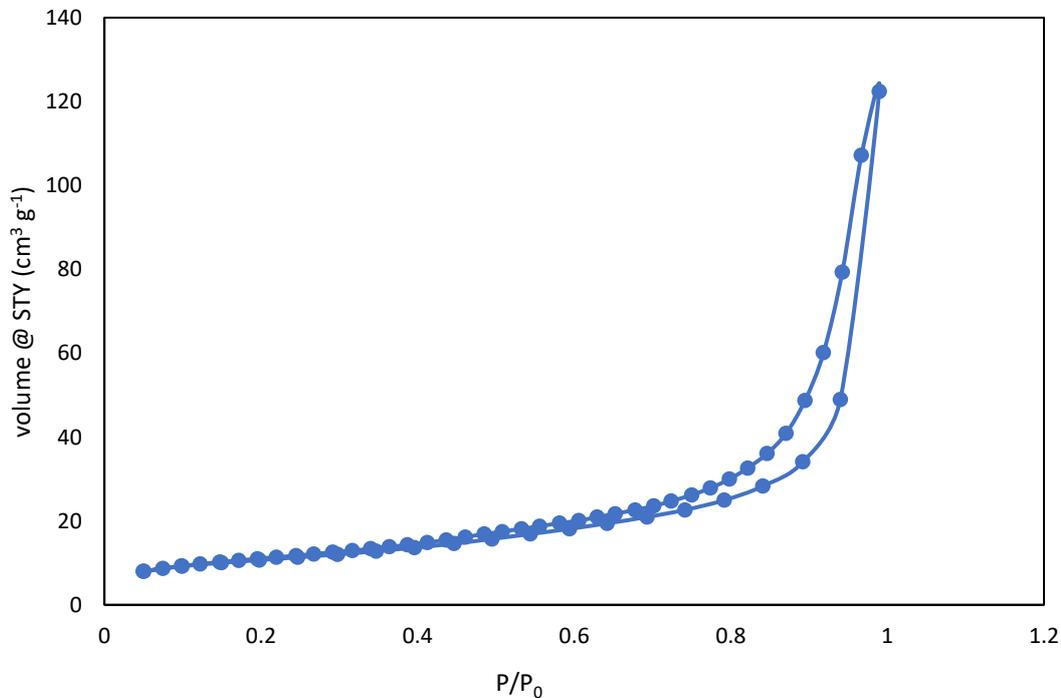
Figure 8. N$_2$ sorption isotherm for MgO_450
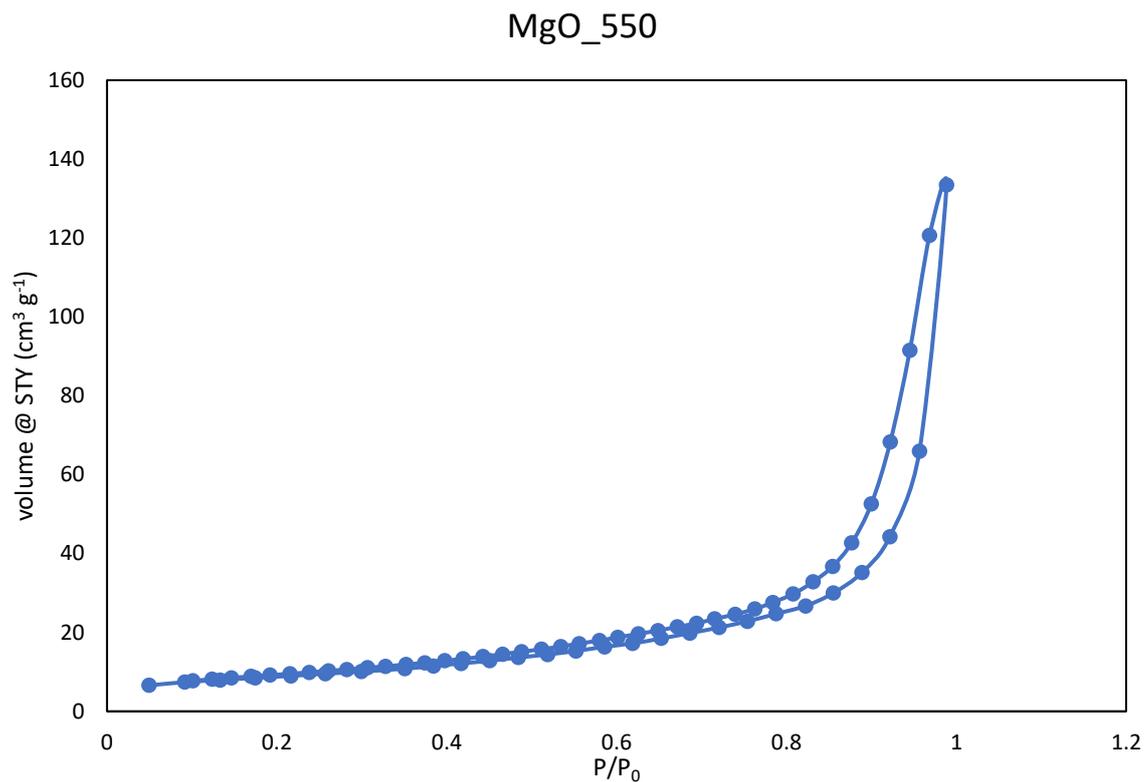
MgO_550

Figure 9. N$_2$ sorption isotherm for MgO_550.
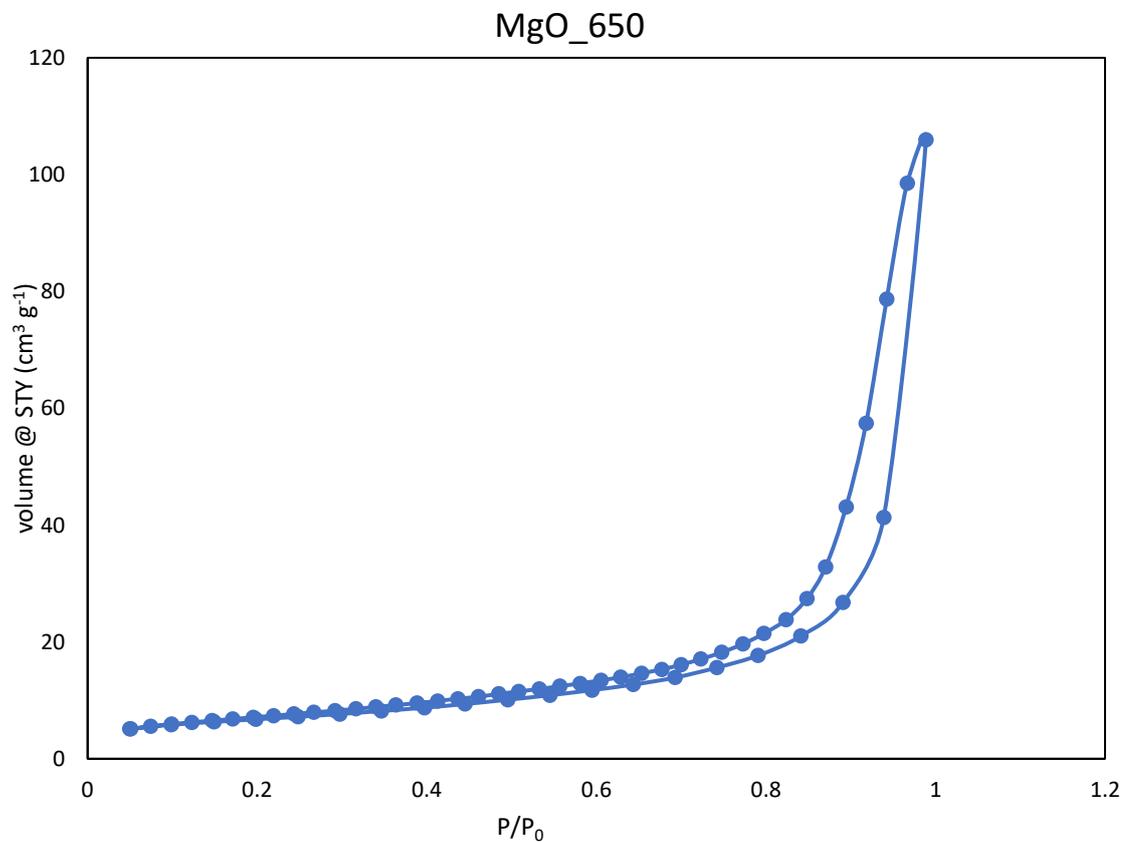
MgO_650

Figure 10. N$_2$ sorption isotherm for MgO_650.
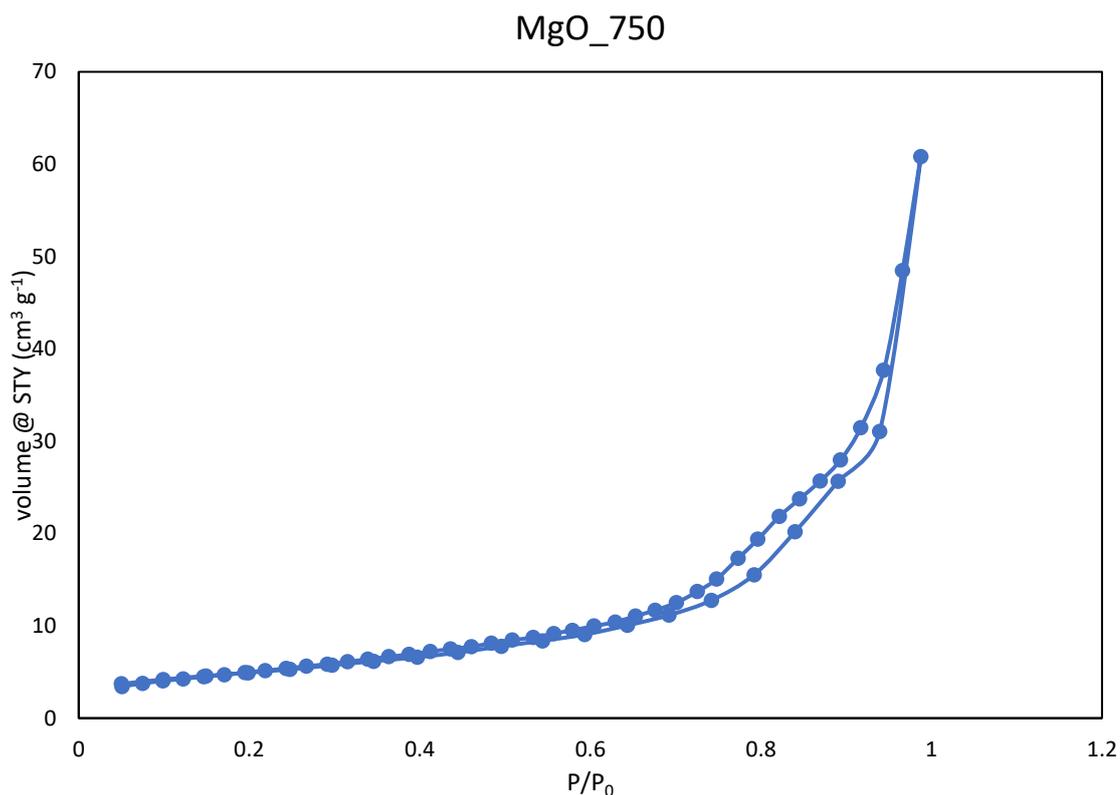
Figure 11. N₂ sorption isotherm for MgO_750.

6.3.2 XRD patterns of different stages of catalyst preparation
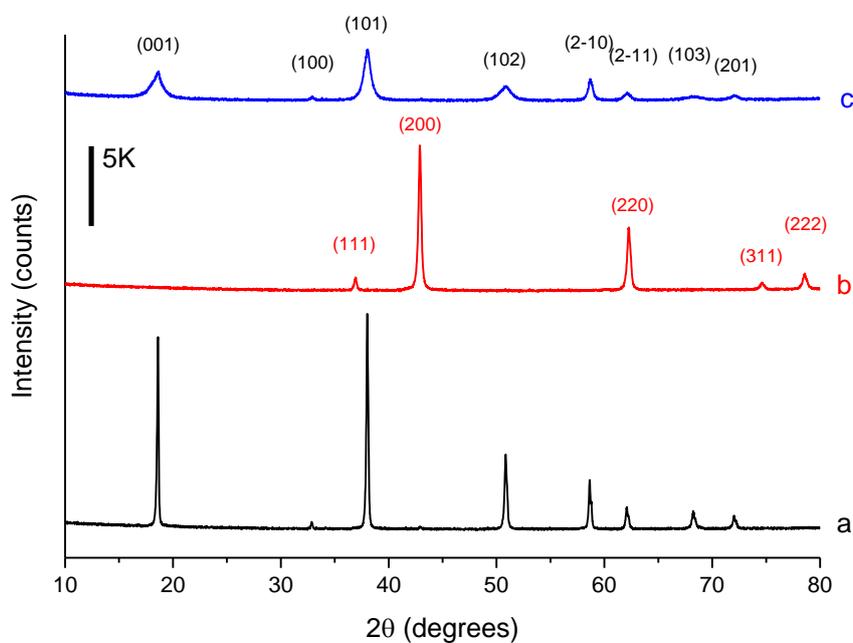
Figure 12. XRD patterns for (a) commercial Mg(OH)₂, (b) MgO after calcination at 450 ˚C for 2 h, (c) Mg(OH)₂ after refluxing in water and drying at 110 ˚C for 16 h.

6.2.3 Mass spectrums from MgO LCMS

(a)

(b)

(c)

(d)

(e)

(f)

(g)

SHT_MS35541A_LCMS 514 (4.536) Cm (503:516-475:484)
1: TOF MS ES+
1.90e6

215.0919
267.9536
357.8405

(h)

SHT_MS35541A_LCMS 537 (4.734) Cm (532:540-(522+543))
1: TOF MS ES+
9.38e5

245.0992
195.9125
357.8405
446.8658

(i)

SHT_MS35541A_LCMS 556 (4.897) Cm (542:575-(534:546+579:592))
1: TOF MS ES+
1.49e7

245.0992
307.0703

(j)

(k)

(l)

220
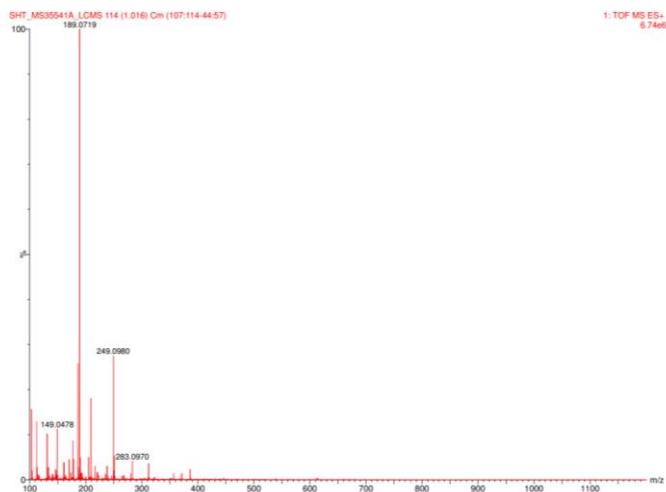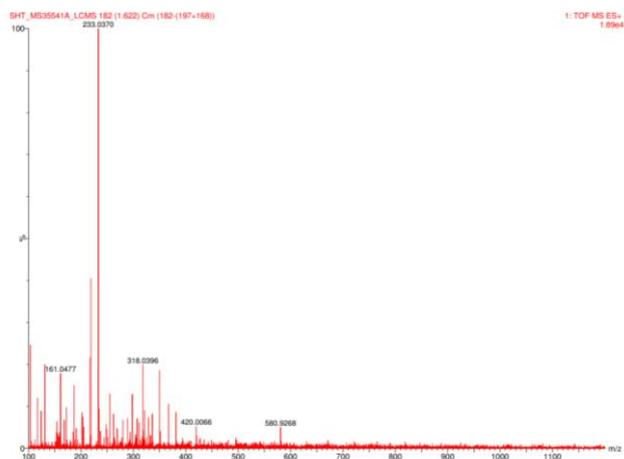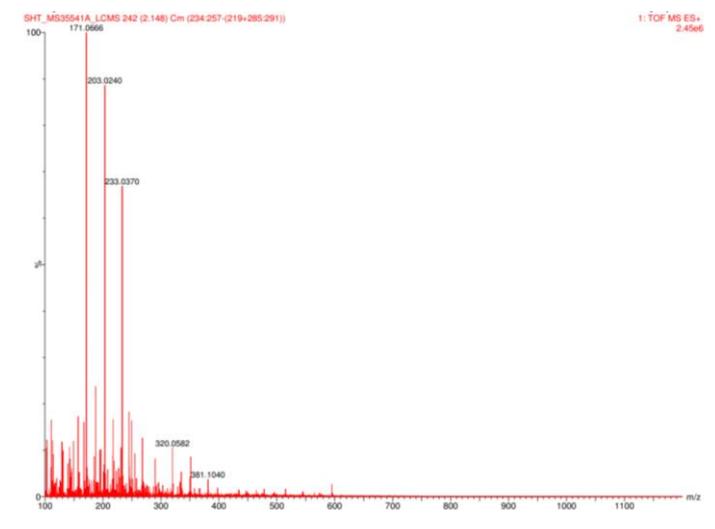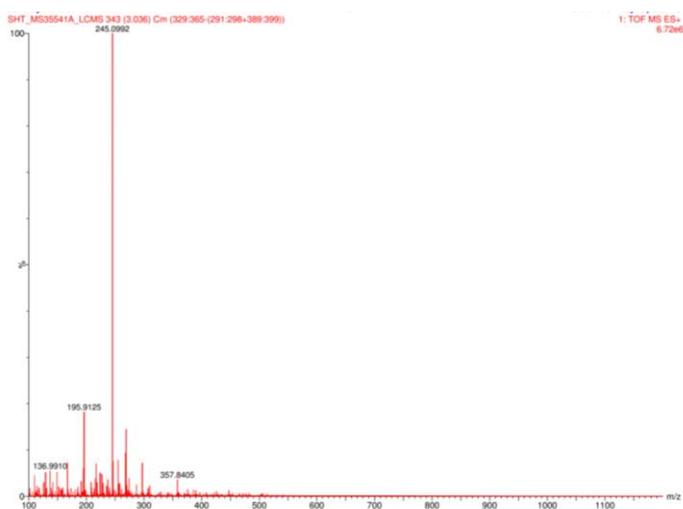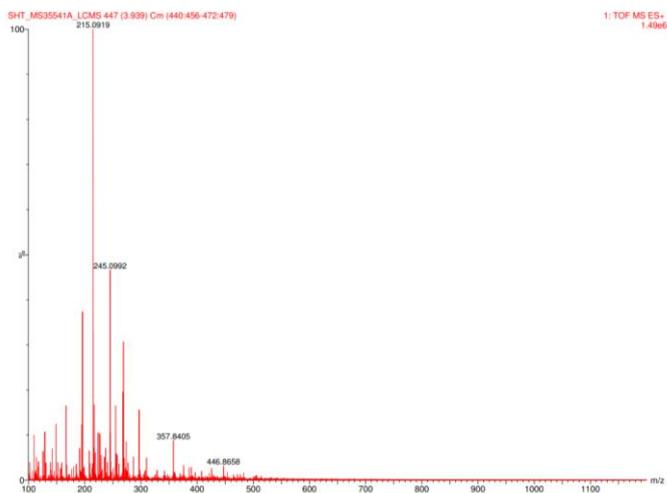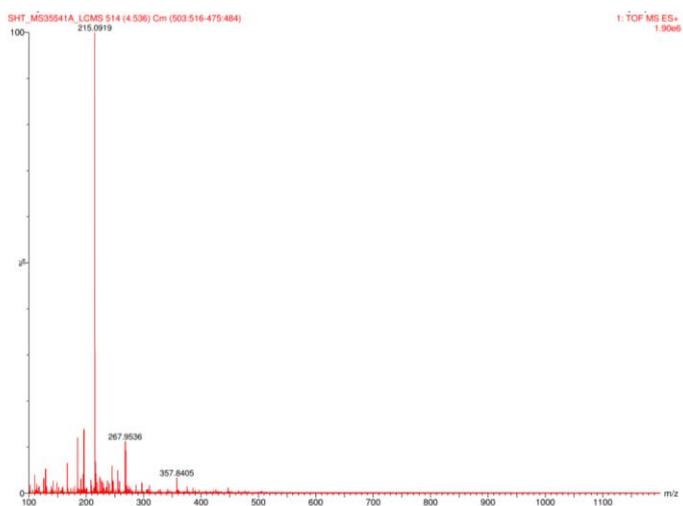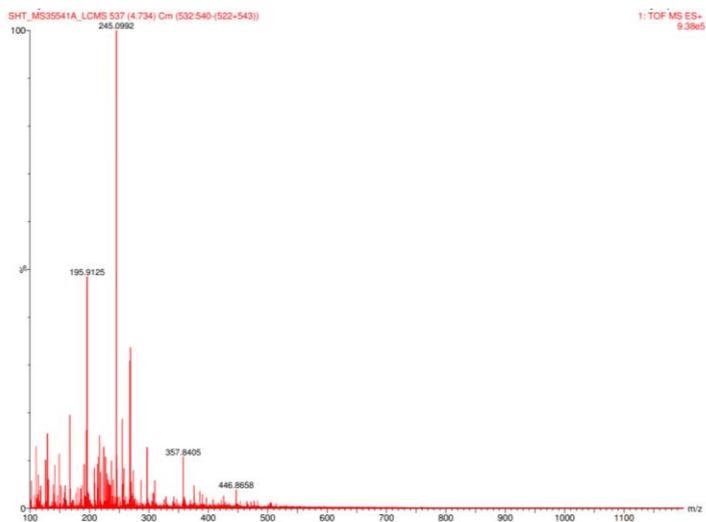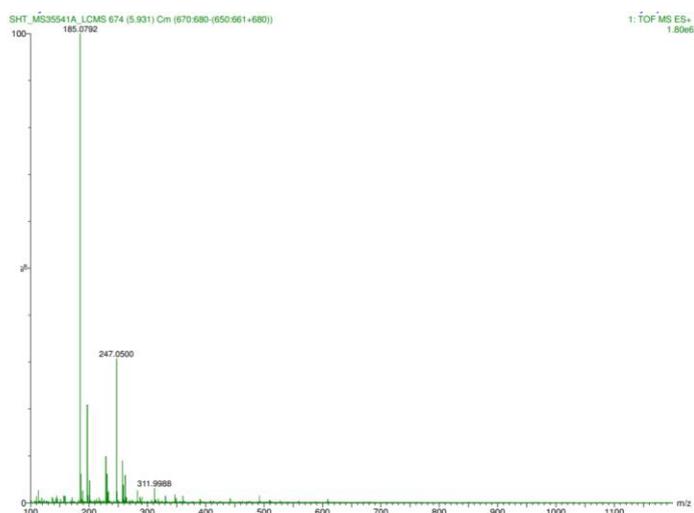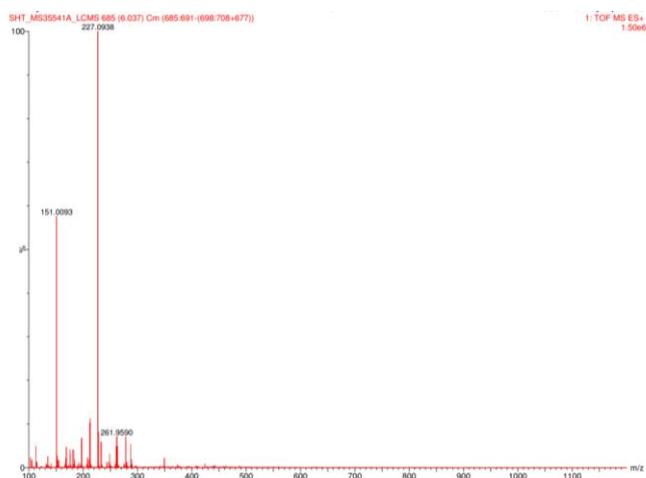
(m)
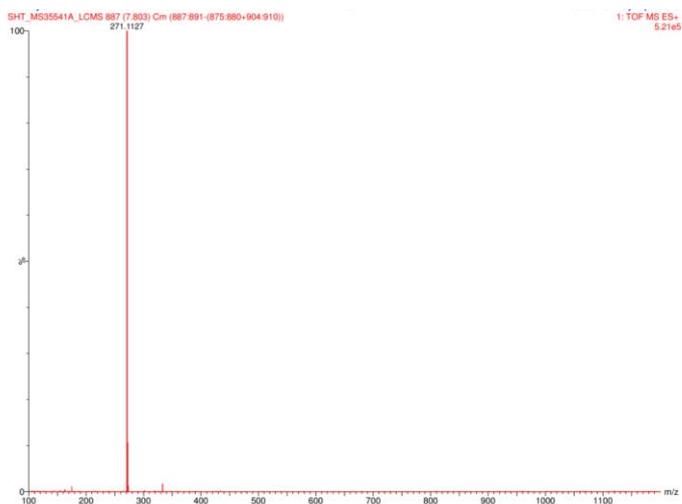
Figure 13. LC-MS mass spectrums selection corresponding to the post reaction solution of a reaction run over MgO_450. Detection parameters are fixed at 100 - 1000 m/z. Retention time mins; (a) 1.016 (b) 1.113 (c) 1.622 (d) 2.148 (e) 3.036 (f) 3.939 (g) 4.536 (h) 4.734 (i) 4.897 (j) 5.537 (k) 5.931 (l) 6.037 (m) 7.803. Reaction conditions: 360 °C, glycerol flow (0.016 mL min-1), 0.5 g MgO, 50 mL min-1 Ar, 3 hours.

6.3.4 Coking of post reaction catalyst - TGA
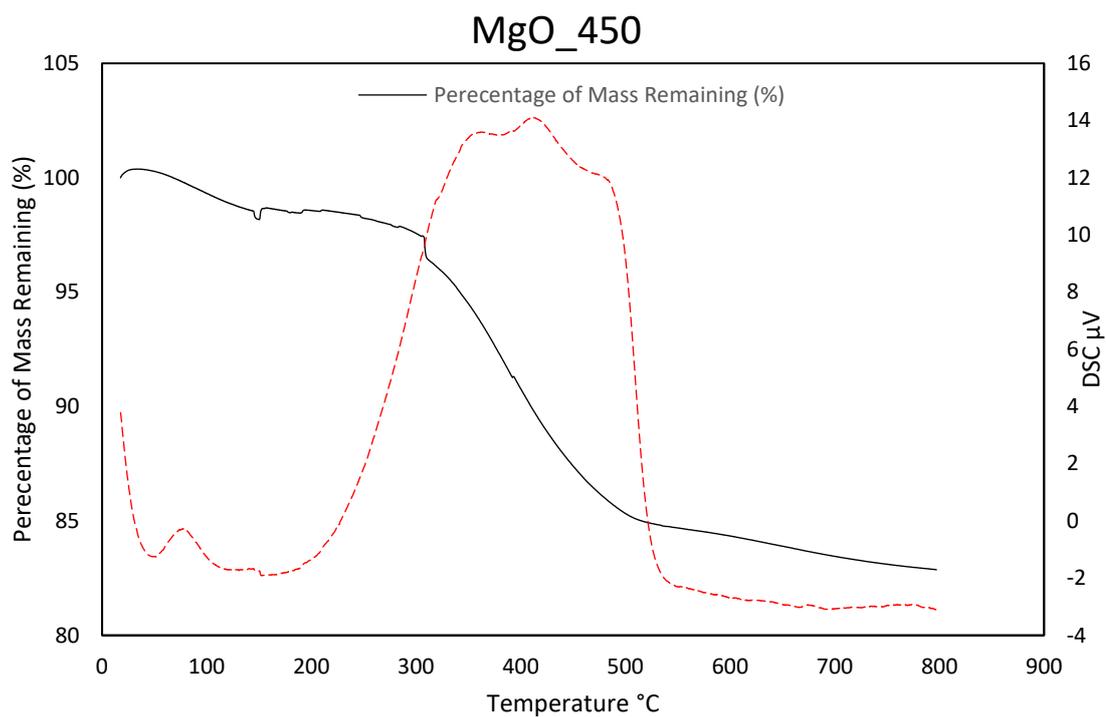
MgO_450

Figure 14. Thermogravimetric analysis of MgO_450 showing mass loss (black) and heat flow (red dashed line) after reaction at 360 C with 50 wt.% glycerol.
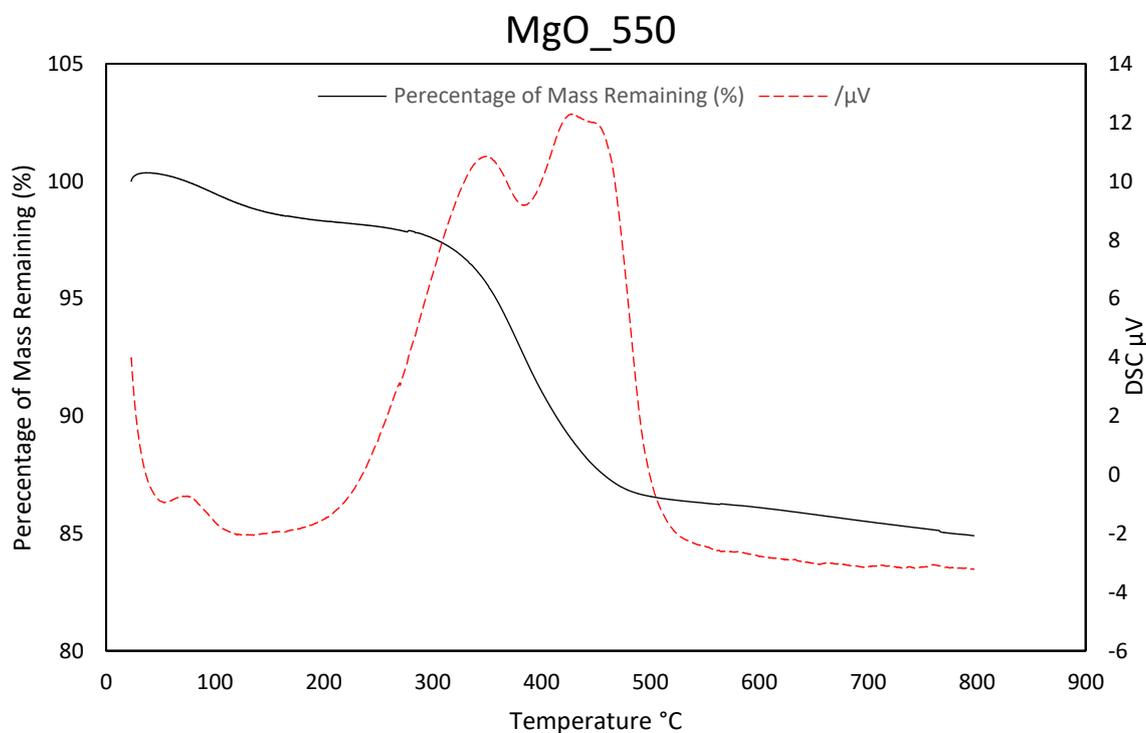
MgO_550

Figure 15. Thermogravimetric analysis of MgO_550 showing mass loss (black) and heat flow (red dashed line) after reaction at 360 C with 50 wt.% glycerol.
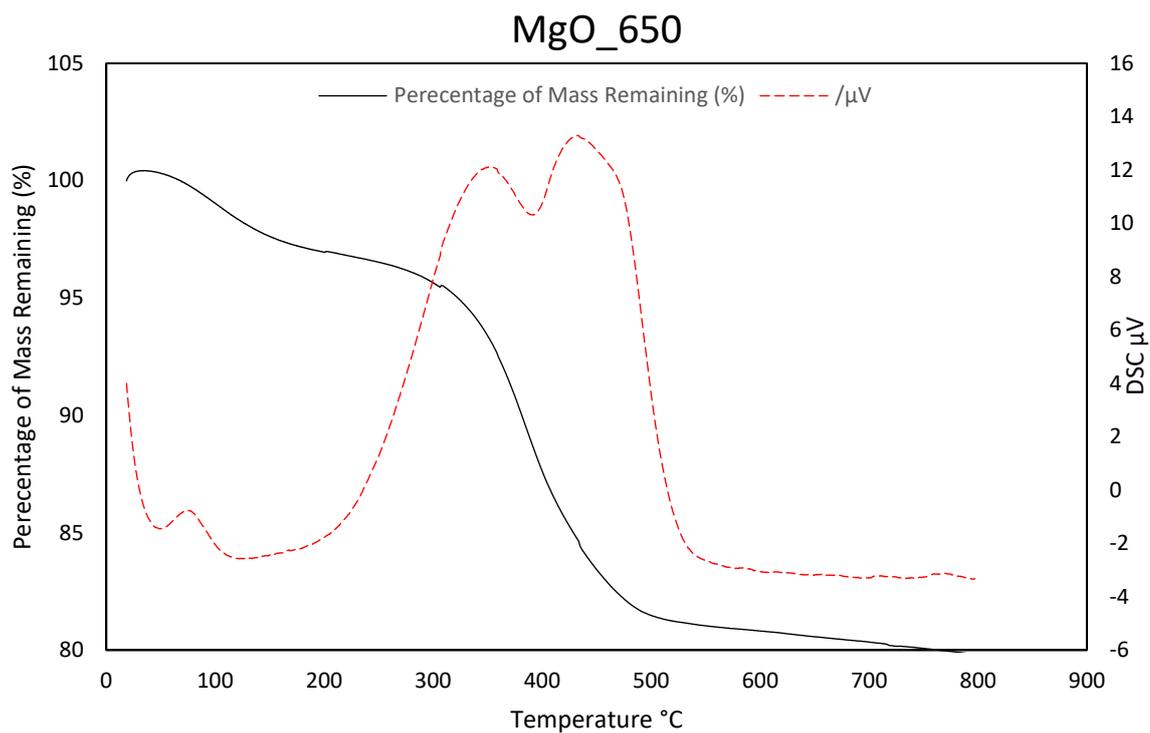
Figure 16. Thermogravimetric analysis of MgO_650 showing mass loss (black) and heat flow (red dashed line) after reaction at 360 C with 50 wt.% glycerol.
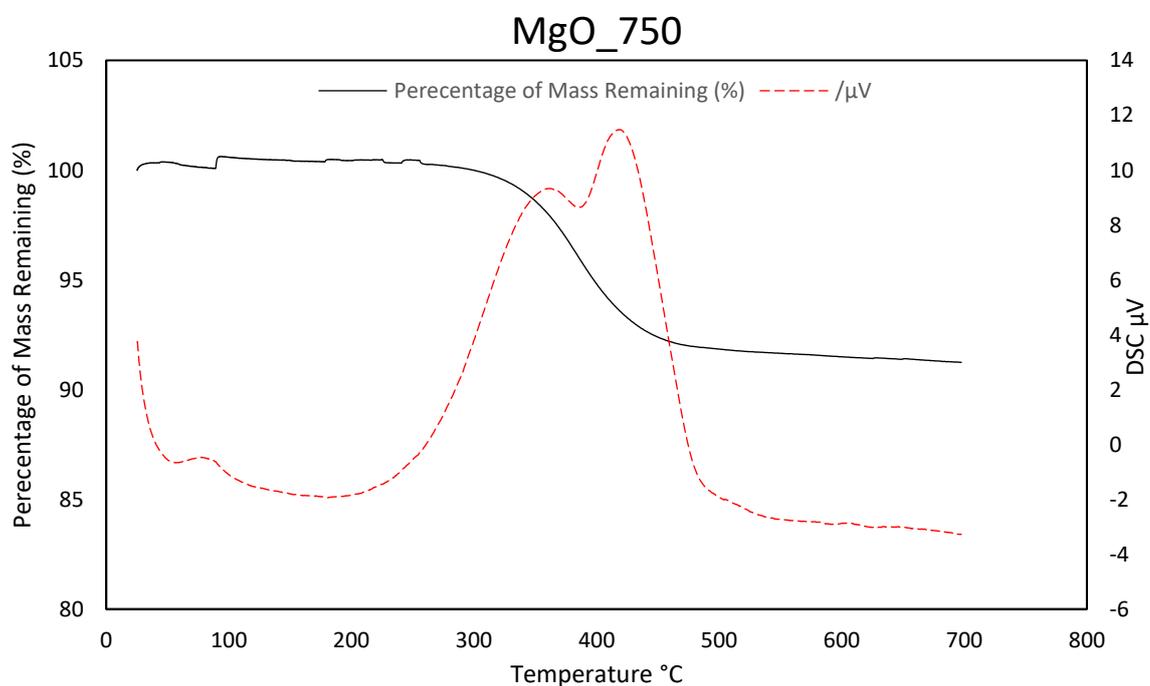

Figure 17. Thermogravimetric analysis of MgO_750 showing mass loss (black) and heat flow (red dashed line) after reaction at 360 C with 50 wt.% glycerol.

6.4 Chapter 4

6.4.1 Unknown GC peaks hydroxyacetone

Table 1. Number of separate unknown GC peaks. Reaction conditions: 320 - 400 °C, 50 wt.% hydroxyacetone, 0.016 mL min^{-1}, 0.5 g catalyst, 50 mL min^{-1} Ar. 3 hours.

	320 °C	360 °C	400 °C
MgO_450	31	39	28
MgO_650	34	38	22

6.4.2 Unknown GC peaks ethylene glycol

Table 2. Number of separate unknown GC peaks. Reaction conditions: 50 wt.% ethylene glycol in water, 320 °C - 440 °C with 0.5 g catalyst. 0.1 mL min^{-1} 15 mins, 0.016 mL min^{-1} 2 hours, 0.016 mL min^{-1} 3 hours collect. 50 mL min^{-1} Ar flow.

	320 °C	360 °C	400 °C	440 °C
MgO_450	20	24	31	68
MgO_650	16	22	54	67

6.4.3 25 %/25 % Ethylene glycol/ glycerol reaction results

Table 3. Reaction conditions: 25 wt.% ethylene glycol 25 wt.% ethylene glycol in water, 400 °C - °C with 0.5 g catalyst. 0.1 mL min^{-1} 15 mins, 0.016 mL min^{-1} 2 hours, 0.016 mL min^{-1} 3 hours collect. 50 mL min^{-1} Ar flow.

	Selectivity %
acetaldehyde	27.7
propionaldehyde	1.2
acetone	0.2
acrolein	8.1
butyraldehyde	0.0
methanol	16.1
2-propanol	0.0
ethanol	1.9
2,3-butanedione	1.5
2-butanol	0.0
1-propanol	0.3
3-hexanone	0.2
2-hexanone	0.0
2-methyl-1-propanol	0.0
allyl alcohol	1.2
cyclopentanone	0.8
hydroxyacetone	19.8
3-ethoxy-1-propanol	0.0
acetic acid	1.8
Glycidol	0.6
propionic acid	0.2
1,2-propanediol	4.3
unknown(s)	7.8
ethylene glycol	0.0
1,3-propanediol	0.7
phenol	0.0
CO	2.8
CO2	2.9
Glycerol conversion	87
Carbon balance	49
MeOH carbon selectivity	16
MeOH STY g h^{-1} kg h^{-1}	77

6.5 References

(1)   Haider, M. H.; Dummer, N. F.; Knight, D. W.; Jenkins, R. L.; Howard, M.; Moulijn, J.; Taylor, S. H.; Hutchings, G. J. Efficient Green Methanol Synthesis from Glycerol. *Nat. Chem.* **2015**, *7* (12), 1028–1032. https://doi.org/10.1038/nchem.2345.

(2)   Bamford, C. H.; Norrish, R. G. W. Photodecomposition of Aldehydes and Ketones. *Nature* **1936**, *874* (1934), 1016.

(3)   Norrish Type I Reaction. In *Comprehensive Organic Name Reactions and Reagents*; John Wiley & Sons, Ltd, 2010; pp 2062–2066. https://doi.org/https://doi.org/10.1002/9780470638859.conrr464.